
VALIDATION OF NOMINATIONS IN GAS NETWORKS AND
PROPERTIES OF TECHNICAL CAPACITIES

Von der Fakultät für Mathematik und Physik
der Gottfried Wilhelm Leibniz Universität Hannover
zur Erlangung des akademischen Grades

Doktor der Naturwissenschaften
Dr. rer. nat.

genehmigte Dissertation
von

Dipl.-Math. Bernhard Michael Willert

geboren am 10. Februar 1984 in München

2014

Referent: Prof. Dr. Marc C. Steinbach, Leibniz Universität Hannover
Korreferent: Prof. Dr. Marc Pfetsch, Technische Universität Darmstadt
Tag der Promotion: 16. Juli 2014

For my little one, a natural born explorer.

Abstract

Traditional methods in planning of gas transport networks rely on series of network simulations. New legal and economical requirements render these methods insufficient, so alternative approaches for accurate planning of large-scale networks are highly desired. The increasing importance of natural gas in Europe and new demands imposed by new techniques like power to gas drive the need for an automated determination of optimal network settings.

This thesis covers two optimization problems occurring in gas transportation. The problem of validation of nominations rises the question, if given supply and discharge rates at the entries and exits of the network result in a feasible network state. To this end, a MINLP model is presented including a detailed description of stationary gas physics and technical properties of the network elements. To be able to apply general-purpose nonlinear solvers, two separate optimization problems are described. A nonlinear model with reduced complexity is derived from the MINLP model. Complementarity constraints model discrete aspects. This results in a mathematical program with equilibrium constraints (MPEC). Furthermore, a highly accurate NLP model is described, covering all physical aspects of the MINLP model under given discrete decisions. Numerical experiments on large-scale networks show the applicability of regularization techniques on the MPEC and the success in validating nominations when both models are combined. Comparisons with commercial simulation software underline the high level of detail of the gained solutions.

The second problem discussed in this thesis is the determination of technical capacities of a network. A mathematical problem description of this new problem class is derived from the legal regulations resulting in a mixed-integer nonlinear adjustable robust problem. It turns out that the criteria for an optimal capacity are not well-defined. A sensible interpretation results in a Pareto optimization problem. Analysis of the capacity problem shows that monotony and convexity of technical capacities are typically not given in reality. The implications are explained based on small network examples.

Keywords: technical capacities of gas networks, mixed-integer nonlinear optimization, complementarity constraints, MPEC

Zusammenfassung

Etablierte Methoden zur Planung von Gastransportnetzen beruhen auf Simulationen verschiedener Netzzustände. Durch neue rechtliche und wirtschaftliche Anforderungen ist dieses Vorgehen häufig nicht mehr ausreichend und neue Ansätze sind gefordert. Neue Bedürfnisse durch die Entwicklung des Energiemarktes machen eine automatisierte Bestimmung optimaler Netzentscheidungen notwendig.

In dieser Arbeit werden zwei Probleme der Gastransportplanung näher betrachtet. Bei der Nominierungsvalidierung wird eine zulässige Netzkonfiguration zu gegebenen Ein- und Ausspeisungen gesucht. Hierfür wird eine detaillierte Abbildung der physikalischen und technischen Eigenschaften in einem MINLP Modell vorgestellt. Um moderne NLP-Löser anwenden zu können, wird ein nichtlineares Modell mit reduziertem Detailgrad abgeleitet. Diskrete Entscheidungen werden mittels Komplementaritätsbedingungen abgebildet. Desweiteren wird ein nichtlineares Modell hoher Modellgenauigkeit vorgestellt, das gegebene diskrete Entscheidungen voraussetzt. Numerische Untersuchungen auf realistischen Gasnetzen zeigen die Praktikabilität verschiedener Regularisierungsansätze für die Komplementaritätsbedingungen und den Erfolg der beiden Modelle bei der Nominierungsvalidierung. Vergleiche mit kommerziellen Simulationsprogrammen bestätigen den hohen Detailgrad der Lösungen.

Der zweite Aspekt dieser Arbeit ist die Bestimmung technischer Kapazitäten von Gasnetzen. Anhand der rechtlichen Vorschriften wird ein gemischt-ganzzahliges, nichtlineares, anpassbar robustes Problem hergeleitet, wobei sich herausstellt, dass die rechtliche Vorgabe nicht zu einem wohldefinierten Problem führt. Eine mögliche Interpretation der Vorschriften führt zu einem Pareto-Optimum. Eine Analyse des Kapazitätsproblems zeigt, dass Monotonie und Konvexität im Allgemeinen nicht angenommen werden können. Auswirkungen werden anhand kleiner Beispielnetze erläutert.

Schlüsselworte: technische Kapazitäten von Gasnetzen, gemischt-ganzzahlige nichtlineare Optimierung, Komplementaritätsbedingungen, MPEC

Contents

Abstract	v
Zusammenfassung	vii
List of Figures	xiv
1. Introduction	1
2. Theoretical Basics	5
2.1. An Introduction to the Theory of NLPs	5
2.2. An Introduction to the Theory of MPECs	8
2.2.1. Definition of an MPEC	8
2.2.2. Constraint Qualifications for MPECs	9
2.2.3. Stationarity Concepts for MPECs	12
2.2.4. Solution Strategies for MPECs	13
3. Validation of Nominations	17
3.1. Graph Topology and Notation	20
3.2. A Nonsmooth MINLP Model with ODE Constraints	21
3.2.1. Component-Unspecific Aspects	22
3.2.2. Nodes and Arcs	24
3.2.3. Pipes	26
3.2.4. Resistors	32
3.2.5. Valves	33
3.2.6. Shortcuts	34
3.2.7. Control Valves	34
3.2.8. Compressor Groups	38
3.2.9. Variable Bounds	47
3.3. Handling Discrete Decisions by Complementarity Constraints	48
3.3.1. Nodes and Arcs	49

Contents

3.3.2.	Pipes	50
3.3.3.	Resistors	53
3.3.4.	Valves and Shortcuts	54
3.3.5.	Control Valves	55
3.3.6.	Compressor Groups	58
3.3.7.	Complete MPEC Model	58
3.3.8.	An Heuristic to Determine Active Configurations	59
3.4.	High Accuracy Optimization (ValNLP)	65
3.4.1.	Common Model Aspects	66
3.4.2.	Nodes and Arcs	67
3.4.3.	Pipes	69
3.4.4.	Resistors	75
3.4.5.	Valves and Shortcuts	76
3.4.6.	Control Valve Stations	76
3.4.7.	Compressor Groups	78
3.4.8.	A Concrete Validation Model	85
3.4.9.	Relaxations	87
4.	Numerical Experiments	91
4.1.	Solving Mixed-Integer Nonlinear Problems Directly	91
4.2.	Solving NoVa with the MPEC Approach	94
4.2.1.	Direct Approach	96
4.2.2.	Penalization Approach	100
4.2.3.	Relaxation Approach	104
4.2.4.	Further Approaches	111
4.2.5.	Conclusion	112
4.3.	Accuracy of the Validation NLP	116
4.3.1.	Pipes	117
4.3.2.	Resistors	121
4.3.3.	Control Valves with Remote Access	125
4.3.4.	Compressors	125
4.3.5.	Conclusion	129
5.	Technical Capacities of Gas Networks	131
5.1.	Problem Description	131
5.2.	Relation to Robust Optimization	134

5.3. Properties of Technical Capacities and the Set of Feasible Nominations . .	137
5.3.1. Existence and Uniqueness of Technical Capacities	138
5.3.2. Geometry of the Set of Feasible Nominations	140
5.4. Approaches	145
6. Conclusion	149
A. Appendix	153
A.1. Symbols of Network Elements	153
A.2. Physical Quantities	153
A.3. List of Used GasLib-582 Instances	155

List of Figures

2.1. Feasible set of the relaxation scheme	14
3.1. Comparison of friction models	28
3.2. Pressure and temperature profiles	32
3.3. Schematic control valve station	36
3.4. Configurations of a compressor group	39
3.5. Configuration with two serial stages of parallel units	39
3.6. Subgraph of a compressor group	40
3.7. Schematic turbo compressor	42
3.8. Examples of characteristic diagrams	43
3.9. Smooth approximation of the friction term	52
3.10. Smoothings of sign and the absolute value	53
3.11. Schematic idea of the compressor group heuristic	60
3.12. Models of gas temperature	72
3.13. Subgraph of a compressor group	79
4.1. Direct approach: successfully solved instances	96
4.2. Modified direct approach: successfully solved instances	99
4.3. Penalization approach: successfully solved instances	101
4.4. Alternative penalization approach: successfully solved instances	103
4.5. Relaxation approach: successfully solved instances	105
4.6. Symmetric relaxation: successfully solved instances	107
4.7. Alternative symmetric relaxation: successfully solved instances	109
4.8. Variable splitting: successfully solved instances	110
4.9. Alternative variable splitting: successfully solved instances	112
4.10. Overview per solver	115
4.11. Absolute deviations in pressure and temperature at pipes	119
4.12. Pressure profile of an exemplary pipe	120
4.13. Temperature profile of an exemplary pipe	120
4.14. Comparison of SIMONE versions	121

List of Figures

4.15. Temperature deviations of resistors with linear pressure loss model	123
4.16. Pressure deviations of resistors with nonlinear pressure loss model	123
4.17. Temperature deviations of resistors with nonlinear pressure loss model . .	124
4.18. Temperature deviations of control valves	126
4.19. Deviations of quantities of piston compressors	127
4.20. Deviations of quantities of turbo compressors	128
5.1. Flow sets concerning technical capacities	133
5.2. All network topologies up to a specific size	138
5.3. Single pipe a connecting entry u and exit v	138
5.4. Network with infinite possible technical capacities	139
5.5. Y-shaped network with entry u and exits μ and ν	141
5.6. Set of feasible flows of the Y-shaped network	141
5.7. Set of feasible flows of the Y-shaped network with nonlinear model	142
5.8. Y-shaped network with a compressor group	143
5.9. Nonconvex set of feasible nominations	143
5.10. Disconnected sets of feasible nominations	144
5.11. Consequence of infeasible instances	146

1. Introduction

Production and distribution of energy is one of the main problems of modern humanity. Besides crude oil and coal, natural gas is still one of the most important sources of primary energy. It is required for heating, power generation and industrial processes. However, the distribution of gas sources does usually not coincide with the main consumers. The total consumption of natural gas in the European Union amounts to $443.9 \times 10^9 \text{ m}^3$ but only $164.6 \times 10^9 \text{ m}^3$ are extracted within the EU. Germany alone consumes $75.2 \times 10^9 \text{ m}^3$ and covers only 12% by own extraction [21]. The main suppliers of Germany in 2013 were Russia (38.7%), Norway (29.4%), Netherlands (26.1%) and others, including Denmark and the United Kingdom (5.8%) [15]. Most of this gas is gained from gas fields in the North Sea and Siberia.

Normally, the location, where natural gas is extracted, is far away from the place, where the majority is consumed. Depending on the distance and target area, different means of transportation are possible. For distances above 2000 km or to reach isolated islands liquefied natural gas (LNG) carriers are the most economic choice. On the other side, tank trucks may be the only sensible choice to supply rural regions. Nevertheless, one of the most important ways to transport gas from its sources to consumers are gas transport networks. These technical facilities consist mainly of pipelines and pressure-regulating devices.

Natural gas is of increasing importance for the medium-term energy supply. The reduction of nuclear energy increases the demand for other energy sources. Natural gas is the fossil fuel with lowest carbon dioxide output, which helps to satisfy the self-appointed carbon dioxide limits in Europe until the energy output of regenerative energies has improved. New pipeline projects like Nord Stream, Nabucco and the Trans Adriatic Pipeline, as well as planned LNG capable ports underline the importance of natural gas. Furthermore, the existing infrastructure can be used by power-to-gas technologies. Here, excess power is transformed into fuel gas like hydrogen or methane that is then supplied into the gas transport network. By doing so the fluctuating output of regenerative fuels is balanced out.

1. Introduction

On the other hand, the foreseeable shortage of fossil fuel and increasing environmental concerns have strengthened the focus on an efficient operation of the transport systems. To gain an increase in efficiency, the European Union decided to liberalize the gas market. New legal regulations in course of the market liberalization put new requirements on the transport system operators. The unbundling of the gas market enforces the independence of the transport system operator from customers and traders.

Prior to the market restructuring, the network operator was also the gas trader. Often, they also possessed storage facilities and extraction sites. Network customers usually had no alternative when buying gas since the owner of the local transport network was also the responsible trader. Without market competition the gas companies had a price monopoly at their trading points. Covering the whole value chain was a big strategic and organizational advantage for the gas companies.

The unbundling process led to a separation of transport, trading and shipping to open the market and increase competition and transparency of transport. Network operators have the obligation to determine and offer the maximum possible capacities independent of predefined transport paths. To ensure security of supply all stakeholders are obliged to cooperate. Furthermore, network operators have to reinvest their revenues to eliminate network congestions and increase the maximum capacities. The legal requirements are laid down in the GasNZV [16].

In practice, a transport customer books capacity rights prior to the actual transport, usually some weeks to years in advance. The day before he supplies or discharges the gas, the customer nominates the actual amount he trades within the bounds he has booked. Usually, he can change his nomination up to two hours prior to the trade. This process has several challenges for the transporting company. First, he has to check whether the booking can be accepted. To this end a certain percentage of partial nominations has to be realizable to minimize the risk of contractual penalties on one hand and omitting improbable infeasible nominations on the other hand. In course of the booking validation and when the customer communicates his nomination the question for possible transport routes arises. If several possibilities exist, it is desirable to find the most efficient one. If however a booking must be declined, the network operator is obliged to check for reasonable network extensions to resolve the congestion.

The traditional work flow handling these problems typically incorporates one or several expert-generated nominations that are validated by a series of simulation runs until working network settings are determined.

Due to the increasing importance of natural gas along with enforced legal requirements current manual approaches are not sufficient anymore. The recent development of the gas market introduced new challenges. The unbundling results in a reduction of available information, the development of future demand is unknown, discrepancies between legal definitions and their practical realizations exists and the increasing importance strengthen the need for an efficient transport and maximum capacities. German network operators are now obliged by law to publish still available capacities of the network. New pipeline projects and changing consumption profiles require the extension of existing infrastructure, resulting in network topology problems. This thesis concentrates on two problem classes of gas transport networks and their formulation as a mathematical optimization problem, validation of nominations (NoVa) and the determination of technical capacities. The aim is to solve both problems by applying general-purpose nonlinear problem (NLP) solvers.

Transport networks span large distances in order to direct gas from the sources to customers and local distribution networks. They consist mainly of pipelines and connect places where gas is supplied into the network, so called entries, with places where gas is discharged, so called exits. Typical suppliers are gas fields and LNG capable ports, while typical recipients of gas are power plants, industrial customers, and connection points to local distribution networks. Some connection points may belong to either group, depending on the situation. Typical examples of these bidirectional places are storage facilities and network gateways, i.e. connection points to adjacent transport networks.

In general, gas flows from high pressure to low pressure. Thus, pressure regulating devices are required in the gas network to control the flow of the gas and to balance out the pressure loss caused inside the pipelines. The energy for the transport process can conveniently be taken from the network itself. Since this consumed energy reduces the amount of actually usable gas, it is an obvious demand to minimize its amount. Conversely, gas transport networks are a critical factor for the society and any interruption is not justifiable. Thus, the gas transport has to be modeled highly accurate to prevent misconfigurations and a stop in support.

Subsequent to this introduction to gas networks, an overview of the basic theory of nonlinear optimization and mathematical programs with equilibrium constraints (MPEC) is given. Both classes will be used in the third chapter to describe a solution approach for the NoVa problem. The approach is based on a solution framework developed in course of the research project ForNe [71], in which the Zuse-Institute Berlin, Technische Universität Darmstadt, Friedrich-Alexander-Universität Erlangen-Nürnberg, Leibniz Universität Hannover, Universität Duisburg-Essen, Humboldt-Universität zu Berlin, and

1. Introduction

Weierstrass Institute for Applied Analysis and Stochastics cooperate with Open Grid Europe to find optimal solutions to the upper problem classes. A mixed-integer nonlinear model of physical and technical properties of gas networks is first described. Afterwards an MPEC is derived from this model and discrete model aspects are reformulated using complementarity constraints. In Section 3.4 an NLP model is described with variants for several model aspects, making it customizable for different problem requirements.

In Chapter 4 numerical experiments based on the public gas library GasLib [56] prove the applicability of the MPEC approach on realistic nominations and network sizes. A large-scale analysis of network elements also shows the comparability of variants of the NLP model with current commercial simulation packages.

Technical capacities are the subject of Chapter 5. A problem description is derived from the legal regulations and the relation to robust optimization is explained. Deficiencies in the legal definitions and possible interpretations are illustrated. Properties of technical capacities and related sets are examined and minimal network examples illustrate the findings. A short outlook on possible solution strategies and their pitfalls is finally given. Chapter 6 summarizes the results of this thesis and offers some ideas for future research.

For a better readability, notation is kept consistent throughout this thesis. Constraints are denoted by c , a constraint indexed by a set represents the vector of constraints with an index of the index set, e.g., $c_{\mathcal{E}}$ is equivalent to the vector $(c_i)_{i \in \mathcal{E}}$. Continuous variables are usually denoted by x and z represents a discrete variable. If vectors are compared by relations like $=$, \geq or $>$, the relation is defined component-wise, i.e. $c_{\mathcal{I}}(x) \geq 0$ means $c_i(x) \geq 0$ for all $i \in \mathcal{I}$. Upper and lower bounds of a variable x are denoted by x^- and x^+ . Notation specific to gas networks will be discussed in Section 3.1.

Parts of Section 3.3, Section 3.4 and Chapter 4 have been published in [54, 114] or will be published in [71, 104] together with the results of the project ForNe.

This work has been supported by the German Federal Ministry of Economics and Technology owing to a decision of the German Bundestag.

2. Theoretical Basics

2.1. An Introduction to the Theory of Nonlinear Programs

Nonlinear programs (NLP) model optimization tasks where the objective function and constraints may be described by nonlinear functions. A typical field of application is engineering, where the fundamental physics is often highly nonlinear.

The aim of a nonlinear program is to find values of a variable vector $x \in \mathbb{R}^n$ that minimizes an objective function f . In addition, the solution has to satisfy a set of equality constraints $c_{\mathcal{E}}(x) = 0$, and a set of inequality constraints $c_{\mathcal{I}}(x) \geq 0$. \mathcal{E} denotes the finite index set of the equality constraints and \mathcal{I} is the finite index set of the inequality constraints. Both index sets are disjoint. The notation and structure of this section is based on [94].

Generally, nonlinear programs can be formulated as

$$\min_{x \in \mathbb{R}^n} f(x) \tag{2.1a}$$

$$\text{s.t. } c_{\mathcal{E}}(x) = 0, \tag{2.1b}$$

$$c_{\mathcal{I}}(x) \geq 0, \tag{2.1c}$$

$$x \in [x^-, x^+]. \tag{2.1d}$$

The objective function $f : \mathbb{R}^n \rightarrow \mathbb{R}$ and the constraints $c_i : \mathbb{R}^n \rightarrow \mathbb{R}$ have to be smooth, i.e. twice continuously differentiable.

Definition 1 (Feasible point). *A variable vector $x^* \in \mathbb{R}^n$ is called feasible, when it satisfies all equality and inequality constraints, i.e.*

$$c_{\mathcal{E}}(x^*) = 0, \quad c_{\mathcal{I}}(x^*) \geq 0.$$

Thus, the set of feasible points is defined as

$$\mathcal{F} = \{x \in \mathbb{R}^n : c_{\mathcal{E}}(x) = 0, c_{\mathcal{I}}(x) \geq 0\}.$$

2. Theoretical Basics

Since the desired solution of the nonlinear program (2.1) needs to fulfill all constraints, it is part of the feasible set \mathcal{F} .

Definition 2 (Active set). *Let $x^* \in \mathbb{R}^n$ be a feasible point of the NLP (2.1). A constraint c_i , $i \in \mathcal{E} \cup \mathcal{I}$, is called active, if $c_i(x^*) = 0$. The set of active constraints $\mathcal{A}(x^*)$ is defined by*

$$\mathcal{A}(x^*) = \mathcal{E} \cup \{i \in \mathcal{I} : c_i(x^*) = 0\}.$$

Note that equality constraints are always active at a feasible point. Inequality constraints, which are not active, are called inactive.

Definition 3 (Local solution). *Let $x^* \in \mathbb{R}^n$ be a feasible point of the NLP (2.1). x^* is called a local solution of the NLP (2.1), if there exists a neighborhood \mathcal{N} of x^* , such that*

$$f(x^*) \leq f(x) \quad \text{for all } x \in \mathcal{N} \cap \mathcal{F}.$$

The feasible set may contain several local solutions. In contrast to convex and linear optimization, a local solution is not automatically a feasible point with the overall best value of the objective function, i.e. a global solution, but for many applications a local solution is sufficient. In the following, first order necessary conditions of local solutions, the so-called Karush-Kuhn-Tucker (KKT) conditions, are described. For the KKT conditions to hold at a minimizer, the constraints must fulfill a constraint qualification. For details see [57, 94]. Two constraint qualifications are stated here, which guarantee the required properties at a given feasible point.

Definition 4 (LICQ). *Let $x^* \in \mathbb{R}^n$ be a feasible point of the NLP (2.1) and let $\mathcal{A}(x^*)$ be the according active set. The linear independence constraint qualification (LICQ) holds at x^* , if the set of gradients*

$$\{\nabla c_i(x^*) : i \in \mathcal{A}(x^*)\}$$

is linearly independent.

Definition 5 (MFCQ). *Let $x^* \in \mathbb{R}^n$ be a feasible point of the NLP (2.1). The Mangasarian–Fromovitz constraint qualification (MFCQ) holds at x^* , if there is a vector $d \in \mathbb{R}^n$ satisfying*

$$\begin{aligned} \nabla c_i(x^*)^T d &> 0 \quad \text{for all } i \in \mathcal{A}(x^*) \cap \mathcal{I}, \\ \nabla c_i(x^*)^T d &= 0 \quad \text{for all } i \in \mathcal{E}, \end{aligned}$$

and if the set $\{\nabla c_i(x^) : i \in \mathcal{E}\}$ is linearly independent.*

Theorem 1. *LICQ implies MFCQ.*

Proof. Since LICQ holds, all constraint gradients are linearly independent, in particular the subset $\{\nabla c_i(x^*) : i \in \mathcal{E}\}$. Due to the linear independence, the matrix

$$M = \begin{pmatrix} \nabla c_i(x^*)^T \\ \nabla c_j(x^*)^T \end{pmatrix}_{i \in \mathcal{A}(x^*) \cap \mathcal{I}, j \in \mathcal{E}}$$

has full rank. Thus, for every $b \in \mathbb{R}^{|\mathcal{A}(x^*)|}$ there exists a vector $d \in \mathbb{R}^n$ such that

$$Md = b.$$

Choose the first $|\mathcal{A}(x^*) \cap \mathcal{I}|$ entries of b as 1 and the others as 0. Then a $d \in \mathbb{R}^n$ exists satisfying $Md = b$, i.e.

$$\begin{aligned} \nabla c_i(x^*)^T d &= 1 > 0 && \text{for all } i \in \mathcal{A}(x^*) \cap \mathcal{I}, \\ \nabla c_i(x^*)^T d &= 0 && \text{for all } i \in \mathcal{E}, \end{aligned}$$

so MFCQ holds. □

MFCQ is weaker than LICQ, i.e. the reverse direction of Theorem 1 does not hold. For a detailed analysis of the differences see Henrion [61].

The stationarity concept which is used in the KKT condition is based on the Lagrangian function

$$\mathcal{L}(x, \lambda) = f(x) - \sum_{i \in \mathcal{E} \cup \mathcal{I}} \lambda_i c_i(x).$$

The entries of the variable vector λ are called the Lagrangian multipliers or dual variables.

Definition 6 (KKT-stationarity). *A feasible point x^* is called KKT-stationary, if there exists a Lagrangian multiplier λ^* , so that the KKT-conditions*

$$\nabla_x \mathcal{L}(x^*, \lambda^*) = 0, \tag{2.2a}$$

$$c_{\mathcal{E}}(x^*) = 0, \tag{2.2b}$$

$$c_{\mathcal{I}}(x^*) \geq 0, \tag{2.2c}$$

$$\lambda_{\mathcal{I}}^* \geq 0, \tag{2.2d}$$

$$c_{\mathcal{I}}(x^*)^T \lambda_{\mathcal{I}}^* = 0, \tag{2.2e}$$

2. Theoretical Basics

are satisfied.

The conditions (2.2b) and (2.2c) ensure primal feasibility. Since x^* is feasible, these are automatically satisfied. Condition (2.2d) is the dual feasibility. The last condition is the complementarity condition, which states that c_i , $i \in \mathcal{I}$, is active or $\lambda_i = 0$ holds for the corresponding multiplier. Based on this stationarity concept first order necessary conditions are now stated.

Theorem 2 (First order necessary conditions based on MFCQ). *Let $x^* \in \mathbb{R}^n$ be a local solution of the NLP (2.1) and assume that MFCQ holds at x^* . Then there exists a bounded set of dual variables λ^* , so that x^* is KKT-stationary.*

A proof is given in [57].

Theorem 3 (First order necessary conditions based on LICQ). *Let x^* be a local solution of (2.1) and assume that LICQ holds at x^* . Then there exist unique dual variables λ^* , so that x^* is KKT-stationary.*

Proof. Since LICQ implies MFCQ, the KKT-stationarity follows directly from Theorem 2. Condition (2.2e) implies $\lambda_i = 0$ for $i \notin \mathcal{A}(x^*)$. From condition (2.2a) and the definition of LICQ follows the uniqueness of $\lambda_{\mathcal{A}(x^*)}$. \square

2.2. An Introduction to the Theory of Mathematical Programs with Equilibrium Constraints

2.2.1. Definition of an MPEC

Mathematical programs with equilibrium constraints (MPEC) have been an important topic of research in the recent decades. They are strongly related to the problem of Stackelberg game and bilevel programming [79]. MPEC formulations are also applied to a large number of problems in economics and industry like spot market models [70, 125], robotics [101, 102], and chemical engineering [6]. For a large number of examples see the survey of Ferris and Pang [40].

In the following, we concentrate on MPECs of the form

$$\min_{x \in \mathbb{R}^n} f(x) \quad (2.3a)$$

$$\text{s.t. } c_{\mathcal{E}}(x) = 0, \quad (2.3b)$$

$$c_{\mathcal{I}}(x) \geq 0, \quad (2.3c)$$

$$0 \leq \phi(x) \perp \psi(x) \geq 0. \quad (2.3d)$$

Equation (2.3d) states, that the two functions $\phi : \mathbb{R}^n \rightarrow \mathbb{R}^{|\mathcal{C}|}$ and $\psi : \mathbb{R}^n \rightarrow \mathbb{R}^{|\mathcal{C}|}$ are disjunctive, i.e. $\phi(x)^T \psi(x) = 0$. \mathcal{C} denotes the index set of the disjunctive functions. Equivalent formulations of this complementary are

$$\phi(x) \geq 0, \quad \psi(x) \geq 0, \quad \phi(x)^T \psi(x) = 0, \quad (2.4)$$

$$\phi(x)_i \geq 0, \quad \psi(x)_i \geq 0, \quad \phi(x)_i \psi(x)_i = 0 \quad \text{for all } i \in \mathcal{C}, \quad (2.5)$$

$$\min(\phi(x)_i, \psi(x)_i) = 0 \quad \text{for all } i \in \mathcal{C}. \quad (2.6)$$

The notation and structure of this section is based on [94] and [111].

By applying the reformulation (2.4) or (2.5), the MPEC (2.3) is in accordance with (2.1), thus it is an NLP.

2.2.2. Constraint Qualifications for MPECs

Despite the fact that MPECs of type (2.3) can be formulated as NLPs by applying (2.4), many results of NLP theory cannot be applied directly. A central difficulty of MPECs is that many common constraint qualifications do not hold at any feasible point. The proof of the following theorem is based on [47].

Theorem 4. *At every feasible point $x^* \in \mathbb{R}^n$ of (2.3) MFCQ is violated.*

Proof. Let $c_{\perp}(x) = \phi(x)^T \psi(x)$ denote the complementarity constraint and let x^* be a feasible point of (2.3). Define the index sets

$$\mathcal{A}_{\phi} = \{i \in \mathcal{C} : \phi_i(x^*) = 0\},$$

$$\mathcal{A}_{\psi} = \{i \in \mathcal{C} : \psi_i(x^*) = 0\},$$

$$\mathcal{A}_{\phi\psi} = \mathcal{A}_{\phi} \cap \mathcal{A}_{\psi}.$$

2. Theoretical Basics

As a consequence $\mathcal{C} = \mathcal{A}_\phi \cup \mathcal{A}_\psi$ is true. Assume that MFCQ holds for the MPEC in x^* . If $\mathcal{A}_{\phi\psi} = \mathcal{C}$, it follows that

$$\nabla c_\perp(x^*) = \sum_{i \in \mathcal{C}} (\phi_i(x^*) \nabla \psi_i(x^*) + \psi_i(x^*) \nabla \phi_i(x^*)) = 0,$$

since $\phi_i(x^*) = \psi_i(x^*) = 0$ for all $i \in \mathcal{C}$.

By this, $\nabla c_\perp(x^*)$ is not linearly independent to the other constraint gradients, which contradicts the requirement of MFCQ, that the gradients of the active constraints need to be linearly independent, see Definition 5.

If $\mathcal{C} \setminus \mathcal{A}_{\phi\psi} \neq \emptyset$, then

$$\begin{aligned} \nabla c_\perp(x^*)^T d &= d^T \left(\sum_{i \in \mathcal{C}} (\phi_i(x^*) \nabla \psi_i(x^*) + \psi_i(x^*) \nabla \phi_i(x^*)) \right) \\ &= \sum_{i \in \mathcal{A}_\psi \setminus \mathcal{A}_\phi} \phi_i(x^*) \nabla \psi_i(x^*)^T d + \sum_{i \in \mathcal{A}_\phi \setminus \mathcal{A}_\psi} \psi_i(x^*) \nabla \phi_i(x^*)^T d > 0 \end{aligned}$$

holds, since

$$\begin{aligned} \phi_i(x^*), \nabla \psi_i(x^*)^T d &> 0 \quad \text{for all } i \in \mathcal{A}_\psi \setminus \mathcal{A}_\phi, \\ \psi_i(x^*), \nabla \phi_i(x^*)^T d &> 0 \quad \text{for all } i \in \mathcal{A}_\phi \setminus \mathcal{A}_\psi, \end{aligned}$$

due to MFCQ. This contradicts the condition $\nabla c_\perp(x^*)^T d = 0$ of MFCQ. \square

Lemma 1. *LICQ is violated at every feasible point $x^* \in \mathbb{R}^n$ of the MPEC.*

Proof. This follows directly from Theorem 4 and Theorem 1. \square

Since LICQ, MFCQ and further standard constraint qualifications do not hold at any feasible point in case of MPECs [48], the central stationarity and optimality results of NLPs cannot be applied to MPECs. In particular, the Karush-Kuhn-Tucker theorems 2 and 3 do not hold, which are a core element of most NLP algorithms. As a result, new MPEC-specific constraint qualifications are developed, under which a minimizer of the MPEC satisfies some kind of stationarity concept, see [47, 67, 79, 100, 111, 125].

Let $x^* \in \mathbb{R}^n$ be a feasible point of 2.3. The NLP

$$\begin{aligned}
 & \min_{x \in \mathbb{R}^n} f(x) \\
 & \text{s.t. } c_{\mathcal{E}}(x) = 0, \\
 & \quad c_{\mathcal{I}}(x) \geq 0, \\
 & \quad \phi_{\mathcal{A}_{\phi}}(x) = 0, \quad \phi_{\mathcal{A}_{\psi} \setminus \mathcal{A}_{\phi}}(x) \geq 0, \\
 & \quad \psi_{\mathcal{A}_{\psi}}(x) = 0, \quad \psi_{\mathcal{A}_{\phi} \setminus \mathcal{A}_{\psi}}(x) \geq 0,
 \end{aligned} \tag{TNLP}(x^*)$$

is called the tightened NLP in x^* (TNLP(x^*)). Based on the TNLP, Scheel and Scholtes [111] define the constraint qualifications MPEC-LICQ and MPEC-MFCQ.

Definition 7 (MPEC-MFCQ, MPEC-LICQ). *Let $x^* \in \mathbb{R}^n$ be a feasible point of the MPEC (2.3). The MPEC satisfies MPEC-LICQ (MPEC-MFCQ) in x^* , if TNLP(x^*) satisfies LICQ (MFCQ) in x^* .*

Alternatively, these constraint qualifications can be defined by using the relaxed NLP (RNLP(x^*)) at a feasible point x^* ,

$$\begin{aligned}
 & \min_{x \in \mathbb{R}^n} f(x) \\
 & \text{s.t. } c_{\mathcal{E}}(x) = 0, \\
 & \quad c_{\mathcal{I}}(x) \geq 0, \\
 & \quad \phi_{\mathcal{A}_{\phi} \setminus \mathcal{A}_{\psi}}(x) = 0, \quad \phi_{\mathcal{A}_{\psi}}(x) \geq 0, \\
 & \quad \psi_{\mathcal{A}_{\psi} \setminus \mathcal{A}_{\phi}}(x) = 0, \quad \psi_{\mathcal{A}_{\phi}}(x) \geq 0.
 \end{aligned} \tag{RNLP}(x^*)$$

The only difference to TNLP(x^*) lies in the handling of the biactive complementarity constraints, i.e. those with an index in the set $\mathcal{A}_{\phi\psi}(x^*)$.

Lemma 2. *The RNLP(x^*) satisfies LICQ(MFCQ) in x^* , if and only if TNLP(x^*) satisfies LICQ(MFCQ) in x^* .*

Proof. The set of active constraints in x^* is identical for RNLP(x^*) and TNLP(x^*). \square

Besides the MPEC-LICQ and MPEC-MFCQ, several other constraint qualifications are examined in the context of MPECs, e.g. the Abadie constraint qualification, resulting in MPEC-ACQ [48], and the Guignard constraint qualification (GCQ) [50]. An overview of the relations of many constraint qualifications are given in [139]. Together with the

2. Theoretical Basics

MPEC-specific constraint qualifications, stationarity concepts are in the focus of recent research.

2.2.3. Stationarity Concepts for MPECs

Associate with an MPEC the Lagrangian function of (2.3) without the complementarity constraints, i.e.

$$\mathcal{L}(x, \lambda_{\mathcal{E}}, \lambda_{\mathcal{I}}, \lambda_{\phi}, \lambda_{\psi}) = f(x) - \lambda_{\mathcal{E}}^T c_{\mathcal{E}}(x) - \lambda_{\mathcal{I}}^T c_{\mathcal{I}}(x) - \lambda_{\phi}^T \phi(x) - \lambda_{\psi}^T \psi(x).$$

This resembles the Lagrangian function of TNLP(x^*) and RNLP(x^*) for any feasible x^* .

Definition 8 (B-stationary). *Let $x^* \in \mathbb{R}^n$ be a feasible point of (2.3). It is called Bouligand-stationary (B-stationary), if it is a local minimizer of the linearized MPEC, i.e. $\nabla f(x^*)^T d \geq 0$ for all d :*

$$\begin{aligned} \nabla c_i(x^*)^T d &\geq 0 && \text{for all } i \in \mathcal{A}(x^*) \cap \mathcal{I} \\ \nabla c_i(x^*)^T d &= 0 && \text{for all } i \in \mathcal{E} \\ \nabla \phi_i(x^*)^T d &= 0 && \text{for all } i \in \mathcal{A}_{\phi} \setminus \mathcal{A}_{\psi} \\ \nabla \phi_i(x^*)^T d &= 0 && \text{for all } i \in \mathcal{A}_{\psi} \setminus \mathcal{A}_{\phi} \\ \min\{\nabla \phi_i(x^*)^T d, \nabla \psi_i(x^*)^T d\} &= 0 && \text{for all } i \in \mathcal{A}_{\phi\psi}. \end{aligned}$$

Definition 9 (W-stationarity). *Be $x^* \in \mathbb{R}^n$ a feasible point of the MPEC (2.3). It is called weakly stationary (W-stationary), if it is a KKT-stationary point of TNLP(x^*).*

Definition 10 (S-stationarity). *Be $x^* \in \mathbb{R}^n$ a feasible point of the MPEC (2.3). It is called strongly stationary (S-stationary), if it is a KKT-stationary point of RNLP(x^*).*

Definition 11 (C-stationarity). *Be $x^* \in \mathbb{R}^n$ a feasible point of the MPEC (2.3). It is called Clarke stationary (C-stationary), if it is weakly stationary and in addition $\lambda_{\phi,i} \lambda_{\psi,i} = 0$ for all $i \in \mathcal{A}_{\phi\psi}$.*

For a detailed analysis of these stationarity concepts and their relations see [111]. Further stationarity concepts have been discussed in the literature, like M-stationarity [49, 51, 100, 139] and A-stationarity [47, 50]. Based on these stationarity concepts and constraint qualifications, first order necessary conditions for MPECs are deduced.

Lemma 3. *Let $x^* \in \mathbb{R}^n$ be a local minimizer of the MPEC (2.3) and assume that MPEC-MFCQ holds in x^* . Then x^* is C-stationary and W-stationary.*

A proof is given in [111]. For further first order necessary conditions see [47, 111, 139].

2.2.4. Solution Strategies for MPECs

For nonlinear programs, a large number of field-tested and successful algorithms have been developed in the recent decades. However, most of them require LICQ or MFCQ to hold for the problem to solve. Since this is not the case for MPECs at any feasible point, these algorithms do not necessarily converge to a (local) minimum, so different solution approaches are required. Mainly, two different groups of strategies exist currently for solving MPECs.

The first group of approaches suggests new algorithms based on stationarity concepts mentioned above or similar ones. Partly these algorithms require a specific form of the MPEC, as the trust region methods suggested in [98, 99]. For general MPECs, sequential methods solving a series of partly linearized problems were suggested by Stöhr [124], and Leyffer and Munson [77].

The second group acts on the assumption that an NLP solver is available. The common idea is to replace the MPEC by an parameterized nonlinear problem $\text{NLP}(\xi)$. By this, the NLP solver can be applied directly or with minor modifications. These so-called regularization schemes usually solve a sequence $\text{NLP}(\xi_k)$, $\xi_k \rightarrow 0$, with the aim that the solutions of the sequence converge to a solution of the original MPEC. Three groups of these regularization schemes are mainly used: penalization, relaxation and smoothing.

The penalization approach removes the complementarity constraint from the model and penalizes its violation in the objective function. This results in the NLP

$$\min_{x \in \mathbb{R}^n} f(x) + \frac{1}{\xi} \Pi(\phi(x), \psi(x)) \quad (2.9a)$$

$$\text{s.t. } c_{\mathcal{E}}(x) = 0, \quad c_{\mathcal{I}}(x) \geq 0, \quad (2.9b)$$

$$\phi(x) \geq 0, \quad \psi(x) \geq 0, \quad (2.9c)$$

with a twice continuously differentiable penalization function Π ,

$$\Pi(\phi(x), \psi(x)) = 0 \iff \phi(x) = 0 \text{ or } \psi(x) = 0.$$

2. Theoretical Basics

The intuitive candidate $\Pi(\phi(x), \psi(x)) = \phi(x)^T \psi(x)$ was successfully applied by Tin-Loi [41, 42, 130]. A detailed examination of the general case (2.9) by Hu and Ralph [63] shows, that the sequence of stationary points $x^*(\xi_k)$ of $\text{NLP}(\xi_k)$, $\xi_k \rightarrow 0$, converges to a C-stationary point x^* of the original MPEC under MPEC-LICQ. Under additional conditions B-stationarity is shown.

Scholtes proposed in [117] the relaxation scheme based on the relaxation of the complementarity function:

$$\min_{x \in \mathbb{R}^n} f(x) \quad (2.10a)$$

$$\text{s.t.} \quad c_{\mathcal{E}}(x) = 0, \quad c_{\mathcal{I}}(x) \geq 0, \quad (2.10b)$$

$$\phi(x) \geq 0, \quad \psi(x) \geq 0, \quad (2.10c)$$

$$\phi(x)_i \psi(x)_i \leq \xi, \quad i \in \mathcal{C}. \quad (2.10d)$$

By this modification, the feasible set of the complementarity constraint is not restricted to the lines $\phi(x) = 0$ and $\psi(x) = 0$, but has now an interior, see Figure 2.1 for an illustration.

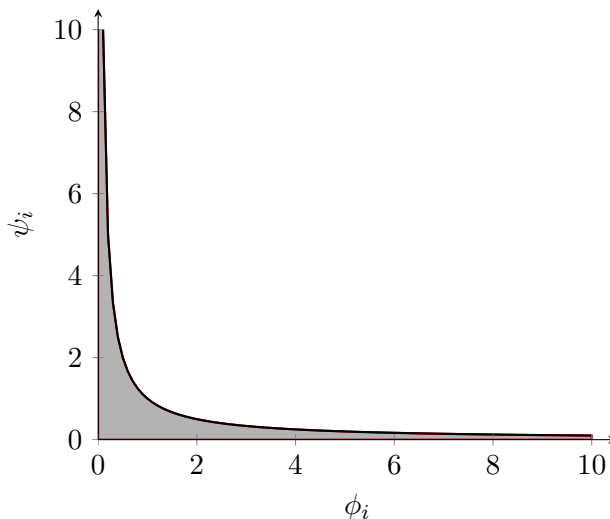


Figure 2.1. Feasible set of the relaxation scheme in the ϕ_i - ψ_i -plane, $\xi = 1$

Scholtes [117] was able to show, that if the sequence of feasible points $x^*(\xi)$ of $\text{NLP}(\xi)$ converges and MPEC-LICQ holds in the limit x^* , then x^* is C-stationary. Under additional assumptions the limit x^* is B-stationary.

DeMiguel et al. [28] extend this scheme by relaxing (2.10c) to

$$\phi(x), \psi(x) \geq -\theta, \quad \text{with } \theta \geq 0.$$

Here, either ξ or θ is driven to zero. By this, the feasible set has a nonempty interior even in the limit. Under certain assumptions, S-stationarity can be shown for this scheme, see [28].

The third group of approaches, called smoothing approaches, replaces the complementarity constraint by a smoothed NCP-function.

Definition 12 (NCP-function). *A function $F : \mathbb{R}^2 \rightarrow \mathbb{R}$ is called NCP-function, if*

$$F(x, y) = 0 \iff x, y \geq 0, \quad xy = 0.$$

These functions originate from the analysis of nonlinear complementarity problems (NCP) [22, 24, 68, 126], which are a specialization of the complementarity constraint (2.4). Two popular NCP-functions are the Fischer-Burmeister function [45]

$$F^{\text{FB}}(x, y) = x + y - \sqrt{x^2 + y^2},$$

and the minimum function

$$F^{\text{min}}(x, y) = \min(x, y) = \frac{1}{2} \left(x + y - \sqrt{(x - y)^2} \right).$$

Both functions are not twice continuously differentiable in the origin, thus cannot replace the complementarity constraints directly, when an NLP is desired. Nevertheless, both functions can be smoothed by

$$F^{\text{FB-s}}(x, y, \xi) = x + y - \sqrt{x^2 + y^2 + \xi}, \quad (2.11)$$

$$F^{\text{min-s}}(x, y, \xi) = \frac{1}{2} \left(x + y - \sqrt{(x - y)^2 + \xi} \right), \quad (2.12)$$

or a similar smoothing. Leyffer [75] has shown strong stationarity for the smoothed Fischer-Burmeister function.

All regularization schemes need to drive a parameter ξ to zero for gaining a solution of the original MPEC. Typically, the stationarity proofs assume a series of NLP(ξ_k) with $\xi_k \rightarrow 0$, where for each ξ_k an NLP is solved. Every single NLP has to be solved to optimality for convergence of the algorithm. In addition, solving several nonlinear problems may be very

2. Theoretical Basics

time-consuming. Therefore, different approaches have been suggested, e.g. controlling ξ between the iterations of an interior point method (IPM), see [76, 113], or sequential quadratic programming (SQP) framework, see [75]. A different idea is to handle the parameter ξ as a variable and reduce it by a suitable constraint, e.g.

$$e^\xi - 1 = 0, \tag{2.13}$$

assuming a positive initial value [66]. Another way of reducing ξ without solving a sequence of NLPs is to minimize the parameter in the objective function [4].

3. Validation of Nominations

When a customer of a gas network is going to supply or discharge gas, he contacts the network operator and nominates the required amounts. The operator ensures, that the planned transactions are within the bounds of the contract with the customer and that the combined transport situation considering all customers is realizable. To check this, the operator collects information about the balanced demands of his customers at the entries and exits, the contractual pressure bounds of the network and the supplied gas composition at each entry. The validation of nominations (NoVa) verifies whether this nomination is realizable or not.

The validation of nominations is an important problem of mid-term planning of gas networks and it is a core aspect of several other problems, like booking validation or the determination of technical capacities. The current state-of-the-art to validate a nomination is based on repetitive simulation of a stationary, i.e. time-independent, network model. A specialist with profound knowledge of the transport network decides the settings of all controllable network elements and checks his decision with a simulation of the network. If this check turns out successful, the nomination is validated. Otherwise other settings are tested until the nomination is validated or no feasible setting has been found after several tries and the nomination is finally rejected.

Simulating gas networks has a long history and highly accurate models exist for several decades. Transient simulation models of long pipelines including partial differential systems and isothermal ideal gas were already formulated in the 1960s and 1970s [129, 135]. Single effects like temperature dynamics [69, 133] or supercompressibility [2, 74, 103, 122] were researched and found their way into simulation models. For an overview of the simulation models of this time see Fincham and Goldwater [43]. Detailed models for other network elements like compressor groups were also developed [72]. A detailed overview of network elements and model alternatives is given in [85] and [97]. These results lead to highly detailed, non-isothermal simulation of gas networks and tracking of gas composition [14, 112, 140]. The simulation models were also extended to special situations like ruptures [46].

3. Validation of Nominations

While simulation models are well developed and are applicable even for large networks, the described process to validate a nomination is highly tedious and a feasible setting may be missed. Hence, validation of nominations can strongly profit from mathematical optimization. The optimization of gas networks is young compared to simulation approaches. Suggestions for stationary [64] and transient [65, 132] optimization models and procedures were derived from the experiences of the simulation models. These attempts still based on predefined decisions of the active elements. Later studies developed heuristics and nonlinear mixed-integer models of compressor groups for given flow and pressure situations [19, 96, 136]. These works often based on linear pressure change and simplified models of the power consumption and specific change in adiabatic enthalpy. Further works study discontinuities of gas network optimization models [20] and more sophisticated models of compressors [12, 95, 138].

Later, the results were combined and first attempts were started to handle nonlinearities and discrete decisions of stationary models. The resulting MINLP models proved to be intractable by current optimization algorithms [30]. Two groups of approaches emerged, both try to circumvent the weaknesses of general purpose MINLP solvers.

The first type of approaches focuses on a linearization of the nonlinear aspects, leading to a mixed-integer linear problem (MILP) [27, 58, 60, 83, 84, 87, 105, 118, 119]. The results are extended on transient models [82, 90]. The second type of approaches introduces two steps. The discrete aspects are decided by a coarse MILP model and are fixed in a subsequent, purely nonlinear model [10, 11, 107, 108, 131, 137]. Again, some results are developed for transient models [37, 38, 123]. Domschke et al. [30] offer a comparison of both groups.

In both approaches the pressure loss on pipes is mostly based on a quadratic approximation, only a few publications consider discretizations of ordinary differential equations of the gas dynamics [37, 38, 123]. The considered networks typically have a lower double-digit number of network elements. The aim of this work is to solve large gas distribution network of real-world size with a detailed model of the physical phenomena and technical devices. To this end, Section 3.1 introduces a graph notation for gas transport networks. Based on this notation a nonsmooth stationary MINLP model with differential algebraic equations (DAE) as constraints is described in Section 3.2. The work is based on recent results developed in the project ForNe [54, 71, 81, 104, 115, 116]. This optimization problem is too complex to be solved by current optimization software. Even an MINLP model of a realistic network with approximated differential equations, constant temperature and

gas quality parameters cannot be solved by general-purpose MINLP solvers at the time [104].

To be able to validate nominations on real-world networks anyway, the subsequent sections present a new two-step approach based on the detailed MINLP model. The two-step framework was developed in the project ForNe in cooperation with the workgroups of M. Grötschel (Zuse-Institute Berlin), M. Pfetsch (Technische Universität Darmstadt), A. Martin (Friedrich-Alexander-Universität Erlangen-Nürnberg), R. Schultz (Universität Duisburg-Essen), W. Römisches (Humboldt-Universität zu Berlin), and R. Henrion (Weierstrass Institute for Applied Analysis and Stochastics). In the first step, discrete decisions of active network elements are determined and a solution of the network situation is gained. The solution is verified in the second step by a highly accurate NLP, resulting in a more detailed solution. For details, including several alternatives for the first step, see [71].

Section 3.3 describes a heuristic to decide the states of active elements, like valves, control valves and compressor groups, and the active configurations of compressor groups in the first step. This approach is based on a nonlinear model of the main aspects of a gas network derived from the model described in Section 3.2. The discrete states of the active network elements are modeled by complementarity constraints

$$\chi_1(x)^T \chi_2(x) = 0, \quad \chi_1(x), \chi_2(x) \geq 0.$$

This results in a mathematical program with equilibrium constraints (MPEC). By applying several smoothing techniques, approximations and regularization schemes, the MPEC model is further reformulated into a nonlinear problem, which can be solved by general-purpose NLP solvers.

The central aim of this MPEC approach is to find reliable solutions fast. It can be applied as an initial heuristic in a MIP or MINLP framework, or it can be used as a stand-alone solution approach.

In the second step, the solution of the MPEC approach is validated by an NLP (ValNLP), which is introduced in Section 3.4. The ValNLP model is closely related to the descriptions in Section 3.2 resulting in a highly detailed model. The states of the active elements and the flow directions on the arcs are adopted from the solution of the MPEC approach, thus the discrete decisions are eliminated. The initial values for the ValNLP are extrapolated from the solution of the MPEC approach. The resulting nonlinear problem is suited

3. Validation of Nominations

for standard NLP solvers. By including multiple choices for several model aspects, the ValNLP offers an adjustable trade-off between solution accuracy and solving time.

3.1. Graph Topology and Notation

The topology of transport networks offers an immanent structure which is a great starting point for a mathematical model. A natural way to use this problem topology is to model the network as a directed graph $\mathbb{G} = (\mathbb{V}, \mathbb{A})$. In gas transport networks the set of vertices \mathbb{V} includes entries \mathbb{V}_+ , exits \mathbb{V}_- and junctions \mathbb{V}_0 . Entries are also known as sources and describe places where gas is supplied into the network. Exits, also known as sinks, are locations, where gas is discharged from the network. Vertices, where no gas exchange takes place, are represented by junctions. Entries and exits are summarized as boundary nodes \mathbb{V}° , since they are the connection points to industrial customers, storage facilities and other transport networks.

Each arc $a = (u, v)$ in the set of arcs \mathbb{A} connects its tail u with its head v . The set of arcs can be separated into pipes \mathbb{A}_{pi} , compressor groups \mathbb{A}_{cg} , valves \mathbb{A}_{vl} , control valves \mathbb{A}_{cv} , resistors \mathbb{A}_{re} and shortcuts \mathbb{A}_{sc} .

Based on the graph topology, a node u may be the head of one or several arcs, so-called inlet arcs of u ,

$$\delta_u^- = \{a \in \mathbb{A} : a = (v, u)\},$$

and it may be the tail of other arcs, so-called outlet arcs of u ,

$$\delta_u^+ = \{a \in \mathbb{A} : a = (u, v)\}.$$

The set of all incident arcs is δ_u . The degree of a node is the combined number of inlet and outlet arcs. Note, that a node with degree one is typically a boundary node.

The models of the next sections make strong use of the graph topology. Variables and constraints belonging to a network element are indexed with the element, e.g. p_u is the pressure at node u and q_a is the mass flow at arc a . Some quantities x like gas temperature change along an arc. Their values at the tail u and head v of the arc differ and are denoted with $x_{a:u}$ and $x_{a:v}$. These quantities are often discontinuous at a node, i.e. $x_{a:u}$ and $x_{b:u}$ of two incident arcs a and b are not necessarily equal.

Certain constraints depend on the direction of flow. A flow from tail to head is defined as positive and a flow from head to tail is defined as negative. Accordingly, at every node u

3.2. A Nonsmooth MINLP Model with ODE Constraints

there exist inflow arcs \mathcal{I}_u and outflow arcs \mathcal{O}_u ,

$$\begin{aligned}\mathcal{I}_u &= \{a \in \delta_i^- : q_a \geq 0\} \cup \{a \in \delta_i^+ : q_a \leq 0\}, \\ \mathcal{O}_u &= \{a \in \delta_i^- : q_a < 0\} \cup \{a \in \delta_i^+ : q_a > 0\}.\end{aligned}$$

Similarly, the tail u is called the inflow node of arc (u, v) in case of positive flow and outflow node otherwise. The values at the inflow node and outflow node of a quantity x that varies along an arc are written as

$$x_a^{\text{in}} = \begin{cases} x_{a:u}, & q_a \geq 0, \\ x_{a:v}, & q_a < 0, \end{cases} \quad x_a^{\text{out}} = \begin{cases} x_{a:v}, & q_a \geq 0, \\ x_{a:u}, & q_a < 0. \end{cases} \quad (3.1)$$

if $x_{a:u}$ and $x_{a:v}$ are defined, otherwise the values at the appropriate nodes are used, i.e.

$$x_a^{\text{in}} = \begin{cases} x_u, & q_a \geq 0, \\ x_v, & q_a < 0, \end{cases} \quad x_a^{\text{out}} = \begin{cases} x_v, & q_a \geq 0, \\ x_u, & q_a < 0. \end{cases} \quad (3.2)$$

Models using these inflow and outflow values often have a nonsmooth transition when the flow direction changes.

3.2. A Nonsmooth MINLP Model with ODE Constraints

Given a gas network $\mathbb{G} = (\mathbb{V}, \mathbb{A})$, pressure bounds p_u^-, p_u^+ for all $u \in \mathbb{V}$ and supplied gas q_u with gas parameters X_u for all $u \in \mathbb{V}_+$, is there a setting for the active network devices, such that all demanded flows $q_v, v \in \mathbb{V}_-$ are satisfied?

To answer this question, a mathematical model of a gas network is necessary, which has to combine several different aspects. Stationary gas physics is partially based on ordinary differential equations (ODE) and contains nonsmooth phenomena, the states of controllable network elements introduce discrete decisions and the technical properties of network devices are only known by empirical data in many cases.

3. Validation of Nominations

In this section, MINLP-techniques are used to create an existence problem of type

$$\begin{aligned} \exists \quad & x \in \mathbb{R}^{n_x}, y \in \mathbb{R} \rightarrow \mathbb{R}^{n_y}, z \in \{0, 1\}^{n_z} \\ \text{s.t.} \quad & c_{\mathcal{E}}(x, z) = 0, \\ & c_{\mathcal{I}}(x, z) \geq 0, \\ & c_{\mathcal{D}}(x, y, \dot{y}) = 0, \\ & c_{\mathcal{A}}(x, y) = 0, \end{aligned}$$

which is a MINLP with nonsmooth constraints $c_{\mathcal{E}}(x, z)$, $c_{\mathcal{I}}(x, z)$, and differential algebraic equations (DAE) as constraints $c_{\mathcal{D}}(x, y, \dot{y})$ and $c_{\mathcal{A}}(x, y)$.

3.2.1. Component-Unspecific Aspects

While often physical equations are designed for ideal gas, the model of a real-world gas network need adjustments, since gas has slightly different attributes in reality. Gas inside transport networks does not consist of a single chemical element, but is a combination of methane, ethane, propane, butane and others. Due to interaction between the gas particles, real gas shows a different relation between pressure, temperature and volume than ideal gas, which has an impact on many physical phenomena. To model this difference, a compressibility factor z is introduced. This factor depends on the pressure p , temperature T and the gas composition. During the last decades several different empirical models of this compressibility factor have been developed. Two examples are the equation of the American Gas Association (AGA), see [73],

$$z^{\text{AGA}}(p, T, p_c, T_c) = 1 + 0.257 \frac{p}{p_c} - 0.533 \frac{p}{p_c} \frac{T_c}{T}, \quad (3.4)$$

which is sufficiently accurate for pressures up to 70 bar [78], and the Papay's equation [103, 110]

$$z^{\text{Papay}}(p, T, p_c, T_c) = 1 - 3.52 \frac{p}{p_c} e^{-2.26 \frac{T}{T_c}} + 0.274 \left(\frac{p}{p_c} \right)^2 e^{-1.878 \frac{T}{T_c}}, \quad (3.5)$$

which is appropriate up to 150 bar [78]. The gas parameter p_c denotes the pseudocritical pressure and T_c the pseudocritical temperature of the real gas.

Several other models are known in the literature. High-detailed online simulation often incorporates the detailed models AGA-DC92 [122] or GERG-2004 [74]. These sophisticated models consist of a system of nonlinear equations and require detailed information on the

3.2. A Nonsmooth MINLP Model with ODE Constraints

specific gas consumption for an increased accuracy. In mid-term planning processes, the required information is usually only partially known and has to be estimated, effectively eliminating the advantage in accuracy.

Besides the compressibility, other main differences between ideal and real gas are the specific heat capacity c_p and the molar heat capacity $\tilde{c}_p = mc_p$ of real gas. These sizes express the energy, which is necessary to increase the temperature of one kilogram or mole of gas by one Kelvin at a fixed pressure. They are modeled by

$$c_p = \frac{1}{m} \left(\tilde{c}_p^0(T, \tilde{A}, \tilde{B}, \tilde{C}) + \Delta\tilde{c}_p(p, T, p_c, T_c) \right), \quad (3.6a)$$

$$\tilde{c}_p^0 = \tilde{A} + \tilde{B}T + \tilde{C}T^2, \quad (3.6b)$$

$$\Delta\tilde{c}_p = -R \int_0^p \frac{1}{\tilde{p}} \left(2T \frac{\partial z(\tilde{p}, T, p_c, T_c)}{\partial T} + T^2 \frac{\partial^2 z(\tilde{p}, T, p_c, T_c)}{\partial T^2} \right) d\tilde{p}. \quad (3.6c)$$

The molar heat capacity consists of the molar heat capacity of ideal gas \tilde{c}_p^0 and a correction term for real gas $\Delta\tilde{c}_p$. \tilde{c}_p^0 is modeled by a least squares fit using the parameters $\tilde{A}, \tilde{B}, \tilde{C}$, which depend on the specific gas composition. The correction term expresses the difference to ideal gas. If the AGA formula (3.4) is chosen to model the compressibility factor, the correction term evaluates to zero. For Papay's equation the integral can be solved analytically [71].

The density of gas ρ is strongly related to the pressure p and temperature T . For increasing pressure the density also increases, while the density decreases when the temperature rises. This interrelation is modeled by an equation of state. Several equations of state with different ranges of validity exists, common ones are the thermodynamical standard equation [122] and the empirical equation of state of Redlich–Kwong [106].

The thermodynamical standard equation incorporates the molar mass m and the compressibility factor z . The formula is

$$0 = \rho z(p, T, p_c, T_c) RT - pm. \quad (3.7)$$

The Redlich–Kwong equation is defined as

$$\begin{aligned} 0 &= \frac{RT}{V_m - b} - \frac{a}{\sqrt{T}V_m(V_m + b)} - p, \\ a &= 0.4278 \frac{R^2 T_c^{2.5}}{p_c}, \\ b &= 0.0867 \frac{RT_c}{p_c}. \end{aligned}$$

3. Validation of Nominations

In addition to pressure, temperature and density, the equation uses the molar volume $V_m = m/\rho$ and the universal gas constant $R = 8.3144621 \text{ J K}^{-1} \text{ mol}^{-1}$.

At several network elements a pressure change occurs without heat transfer to the environment. This results in a temperature change, described by the Joule–Thomson effect,

$$T_2 - T_1 = \int_{p_1}^{p_2} \mu_{\text{JT}}(p, T) dp, \quad \mu_{\text{JT}}(p, T) = \frac{T^2}{p} \frac{R}{\tilde{c}_p} \frac{\partial z}{\partial T}. \quad (3.9)$$

3.2.2. Nodes and Arcs

Every node $u \in \mathbb{V}$ holds information about the pressure $p_u \in [p_u^-, p_u^+]$ and $T_u \in [T_u^-, T_u^+]$ at this location, and the adjacent arcs define the relations of these values to the connected nodes.

The mass flow, which is discharged or supplied at a boundary node u , is denoted by $q_u \in [q_u^-, q_u^+]$, with

$$\begin{aligned} q_u &\geq 0, & u \in \mathbb{V}_+, \\ q_u &\leq 0, & u \in \mathbb{V}_-, \\ q_u &= 0, & u \in \mathbb{V}_0. \end{aligned}$$

At every node u of the network graph the law of Kirchhoff defines a flow balance. It states that the amount of inlet mass flow and supplied mass flow equals the amount of outlet mass flow and discharged mass flow, i.e.

$$0 = q_u + \sum_{a \in \delta_u^-} q_a - \sum_{a \in \delta_u^+} q_a, \quad (3.10)$$

with q_a denoting the mass flow on arc a . Based on the common linguistic usage nominated gas is defined as a non-negative flow value $q^{\text{ext}} \geq 0$ and it is considered in the model by

$$\begin{aligned} q_u &= q_u^{\text{ext}}, & \text{for all } u \in \mathbb{V}_+, \\ q_u &= -q_u^{\text{ext}}, & \text{for all } u \in \mathbb{V}_-. \end{aligned}$$

Adding up all balance equations (3.10) and considering $q_{\mathbb{V}_+}^{\text{ext}} = q_{\mathbb{V}_+}$ and $q_{\mathbb{V}_-}^{\text{ext}} = -q_{\mathbb{V}_-}$ results in the equality

$$\sum_{u \in \mathbb{V}_+} q_u^{\text{ext}} = \sum_{u \in \mathbb{V}_-} q_u^{\text{ext}},$$

i.e. a nomination has to be balanced [53].

At nodes, the inflow gas is mixed and flows into the outlet arcs. The mixing has a strong impact on the composition of the gas inside the pipeline. The composition of supplied gas depends on the original source of the gas. Since chemical properties of the gas like molar mass m , calorific value H_c , pseudocritical pressure p_c , pseudocritical temperature T_c and coefficients of the heat capacity \tilde{A} , \tilde{B} and \tilde{C} depend on the composition, knowledge of the exact ratios increases the accuracy of the data basis of the physical and technical constraints. The importance of composition tracking will further increase in the future, when biogas and power to gas techniques, like methanation or electrolysis, further diversify the gas composition.

Mixing of the gas parameters $X = (m, H_c, p_c, T_c, \tilde{A}, \tilde{B}, \tilde{C})$ takes place with respect to the molar flow $\hat{q} = q/m$. Which gas is mixed at a node depends on the flow direction of incident arcs.

Based on the sets \mathcal{I}_u and \mathcal{O}_u , the gas mixture at node u is defined as

$$X_u = \frac{([\hat{q}_u]^+ X_u^{\text{ext}} + \sum_{a \in \mathcal{I}_u} |\hat{q}_a| X_a)}{([\hat{q}_u]^+ + \sum_{a \in \mathcal{I}_u} |\hat{q}_a|)}, \quad X_a = X_u, \quad \forall a \in \mathcal{O}_u, \quad (3.11)$$

and the mixed gas parameters are propagated on the outlet arcs. Here X_u^{ext} denotes the gas parameters of supplied gas at node $u \in \mathbb{V}_+$. At junctions and exits, this vector is assumed to be zero. The vector X_a describes the gas parameters at arc a , and $[\hat{q}_u]^+$ is the supplied molar flow \hat{q}_u , i.e.

$$[\hat{q}_u]^+ = \begin{cases} \hat{q}_u, & \text{if } u \in \mathbb{V}_+, \\ 0, & \text{else.} \end{cases}$$

The temperature of gas arriving at a node varies between the inflow arcs. When the gas of the inflow arcs is mixed an average temperature results. The mixing equation for the temperature is derived from the conservation of energy and has the same structure as (3.11). Using the molar heat capacity \tilde{c}_p the mixed temperature T_u at node u is

$$T_u = \frac{\tilde{c}_{p,u}^{\text{ext}} [\hat{q}_u]^+ T_u^{\text{ext}} + \sum_{a \in \mathcal{I}_u} \tilde{c}_{p,a} |\hat{q}_a| T_{a:u}}{\tilde{c}_{p,u}^{\text{ext}} [\hat{q}_u]^+ + \sum_{a \in \mathcal{I}_u} \tilde{c}_{p,a} |\hat{q}_a|}, \quad (3.12)$$

where $\tilde{c}_{p,u}^{\text{ext}}$ denotes the constant molar capacity of the supplied gas and T_u^{ext} its temperature.

3. Validation of Nominations

Note that all mixing equations are discontinuous, since the gas is mixed with respect to the absolute value of the mass flow on the inflow arcs and the set of inflow arcs depend on the flow direction.

3.2.3. Pipes

When people think of gas networks, they usually have a picture of large tubes made of metal or plastic in mind. Indeed, pipes outnumber all other network elements of a gas network, and they are the only elements with a noteworthy length L_a , compared to the size of the network.

A pipe is characterized by its length L_a , diameter D_a and integral roughness k_a . The cross-sectional area A_a of a pipe is considered to be circular, so

$$A_a = \frac{\pi}{4} D_a^2.$$

The slope of a pipe is assumed to be constant, $s_a = \Delta h/L_a$. The roughness of the pipe describes the quality of the internal pipe wall. In this work the integral (or average) roughness k_a is used. It summarizes the effects of several aspects of a pipe causing friction and hence pressure loss: wall roughness, sedimentation, measurement devices, welding seams, production tolerances in pipe diameters and similar. While a detailed knowledge is useful or even necessary for the in-depth analysis of fluid dynamics inside a pipe like in [3], most of the single aspects are hard or impossible to determine when solving problems on an operating gas network however. Hence the integral roughness is used, since it can comparatively easily be measured or estimated. It is the foundation of historical data and research, and it allows some tolerances for the manufacturer [128].

The roughness of the pipe has a major influence on the friction factor $\lambda(q_a)$ and thereby on the pressure loss inside the pipe. Other aspects influencing the friction factor are the diameter of the pipe and the Reynolds number of the current flow situation,

$$\text{Re}(q_a) = \frac{D_a}{A_a \eta} |q_a|,$$

η denotes the dynamic viscosity. Two kinds of friction factors are common in the literature: the Darcy friction factor λ_d and the Fanning friction factor λ_f . They only differ in a scaling constant:

$$\lambda_d = 4\lambda_f.$$

In this work the Darcy friction factor is used and the index is omitted.

3.2. A Nonsmooth MINLP Model with ODE Constraints

The dimensionless Reynolds number Re characterizes types of flow in a pipe [85]. For small mass flows q_a , the flow inside the pipe is laminar. Here, the friction factor is expressed exactly by the law of Hagen–Poiseuille [44, 85],

$$\lambda^{\text{HP}}(q_a) = \frac{64}{\text{Re}(q_a)}. \quad (3.13)$$

For larger mass flows with a Reynolds number above the critical value $\text{Re}_{\text{crit}} \approx 2320$, the flow situation is turbulent. Here, laminar flow breaks down and vortices occur [97]. For this situation no exact law is known, but a lot of empirical models have been developed in the last century. One of the pioneers of this research area was Johann Nikuradse, who roughened the inside of pipes by applying grains of sand with a known size and made a detailed analysis on these pipes in 1933 [92, 93]. He developed the formula

$$\lambda^{\text{Nik}} = \frac{1}{\left(1.74 + 2 \log \left(\frac{D_a}{2k_a}\right)\right)^2}.$$

This model is independent of the flow, i.e. it is constant for a given pipe. In 1939 Colebrook [26] published an implicit formula regarding the flow,

$$\frac{1}{\sqrt{\lambda^{\text{PC}}(q_a)}} = -2 \log_{10} \left(\frac{2.51}{\text{Re}(q_a) \sqrt{\lambda^{\text{PC}}(q_a)}} + \frac{k_a}{3.71 D_a} \right). \quad (3.14)$$

This formula is generally known as the Colebrook–White equation, in German literature sometimes also Prandtl–Colebrook equation, or just Colebrook equation. Originally, this formula could not be used directly due to its implicit nature, so graphical representations were created. Examples are the Rouse diagram [109] and the Moody diagram [88]. With the upcoming of computers, the equations could be solved iteratively. In the recent years explicit reformulations have been found [89].

Several other equations of the friction have been developed, like the Hofer equation [62, 86]

$$\lambda^{\text{Hof}}(q_a) = \left(-2 \log \left(\frac{4.518}{\text{Re}(q_a)} \log \left(\frac{\text{Re}(q_a)}{7} \right) + \frac{k_a}{3.71 D_a} \right) \right)^{-2},$$

or the PMT-1025 equation [25, 86]

$$\lambda^{\text{PMT}}(q_a) = 0.067 \left(\frac{158}{\text{Re}(q_a)} + \frac{2k_a}{D_a} \right)^{0.2}.$$

Hofer’s formula is an explicit approximation of the Colebrook equation [86]. For $q_a \rightarrow \infty$

3. Validation of Nominations

the result of Hofer's formula converges to the value of Nikuradse's formula. Further friction models are given in [13, 85, 86, 97].

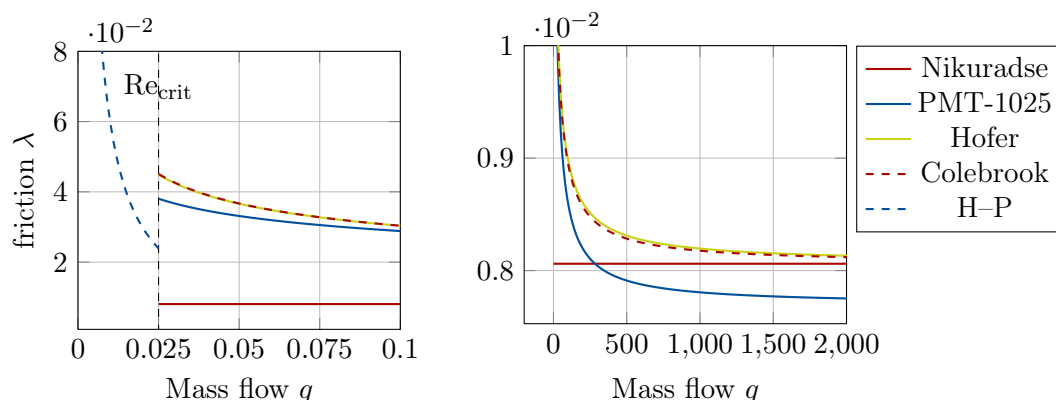


Figure 3.1. Comparison of friction models for small and large mass flow ($D_a = 1$ m, $k_a = 10^{-6}$ m)

The stated friction models are displayed in Figure 3.1 for the transition point between laminar and turbulent flow, and for large flow. While the graphs of Hofer and Colebrook–White are hardly distinguishable, the PMT-1025 formula leads to significantly smaller values in case of large flows. The constant value of Nikuradse's formula is inaccurate for small flow values but closes in to the values of Colebrook's and Hofer's formulas for growing flow values. This is to be expected, since it is the convergence limit of Hofer's formula for large mass flows. At the transition from laminar to turbulent, i.e. at the critical Reynolds number, there exists a jump discontinuity between the law of Hagen–Poiseuille and the turbulent models.

Resistance and gravitational forces based on friction and slope have a major impact on pressure and temperature change along a pipe. In full complexity, these changes and the conservation of mass are described by Euler equations for compressible fluids in cylindrical pipes, which are a specialization of the Navier–Stokes equations [39]. In the following, these equations are stated as partial differential equations in location x and time t , together with some short motivations, based on [5, 73, 80].

The continuity equation is derived from the mass conservation law

$$\frac{d}{dt} \int_{x_1(t)}^{x_2(t)} A_a \rho_a(x, t) dx = 0$$

using the density at position x at time t in an arbitrary pipe segment $[x_1(t), x_2(t)]$. Based

on Reynolds' transport theorem, this is equivalent to

$$\int_{x_1(t)}^{x_2(t)} A_a \frac{\partial}{\partial t} \rho_a(x, t) dx + A_a \rho_a(x, t) \Big|_{x_2(t)} \frac{dx_2}{dt} - A_a \rho_a(x, t) \Big|_{x_1(t)} \frac{dx_1}{dt} = 0.$$

The terms dx_1/dt and dx_2/dt correspond to the velocities $v(x_1, t)$ and $v(x_2, t)$ at the bounds of the considered pipe segment. Hence,

$$\begin{aligned} & \int_{x_1(t)}^{x_2(t)} A_a \frac{\partial}{\partial t} \rho_a(x, t) dx + A_a v_a(x, t) \rho_a(x, t) \Big|_{x_2(t)} - A_a v_a(x, t) \rho_a(x, t) \Big|_{x_1(t)} = 0 \\ \iff & \int_{x_1(t)}^{x_2(t)} A_a \frac{\partial}{\partial t} \rho_a(x, t) dx + \int_{x_1(t)}^{x_2(t)} A_a \frac{\partial}{\partial x} [v_a(x, t) \rho_a(x, t)] dx = 0 \\ \iff & \int_{x_1(t)}^{x_2(t)} \frac{\partial \rho_a(x, t)}{\partial t} + \frac{\partial (v_a(x, t) \rho_a(x, t))}{\partial x} dx = 0. \end{aligned}$$

Since these equations hold for any segment $[x_1(t), x_2(t)]$, the continuity equation

$$\frac{\partial \rho_a}{\partial t} + \frac{\partial v_a \rho_a}{\partial x} = 0 \quad (3.15)$$

is gained.

The momentum equation is based on Newton's second law of motion, the sum of forces acting on an object equals the change in time of its momentum. The relevant forces are the pressure force

$$A_a \int_{x_1(t)}^{x_2(t)} \frac{\partial p_a(x, t)}{\partial x} dx,$$

the gravitational force with the gravitational acceleration g

$$A_a \int_{x_1(t)}^{x_2(t)} \rho_a(x, t) g s_a dx,$$

and the friction forces

$$A_a \int_{x_1(t)}^{x_2(t)} \frac{\lambda(q_a)}{2D_a} \rho_a(x, t) |v_a(x, t)| v_a(x, t) dx.$$

3. Validation of Nominations

In summary, Newton's second law is stated as

$$0 = A_a \frac{d}{dt} \int_{x_1(t)}^{x_2(t)} v_a \rho_a dx - A_a \int_{x_1(t)}^{x_2(t)} \frac{\partial p_a}{\partial x} dx - A_a \int_{x_1(t)}^{x_2(t)} \rho_a g s_a dx - A_a \int_{x_1(t)}^{x_2(t)} \frac{\lambda(q_a)}{2D_a} \rho_a |v_a| v_a dx.$$

By applying Reynolds' transport theorem, this results in

$$0 = \int_{x_1(t)}^{x_2(t)} \frac{\partial v_a \rho_a}{\partial t} + \frac{\partial \rho_a v_a^2}{\partial x} dx - \int_{x_1(t)}^{x_2(t)} \frac{\partial p_a}{\partial x} + \rho_a g s_a + \frac{\lambda(q_a)}{2D_a} \rho_a |v_a| v_a dx \quad (3.16)$$

$$\iff 0 = \frac{\partial \rho_a v_a}{\partial t} + \frac{\partial \rho_a v_a^2}{\partial x} - \frac{\partial p_a}{\partial x} - \rho_a g s_a - \frac{\lambda(q_a)}{2D_a} \rho_a |v_a| v_a, \quad (3.17)$$

since the equation holds for any x_1 and x_2 . Some publications describe the equivalent formulation

$$\rho_a \frac{\partial v_a}{\partial x} + \rho_a v_a \frac{\partial v_a}{\partial x} - \frac{\partial p_a}{\partial x} - \rho_a g s_a - \frac{\lambda(q_a)}{2D_a} \rho_a |v_a| v_a = 0.$$

This is achieved by applying the product rule and (3.15) on the first and second term of (3.17) [80].

The temperature dynamics are described by the law of energy conservation. Here, they are modeled by the same differential equation as in [78]. Essentially, this equation incorporates changes due to the Joule–Thomson effect (3.9) and heat exchange with the environment,

$$0 = A_a \rho_a c_p \left(\frac{dT_a}{dt} - \mu_{JT} \frac{dp_a}{dt} \right) - A_a \frac{dp_a}{dt} + A_a v_a g \rho_a s_a + \pi D_a c_{HT} (T_a - T_{soil}).$$

The specific heat capacity is abbreviated by $c_{p,a}$, c_{HT} denotes the constant heat transfer coefficient of the pipe and the temperature of the surrounding soil is written as T_{soil} . By expanding the total derivatives and applying (3.9) the equation is transformed into the energy equation

$$0 = A_a \rho_a c_{p,a} \left(\frac{\partial T_a}{\partial t} + v_a \frac{\partial T_a}{\partial x} \right) - A_a \left(1 + \frac{T_a}{z_a} \frac{\partial z_a}{\partial T_a} \right) \frac{\partial p_a}{\partial t} - A_a v_a \frac{T_a}{z_a} \frac{\partial z_a}{\partial T_a} \frac{\partial p_a}{\partial x} + A_a \rho_a v_a g s_a + \pi D_a c_{HT} (T_a - T_{soil}).$$

The compressibility factor $z(p_a(x, t), T_a(x, t), p_{c,a}, T_{c,a})$ is abbreviated by z_a .

3.2. A Nonsmooth MINLP Model with ODE Constraints

In summary, the transient gas dynamics are modeled by

$$0 = \frac{\partial \rho_a}{\partial t} + \frac{\partial(\rho_a v_a)}{\partial x}, \quad (3.18a)$$

$$0 = \frac{\partial(\rho_a v_a)}{\partial t} + \frac{\partial p_a}{\partial x} + \frac{\partial(\rho_a v_a^2)}{\partial x} + g \rho_a s_a + \lambda(q_a) \frac{|v_a| v_a}{2D_a} \rho_a, \quad (3.18b)$$

$$0 = A_a \rho_a c_{p,a} \left(\frac{\partial T_a}{\partial t} + v_a \frac{\partial T_a}{\partial x} \right) - A_a \left(1 + \frac{T_a}{z_a} \frac{\partial z_a}{\partial T_a} \right) \frac{\partial p_a}{\partial t} - A_a v_a \frac{T_a}{z_a} \frac{\partial z_a}{\partial T_a} \frac{\partial p_a}{\partial x} + A_a \rho_a v_a g s_a + \pi D_a c_{HT} (T_a - T_{\text{soil}}). \quad (3.18c)$$

The gas velocity v_a is expressed by the mass flow q_a , density ρ_a and the cross-sectional area of the pipe A_a using

$$q_a(x, t) = A_a \rho_a(x, t) v_a(x, t). \quad (3.19)$$

In practice, the gas velocity is desired to be in specific bounds, since high velocities create a considerable sound pollution which is not acceptable in inhabited areas and the resulting vibrations could damage the wall material.

For a stationary model of a pipe $a = (u, v)$ the time-dependent partial derivatives are dropped from (3.18). Together with (3.19) and an equation of state, e.g. the thermodynamical standard equation (3.7), this results in a differential algebraic equation (DAE)

$$0 = \frac{\partial q_a(x)}{\partial x}, \quad (3.20a)$$

$$0 = \frac{\partial p_a(x)}{\partial x} + \frac{q_a^2(x)}{A_a^2} \frac{\partial}{\partial x} \frac{1}{\rho_a(x)} + g \rho_a(x) s_a + \lambda(q_a(x)) \frac{|q_a(x)| q_a(x)}{2A_a^2 D_a \rho_a(x)}, \quad (3.20b)$$

$$0 = q_a(x) c_{p,a} \frac{\partial T_a(x)}{\partial x} - \frac{q_a(x) T_a(x)}{\rho_a(x) z_a} \frac{\partial z_a}{\partial T_a(x)} \frac{\partial p_a(x)}{\partial x} + q_a(x) g s_a + \pi D_a c_{HT} (T_a(x) - T_{\text{soil}}), \quad (3.20c)$$

$$0 = \rho_a(x) z_a R T_a(x) - p_a(x) m, \quad (3.20d)$$

$$0 = p_a(0) - p_u, \quad (3.20e)$$

$$0 = T_a(0) - T_u, \quad (3.20f)$$

$$0 = q_a(0) - q_a. \quad (3.20g)$$

It follows from the continuity equation (3.20a) that the gas flow $q_a(x)$ through the pipe is constant.

3. Validation of Nominations

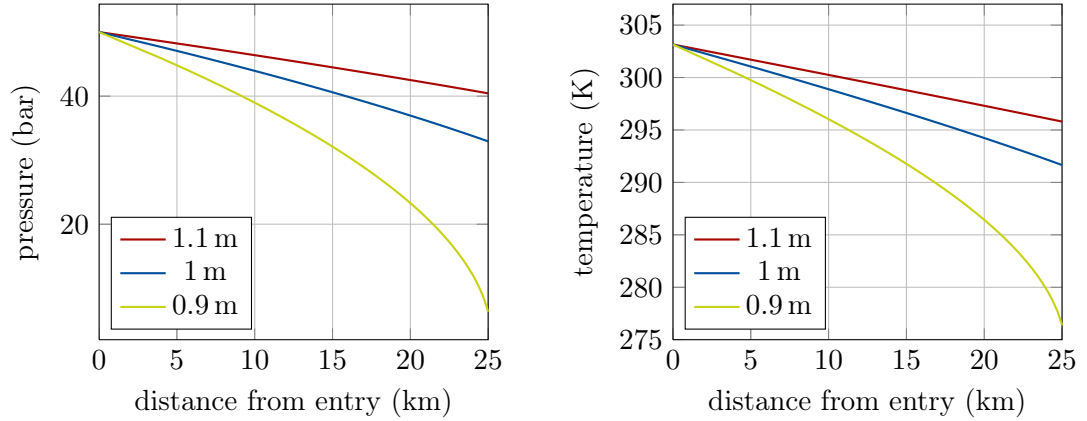


Figure 3.2. Profiles of pressure and temperature of three horizontal pipes with differing diameters ($L_a = 25$ km, $k_a = 0.06$ mm, $q_a = 500$ kg s⁻¹).

Figure 3.2 displays the change of pressure and temperature along a pipe and the influence of the diameter. It shows the increasing loss in pressure and temperature for decreasing diameter. The trends of pressure and temperature are quite similar.

3.2.4. Resistors

Some network devices, like measurement devices, narrow kinks in pipes, filters and internal station piping lead to additional pressure loss. Sometimes, it is not desirable to incorporate this into the integral roughness of a pipe or it is just not possible, since the devices are attached to other network elements than pipes. Typically, the exact characteristics of the pressure loss are unknown and only empirical data is available. To model the pressure drop anyway, fictitious resistors are included.

Two different models are presented for these fictitious network elements, depending on the available data. The first model of a resistor $a = (u, v)$ is based on a constant non-negative pressure loss ξ_a ,

$$0 = p_u - p_v - \text{sign}(q_a)\xi_a. \quad (3.21)$$

The second model incorporates a pressure loss similar to the Darcy–Weisbach equation [44, 80] with fictitious diameter D_a :

$$0 = p_u - p_v - \frac{1}{2}\zeta_a\rho_{\text{in}}|v_{\text{in}}|v_{\text{in}} = p_u - p_v - \frac{8\zeta_a}{\pi^2 D_a^4} \frac{|q_a|q_a}{\rho_{\text{in}}}. \quad (3.22)$$

Here, ζ_a denotes a non-negative resistance coefficient. The change of pressure leads to a change of temperature. This effect is governed by the Joule–Thomson effect (3.9).

Note, that in both models the pressure loss depends on the flow direction. Values indexed by $_{\text{in}}$ refer to the inflow side of the resistor. This results in nonsmooth aspects in both models. The sign function in (3.21) introduces a nonsmoothness of first order and the absolute value in (3.22) introduces a nonsmoothness of second order.

3.2.5. Valves

Valves are controlled by the network operator to redirect the flow of the gas. Thus, they are active network elements and they can be either open or closed. An open valve does not influence the gas, i.e. there is no change of pressure, temperature or flow. On the opposite, a closed valve prevents any gas from passing through, and the closed valve induces no relation between the values at the beginning of the valve and its end. The consequences of both states are listed in Table 3.1.

	open	closed
flow:	–	$q_a = 0$
pressure:	$p_u = p_v$	–

Table 3.1. States of a valve $a = (u, v)$ and their consequences on pressure and flow

By closing valves, subnetworks can be decoupled, e.g. for maintenance, and the route of the flow can be controlled, e.g. to direct gas to a compressor group. Therefore, valves are frequently found in combination with compressor groups and control valve stations.

Several types of valves exist, but typically they have some kind of changeable obstacle to close themselves. For example, a gate valve raises or drops a wall-like barrier into the pipe, whereas a ball valve is based on a ball with a cylindrical hole through its center. When the hole is parallel to the valve, the gas can flow freely, while the gas flow is interrupted, when the hole is perpendicular to the valve.

A valve $a \in \mathbb{A}_{\text{vl}}$ is described by a linear mixed-integer model using big- M -formulations. It uses sufficiently large constants $M_p, M_T > 0$ and a discrete variable $z_a \in \{0, 1\}$ which describes the state of the valve. An open valve is represented by $z_a = 1$, while a closed

3. Validation of Nominations

valve is represented by $z_a = 0$. The resulting mixed-integer model is

$$\begin{aligned}
0 &\leq (1 - z_a)M_p^+ + (p_u - p_v), \\
0 &\leq (1 - z_a)M_p^- - (p_u - p_v), \\
0 &\leq (1 - z_a)M_T^+ + (T_{a:u} - T_{a:v}), \\
0 &\leq (1 - z_a)M_T^- - (T_{a:u} - T_{a:v}), \\
0 &\leq z_a q_a^+ - q_a, \\
0 &\leq q_a - z_a q_a^-.
\end{aligned}$$

The smallest possible constants are $M_p^+ = p_u^+ - p_v^-$, $M_p^- = p_v^+ - p_u^-$, $M_T^+ = T_{a:u}^+ - T_{a:v}^-$ and $M_T^- = T_{a:v}^+ - T_{a:u}^-$. If any of these constants is negative there has to be a difference in temperature or pressure between the nodes, thus the valve has to be closed.

3.2.6. Shortcuts

Similar to resistors, shortcuts are fictitious network elements. They are introduced to simplify the modeling of sophisticated network situations, like combinations of compressor groups or exchange nodes, which can be both entries and exits (just not at the same time). The model is similar to an open valve, i.e.

$$0 = p_u - p_v, \tag{3.23a}$$

$$0 = T_{a:u} - T_{a:v}. \tag{3.23b}$$

3.2.7. Control Valves

Typically, the pressure levels of gas transporting networks are too high for attached distribution networks and industrial customers. To fit their demands on the maximum allowed pressure, control valve stations are incorporated into the network to decrease the gas pressure. Two kinds of control valves are presented here: those with remote access and those without.

The pressure loss at a control valve with remote access is directly controlled by the network operator. This is not the case for control valves without remote access. Here, a pressure value p_{set} is set and the pressure is reduced to this value, if the inflow pressure is larger. If the pressure in the subsequent subnetwork rises above the preset value, the control valve without remote access closes automatically.

3.2. A Nonsmooth MINLP Model with ODE Constraints

A control valve station of either type consists of several elements. The actual reduction of pressure is done by the control valve. Additional devices like filters, station piping or measurement devices reduce the pressure loss further and are summarized in inlet and outlet resistors, see Section 3.2.4 for modeling details. A large pressure drop may lead to hydratized gas, which is undesirable in gas transport networks. To prevent this from happening, a gas preheater is activated, when the gas temperature falls below a given minimum $T_{a:v}^-$. In (transient) reality, the preheater heats the gas in front of the active control valve based on readings of temperature sensors located behind the control valve. Here, the model is simplified and the preheater has direct control of the outlet temperature.

A control valve station is either active, closed or bypassed. In case of an active control valve station, the operator specifies the pressure drop Δp caused by the control valve, when remote access is available. Otherwise, the outlet pressure is reduced to a preset pressure value p_{set} . The pressure reduction leads to a change of temperature based on the Joule–Thomson effect, see (3.9). The inlet and outlet resistors result in additional changes of pressure and temperature. An active control valve station can only operate in direction of the arc, so the flow through the station has to be positive, $q_a \geq 0$.

A closed control valve station interrupts the gas flow and decouples the ends of the element. It is modeled like a closed valve.

A control valve station in bypass has no influence on the pressure and the gas can flow freely through the element. Whether the resistors are circumvented in bypass mode depends on the type of the control valve. If remote access is available, the resistors are also bypassed, otherwise they are always regarded. The states and their conditions of a control valve with remote access are summarized in Table 3.2. The same information is given for control valves without remote access in Table 3.3.

	open		closed
	active	bypass	
flow:	$q_a \geq 0$	–	$q_a = 0$
pressure:	$p_u \geq p_v$	$p_u = p_v$	–

Table 3.2. States and their consequences on pressure and flow of a control valve with remote access $a = (u, v)$.

3. Validation of Nominations

	active	bypass	closed
flow:	$q_a \geq 0$	–	$q_a = 0$
pressure at tail:	$p_1 \geq p_{\text{set},a}$	$p_1 \leq p_{\text{set},a}$	–
pressure at head:	$p_2 = p_{\text{set},a}$	$p_2 = p_1$	$p_2 \geq p_{\text{set},a}$

Table 3.3. States and their consequences on pressure and flow of a control valve without remote access $a = (u, v)$.

Similar to valves, a mixed-integer formulation models the control valve station. Since a control valve station has three possible states, two binary variables $z_1, z_2 \in \{1, 0\}$ are required. In the following model, z_1 represents the decision between an open ($z_1 = 1$) and closed ($z_1 = 0$) station, while z_2 represents an active control valve station ($z_2 = 1$) or an inactive one ($z_2 = 0$). Thus, the states of the control valve station are represented by

$$\begin{aligned} \text{closed:} & \quad z_1 = 0, z_2 = 0, \\ \text{bypass:} & \quad z_1 = 1, z_2 = 0, \\ \text{active:} & \quad z_1 = 1, z_2 = 1. \end{aligned}$$

Since an active station has to be open, the choice $z_1 = 0, z_2 = 1$ is not possible.

Additional nodes and arcs have to be introduced, since a control valve station consists of several devices. The whole control valve station is modeled as a subgraph, see Figure 3.3.

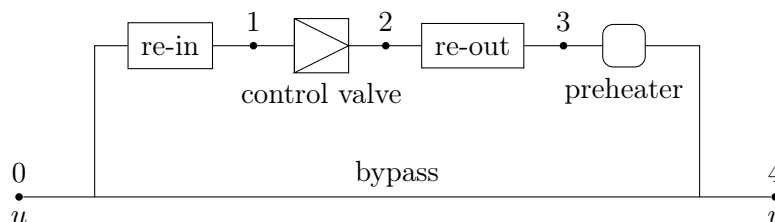


Figure 3.3. Schematic control valve station

When regarding the control valve as sub-arc a_1 , the inlet resistor is sub-arc a_0 , the outlet resistor is sub-arc a_2 and the preheater is the sub-arc a_3 . In summary, an active control valve station consists of four sub-arcs. Each sub-arc a_i connects sub-node i with sub-node $i + 1$. Each sub-node $i = 1, 2, 3$, has a pressure and temperature variable, thus define $x_i = (p_i, T_i)$, $i = 1, 2, 3$. The sub-node 0 is identified with u and sub-node 4 with v .

Let the inlet resistor be represented by $c_{a_0}(q_a, p_u, p_1, T_{a:u}, T_1) = 0$ and the outlet resistor by $c_{a_2}(q_a, p_2, p_3, T_2, T_3) = 0$. In addition, let the Joule–Thomson effect (3.9) at an active

3.2. A Nonsmooth MINLP Model with ODE Constraints

control valve be modeled by $c^{\text{jt}}(p_1, p_2, T_1, T_2) = 0$. The constraints

$$0 = T_{a:v} - \max(T_3, T_{a:v}^-), \quad (3.24a)$$

$$0 = p_3 - p_v, \quad (3.24b)$$

$$0 \leq (1 - z_1)M_{\text{jt}} - c^{\text{jt}}(p_1, p_2, T_1, T_2), \quad (3.24c)$$

$$0 \leq (1 - z_1)M_{\text{jt}} + c^{\text{jt}}(p_1, p_2, T_1, T_2), \quad (3.24d)$$

$$0 \leq z_1 q_a^+ - q_a, \quad (3.24e)$$

$$0 \leq q_a - z_1 q_a^-, \quad (3.24f)$$

$$0 \leq q_a - (1 - z_2)q_a^-, \quad (3.24g)$$

$$0 \leq z_1 - z_2 \quad (3.24h)$$

are valid for both types of control valves. The equations (3.24a) and (3.24b) model the gas preheater.

The model of a control valve station with remote access contains the additional constraints

$$0 \leq (1 - z_1)M_{a_0} - c_{a_0}(q_a, p_u, p_1, T_{a:u}, T_1), \quad (3.25a)$$

$$0 \leq (1 - z_1)M_{a_0} + c_{a_0}(q_a, p_u, p_1, T_{a:u}, T_1), \quad (3.25b)$$

$$0 \leq (1 - z_1)M_{a_2} + c_{a_2}(q_a, p_2, p_3, T_2, T_3), \quad (3.25c)$$

$$0 \leq (1 - z_1)M_{a_2} - c_{a_2}(q_a, p_2, p_3, T_2, T_3), \quad (3.25d)$$

$$0 \leq (1 - z_1)M_{a_1} - (p_1 - p_2 - z_2 \Delta p), \quad (3.25e)$$

$$0 \leq (1 - z_1)M_{a_1} + (p_1 - p_2 - z_2 \Delta p). \quad (3.25f)$$

The vector-valued constants M_{jt} , M_{a_0} , M_{a_1} and M_{a_2} are sufficiently large.

The state of a control valve without remote access depends on the relation of the inflow pressure p_1 and the outlet pressure p_2 to the preset pressure $p_{\text{set},a}$. Based on the properties stated in Table 3.3 for a control valve without remote access, the mutual constraints (3.24) are extended by the constraints

$$0 = c_0(q_a, p_u, p_1, T_{a:u}, T_1),$$

$$0 = c_2(q_a, p_2, p_3, T_2, T_3),$$

$$0 \leq (p_1^- - p_{\text{set},a})z_2 + p_1 - p_1^-,$$

$$0 \leq (p_{\text{set},a} - p_2^+)z_1 - p_2 + p_2^+,$$

$$0 \leq (p_{\text{set},a} - p_1^+)(z_1 - z_2) - p_1 + p_1^+,$$

3. Validation of Nominations

$$\begin{aligned}
0 &\leq (p_{\text{set},a} - p_2^-)(z_1 - z_2) + p_2 - p_{\text{set},a}, \\
0 &\leq (p_2^+ - p_1^-)(1 - z_1) - (p_2 - p_1), \\
0 &\leq (p_1^+ - p_{\text{set},a})(1 + z_2 - z_1) - (p_1 - p_2).
\end{aligned}$$

The models of both types of control valves combine discrete variables z_1 and z_2 , mixed-integer linear functions, nonlinear functions c_0 , c_2 and c^{jt} , and a nonsmooth temperature model of the gas preheater (3.24a).

3.2.8. Compressor Groups

Due to the pressure loss inside the network, the pressure of the input gas may not be sufficient to transport gas to all exits and to satisfy the lower pressure limits at exchange points to adjacent transport networks. Compressor groups offer the network operator the ability to increase the pressure within certain technical limits. Thus, pressure losses are compensated and it is possible to transport gas over larger distances.

The network operator has the choice to either close a compressor group, bypass it or let the group operate actively. A closed compressor group acts similar to a closed valve, i.e. the mathematical model is just

$$q_a = 0.$$

When the compressor group is bypassed, pressure and temperature are not influenced and gas can flow in either direction. The model is similar to a shortcut,

$$\begin{aligned}
0 &= p_u - p_v, \\
0 &= T_u - T_v.
\end{aligned}$$

In case of an active compressor group $a = (u, v)$ several technical devices have impact on the gas passing the group. Filters, sensors, interior pipings and other elements causing additional pressure loss are modeled by inflow and outflow resistors. One or several active compressor units increase the pressure at a compressor group and a gas cooler is activated, when a critical gas temperature is reached.

The pressure increase at the compressor group is generated by multiple compressor units and each compressor unit is powered by a drive. Each compressor unit has a specific

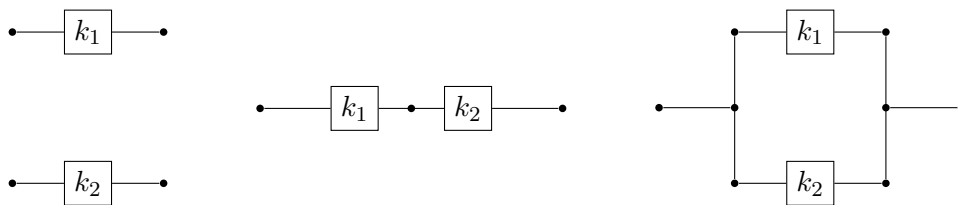


Figure 3.4. All possible configurations of a compressor group with two units k_1 and k_2

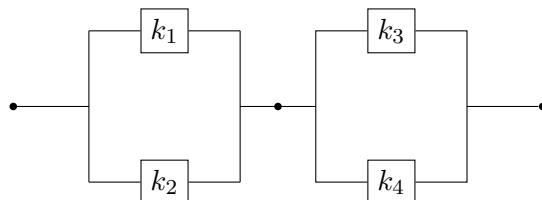


Figure 3.5. Configuration with two serial stages of parallel units

range of operation, which induces lower and upper bounds on the gas flow and pressure increase.

The technical description of a compressor group a typically contains a set of configurations \mathcal{K}_a , which describes all possible combinations of the compressor units of the compressor group. Each configuration $i \in \mathcal{K}_a$ consists of a set of serial stages \mathcal{S}_i and each stage $j \in \mathcal{S}_i$ contains a set of compressor units \mathcal{U}_j which are operated in parallel. Only a single configuration can be active at the same time.

Figure 3.4 lists all possible configurations of a compressor group with two compressor units: there is either a single unit active or they operate serially or in parallel. When compressor units work parallel, the overall flow is split between the units and the maximum flow the station is larger than when a single unit is active. The drawback is, that the pressure increase is limited by the weakest unit, i.e. the unit with the smallest possible pressure increase, since the outflow pressures of the parallel units are identical. In contrast, the serialization of compressor units allows successive pressure increase and thereby a larger outflow pressure than a single unit. The maximum possible flow which can be compressed by a serialization of units is bounded by the smallest maximum flow the serial stages can handle. If more than two units belong to a compressor group these settings can be combined. Figure 3.5 shows a configuration with four active compressor units arranged in two serial stages with two parallel units each. A schematic graph of a compressor group is illustrated in Figure 3.6.

The feasible set of a configuration \mathcal{F}_i , $i \in \mathcal{K}_a$, depends on the included compressor units and how they are combined. At each serial stage $j \in \mathcal{S}_i$ the flow through the compressor

3. Validation of Nominations

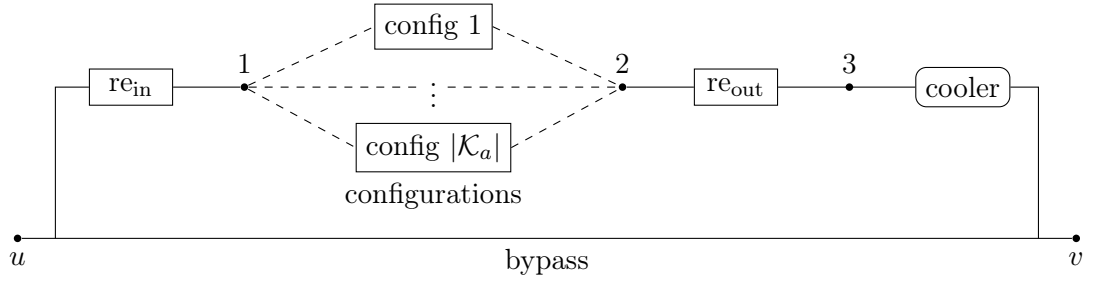


Figure 3.6. Subgraph of a compressor group

group is divided between the compressor units $k \in \mathcal{U}_j$ of this stage,

$$0 = q_a - \sum_{k \in \mathcal{U}_j} q_k \quad \forall j \in \mathcal{S}_i. \quad (3.26)$$

The outlet pressure p_j of a stage j is the inlet pressure of the compressor units in the subsequent stage $j + 1$. The outlet temperatures T_k^{out} , $k \in \mathcal{U}_j$, are mixed according to (3.12), the mixed temperature T_j is the inlet temperature of the subsequent stage.

Two kinds of compressor units are common: turbo compressors and piston compressors. Both types are based on different mechanical principles. Nevertheless, they have some basics in common.

The compression of the gas is adiabatic, i.e. the pressure increase takes place without heat transfer, and is reversible, hence it is isentropic. The energy, which is necessary to compress 1 kg real gas from given pressure and temperature to a target pressure, is expressed by the specific change in adiabatic enthalpy H_{ad} . For a compressor unit k the specific change in adiabatic enthalpy is modeled by

$$H_{\text{ad},k} = z_{j-1} T_{j-1} \frac{R}{m_a} \frac{\kappa_k}{\kappa_k - 1} \left(\left(\frac{p_j}{p_{j-1}} \right)^{\frac{\kappa_k - 1}{\kappa_k}} - 1 \right),$$

$$z_{j-1} = z(p_{j-1}, T_{j-1}, p_{c,a}, T_{c,a}),$$

with the universal gas constant R and the isentropic exponent κ . The isentropic exponent depends on the change in pressure and temperature. Several empirical models of the isentropic exponent exist. The following selection is based on [78]. In the most detailed model presented in this work κ is a mean value, modeled by

$$\kappa_k = \frac{1}{2} (\kappa_k^{\text{in}} + \kappa_k^{\text{out}}), \quad (3.27)$$

3.2. A Nonsmooth MINLP Model with ODE Constraints

where κ^{in} and κ^{out} are the adiabatic efficiencies with respect to the inflow and outflow gas of the compressor unit. They are both computed via

$$\begin{aligned}\kappa_k^{\text{in}} &= \kappa^{\text{def}}(p_{j-1}, T_{j-1}, c_{p,j-1}, m_a, p_{c,a}, T_{c,a}), \\ \kappa_k^{\text{out}} &= \kappa^{\text{def}}(p_j, T_k^{\text{out}}, c_p^{\text{out}}, m_a, p_{c,a}, T_{c,a}),\end{aligned}$$

using the functions

$$\kappa^{\text{def}}(p, T, c_p, m_a, p_{c,a}, T_{c,a}) = \frac{m_a c_p z(p, T, p_{c,a}, T_{c,a})}{m c_p Z_p(p, T, p_{c,a}, T_{c,a}) - Z_T(p, T, p_{c,a}, T_{c,a})^2 R_s}, \quad (3.28)$$

$$Z_p(p, T, p_{c,a}, T_{c,a}) = z - p \frac{\partial z}{\partial p}, \quad (3.29)$$

$$Z_T(p, T, p_{c,a}, T_{c,a}) = z + T \frac{\partial z}{\partial T}. \quad (3.30)$$

The quantities $c_{p,j-1}$ and c_p^{out} denote the heat capacity of the inflow and outflow gas, see (3.6).

An alternative model makes use of a mean temperature $T_{m,k}$, e.g.

$$T_{m,k} = \frac{1}{2} (T_{j-1} + T_k^{\text{out}}),$$

and expresses the isentropic exponent by

$$\kappa_k = 1.29 + 5.8824 \times 10^{-4} (T_{m,k} - T_0).$$

By choosing the mean temperature as the constant value T_0 , this model further simplifies to $\kappa = 1.29$. In practice, this constant value is often chosen instead of a more sophisticated model.

The power P consumed by the compressor depends on the flow through the unit, the specific change in adiabatic enthalpy H_{ad} and the adiabatic efficiency η_{ad} ,

$$P_k = \frac{q_a H_{\text{ad},k}}{\eta_{\text{ad},k}}.$$

The pressure increase at a compressor results in a temperature increase of the gas. Again, several empirical models exist. All models given in [115] base on a certain number of fixed-point iterations using

$$T_k^{l+1} = T_k^{\text{init}} \frac{z(p_{j-1}, T_{j-1}, p_{c,a}, T_{c,a})}{z(p_j, T_k^l, p_{c,a}, T_{c,a})}, \quad T_k^0 = T_k^{\text{init}}, \quad j = 0, 1, 2, \dots, \quad (3.31)$$

3. Validation of Nominations

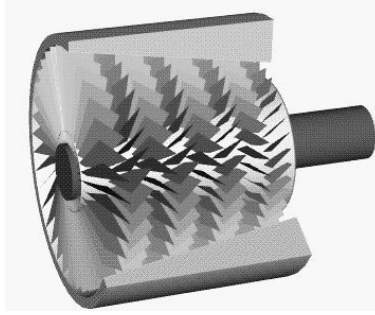


Figure 3.7. Schematic turbo compressor [91]

with a certain choice of the initial temperature T^{init} . The standard model uses a single iteration, $T_k^{\text{out}} = T_k^1$, and defines

$$T_k^{\text{init}} = T_{j-1} \left(\frac{p_j}{p_{j-1}} \right)^{(\kappa_k - 1) / (\kappa_k \eta_{\text{ad}, k})}. \quad (3.32)$$

Most of the type-specific, technical restrictions are modeled by least-squares fits based on empirical measurements. The resulting polynomials are either of the form

$$\psi(x; \beta) = \beta_0 + \beta_1 x + \beta_2 x^2 \quad (3.33)$$

or

$$\chi(x, y; B) = \begin{pmatrix} 1 \\ x \\ x^2 \end{pmatrix}^T \begin{pmatrix} b_{00} & b_{01} & b_{02} \\ b_{10} & b_{11} & b_{12} \\ b_{20} & b_{21} & b_{22} \end{pmatrix} \begin{pmatrix} 1 \\ y \\ y^2 \end{pmatrix}. \quad (3.34)$$

B and b are the unit-specific and constraint-specific fitted parameters.

Turbo compressors are designed for large throughput by moderate compression. Their principle of operation resembles a jet turbine, and essentially they share the same build-up. Figure 3.7 contains a schematic representation of a turbo compressor. The displayed rows of airfoils alternate between rotating and stationary. The rotating rows accelerate the gas, while the stationary rows transform the increased kinetic energy to a pressure increase by diffusion.

The set of feasible working points of a turbo compressor, i.e. tuples of specific change in adiabatic enthalpy and volumetric flow, is described by a characteristic diagram. An example is given in Figure 3.8a.

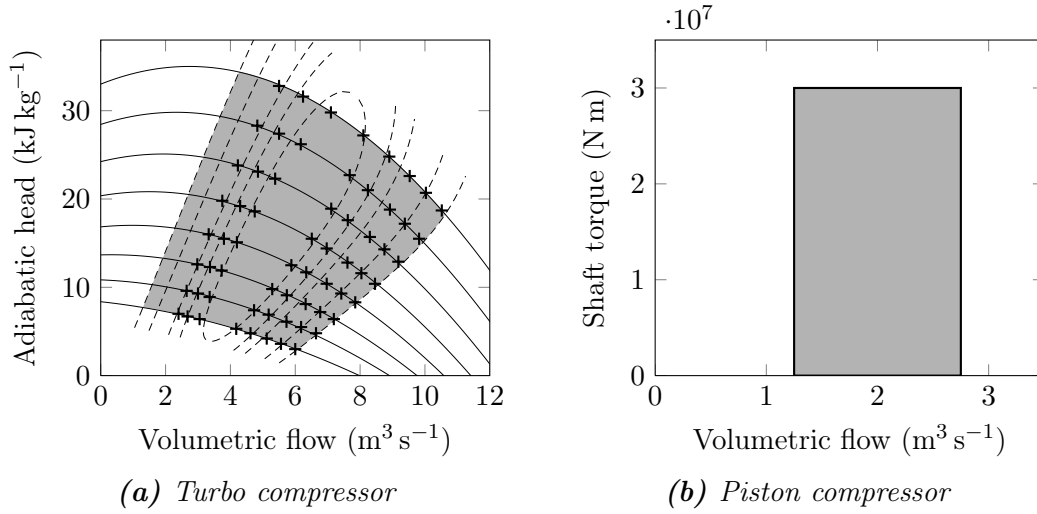


Figure 3.8. Examples of characteristic diagrams

The diagram is defined by the isolines for speed

$$H_{\text{ad}}(Q, n) = \chi(Q, n; B_{H_{\text{ad}}}), \quad (3.35)$$

and the isolines for adiabatic efficiency

$$\eta_{\text{ad}}(Q, n) = \chi(Q, n; B_{\eta_{\text{ad}}})$$

and limits to the left and right. The volumetric flow Q results from mass flow and density by the equation $Q = q_a/\rho$. Since the range of the compressor speed n is limited, the set of feasible working points has upper and lower limits defined by the maximum and minimum speed isolines. The left limit of the characteristic diagram is called the surgeline. Left-above this line, there is not enough gas flowing through the compressor unit to realize the desired specific change in adiabatic enthalpy, so

$$H_{\text{ad},k} \leq \psi(Q_k; \beta_{\text{surge}}).$$

On the right side the feasible operating range of the compressor unit is restricted by the chokeline. Points below and at the right of this line overcharge the compressor unit, i.e. the amount of gas through the unit is too large to be compressed any further than this line allows,

$$H_{\text{ad},k} \geq \psi(Q_k; \beta_{\text{choke}}).$$

3. Validation of Nominations

Both surgeline and chokeline do not necessarily coincide with an isoline for adiabatic efficiency.

Piston compressors periodically capsule a certain amount of gas, compress it and release it into the network. Its basic principle is similar to an air pump. Compared to turbo compressors, they can reach higher compression ratios, but compress a smaller amount of gas in the same time span. Their characteristic diagram is defined by volumetric flow Q and the shaft torque M . An example is given in Figure 3.8b. The diagram is less sophisticated than its counterpart of turbo compressors. The volumetric flow a piston compressor can handle is defined by the operating volume V_0 , i.e. the volume which is compressed during one cycle and the speed of the crankshaft which is driving the unit,

$$Q_k = V_{0,k} n_k.$$

It is bounded by the feasible range of the compressor speed $n \in [n^-, n^+]$.

The torque of the shaft M is defined by

$$M_k = \frac{V_{0,k} H_{ad,k}}{2\pi \eta_{ad,k}} \rho_{j-1},$$

where ρ_{j-1} denotes the density of the inflow gas of a compressor in stage j . In case of piston compressors the adiabatic efficiency η_{ad} is a constant parameter of the unit. Depending on the specific piston compressor $k \in \mathcal{U}_j$ and the available technical data, the compression ratio is limited by one of the inequalities

$$\begin{aligned} p_j &\leq \epsilon_k^+ p_{j-1}, \\ p_j &\leq p_{j-1} + \Delta p_k^+, \\ M_k &\leq M_k^+, \end{aligned}$$

using a constant maximum ration ϵ_k^+ , constant maximum pressure increase Δp_k^+ or constant maximum torque M_k^+ .

All compressor units are powered by drives. The correlation of drive d and compressor unit k is defined by the mapping $\sigma(k) = d$. While every compressor has one drive attached, some may share the same drive, i.e. a single drive may power several compressor units. Three different types of drives are presented in the following: gas turbines, gas driven motors and electric motors. Gas turbines and gas driven motors use gas from the network as a power source. They are combined in the set of gas consuming drives, \mathbb{A}_{fuel} . In contrast, electrical motors use electrical power. They build the set of electricity

3.2. A Nonsmooth MINLP Model with ODE Constraints

consuming drives, \mathbb{A}_{el} . The maximum power P_d^+ , that a drive d can deliver, is the upper bound of the combined powers the connected compressor units can consume, i.e.

$$\sum_{k \in \sigma^{-1}(d)} P_k = P_d \leq P_d^+.$$

The maximal power depends on the speed of the drive, which equals the speed of the connected compressors. If several units are connected, their speeds are therefore identical.

Additionally, all types of drives are modeled by a subset of the equations

$$b_d = \psi(P_d; \beta_{b_d}), \quad (3.37)$$

$$P_d^+ = \chi(n_k, T_{\text{amb}}; B_{P_d^+}), \quad (3.38)$$

$$P_d^+ = \psi(n_k; \beta_{P_d^+}), \quad (3.39)$$

where b_d denotes the specific energy consumption rate. Which equations of (3.37) to (3.39) are appropriate for a drive depends on its type.

The model of gas turbines is defined by the specific energy consumption rate b_d , the generated power and a relation between the maximal power P_d^+ , the speed of the compressor n_k , and the constant ambient temperature T_{amb} , thus, gas turbines are modelled by (3.37) and (3.38). Gas driven motors behave like gas turbines except that the maximal power does not depend on the ambient temperature, i.e. they are modelled by (3.37) and (3.39). Electric motors do not consume fuel gas, but electrical power. Depending on the drive the ambient temperature may or may not have an influence on the upper power limit, hence they are modeled either by (3.38) or (3.39).

The fuel which is consumed by a gas driven motor or a gas turbine is calculated via

$$q_d^{\text{fuel}} = \frac{b_d m_a}{H_{u,a}}.$$

H_u denotes the lower calorific value, which is a constant fraction of the calorific value H_c , thus $H_u = cH_c$.

In summary, the model of a compressor group contains descriptions of the inlet and outlet resistors, constraints representing the configurations and a model of the gas cooler. Three additional nodes are introduced to describe the relation between these model aspects: the node $a : 1$ between the inflow resistor and the configurations, node $a : 2$ between the

3. Validation of Nominations

configurations and the outflow resistor, and node $a : 3$ between the outflow resistor and the gas cooler. See the graph of a compressor group in Figure 3.6 for an illustration.

A model of a configuration summarizes the models of all of its stages and links the stage models up. The model of a stage consists of the flow distribution (3.26), constraints modeling the feasible working sets of the corresponding compressor units and their drives, and a mixing equation for the gas temperature leaving the compressor units. The feasible set of a configuration $i \in \mathcal{K}_a$ is thus modeled by a set of constraints

$$\begin{aligned} 0 &= c_{\mathcal{E},a,i}(q_a, p_{a:1}, T_{a:1}, p_{a:2}, T_{a:2}, x_i), \\ 0 &\leq c_{\mathcal{I},a,i}(q_a, p_{a:1}, T_{a:1}, p_{a:2}, T_{a:2}, x_i), \end{aligned}$$

and additional variables required for the intermediate stages denoted by x_i . Inlet and outlet resistors are modeled by

$$\begin{aligned} 0 &= c_a^{\text{resIn}}(q_a, p_{a:1}, p_{a:2}, T_{a:1}, T_{a:2}, x_a^{\text{resIn}}), \\ 0 &= c_a^{\text{resOut}}(q_a, p_{a:2}, p_{a:3}, T_{a:2}, T_{a:3}, x_a^{\text{resOut}}), \end{aligned}$$

for details see the description of the model of a resistor stated in Section 3.2.4.

The compression of the gas leads to an increase in temperature. The temperature may reach a critical level, hence a gas cooler is commonly part of a compressor group. If the outflow temperature of the outlet resistor $T_{a:3}$ exceeds the critical limit $T_{a:v}^+$, the gas cooler is activated to reduce the temperature to a save value,

$$0 = c_a^{\text{cooler}}(p_{a:3}, p_v, T_{a:3}, T_{a:v}) = \begin{pmatrix} p_{a:3} - p_v \\ T_{a:v} - \min(T_{a:3}, T_{a:v}^+) \end{pmatrix}. \quad (3.40)$$

Similar to control valves and valves, a compressor group can be modeled using a big-M-notation, but with a potentially much larger number of discrete variables, since the choice of the active configuration has to be regarded as well. Denote the set of configurations as \mathcal{K}_a and a single configuration by $i \in \mathcal{K}_a$. Then, the discrete variables $z_i \in \{0, 1\}$, $i \in \mathcal{K}_a$, represent the configurations. In addition, the discrete variable $z_{a,\text{open}} \in \{0, 1\}$ represents the choice between open and closed, while the discrete variable $z_{a,\text{active}} \in \{0, 1\}$ represents the choice between active and inactive.

The compressor group is working, when it is open, i.e. $z_{a,\text{open}} = 1$, and active, i.e. $z_{a,\text{active}} = 1$. When the group is in bypass mode, $z_{a,\text{open}} = 1$ and $z_{a,\text{active}} = 0$ hold. A closed group is represented by $z_{a,\text{open}} = 0$ and $z_{a,\text{active}} = 0$. Logically, an active group

cannot be closed. Since the choice of the active configuration is unique, only one of the variables $z_i, i \in \mathcal{K}_a$ differs from zero. In addition, a configuration is only active, when the group is active. By representing the feasible set of a configuration i with $c_{\mathcal{E},a,i}(q_a, p_{a:1}, p_{a:2}, T_{a:1}, T_{a:2})$ and $c_{\mathcal{I},a,i}(q_a, p_{a:1}, p_{a:2}, T_{a:1}, T_{a:2})$ the model of the compressor group a is

$$\begin{aligned}
 0 &\leq z_2 M_a^{\text{resIn}} + c_a^{\text{resIn}}(q_a, p_{a:0}, p_{a:1}, T_{a:0}, T_{a:1}, x_a^{\text{resIn}}), \\
 0 &\leq z_2 M_a^{\text{resIn}} - c_a^{\text{resIn}}(q_a, p_{a:0}, p_{a:1}, T_{a:0}, T_{a:1}, x_a^{\text{resOut}}), \\
 0 &\leq z_2 M_a^{\text{resOut}} + c_a^{\text{resOut}}(q_a, p_{a:2}, p_{a:3}, T_{a:2}, T_{a:3}), \\
 0 &\leq z_2 M_a^{\text{resOut}} - c_a^{\text{resOut}}(q_a, p_{a:2}, p_{a:3}, T_{a:2}, T_{a:3}), \\
 0 &\leq z_2 M_a^{\text{cooler}} + c_a^{\text{cooler}}(p_{a:3}, p_v, T_{a:3}, T_{a:v}), \\
 0 &\leq z_2 M_a^{\text{cooler}} - c_a^{\text{cooler}}(p_{a:3}, p_v, T_{a:3}, T_{a:v}), \\
 0 &\leq z_i M_{a,\mathcal{E},i} + c_{\mathcal{E},a,i}(q_a, p_{a:1}, p_{a:2}, T_{a:1}, T_{a:2}, x_i), \quad \text{for all } i \in \mathcal{K}_a, \\
 0 &\leq z_i M_{a,\mathcal{E},i} - c_{\mathcal{E},a,i}(q_a, p_{a:1}, p_{a:2}, T_{a:1}, T_{a:2}, x_i), \quad \text{for all } i \in \mathcal{K}_a, \\
 0 &\leq z_i M_{a,\mathcal{I},i} - c_{\mathcal{I},a,i}(q_a, p_{a:1}, p_{a:2}, T_{a:1}, T_{a:2}, x_i), \quad \text{for all } i \in \mathcal{K}_a, \\
 0 &\leq z_{a,\text{open}} q_a^+ - q_a, \\
 0 &\leq q_a - z_{a,\text{open}} q_a^-, \\
 0 &\leq q_a - (1 - z_{a,\text{active}}) q_a^-, \\
 0 &\leq z_{a,\text{open}} - z_{a,\text{active}}, \\
 0 &= z_{a,\text{active}} - \sum_{i \in \mathcal{K}_a} z_i.
 \end{aligned}$$

3.2.9. Variable Bounds

Almost all of the introduced quantities possess lower or upper bounds. These bounds results from physical principles, technical restrictions and legal requirements. Technical limitations typically result in stronger bounds than physical principles, e.g. the maximum regulated pressure loss at a control valve is subject to the specific technical capabilities, and the capabilities of compressor units induce lower and upper bounds of the power, specific change in adiabatic enthalpy and volumetric flow. These bounds are chosen according to the specific element.

Other restrictions are introduced for security reasons and legal requirements, e.g. the velocity of gas inside the network is restricted to reduce vibrations which cause noise pollution and may lead to material failure. In addition, regulation agencies define

3. Validation of Nominations

specifications of maximum permitted pressure bounds and their interrelation in connected subnetworks to prevent pipeline ruptures.

Note that even wide physical bounds should be modeled explicitly, since empirical and approximated model aspects may lead to meaningless values, e.g. the natural lower bound of the compressibility factor is zero, but the presented models (3.4) and (3.5) result in negative values for z for physically possible values of pressure and temperature outside the range of validity of the equations.

3.3. Handling Discrete Decisions by Complementarity Constraints

In this section a mathematical program with equilibrium constraints,

$$\min_{x \in \mathbb{R}^n} f(x) \tag{3.41a}$$

$$\text{s.t.} \quad c_{\mathcal{E}}(x) = 0, \quad c_{\mathcal{I}}(x) \geq 0, \tag{3.41b}$$

$$\phi(x) \geq 0, \quad \psi(x) \geq 0, \tag{3.41c}$$

$$\phi(x)^T \psi(x) = 0, \tag{3.41d}$$

is derived based on the model described in Section 3.2. The aim is an approach which determines the decisions for the active network elements fast and reliable. As described in Section 2.1, the objective function $f : \mathbb{R}^n \rightarrow \mathbb{R}$ and constraints $c_i(x) : \mathbb{R}^n \rightarrow \mathbb{R}$ are supposed to be twice continuously differentiable and the variable vector x is an element of \mathbb{R}^n . The model of Section 3.2 has to be adjusted in several points to meet these conditions. The differential equations (3.20) with their continuous variables have to be described by a finite dimensional model. Nonsmooth model aspects, e.g. for resistors and pipes, need to be smoothed and discrete model aspects have to be replaced.

The level of detail is reduced in comparison to Section 3.2. Some of the chosen adjustments are approximative. Furthermore, the model described in this section is isothermal, i.e. the gas temperature T is assumed to be constant, and the gas composition is uniform, i.e. the gas parameters X are globally constant. Besides resulting in a reduced model complexity these decisions avoid the nonsmoothness of the mixing constraints (3.11) and (3.12). The small additional pressure losses occurring in control valve stations and compressor groups are neglected, thus inflow and outflow resistors are not regarded. Stand-alone resistors however are modeled. The main focus of the MPEC approach lies on finding feasible

3.3. Handling Discrete Decisions by Complementarity Constraints

decisions for the active network elements with. The subsequent ValNLP on the other hand will govern the missing physical aspects.

The MPEC approach described in this section consists of two stages, each modeled by its own optimization problem. The first stage is an MPEC strongly based on the 2-state models described in [114]. To this end, characteristic functions χ are introduced to represent the states of the active network elements:

$$\chi_A(x) = 0 \iff \text{all conditions of state } A \text{ are satisfied.}$$

The characteristic functions corresponding to the same network element are coupled by complementarity constraints.

The aim of the first stage is to determine for each active element in the network, whether the element is closed or open. In case of control valves and compressor groups the first stage determines also if the element is active or in bypass, providing that it is open. In a second stage the decisions of the first stage are fixed. An NLP is solved to determine the active configurations of the compressor groups heuristically.

3.3.1. Nodes and Arcs

For every node $u \in \mathbb{V}$ of the network a pressure variable $p_u \in [p_u^-, p_u^+]$ is introduced. Since the MPEC model is isothermal, no temperature variable and no temperature tracking constraints like (3.12) are required. Since the gas composition is assumed to be uniform, parameter mixing based on (3.11) is not necessary either. For the same reason, no temperature variable and variables for gas composition quantities are required for arcs. The vector of variables that are common for all types of arcs x_a^{base} , $a = (u, v) \in \mathbb{A}$, consists solely of the mass flow $q_a \in [q_a^-, q_a^+]$.

The only constraint introduced at a node governs the mass balance (3.10),

$$0 = c^{\text{mass-bal}}(q_{\delta_u}, q_u) = q_u + \sum_{a \in \delta_u^-} q_a - \sum_{a \in \delta_u^+} q_a, \quad (3.42)$$

with q_{δ_u} denoting the vector of mass flows on all incident arcs. The mass flow exchanged at the node q_u is fixed in the NoVa problem according to flow given by the specific

3. Validation of Nominations

nomination $q_u^{\text{ext}} \geq 0$,

$$\begin{aligned} 0 &= c^{\text{flow-fix}}(q_u) = q_u - q_u^{\text{ext}}, & u \in \mathbb{V}_+, \\ 0 &= c^{\text{flow-fix}}(q_u) = q_u + q_u^{\text{ext}}, & u \in \mathbb{V}_-. \end{aligned}$$

The full model of a node u consists of the constraints

$$0 = c_{\mathcal{E},u}(x_{\delta_u}^{\text{base}}, q_u) = \begin{pmatrix} c^{\text{flow-fix}}(q_u) \\ c^{\text{mass-bal}}(q_{\delta_u}, q_u) \end{pmatrix}$$

and the variable $x_u = (q_u, p_u)$.

The model of an arc depends on the type of network device it is representing. In most cases the type-specific model introduces additional variables.

3.3.2. Pipes

The central aspects of the model of a pipe $a = (u, v) \in \mathbb{A}_{\text{pi}}$ in Section 3.2.3 are the differential algebraic equations consisting of the differential equations (3.20) and an equation of state, e.g. (3.7), which couples pressure, temperature and density. In the stationary, isothermal case this model is simplified. The continuity equation (3.20a) implies a constant flow on the arc which is governed by the variable of the mass flow on the arc. The energy equation (3.20c) is not necessary, since the model is isothermal. The remaining momentum equation is replaced by a nonlinear approximation. Using nonlinear approximations of the momentum equation has a long history in gas engineering, so several suitable and field-tested formulations are given in the literature [85].

Under the assumption of an isothermal, stationary gas model and mean compressibility $z_{m,a}$, the solution of the momentum equation of a sloped pipe is approximated by the equation

$$0 = p_v^2 - \left(p_u^2 - \Lambda_a(z_{m,a}) \lambda_a(q_a) |q_a| q_a \frac{e^{S_a(z_{m,a})} - 1}{S_a(z_{m,a})} \right) e^{-S_a(z_{m,a})}, \quad (3.43)$$

where Λ_a and S_a are defined by

$$\begin{aligned} \Lambda_a(z_{m,a}) &= \frac{L_a}{A_a^2 D_a} \frac{z_{m,a} T R}{m}, \\ S_a(z_{m,a}) &= 2 \frac{g L_a s_a m}{z_{m,a} T R}, \end{aligned}$$

3.3. Handling Discrete Decisions by Complementarity Constraints

cf. [5, 80]. In case of a horizontal pipe, the equation simplifies to

$$0 = p_v^2 - (p_u^2 - \Lambda_a(z_{m,a})\lambda_a(q_a)|q_a|q_a).$$

Both depend on the constant molar mass m , the constant temperature T , the universal gas constant R and a mean compressibility factor $z_{m,a}$. The compressibility factor is based on a mean pressure $p_{m,a}$ and the AGA formula (3.4),

$$c^{z\text{-mean}}(z_{m,a}, p_{m,a}) = z_{m,a} - z^{\text{AGA}}(p_{m,a}, T, p_c, T_c).$$

Since the gas composition is uniform, the pseudocritical pressure p_c and pseudocritical temperature T_c are constant.

In the MPEC approach, the mean pressure is defined by

$$c^{\text{p-mean}}(p_u, p_v, p_{m,a}) = p_{m,a} - \frac{2}{3} \left(p_u + p_v - \frac{p_u p_v}{p_u + p_v} \right).$$

See [85] for this equation and some alternatives.

By using equation (3.43), the momentum equation is successfully replaced by a nonlinear equation. However, the friction term $\lambda_a(q_a)$ is not continuous for the transition between laminar and turbulent flow, as long as it is based on the models described in Section 3.2.3. In addition, the term $|q_a|q_a$ is nonsmooth for zero flow. Hence, the term $\lambda_a|q_a|q_a$ is replaced by a smooth friction approximation $\phi_a(q_a)$, based on the law of Hagen–Poiseuille (3.13) and the equation of Colebrook–White (3.14). This approximation has originally been developed for water networks [17, 18], but applies also to gas networks [115]. The corresponding constraint reads

$$0 = c_a^{\text{sfa}}(\phi_a, q_a) = \phi_a - q_a \tilde{\lambda}_a \left(\sqrt{q_a^2 + e_a^2} + b_a + \frac{c_a}{\sqrt{q_a^2 + d_a^2}} \right), \quad (3.44)$$

$$\begin{aligned} \tilde{\lambda}_a &= (2 \log_{10} \beta_a)^{-2}, & b_a &= 2\delta_a, & c_a &= (\ln \beta_a + 1)\delta_a^2 - \frac{e_a^2}{2}, \\ \alpha_a &= \frac{2.51A_a\eta}{D_a}, & \beta_a &= \frac{k_a}{3.71D_a}, & \delta_a &= \frac{2\alpha_a}{\beta_a \ln 10}. \end{aligned}$$

The approximation (3.44) is asymptotically correct for $|q| \rightarrow \infty$ and the two smoothing parameters d_a, e_a have to be positive [18].

3. Validation of Nominations

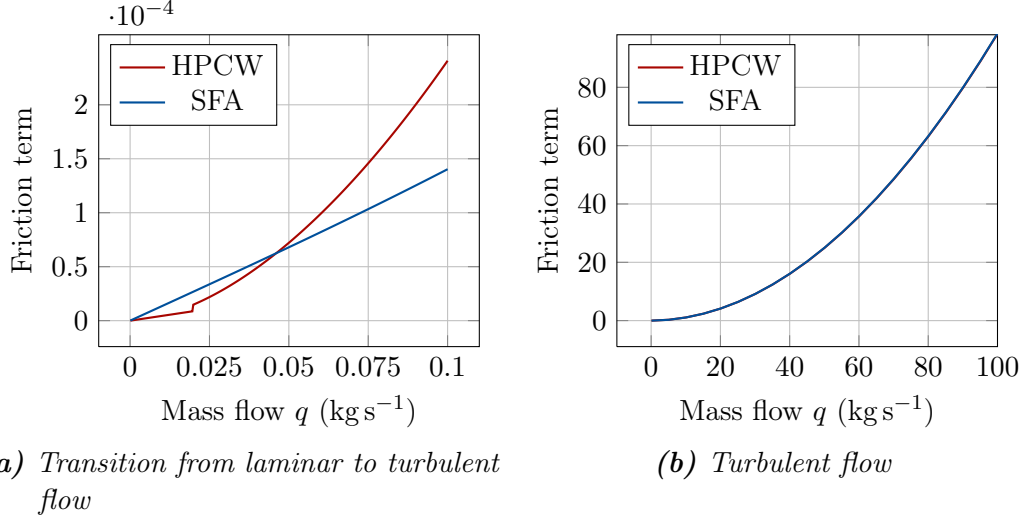


Figure 3.9. Friction term $\lambda(q)|q|q$ according to Hagen–Poiseuille and Colebrook–White (HPCW) and smooth approximation $\phi(q)$ (SFA) vs. mass flow q in kg s^{-1}

Figure 3.9 illustrates the graphs of the nonsmooth friction model and the smooth approximation. The smoothing of the nonsmooth transition between laminar and turbulent flows results in a small deviation for tiny mass flows, but the smooth friction approximation converges fast against the values of the Colebrook–White formula, so that there is no visible difference in Figure 3.9b.

Applying the smooth friction approximation yields the smooth pressure loss constraint

$$c_a^{\text{mom-approx}}(p_u, p_v, \phi_a, z_{m,a}) = p_v^2 - \left(p_u^2 - \Lambda_a(z_{m,a})\phi_a \frac{e^{S_a(z_{m,a})} - 1}{S_a(z_{m,a})} \right) e^{-S_a(z_{m,a})}$$

in case of a sloped pipe and

$$c_a^{\text{mom-approx}}(p_u, p_v, \phi_a, z_{m,a}) = p_v^2 - (p_u^2 - \Lambda_a(z_{m,a})\phi_a)$$

otherwise. Finally, the complete pipe model is given by

$$c_{\mathcal{E},a}(x_u, x_v, x_a) = \begin{pmatrix} c_a^{\text{mom-approx}}(p_u, p_v, \phi_a, z_{m,a}) \\ c_a^{\text{sfa}}(\phi_a, q_a) \\ c^{\text{p-mean}}(p_u, p_v, p_{m,a}) \\ c^{\text{z-mean}}(z_{m,a}, p_{m,a}) \end{pmatrix},$$

$$x_a = (x_a^{\text{base}}, \phi_a, z_{m,a}, p_{m,a}).$$

3.3.3. Resistors

Both resistor models presented in Section 3.2.4 have to be sufficiently smoothed for the desired MPEC model, since they contain first and second order discontinuities. The resistor model with linear pressure loss (3.21) contains the discontinuous sign function, the nonlinear pressure loss model (3.22) contains the second-order discontinuous term $|q_a|q_a$ and the inflow density required in model (3.22) depends on the flow direction through the resistor.

Since $\text{sign}(q_a) = q_a/|q_a|$, a smooth approximation of the absolute value function resolves the first two discontinuities. An appropriate smoothing is $|x| \approx \sqrt{x + \epsilon}$ with a smoothing parameter $\epsilon > 0$. The impact of different values of ϵ on the smoothing function is illustrated in Figure 3.10. For decreasing ϵ , the quality of the smoothing improves, but in case of the sign-function, the derivation in the origin increases fast and in case of the absolute value, the second derivation increases.

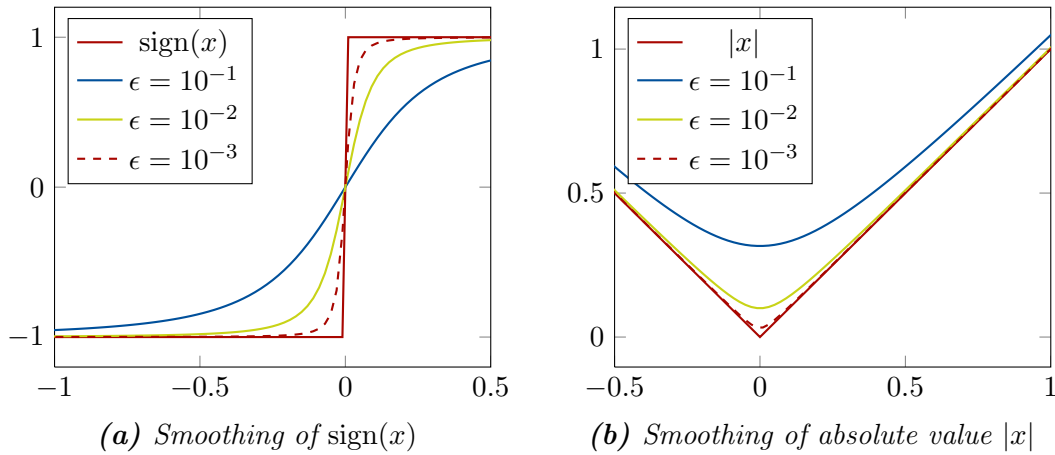


Figure 3.10. Smoothings of sign and the absolute value for some values of ϵ

The smoothed linear pressure loss model is expressed by the constraint

$$0 = c_{\mathcal{E},a}(x_u, x_v, x_a) = p_u - p_v - \frac{q_a}{\sqrt{q_a + \epsilon}} \xi_a.$$

No additional variables are required, thus $x_a = x_a^{\text{base}}$.

The nonlinear pressure loss equation (3.22) of $a = (u, v)$ requires the inflow density ρ_a^{in} . Since the flow direction is usually unknown a priori, it is unclear whether the inflow

3. Validation of Nominations

density corresponds to the density at the tail $\rho_{a:u}$ or to the density at the head ρ_v . Hence, the inflow density is replaced by a mean density $\rho_{m,a}$, which is defined by the constraint

$$0 = c^{\text{d-mean}}(\rho_{m,a}, \rho_{a:u}, \rho_{a:v}) = 2\rho_{m,a} - (\rho_{a:u} + \rho_{a:v}).$$

The densities at the head and tail of the resistor are computed via the equation of state (3.7). The AGA formula (3.4) is chosen for the required compressibility factors. This leads to the constraints

$$\begin{aligned} 0 &= c^{\text{d-tail}}(\rho_{a:u}, z_{a:u}, p_u) = \rho_{a:u} z_{a:u} RT - p_u m, \\ 0 &= c^{\text{d-head}}(\rho_{a:v}, z_{a:v}, p_v) = \rho_{a:v} z_{a:v} RT - p_v m, \\ 0 &= c^{\text{z-tail}}(z_{a:u}, p_u) = z_{a:u} - z^{\text{AGA}}(p_u, T, p_c, T_c), \\ 0 &= c^{\text{z-head}}(z_{a:v}, p_v) = z_{a:v} - z^{\text{AGA}}(p_v, T, p_c, T_c). \end{aligned}$$

Combining the smoothing of the absolute value and the mean density with the pressure loss equation (3.22) results in the pressure loss constraint

$$0 = c_a^{\text{p-loss}}(q_a, p_u, p_v, \rho_{m,a}) = p_u - p_v - \frac{8\zeta_a}{\pi^2 D_a^4} \frac{q_a \sqrt{q_a^2 + \epsilon}}{\rho_{m,a}},$$

which is sufficiently smooth and independent of the flow direction. In summary, the nonlinear pressure loss model of the resistor $a = (u, v)$ consists of the constraints

$$0 = c_{\mathcal{E},a}(x_u, x_v, x_a) = \begin{pmatrix} c^{\text{d-mean}}(\rho_{m,a}, \rho_{a:u}, \rho_{a:v}) \\ c^{\text{d-tail}}(\rho_{a:u}, z_{a:u}, p_u) \\ c^{\text{d-head}}(\rho_{a:v}, z_{a:v}, p_v) \\ c^{\text{z-tail}}(z_{a:u}, p_u) \\ c^{\text{z-head}}(z_{a:v}, p_v) \\ c_a^{\text{p-loss}}(q_a, p_u, p_v, \rho_{m,a}) \end{pmatrix},$$

and the variable vector $x_a = (x_a^{\text{base}}, \rho_{m,a}, \rho_{a:u}, \rho_{a:v}, z_{a:u}, z_{a:v})$.

3.3.4. Valves and Shortcuts

The model of a valve given in Section 3.2.5 contains a discrete variable, which defines the state of a valve $a = (u, v)$. The two possible states are open and closed. Based on the properties stated in Table 3.1, the appropriate characteristic functions are easily

3.3. Handling Discrete Decisions by Complementarity Constraints

derived:

$$\chi_{\text{active}}(p_u, p_v) = p_u - p_v, \quad (3.45)$$

$$\chi_{\text{closed}}(q_a) = q_a. \quad (3.46)$$

Thus, the mixed-integer model of a valve is equivalently reformulated into

$$\begin{aligned} 0 = c_{\mathcal{C},a}(x_u, x_v, x_a) &= \chi_{\text{active}}(p_u, p_v)\chi_{\text{closed}}(q_a), \\ x_a &= x_a^{\text{base}}. \end{aligned}$$

No additional equality or inequality constraints besides the complementarity constraint are necessary.

The model of a shortcut $a = (u, v)$ equals the model of an open valve, i.e.

$$0 = c_{\mathcal{E},a}(x_u, x_v, x_a) = p_u - p_v.$$

No additional variables are required, thus $x_a = x_a^{\text{base}}$.

3.3.5. Control Valves

In Section 3.2.7 two types of control valves are introduced. Both types have the three possible states closed, active and bypass. In the MPEC approach, these states are represented by characteristic functions and the decision process is modeled by complementarity constraints based on the properties stated in Table 3.2 and Table 3.3. The resistors of a control valve station are not regarded in the MPEC approach, thus the control valve directly connects the nodes u and v . Since the temperature is a global constant, a model of the gas preheater is not required.

A closed control valve with remote access interrupts the flow on the arc. The characteristic function is

$$\chi_{\text{closed}}(q_a) = q_a.$$

For an open control valve, the pressure at the tail p_u , the pressure at the head p_v and the non-negative pressure reduction Δp_a at the control valve are related by $p_v = p_u - \Delta p_a$. Consequently, the characteristic function reads

$$\chi_{\text{open}}(p_u, p_v, \Delta p_a) = p_v - p_u + \Delta p_a.$$

3. Validation of Nominations

Whether an open control valve is active or bypassed depends on the flow direction and the pressure reduction $\Delta p_a \geq 0$. If the reduction is positive, the control valve is active, otherwise it is bypassed. An active element can work only in arc direction, i.e.

$$\Delta p_a q_a \geq 0.$$

The full model of a control valve with remote access is

$$0 = c_{\mathcal{C},a}(x_u, x_v, x_a) = \chi_{\text{open}}(p_u, p_v, \Delta p_a) \chi_{\text{closed}}(q_a), \quad (3.47a)$$

$$0 \leq c_{\mathcal{I},a}(x_u, x_v, x_a) = \Delta p_a q_a, \quad (3.47b)$$

$$x_a = (x_a^{\text{base}}, \Delta p_a). \quad (3.47c)$$

Besides the complementarity constraint, no additional equality constraints are necessary. Note that this model is equivalent to an isothermal version of (3.25), only when the inlet and outlet resistors cause no additional pressure loss and the lower bound of the pressure reduction in the MINLP model is zero. Available real-world data never contained a strictly positive lower bound, thus the requirement $\Delta p_a^- = 0$ is not considered to be too restrictive.

A control valve without remote access is more difficult to model, since the state depends on the pressures at the head and tail and their relation to a threshold p_{set} .

Based on the properties stated in Table 3.3, characteristic functions of the states active, bypass and closed are

$$\chi_{\text{active}}(p_u, p_v, q_a) = \min(0, p_u - p_{\text{set},a}) - \min(0, q_a) - (p_v - p_{\text{set},a})^2, \quad (3.48a)$$

$$\chi_{\text{bypass}}(p_u, p_v) = \max(0, p_u - p_{\text{set},a}) - (p_u - p_v)^2, \quad (3.48b)$$

$$\chi_{\text{closed}}(p_v, q_a) = \min(0, p_v - p_{\text{set},a}) - q_a^2. \quad (3.48c)$$

The nonsmoothness introduced by the min and max functions has to be eliminated before these characteristic functions can be used in an MPEC model. A possible way is to use the smoothing functions

$$\min(0, x) \approx \frac{1}{2} \left(x - \sqrt{x^2 + \xi} \right), \quad (3.49)$$

$$\max(0, x) \approx \frac{1}{2} \left(x + \sqrt{x^2 + \xi} \right). \quad (3.50)$$

Applying these approximations on the characteristic functions leads to the smoothed characteristic functions χ_{active}^s , χ_{bypass}^s and χ_{closed}^s . With these functions the model of a

3.3. Handling Discrete Decisions by Complementarity Constraints

control valve without remote control is

$$0 = c_{\mathcal{E},a}(x_u, x_v, x_a) = x_a^{ab} - \chi_{\text{active}}^s(p_u, p_v, q_a) \chi_{\text{bypass}}^s(p_u, p_v), \quad (3.51a)$$

$$0 = c_{\mathcal{C},a}(x_u, x_v, x_a) = x_a^{ab} \chi_{\text{closed}}^s(q_a), \quad (3.51b)$$

$$x_a = \left(x_a^{\text{base}}, x_a^{ab} \right). \quad (3.51c)$$

No inequality constraints are required. Alternatively, a variable splitting

$$x = x^+ - x^-, \quad x^+ x^- = 0, \quad x^+, x^- \geq 0,$$

can be used. The minimum and maximum functions in (3.48) are then represented by $\min(0, x) = -x^-$ and $\max(0, x) = x^+$. In contrast to the smoothed model (3.51), this reformulation is exact, but introduces additional complementarity constraints.

A third approach uses also complementarity constraints, but does not model the characteristic functions of the states explicitly. Instead, addition inequalities ensure the properties stated in Table 3.3. To this end, the pressure related quantities

$$\Delta p_a = p_u - p_v, \quad \tilde{p}_a = p_v - p_{\text{set},a}, \quad \hat{p}_a = \Delta p_a q_a$$

are defined. A control valve without remote control is then modeled by

$$0 = c_{\mathcal{E},a}(x_u, x_v, x_a) = \begin{pmatrix} \Delta p_a - p_u + p_v \\ \tilde{p}_a - p_v + p_{\text{set},a} \\ \hat{p}_a - \Delta p_a q_a \end{pmatrix},$$

$$0 = c_{\mathcal{C},a}(x_u, x_v, x_a) = \hat{p}_a \tilde{p}_a$$

$$0 \leq c_{\mathcal{I},a}(x_u, x_v, x_a) = \begin{pmatrix} -q_a^2 \tilde{p}_a \\ \Delta p_a^2 \tilde{p}_a \\ q_a^2 \Delta p_a \end{pmatrix},$$

$$x_a = \left(x_a^{\text{base}}, \Delta p_a, \tilde{p}_a, \hat{p}_a \right).$$

This model choice contains only a single complementarity constraint $\hat{p}_a \tilde{p}_a = 0$ per control valve.

3. Validation of Nominations

3.3.6. Compressor Groups

The basic decision, whether a compressor group $a = (u, v)$ open, i.e. actively compressing or in bypass, or closed is modeled similarly to a control valve with remote control. The only difference is the direction of the pressure change $\Delta p_a \geq 0$ caused by the element. Hence, the characteristic function of a closed compressor group is

$$\chi_{\text{closed}}(q_a) = q_a,$$

the characteristic function of the open state reads

$$\chi_{\text{open}}(p_u, p_v, \Delta p_a) = p_v - p_u - \Delta p_a,$$

and the complete model of a compressor group is

$$0 = c_{\mathcal{E},a}(x_u, x_v, x_a) = \chi_{\text{open}}(p_u, p_v, \Delta p_a)\chi_{\text{closed}}(q_a), \quad (3.52a)$$

$$0 \leq c_{\mathcal{I},a}(x_u, x_v, x_a) = \Delta p_a q_a, \quad (3.52b)$$

$$x_a = (x_a^{\text{base}}, \Delta p_a). \quad (3.52c)$$

3.3.7. Complete MPEC Model

An MPEC model is derived from the descriptions given in Section 3.2 by smoothing and approximating some model aspects and reformulating discrete decisions as complementarity constraints. The differential algebraic model of pipes is replaced by a smooth approximation of the pressure loss and the descriptions of resistors are smoothed as is the model of a control valve station without remote access in one of the presented model variants. All these techniques lead to the following existence problem with complementarity constraints $c_{\mathcal{C},a}$

$$\exists? x \quad (3.53a)$$

$$\text{s.t. } c_{\mathcal{E},a}(x) = 0, \quad a \in \mathbb{A}, \quad (3.53b)$$

$$c_{\mathcal{I},a}(x) \geq 0, \quad a \in \mathbb{A}_{\text{cg}} \cup \mathbb{A}_{\text{cv}}, \quad (3.53c)$$

$$c_{\mathcal{C},a}(x) = 0, \quad a \in \mathbb{A}_{\text{cg}} \cup \mathbb{A}_{\text{cv}} \cup \mathbb{A}_{\text{vl}}, \quad (3.53d)$$

$$x \in [x^-, x^+]. \quad (3.53e)$$

The variable vector x consists of the arc and node variables $x_{\mathbb{A}}$ and $x_{\mathbb{V}}$.

3.3. Handling Discrete Decisions by Complementarity Constraints

Some complementarity constraints are not of type Equation 2.3d, but at least one of the incorporated functions has a nonzero lower bound or no lower bound at all. If these constraints are biactive or one of ϕ and ψ has the lower bound zero and is active, LICQ and MFCQ are violated. In contrast to the complementarity constraints governed in Section 2.2, this is not the case for every feasible point. However, since the model of the bypass mode of compressor groups and control valves is one of the problematic constellations, both constraint qualifications will be violated with high probability in the optimal solution for realistic network situations.

Besides complementarity constraints, the MPEC (3.53) contains inequality constraints of the form

$$\phi(x)\psi(x) \geq 0, \quad \phi(x) \geq 0. \quad (3.54)$$

Although these are no classical complementarity constraints, they yield similar problems. If the inequality is active for a feasible point x^* because $\phi(x^*) = 0$ holds, LICQ is not satisfied in x^* . These constraints occur in the model of compressor groups (3.52) and control valve stations (3.47). The problematic constellation relates to the bypass mode of both types of network elements and is expected to happen frequently. If in addition $\psi(x)$ is also active, i.e. the inequality constraint $\phi(x)\psi(x) \geq 0$ is biactive, MFCQ is violated also.

3.3.8. An Heuristic to Determine Active Configurations

Solving problem (3.53) results in a description of the stationary flow and pressure distribution in the gas network. The values of the variables coupled by complementarity constraints are translated into decisions whether the valves, control valves and compressor groups are open, closed or bypassed. Still, information about the active configurations is not part of the solution of (3.53). The active configurations are determined in a second stage. Here, an additional optimization problem of the network is solved. The passive network elements pipes, resistors and shortcuts are modeled as in (3.53). Control valves, valves and closed or bypassed compressor groups (denoted by $\mathbb{A}_{\text{cg}}^{\text{inactive}}$) are fixed to the state given by the solution of (3.53), i.e. their model is condensed to the decided state without any complementarity constraints, yielding

$$0 = c_{\mathcal{E},a}^{\text{fix}}(x), \quad a \in \mathbb{A}_{\text{vl}} \cup \mathbb{A}_{\text{cv}} \cup \mathbb{A}_{\text{cg}}^{\text{inactive}}.$$

For compressor groups that are decided as active, a heuristic models the decision between the configurations.

3. Validation of Nominations

The configurations are essentially modeled as in Section 3.2.8. The heuristic described in the following adds all configurations to a compressor group as shown in Figure 3.11.

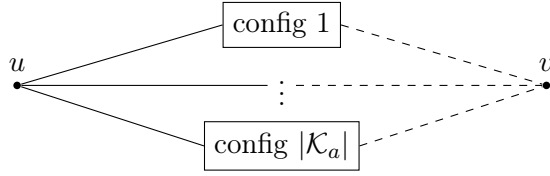


Figure 3.11. Schematic idea of the compressor group heuristic

Inflow and outflow resistors are omitted and a gas cooler is not required since the temperature is constant. The inlet pressure of each configuration equals the inlet pressure of the compressor group p_u and the flow through each configuration equals the flow on the arc of the group q_a . The outlet pressure p_v is a convex combination of the outlet pressures of the configurations $p_{\mathcal{K}_a}^{\text{out}}$,

$$0 = c^{\text{coupl}}(p_v, p_{\mathcal{K}_a}^{\text{out}}, \sigma_{\mathcal{K}_a}) = \begin{pmatrix} p_v - \sum_{i \in \mathcal{K}_a} \sigma_i p_i^{\text{out}} \\ 1 - \sum_{i \in \mathcal{K}_a} \sigma_i \end{pmatrix}. \quad (3.55)$$

A configuration $i \in \mathcal{K}_a$ consists of $|\mathcal{S}_i|$ stages and each stage in turn contains $|\mathcal{U}_j| \geq 1$ parallel compressor units.

The models of the compressors in stage $j \in \mathcal{S}_i$ of configuration $i \in \mathcal{K}_a$ require an inlet pressure p_{j-1} , an inlet density variable ρ_{j-1} and a variable for the compressibility factor of the inflow gas z_{j-1} . The inlet pressure of the first stage of every configuration is identified with the pressure p_u . These three quantities are coupled by the AGA formula (3.4),

$$0 = c^z(z_{j-1}, p_{j-1}) = z_{j-1} - z^{\text{AGA}}(p_{j-1}, T, p_c, T_c),$$

and the equation of state

$$0 = c^{\text{eos}}(\rho_{j-1}, z_{j-1}, p_{j-1}) = \rho_{j-1} z_{j-1} RT - p_{j-1} m.$$

In addition, the model of a single stage $j \in \mathcal{S}_i$ is build up by the models of the contained

3.3. Handling Discrete Decisions by Complementarity Constraints

compressor units and a flow distribution constraint, i.e.

$$\begin{aligned} 0 &= c_{\mathcal{E},j}(x_a^{\text{base}}, x_{j-1}, x_j, x_{\mathcal{U}_j}) = \left(\begin{array}{c} c_j^{\text{flow-dist}}(q_a, q_{\mathcal{U}_j}) \\ (c_{\mathcal{E},k}(x_a^{\text{base}}, x_{j-1}, x_j, x_k))_{k \in \mathcal{U}_j} \end{array} \right), \\ 0 &\leq c_{\mathcal{I},j}(x_a^{\text{base}}, x_{j-1}, x_j, x_{\mathcal{U}_j}) = \left(c_{\mathcal{I},k}(x_a^{\text{base}}, x_{j-1}, x_j, x_k) \right)_{k \in \mathcal{U}_j}. \end{aligned}$$

Here, $k \in \mathcal{U}_j$ denotes a compressor unit of stage $j \in \mathcal{S}_i$. The flow through the compressor group is distributed between these parallel compressor units,

$$0 = c_j^{\text{flow-dist}}(q_a, q_{\mathcal{U}_j}) = q_a - \sum_{k \in \mathcal{U}_j} q_k. \quad (3.56)$$

The feasible operating ranges displayed in Figure 3.8 are modeled in detail for both types of compressor units. Both diagrams are defined in volumetric flow, which is gained from the mass flow via the constraint

$$0 = c^{\text{volconv}}(Q_k, q_k, \rho_{j-1}) = \rho_{j-1} Q_k - q_k.$$

The specific change in adiabatic enthalpy $H_{ad,k}$ of a compressor $k \in \mathcal{U}_j$ of either type is defined by the constraint

$$0 = c^{\text{adiabatic}}(H_{ad,k}, p_{j-1}, p_j, z_{j-1}) = H_{ad,k} - z_{j-1} T \frac{R}{m} \frac{\kappa}{\kappa - 1} \left(\left(\frac{p_j}{p_{j-1}} \right)^{(\kappa-1)/\kappa} - 1 \right).$$

The isentropic exponent κ is set to the constant value 1.29. The power P_k required for increasing the pressure depends on the mass flow q_k through the unit $k \in \mathcal{U}_j$, the specific change in adiabatic enthalpy $H_{ad,k}$ and the adiabatic efficiency $\eta_{ad,k}$:

$$c^{\text{power}}(P_k, q_k, H_{ad,k}, \eta_{ad,k}) = P_k \eta_{ad,k} - q_k H_{ad,k}.$$

A turbo compressor is modeled by the speed isolines

$$0 = c^{\text{speed}}(H_{ad,k}, Q_k, n_k) = H_{ad,k} - \chi(Q_k, n_k; B_{H_{ad,k}}),$$

the efficiency isolines

$$0 = c^{\text{eff}}(\eta_{ad,k}, Q_k, n_k) = \eta_{ad,k} - \chi(Q_k, n_k; B_{\eta_{ad,k}}),$$

3. Validation of Nominations

the surpline

$$0 \leq c^{\text{surge}}(Q_k, H_{ad,k}) = \psi(Q_k, b_{s,k}) - H_{ad,k},$$

and the choke line

$$0 \leq c^{\text{choke}}(Q_k, H_{ad,k}) = H_{ad,k} - \psi(Q_k, b_{c,k}).$$

In summary, the complete model of a turbo compressor k reads

$$\begin{aligned} 0 &= c_{\mathcal{E},k}(x_a^{\text{base}}, x_{j-1}, x_j, x_k) \\ &= \begin{pmatrix} c^{\text{volconv}}(Q_k, q_k, \rho_{j-1}) \\ c^{\text{adiabatic}}(H_{ad,k}, p_{j-1}, p_j, z_{j-1}) \\ c^{\text{power}}(P_k, q_k, H_{ad,k}, \eta_{ad,k}) \\ c^{\text{speed}}(H_{ad,k}, Q_k, n_k) \\ c^{\text{eff}}(\eta_{ad,k}, Q_k, n_k) \end{pmatrix}, \\ 0 &\leq c_{\mathcal{I},k}(x_{j-1}, x_j, x_k) = \begin{pmatrix} c^{\text{surge}}(Q_k, H_{ad,k}) \\ c^{\text{choke}}(Q_k, H_{ad,k}) \end{pmatrix}, \end{aligned}$$

with the vector of variables

$$x_k = (Q_k, q_k, P_k, H_{ad,k}, \eta_{ad,k}, n_k).$$

The model of a piston compressor requires a constraint for the operated volumetric flow,

$$0 = c^{\text{vol}}(Q_k, n_k) = Q_k - V_{0,k} n_k,$$

and a constraint defining the shaft torque M_k ,

$$0 = c^{\text{torque}}(\rho_{j-1}, M_k, H_{ad,k}) = M_k - \frac{V_{0,k} H_{ad,k}}{2\pi \eta_{ad,k}} \rho_{j-1}.$$

Here, the adiabatic efficiency $\eta_{ad,k}$ is a constant parameter.

Depending on the specific machine and the available technical data, the compression ratio

3.3. Handling Discrete Decisions by Complementarity Constraints

is limited in one of the following ways:

$$0 \leq c^{\text{limit}}(p_{j-1}, p_j, M_k) = \begin{cases} \varepsilon^+ - p_j/p_{j-1}, \\ p_{j-1} - p_j + \Delta p^+, \\ M_k^+ - M_k. \end{cases}$$

Here ε^+ denotes an upper limit on the compression ratio, Δp^+ an upper limit on the pressure increase and M_k^+ an upper torque limit.

A piston compressor is thus modeled by the constraints

$$0 = c_{\mathcal{E},k}(x_a^{\text{base}}, x_{j-1}, x_j, x_k) = \begin{pmatrix} c^{\text{volconv}}(Q_k, q_k, \rho_{j-1}) \\ c^{\text{adiabatic}}(H_{ad,k}, p_{j-1}, p_j, z_{j-1}) \\ c^{\text{power}}(P_k, q_k, H_{ad,k}, \eta_{ad,k}) \\ c^{\text{torque}}(\rho_{j-1}, M_k, H_{ad,k}) \\ c^{\text{vol}}(Q_k, n_k) \end{pmatrix},$$

$$0 \leq c_{\mathcal{I},k}(x_{j-1}, x_j, x_k) = c^{\text{limit}}(p_{j-1}, p_j, M_k),$$

and the variables

$$x_k = (Q_k, q_k, P_k, H_{ad,k}, M_k, n_k).$$

Thus, the feasible set \mathcal{F}_i of a configuration $i \in \mathcal{K}_a$ is modeled by the constraints

$$0 = c_{\mathcal{E},i}(x_a^{\text{base}}, x_u, x_i) = \left(c_{\mathcal{E},i}(x_a^{\text{base}}, x_{j-1}, x_j, x_{\mathcal{U}_j}) \right)_{j \in \mathcal{S}_i}$$

$$0 \leq c_{\mathcal{I},i}(x_a^{\text{base}}, x_u, x_i) = \left(c_{\mathcal{I},i}(x_a^{\text{base}}, x_{j-1}, x_j, x_{\mathcal{U}_j}) \right)_{j \in \mathcal{S}_i},$$

and the variable vector

$$x_i = \left(x_{\mathcal{S}_i}, (x_{\mathcal{U}_j})_{j \in \mathcal{S}_i} \right).$$

The predecessor of the first stage is identified with the node u and its associated variables.

Since the configurations of a compressor group are designed to cover a large range of possible situations, their feasible sets have little in common. Hence, with high probability there exists no point x which is feasible for all configurations, so at least one constraint of a configuration is violated. This renders the whole optimization problem infeasible.

To resolve this problem, the constraints of the feasible set of a configuration \mathcal{F}_i are relaxed

3. Validation of Nominations

by the variable vectors $s_{\mathcal{E},i}^+, s_{\mathcal{E},i}^-, s_{\mathcal{I},i}^+ \geq 0$,

$$\begin{aligned} 0 &= \tilde{c}_{\mathcal{E},i}(x_a^{\text{base}}, x_u, x_i) = c_{\mathcal{E},i}(x_a^{\text{base}}, x_u, x_i) + s_{\mathcal{E},i}^+ - s_{\mathcal{E},i}^-, \\ 0 &\leq \tilde{c}_{\mathcal{I},i}(x_a^{\text{base}}, x_u, x_i) = c_{\mathcal{I},i}(x_a^{\text{base}}, x_u, x_i) + s_{\mathcal{I},i}^+, \end{aligned}$$

and the sum of the relaxation variables is minimized in the objective of the second MPEC stage. The model of a compressor group in stage two of the MPEC approach is finally stated as follows:

$$\begin{aligned} 0 &= c_{\mathcal{E},a}(x_u, x_v, x_a) = \left(c^{\text{coupl}}(p_v, p_{\mathcal{K}_a}^{\text{out}}, \sigma_{\mathcal{K}_a}) \right), \\ 0 &\leq c_{\mathcal{I},a}(x_u, x_v, x_a) = \tilde{c}_{\mathcal{I},\mathcal{K}_a}(x_a^{\text{base}}, x_u, x_i). \end{aligned}$$

The resulting problem of the second MPEC stage

$$\min \sum_{i \in \mathcal{K}_a} \sum_{i \in \mathcal{E}} \sum_{j \in \mathcal{I}} s_{i,i}^+ + s_{i,i}^- + s_{i,i}^+ \quad (3.57a)$$

$$\text{s.t. } c_{\mathcal{E},a}(x) = 0, \quad a \in \mathbb{A}, \quad (3.57b)$$

$$c_{\mathcal{I},a}(x) \geq 0, \quad a \in \mathbb{A}_{\text{cg}} \cup \mathbb{A}_{\text{cv}}, \quad (3.57c)$$

$$x \in [x^-, x^+], \quad (3.57d)$$

does not contain any complementarity constraints. Thus, (3.57) is a standard NLP. Its solution is analyzed and based on the sum of relaxation variables $s_{\mathcal{E},i}^+, s_{\mathcal{E},i}^-, s_{\mathcal{I},i}^+$ and the values of the coefficients σ_i a configuration is selected as the active one for each compressor group.

An alternative approach to the described heuristic extracts each compressor group from the gas network and fixes the flow on the arc and the pressures at the head and the tail according to the solution of (3.53). While the MINLP model described in Section 3.2.8 is too difficult to solve on large networks, first promising results have been gained on single compressor groups, see Section 4.1. Solving each compressor group by a small MINLP has the advantage that no heuristic interpretation of relaxation variables and convex coefficients is required. On the other hand the compressor groups are decoupled from the other network elements. The fixed pressure and flow values gained from the simplistic compressor model of the first stage of the MPEC approach may lead to an infeasible MINLP model of a compressor group despite the fact that the MINLP may be feasible under slight changes of the fixed values. Net-wide interactions cannot be

regarded when the compressor groups are solved separately. To generate proposals for active configurations anyway, a relaxation scheme could be applied on the small MINLPs, in the hope that the ValNLP of the following section will compensate minor violations with the help of other network elements.

3.4. High Accuracy Optimization (ValNLP)

Successfully applying the MPEC approach results in discrete decisions for the active network elements and an approximative description of the gas flow inside the network. However, several physical aspects are simplified or neglected at all, like gas temperature or gas composition. The applied approximations and smoothing techniques reduce the level of detail further.

To compensate the reduction of accuracy, a highly detailed NLP model is created based on the solution of the MPEC approach and the model descriptions in Section 3.2. The resulting optimization problem

$$\begin{aligned} \min_{x \in \mathbb{R}^n} \quad & f(x) \\ \text{s.t.} \quad & c_{\mathcal{E}}(x) = 0 \\ & c_{\mathcal{I}}(x) \geq 0 \end{aligned}$$

requires twice continuously differentiable functions f , $c_{\mathcal{E}}$ and $c_{\mathcal{I}}$ and an finite dimensional vector of variables x . Thus, the preconditions are equivalent to the MPEC (3.41), as are the necessary adjustments of the MINLP: The differential equations (3.20) and nonsmooth model aspects have to be replaced by a smooth, finite dimensional model, and discrete model aspects have to be replaced. Latter is achieved by fixing the discrete model aspects a priori according to the solution of the MPEC approach.

While the model requirements of the ValNLP and the MPEC approach are similar, the adjustments of the MINLP model are quite different. Since the discrete aspects are given, the main focus lies on a extensive consideration of the physics and technical descriptions. The sections 3.4.1 through 3.4.8 describe the relating mathematical models. The structure is similar to Section 3.2.1. Where applicable, different model variants are incorporated. This actually results in a family of models for the ValNLP, so the user can choose his desired trade-off between computation time and accuracy. Section 3.4.8 summarizes all aspects in the ValNLP.

3. Validation of Nominations

If the ValNLP converged to a (local) optimum, the solution of the MPEC approach is confirmed as a valid approximation of the underlying MINLP model. However, no immediate conclusion can be drawn, if the validation NLP is not successfully solved. An approach to interpret arising infeasibilities is presented in Section 3.4.9.

3.4.1. Common Model Aspects

In Section 3.2.1 four model aspects are described that are relevant for several network components: the gas compressibility factor, the molar heat capacity, the Joule–Thomson effect and interrelation of pressure temperature and density. All these phenomena depend on the specific gas composition

$$X = (m, H_c, p_c, T_c, \tilde{A}, \tilde{B}, \tilde{C}).$$

The describing equations can mostly be translated into constraints with only minor adjustments.

In the ValNLP, two models for the compressibility factor z are regarded: the AGA equation (3.4) and Papay’s formula (3.5). Since both have a different range of validity, the user chooses the appropriate formula based on the expected pressures in the network. Depending on the user’s choice, the constraint representing the compressibility factor is either

$$0 = c^z(z, p, T, p_c, T_c) = z - z^{\text{aga}}(p, T, p_c, T_c), \quad \text{or} \quad (3.59)$$

$$0 = c^z(z, p, T, p_c, T_c) = z - z^{\text{papay}}(p, T, p_c, T_c). \quad (3.60)$$

In contrast to the MPEC approach, the ValNLP is capable of tracking the gas temperature. For this, a model of the specific or molar heat capacity is required. The model 3.6 leads to the three constraints

$$0 = c^{\text{mhc-real}}(m, c_p, \tilde{c}_p^0, \Delta\tilde{c}_p) = mc_p - (\tilde{c}_p^0 + \Delta\tilde{c}_p), \quad (3.61a)$$

$$0 = c^{\text{mhc-ideal}}(\tilde{c}_p^0, T, \tilde{A}, \tilde{B}, \tilde{C}) = \tilde{c}_p^0 - (\tilde{A} + \tilde{B}T + \tilde{C}T^2), \quad (3.61b)$$

$$0 = c^{\text{mhc-corr}}(\Delta\tilde{c}_p, p, T, p_c, T_c) \quad (3.61c)$$

$$= \Delta\tilde{c}_p + R \int_0^p \frac{1}{p} \left(2T \frac{\partial z}{\partial T}(\tilde{p}, T, p_c, T_c) + T^2 \frac{\partial^2 z}{\partial T^2}(\tilde{p}, T, p_c, T_c) \right) d\tilde{p}. \quad (3.61d)$$

3.4. High Accuracy Optimization (ValNLP)

As already mentioned in Section 3.2.1, the integral in Equation 3.61c vanishes in case of the AGA formula. For Papay's formula it can be solved analytically. The full model of the molar heat capacity is given by the constraint vector

$$0 = c^{\text{heat-cap}}(p, T, X, x^{\text{heat-cap}}) = \begin{pmatrix} c^{\text{mhc-real}}(m, c_p, \tilde{c}_p^0, \Delta\tilde{c}_p) \\ c^{\text{mhc-ideal}}(\tilde{c}_p^0, T, \tilde{A}, \tilde{B}, \tilde{C}) \\ c^{\text{mhc-corr}}(\Delta\tilde{c}_p, p, T, p_c, T_c) \end{pmatrix} \quad (3.62)$$

with associated variables

$$x^{\text{heat-cap}} = (c_p, \tilde{c}_p^0, \Delta\tilde{c}_p).$$

A second phenomenon related to the gas temperature is the Joule–Thomson effect (3.9). Since the relevant data required for temperature calculations like ambient temperature or supplied gas temperature is inaccurate in mid-term planning by nature, a coarse discretization by a single Euler step is typically sufficient thus yielding

$$\begin{aligned} 0 &= c^{\text{jt}}(p_{\text{in}}, p_{\text{out}}, T_{\text{in}}, T_{\text{out}}, X, \mu_{\text{JT}}, c_{p,\text{out}}) \\ &= \begin{pmatrix} \mu_{\text{JT}} - \frac{T_{\text{out}}^2}{p_{\text{out}}} \frac{R}{m c_{p,\text{out}}} \frac{\partial z}{\partial T}(p_{\text{out}}, T_{\text{out}}, p_c, T_c) \\ T_{\text{out}} - T_{\text{in}} - (p_{\text{out}} - p_{\text{in}}) \mu_{\text{JT}} \end{pmatrix}. \end{aligned} \quad (3.63)$$

For the interrelation of pressure temperature and density the thermodynamical standard equation (3.7) is chosen. It results in the constraint

$$0 = c^{\text{eos}}(p, T, \rho, m, z) = \rho z R T - p m. \quad (3.64)$$

3.4.2. Nodes and Arcs

Every node $u \in \mathbb{V}$ has a pressure variable p_u and a temperature variable T_u . The incident arcs define relations between the pressures and temperatures of the connected nodes. While the model of an arc depends on the modeled network component, all arcs have some basic variables in common: a mass flow variable q_a , variables for the gas temperatures at tail and head, $T_{a:u}$ and $T_{a:v}$, and a quality parameter vector X_a . These are summarized in a common basic variable vector

$$x_a^{\text{base}} = (q_a, T_{a:u}, T_{a:v}, X_a).$$

3. Validation of Nominations

At every node, the flows of the incident arcs q_{δ_u} and the supplied and discharged flow q_u yield to a mass balance equation similar to (3.42):

$$0 = c^{\text{mass-bal}}(q_{\delta_u}, q_u) = q_u + \sum_{a \in \delta_u^-} q_a - \sum_{a \in \delta_u^+} q_a. \quad (3.65)$$

The exchanged mass flow q_u is typically fixed to the value in the given nomination, i.e. non-negative supply value and non-positive discharge value. For inner nodes, q_u is set to zero.

Since the NLP model considers the gas composition and gas temperature, the mixing of gas at every node is part of the model. Under the assumption of perfect mixing at the nodes, the gas composition in the outflow arcs is identical. The resulting mixing constraint reads

$$\begin{aligned} 0 &= c_u^{\text{mix}}(q_{\mathcal{I}_u}, X_{\mathcal{I}_u}, X_u) \\ &= X_u \left(\hat{q}_u^{\text{ext}} + \sum_{a \in \mathcal{I}_u} \hat{q}_a \right) - \left(\hat{q}_u^{\text{ext}} X_u^{\text{ext}} + \sum_{a \in \mathcal{I}_u} \hat{q}_a X_a \right). \end{aligned} \quad (3.66)$$

and the propagation is represented by the constraints

$$0 = c_u^{\text{prop}}(X_u, X_a) = X_u - X_a \quad \forall a \in \mathcal{O}_u.$$

The mixture of the gas temperature is described by Equation 3.12. Under the assumption of identical heat capacities the mixture equation for temperature and its propagation is approximated by

$$\begin{aligned} 0 &= c_u^{\text{mix-temp}}(q_{\mathcal{I}_u}, m_{\mathcal{I}_u}, (T_{a:u})_{a \in \mathcal{I}_u}, T_u) \\ &= T_u \left(\hat{q}_u^{\text{ext}} + \sum_{a \in \mathcal{I}_u} \hat{q}_a \right) - \left(\hat{q}_u^{\text{ext}} T_u^{\text{ext}} + \sum_{a \in \mathcal{I}_u} \hat{q}_a T_{a:u} \right), \end{aligned} \quad (3.67)$$

$$0 = c_u^{\text{prop-temp}}(T_u, T_{a:u}) = T_u - T_{a:u} \quad \forall a \in \mathcal{O}_u. \quad (3.68)$$

The heat capacities cancel each other out. Note that all mixing constraints are discontinuous since \mathcal{I}_u and \mathcal{O}_u depend on the flow directions. To obtain a smooth model, we fix all flow directions according to the solution of the MPEC approach by restricting the bounds of q_a to either $[0, q_a^+]$ or $[q_a^-, 0]$.

Summarizing, the full set of constraints at a node u reads

$$0 = c_u(x_u, x_{\delta_u}^{\text{base}}) = \begin{pmatrix} c^{\text{mass-bal}}(q_{\delta_u}, q_u) \\ c_u^{\text{mix}}(q_{\mathcal{I}_u}, X_{\mathcal{I}_u}, X_u) \\ (c_u^{\text{prop}}(X_u, X_a))_{a \in \mathcal{O}_u} \\ c_u^{\text{mix-temp}}(q_{\mathcal{I}_u}, m_{\mathcal{I}_u}, (T_{a:u})_{a \in \mathcal{I}_u}, T_u) \\ (c_u^{\text{prop-temp}}(T_u, T_{a:u}))_{a \in \mathcal{O}_u} \end{pmatrix}$$

with variable vector

$$x_u = (q_u, p_u, T_u, X_u).$$

3.4.3. Pipes

The pipe model (3.20) described in Section 3.2.3 feature a nonsmooth friction term and infinite dimensional variables. Both characteristics are not applicable in an NLP model, thus they have to be cared for.

In Section 3.3.2 the smooth friction approximation (3.44) has already been introduced as an alternative to the friction term $\lambda(q_a)|q_a|q_a$. The corresponding constraint

$$0 = c_a^{\text{sfa}}(\phi_a, q_a) = \phi_a - \tilde{\lambda}_a \left(\sqrt{q_a^2 + e_a^2} + b_a + \frac{c_a}{\sqrt{q_a^2 + d_a^2}} \right) q_a$$

with the constants described in Section 3.3.2 is also applied in the ValNLP model.

For the differential equations (3.20) are replaced by a smooth and finite dimensional model. Since the continuity equation (3.20a) implies constant mass flow along the pipe, its effect is already represented by the unique variable q_a , so there is no need of a representing constraint in the ValNLP model. For the momentum equation and the energy equation two different approaches are introduced.

The first approach is based on a discretization of the momentum equation and energy equation. Depending on an a priori chosen grid, $0 = x_{a,0} < \dots < x_{a,d} = L_a$, the discretization results in a model with a potentially large number of finite-dimensional nonlinear constraints. The accuracy of the model can be controlled via the choice of the grid points. Refining the grid leads to a more accurate model, but also add additional constraints.

3. Validation of Nominations

The continuous variables in (3.20b) and (3.20c) are evaluated at the grid points. For this purpose, the following abbreviations are introduced for $k = 0, \dots, d$:

$$\begin{aligned} p_{a,k} &= p(x_{a,k}), & z_{a,k} &= z(p_{a,k}, T_{a,k}, p_{c,a}, T_{c,a}), \\ T_{a,k} &= T(x_{a,k}), & c_{p,a,k} &= c_p(p_{a,k}, T_{a,k}, X_a), \\ \rho_{a,k} &= \rho(x_{a,k}), & z_{T,a,k} &= \frac{\partial z}{\partial T}(p_{a,k}, T_{a,k}, p_{c,a}, T_{c,a}). \end{aligned}$$

In the following, the discretization is illustrated by applying a simple Euler scheme, but many suitable schemes of higher order exist and may be applied instead. When denoting step sizes by $\Delta x_{a,k} = x_{a,k} - x_{a,k-1}$, the Euler scheme yields the discrete gradients

$$f'(x_{a,k}) \approx \frac{f(x_{a,k}) - f(x_{a,k-1})}{\Delta x_{a,k}} = \frac{\Delta f_{a,k}}{\Delta x_{a,k}}, \quad k = 1, \dots, d,$$

for pressure, temperature and density. This leads to the discretized ODE constraints

$$\begin{aligned} 0 &= c_a^{\text{mom-discr}}(q_a, p_{a,k}, p_{a,k-1}, \rho_{a,k}, \rho_{a,k-1}, \phi_a) \\ &= \rho_{a,k} \frac{\Delta p_{a,k}}{\Delta x_{a,k}} - \frac{q_a^2}{A_a^2} \frac{\Delta \rho_{a,k}}{\Delta x_{a,k}} \frac{1}{\rho_{a,k}} + g \rho_{a,k}^2 s_a + \frac{\phi_a}{2A_a^2 D_a}, \end{aligned} \quad (3.69a)$$

$$\begin{aligned} 0 &= c_a^{\text{ener-discr}}(q_a, p_{a,k}, p_{a,k-1}, T_{a,k}, T_{a,k-1}, \rho_{a,k}, c_{p,a,k}, z_{a,k}, p_{c,a}, T_{c,a}) \\ &= q_a c_{p,a,k} \frac{\Delta T_{a,k}}{\Delta x_{a,k}} - \frac{q_a T_{a,k}}{\rho_{a,k} z_{a,k}} z_{T,a,k} \frac{\Delta p_{a,k}}{\Delta x_{a,k}} + q_a g s_a + \pi D_a c_{\text{HT},a}(T_{a,k} - T_{\text{amb}}). \end{aligned} \quad (3.69b)$$

The model of the dynamic system is completed by additional constraints for the compressibility factor, heat capacity and equation of state in every discretization point:

$$\begin{aligned} 0 &= c_{a,k}^{\text{dyn}}(x_a^{\text{base}}, x_{a,k}^{\text{dyn}}, x_{a,k-1}^{\text{dyn}}, \phi_a, x_u, x_v) \\ &= \begin{pmatrix} c_a^{\text{mom-discr}}(q_a, p_{a,k}, p_{a,k-1}, \rho_{a,k}, \rho_{a,k-1}, \phi_a) \\ c_a^{\text{ener-discr}}(q_a, p_{a,k}, p_{a,k-1}, T_{a,k}, T_{a,k-1}, \rho_{a,k}, c_{p,a,k}, z_{a,k}, p_{c,a}, T_{c,a}) \\ c^{\text{eos}}(p_{a,k}, T_{a,k}, \rho_{a,k}, m_a, z_{a,k}) \\ c^z(z_{a,k}, p_{a,k}, T_{a,k}, p_{c,a}, T_{c,a}), \\ c_a^{\text{heat-cap}}(p_{a,k}, T_{a,k}, X_a, x_{a,k}^{\text{heat-cap}}) \end{pmatrix}, \end{aligned}$$

for $k = 1, \dots, d$, where the required additional dynamic variables are defined as

$$\begin{aligned} x_k^{\text{dyn}} &= (p_{a,k}, T_{a,k}, \rho_{a,k}, z_{a,k}, x_{a,k}^{\text{heat-cap}}), & k &= 1, \dots, d-1, \\ x_k^{\text{dyn}} &= (\rho_{a,k}, z_{a,k}, x_{a,k}^{\text{heat-cap}}), & k &\in \{0, d\}. \end{aligned}$$

3.4. High Accuracy Optimization (ValNLP)

Together with the smooth approximation of the friction term, the complete model of the discretized dynamic system finally reads

$$0 = c_a^{\text{dyn}}(x_a^{\text{base}}, x_a^{\text{dyn}}, x_u, x_v) = \begin{pmatrix} c_a^{\text{sfa}}(\phi_a, q_a) \\ (c_k^{\text{dyn}}(x_a^{\text{base}}, x_k^{\text{dyn}}, x_{a,k-1}^{\text{dyn}}, \phi_a, x_u, x_v))_{k=1}^d \end{pmatrix},$$

$$x_a^{\text{dyn}} = (\phi_a, (x_{a,k}^{\text{dyn}})_{k=0}^d).$$

Depending on the flow direction the presented Euler scheme corresponds to an implicit Euler scheme for positive flow and an explicit Euler scheme otherwise. Since the flow directions are fixed anyway for the mixing equations, an implicit Euler can always be achieved. If the flow directions were not fixed, this could result in decreased accuracy.

A second possible approach replacing the momentum equation has already been presented in Section 3.3.2: the smooth second order approximation (3.43) yielding the constraint

$$\begin{aligned} 0 &= c_a^{\text{mom-approx}}(p_u, p_v, \phi_a, T_{m,a}, z_{m,a}, m_a) \\ &= p_v^2 - \left(p_u^2 - \Lambda_a \phi_a \frac{e^{S_a} - 1}{S_a} \right) e^{-S_a} \end{aligned} \quad (3.70)$$

with

$$\begin{aligned} \Lambda_a &= \Lambda_a(T_{m,a}, z_{m,a}, m_a) = \frac{L_a}{A_a^2 D_a} \frac{z_{m,a} T_{m,a} R}{m_a}, \\ S_a &= S_a(T_{m,a}, z_{m,a}, m_a) = 2g L_a s_a \frac{m_a}{z_{m,a} T_{m,a} R}. \end{aligned}$$

An approximation of the energy equation can be derived under similar assumptions, including a constant heat capacity c_p and a mean density $\rho_{m,a} = p_{m,a}/(R_s z_{m,a} T_{m,a})$ [115]. The resulting smooth nonlinear constraint is

$$\begin{aligned} 0 &= c_a^{\text{ener-approx}}(q_a, p_a^{\text{in}}, p_a^{\text{out}}, T_a^{\text{in}}, T_a^{\text{out}}, \rho_{m,a}, p_{m,a}, T_{m,a}, z_{m,a}, p_{c,a}, T_{c,a}) \\ &= q_a \left(T_a^{\text{out}} - T_a^{\text{in}} + \frac{g s_a L_a}{c_p} \right) - \frac{z_{T,m,a}}{c_p \rho_{m,a} z_{m,a}} T_a^{\text{out}} q_a (p_a^{\text{out}} - p_a^{\text{in}}) \\ &\quad + \frac{\pi D_a c_{\text{HT},a} L_a}{c_p} (T_a^{\text{out}} - T_{\text{soil}}), \end{aligned} \quad (3.71)$$

where

$$z_{T,m,a} = \frac{\partial z}{\partial T}(p_{m,a}, T_{m,a}, p_{c,a}, T_{c,a}).$$

The inflow and outflow values are chosen as described in (3.1) and (3.2). The differences

3. Validation of Nominations

of the discretized energy equation (3.69b) and the approximation (3.71) are illustrated in Figure 3.12. On the left, the temperature profile is displayed with respect to the position in the pipe and on the right it is On the left, the temperature profile along a pipe is displayed along the pipe and on the right the outflow temperature is presented for varying mass flow.

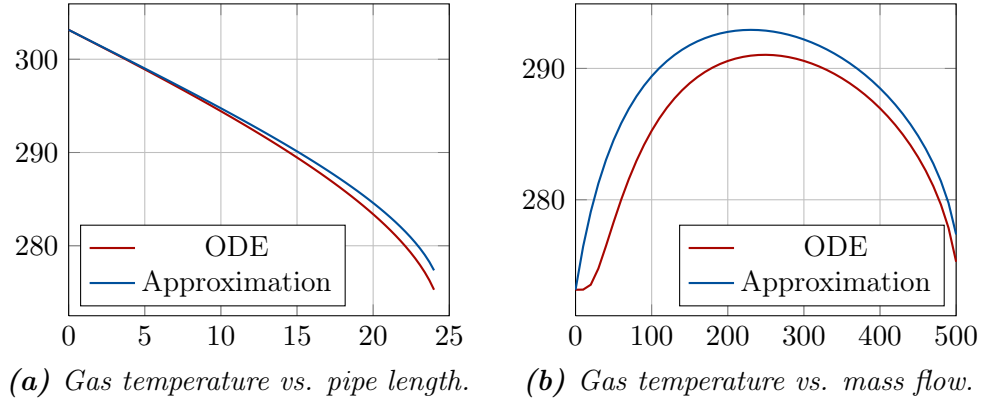


Figure 3.12. Gas temperature according to ODE discretization and approximation ($L = 24$ km, $D = 1$ m, $k = 0.1$ mm, $q = 500$ kg s⁻¹)

Both approximating constraints (3.70) and (3.71) incorporate mean values of pressure $p_{m,a}$ and temperature $T_{m,a}$. A simple method to derive these values is averaging the according variable bounds:

$$p_{m,a} = \frac{1}{2}(\max(p_u^-, p_v^-) + \min(p_u^+, p_v^+)),$$

$$T_{m,a} = \frac{1}{2}(\max(T_{a:u}^-, T_{a:v}^-) + \min(T_{a:u}^+, T_{a:v}^+)).$$

A more sophisticated model contains a constraint to include the mean values as variables that depend on pressures and temperatures at the pipe [85]:

$$0 = c^{\text{mean}}(p_{m,a}, T_{m,a}, p_u, p_v, T_{a:u}, T_{a:v}) = \begin{pmatrix} p_{m,a} - \frac{2}{3}(p_u + p_v - \frac{p_u p_v}{p_u + p_v}) \\ T_{m,a} - \frac{2}{3}(T_{a:u} + T_{a:v} - \frac{T_{a:u} T_{a:v}}{T_{a:u} + T_{a:v}}) \end{pmatrix}.$$

Another possible choice for the mean pressure is [85]

$$0 = p_{m,a} - \frac{2}{3} \left(\frac{p_u^3 - p_v^3}{p_u^2 - p_v^2} \right).$$

Finally, the full approximation model of the differential equations (3.20) with variables for the mean values is thus expressed by the constraints

$$0 = c_a^{\text{approx}}(x_a^{\text{base}}, x_a^{\text{dyn}}, x_u, x_v) = \begin{pmatrix} c_a^{\text{sfa}}(\phi_a, q_a) \\ c_a^{\text{mom-approx}}(p_u, p_v, \phi_a, T_{m,a}, z_{m,a}, m_a) \\ c_a^{\text{ener-approx}}(q_a, p_u, p_v, T_{a:u}, T_{a:v}, \rho_{m,a}, p_{m,a}, T_{m,a}, z_{m,a}, p_{c,a}, T_{c,a}) \\ c^z(z_{m,a}, p_{m,a}, T_{m,a}, p_{c,a}, T_{c,a}) \\ c^{\text{mean}}(p_{m,a}, T_{m,a}, p_u, p_v, T_{a:u}, T_{a:v}) \end{pmatrix}$$

and variables

$$x_a^{\text{approx}} = (\phi_a, \rho_{m,a}, p_{m,a}, T_{m,a}, z_{m,a}).$$

An aspect not governed so far is the restriction of the gas velocity to avoid sound pollution and material failure, see Section 3.2.3. Equation 3.20 leads to a monotone change along the pipe for constant flow. The velocity limits are controlled at the end points of the pipe $a = (u, v)$. To this end, the bounded variables $x_a^{\text{vel}} = (v_{a:u}, v_{a:v})$ and the constraint

$$c_a^{\text{vel-flow}}(q, v, \rho) = A_a \rho v - q \quad (3.72)$$

are introduced. Extended by the necessary constraints for the density this yields the velocity model

$$0 = c_a^{\text{vel}}(x_a^{\text{base}}, x_a^{\text{vel}}, x_u, x_v) = \begin{pmatrix} c_a^{\text{vel-flow}}(q_a, v_{a:u}, \rho_{a:u}) \\ c_a^{\text{vel-flow}}(q_a, v_{a:v}, \rho_{a:v}) \\ c^{\text{eos}}(p_u, T_{a:u}, \rho_{a:u}, m_a, z_{a:u}) \\ c^{\text{eos}}(p_v, T_{a:v}, \rho_{a:v}, m_a, z_{a:v}) \\ c^z(z_{a:u}, p_u, T_{a:u}, p_{c,a}, T_{c,a}) \\ c^z(z_{a:v}, p_v, T_{a:v}, p_{c,a}, T_{c,a}) \end{pmatrix},$$

$$x_a^{\text{vel}} = (v_{a:u}, v_{a:v}, \rho_{a:u}, \rho_{a:v}, z_{a:u}, z_{a:v}).$$

If the discretization scheme is applied on the momentum equation and energy equation, the densities $\rho_{a:u}$ and $\rho_{a:v}$ coincide with the densities ρ_0 and ρ_d , hence the equations of state and the constraints for the compressibility factors are already regarded in the model.

3. Validation of Nominations

The velocity constraints thus reduce to

$$0 = c_a^{\text{vel}}(x_a^{\text{base}}, x_a^{\text{dyn}}, x_a^{\text{vel}}) = \begin{pmatrix} c_a^{\text{vel-flow}}(q_a, v_0, \rho_0) \\ c_a^{\text{vel-flow}}(q_a, v_d, \rho_d) \end{pmatrix}$$

and only variables for velocity have to be added, $x_a^{\text{vel}} = (v_{a:u}, v_{a:v})$. In summary, the complete pipe model consists of the constraints c_a^{dyn} and c_a^{vel} , yielding either

$$0 = c_{\mathcal{E},a}(x_a, x_u, x_v) = \begin{pmatrix} c_a^{\text{approx}}(x_a^{\text{base}}, x_a^{\text{dyn}}, x_u, x_v) \\ c_a^{\text{vel}}(x_a^{\text{base}}, x_a^{\text{dyn}}, x_a^{\text{vel}}) \end{pmatrix}$$

or

$$0 = c_{\mathcal{E},a}(x_a, x_u, x_v) = \begin{pmatrix} c_a^{\text{dyn}}(x_a^{\text{base}}, x_a^{\text{dyn}}, x_u, x_v) \\ c_a^{\text{vel}}(x_a^{\text{base}}, x_a^{\text{dyn}}, x_a^{\text{vel}}, x_u, x_v) \end{pmatrix},$$

$$x_a = (x_a^{\text{base}}, x_a^{\text{dyn}}, x_a^{\text{vel}})$$

with the additional variables $x_a = (x_a^{\text{base}}, x_a^{\text{dyn}}, x_a^{\text{vel}})$, depending on the model of the flow dynamics and the required velocity constraints.

The alternative descriptions of the physical aspects offer several model variants, leading to a family of possible pipe models. A model variant with a small number of nonlinear constraints and modest accuracy is similar to the one proposed for the MPEC approach: the smooth quadratic approximation (3.70) is combined with the choice of the AGA formula for the compressibility factor, constant mean values for pressure and temperature and an isothermal model, so no energy equation will be required. The solution of the MPEC approach will typically offer good initial values for this model choice. While it is one of the most inaccurate choices presented, it proves to be sufficiently accurate for several practical purposes.

A very accurate model choice consists of the discretized ODE equations (3.69a) and (3.69b) and Papay's equation for the compressibility factor. The drawback of this variant is the large number of nonlinear constraints which likely leads to an increased computation time and the model differences to the MPEC approach reduce the quality of the initial may even require different choices for the discrete model aspects.

3.4.4. Resistors

The resistor model in Section 3.2.4 describes points of nonsmooth behavior for both resistor types. The MPEC approach resolves this by appropriate smoothing functions, which introduce inaccuracies for small flow values. In the ValNLP model, the flow direction is fixed a priori to the direction stated in the solution of the MPEC approach. Thus, the pressure loss of a resistor $a = (u, v) \in \mathbb{A}_{\text{re}}$ is either modeled by the linear constraint

$$0 = c_a^{\text{p-loss}}(p_u, p_v, q_a) = p_u - p_v - \text{sign}(q_a)\xi_a, \quad (3.73)$$

or it is modeled by the nonlinear constraint

$$0 = c_a^{\text{p-loss}}(p_u, p_v, q_a, \rho_a^{\text{in}}) = p_u - p_v - \frac{8\zeta_a}{\pi^2 D_a^4} \frac{q_a |q_a|}{\rho_a^{\text{in}}}. \quad (3.74)$$

The pressure loss induces a temperature change due to the Joule–Thomson effect (3.63) yielding additional constraints. Accordingly, the full resistor model is either

$$0 = c_{\mathcal{E},a}(x_u, x_v, x_a) = \begin{pmatrix} c_a^{\text{p-loss}}(q_a, p_u, p_v) \\ c_a^{\text{heat-cap}}(p_u, T_u, X_a, x_{a,\text{out}}^{\text{heat-cap}}) \\ c^{\text{jt}}(p_u, p_v, T_{a:u}, T_{a:v}, X_a, \mu_{\text{JT},a}, c_{p,a,\text{out}}) \end{pmatrix}, \quad (3.75)$$

$$x_a = (x_a^{\text{base}}, x_{a,\text{out}}^{\text{heat-cap}}, \mu_{\text{JT},a})$$

or

$$0 = c_{\mathcal{E},a}(x_u, x_v, x_a) = \begin{pmatrix} c_a^{\text{p-loss}}(q_a, p_u, p_v, \rho_a^{\text{in}}) \\ c_a^{\text{heat-cap}}(p_u, T_u, X_a, x_{a,\text{out}}^{\text{heat-cap}}) \\ c^{\text{jt}}(p_u, p_v, T_{a:u}, T_{a:v}, X_a, \mu_{\text{JT},a}, c_{p,a,\text{out}}) \\ c^{\text{eos}}(p_a^{\text{in}}, T_a^{\text{in}}, \rho_a^{\text{in}}, m_a, z_{u,\text{in}}) \\ c^z(z_u^{\text{in}}, p_a^{\text{in}}, T_a^{\text{in}}, p_c, T_c) \end{pmatrix}, \quad (3.76)$$

$$x_a = (x_a^{\text{base}}, x_{a,\text{out}}^{\text{heat-cap}}, \mu_{\text{JT},a}, \rho_a^{\text{in}}, z_u^{\text{in}}).$$

The pressure loss at resistors, parameter mixing and temperature mixing are the only model aspects that depend on the flow direction. If gas parameters and gas temperature are approximated by mean values and the pressure loss is approximated as in Section 3.3.3, the flow directions do not have to be fixed. Otherwise, information about the flow directions are required in addition to the discrete decisions of the active elements.

3. Validation of Nominations

3.4.5. Valves and Shortcuts

The model (3.23) of a shortcut $a = (u, v) \in \mathbb{A}_{\text{sc}}$ needs no further adjustments, thus the constraints are

$$0 = c_{\mathcal{E},a}(x_u, x_v, x_a) = \begin{pmatrix} p_u - p_v \\ T_{a:u} - T_{a:v} \end{pmatrix}, \quad x_a = x_a^{\text{base}}. \quad (3.77)$$

The state of a valve $a = (u, v) \in \mathbb{A}_{\text{vl}}$ is chosen based on the solution of the given solution of the MPEC approach, so a valve model is required for each state. An open valve is modeled similar to a shortcut by (3.77). A closed valve implies zero flow and decouples the incident pressure and temperature variables:

$$0 = c_{\mathcal{E},a}(x_a) = q_a, \quad x_a = x_a^{\text{base}}. \quad (3.78)$$

3.4.6. Control Valve Stations

Fixing the state of a control valve station $a = (u, v) \in \mathbb{A}_{\text{cv}}$ according to a given solution reduces the complexity of its model considerably. The control valve station is modeled as a subgraph as in the previous models, see Figure 3.3 on page 36.

A closed control valve station is modeled as a closed valve, see Equation 3.78. If the station has no remote access, the lower bounds of the pressure variables p_u and p_v are additionally set to $p_{\text{set},a}$.

The bypass mode of a control valve station differs between stations with and without remote access. A bypassed control valve station with remote access is modeled as an open valve, see (3.77). In contrast, for stations without remote access the inlet resistor a_0 and the outlet resistor a_2 have to be considered,

$$\begin{aligned} 0 &= c_{a_0}(x_u, x_{a,1}, x_a^{\text{base}}, x_{a_0}), \\ 0 &= c_{a_2}(x_{a,2}, x_{a,3}, x_a^{\text{base}}, x_{a_2}), \end{aligned}$$

see Section 3.4.4 for details, and the gas heater is offline. A bypassed control valve without

3.4. High Accuracy Optimization (ValNLP)

remote access is hence represented by

$$0 = c_{\mathcal{E},a}(x_u, x_v, x_a) = \begin{pmatrix} c_{a_0}(x_u, x_{a,1}, x_a^{\text{base}}, x_{a_0}) \\ x_{a,1} - x_{a,2} \\ c_{a_2}(x_{a,2}, x_{a,3}, x_a^{\text{base}}, x_{a_2}) \\ p_{a,3} - p_v \\ T_{a,3} - T_v \end{pmatrix},$$

$$x_a = (x_a^{\text{base}}, x_{a,1}, x_{a,2}, x_{a,3}, x_{a_0}, x_{a_2}),$$

and the upper bound of the incident pressure variables is set to $p_{\text{set},a}$ if it is larger.

An active control valve station with remote access reduces the pressure by Δp_a . The constraint representing the linear pressure loss is

$$0 = c_{a_1}^{\text{p-loss}}(p_{a,1}, p_{a,2}, \Delta p_a) = p_{a,1} - p_{a,2} - \Delta p_a.$$

In case of a control valve without remote access the outlet pressure $p_{a,2}$ is set to $p_{\text{set},a}$,

$$0 = c_{a_1}^{\text{p-loss}}(p_{a,2}) = p_{a,2} - p_{\text{set},a},$$

and the lower bound of the inlet pressure $p_{a,1}$ is increased to $p_{\text{set},a}$, if it is smaller. The pressure decrease results in a temperature change due to the Joule–Thomson effect, thus the control valve model is

$$0 = c_{a_1}(x_{a,1}, x_{a,2}, x_a^{\text{base}}, x_{a_1}) = \begin{pmatrix} c_{a_1}^{\text{p-loss}}(p_{a,1}, p_{a,2}, \Delta p_a) \\ c^{\text{heat-cap}}(p_{a,1}, T_{a,1}, X_a, x_{a_1}^{\text{heat-cap}}) \\ c^{\text{jt}}(p_{a,1}, p_{a,2}, T_{a,1}, T_{a,2}, X_a, \mu_{\text{JT},a_1}, c_{p,a_1}) \end{pmatrix},$$

$$x_{a_1} = (\Delta p_a, \mu_{\text{JT},a_1}, x_{a_1}^{\text{heat-cap}}),$$

for control valves with remote access and otherwise it is

$$0 = c_{a_1}(x_{a,1}, x_{a,2}, x_a^{\text{base}}, x_{a_1}) = \begin{pmatrix} c_{a_1}^{\text{p-loss}}(p_{a,2}) \\ c^{\text{heat-cap}}(p_{a,1}, T_{a,1}, X_a, x_{a_1}^{\text{heat-cap}}) \\ c^{\text{jt}}(p_{a,1}, p_{a,2}, T_{a,1}, T_{a,2}, X_a, \mu_{\text{JT},a_1}, c_{p,a_1}) \end{pmatrix},$$

$$x_{a_1} = (\mu_{\text{JT},a_1}, x_{a_1}^{\text{heat-cap}}).$$

The gas temperature of an active control valve station is controlled by the gas preheater. Its model in Section 3.2.7 is nonsmooth, thus it has to be replaced by a smooth approximation

3. Validation of Nominations

in order to gain an NLP formulation. To this end, the smooth approximation of the minimum function (3.49) is applied, resulting in

$$0 = c_{a_3}(p_{a,3}, p_v, T_{a,3}, T_{a:v}) = \left(T_{a:v} - T_{a:v}^- - \frac{p_{a,3} - p_v}{\frac{1}{2} \left(\sqrt{\Delta T_a^2 + \epsilon} + \Delta T_a \right)} \right),$$

$$\Delta T_a = T_{a,3} - T_{a:v}^-,$$

with a suitable smoothing parameter $\epsilon > 0$. The complete model of an active control valve station then reads

$$0 = c_{\mathcal{E},a}(x_u, x_v, x_a) = \begin{pmatrix} c_{a_0}(x_u, x_{a,1}, x_a^{\text{base}}, x_{a_0}) \\ c_{a_1}(x_{a,1}, x_2, x_a^{\text{base}}, x_{a_1}) \\ c_{a_2}(x_{a,2}, x_{a,3}, x_a^{\text{base}}, x_{a_2}) \\ c_{a_3}(x_{a,3}, x_v, x_a^{\text{base}}) \end{pmatrix},$$

$$x_a = (x_a^{\text{base}}, x_{a,1}, x_{a,2}, x_{a,3}, x_{a_0}, x_{a_1}, x_{a_2}).$$

3.4.7. Compressor Groups

To eliminate the discrete aspects of the compressor group model in Section 3.2.8 information about the general state, i.e. closed, active or bypass, is required and the operating configuration has to be defined in case of an active compressor group. Similar to control valve stations with remote access, a closed compressor group is modeled by (3.78) and a compressor group in bypass mode acts like a shortcut, see (3.77). The model of an active compressor unit is based on a sub-graph representing the compressor group. In contrast to the MINLP model in Section 3.2.8 and the heuristic model in Section 3.3.8, the notation is adjusted, since the configuration is already fixed. The model of an active group includes the inlet resistor a_0 , stages $\mathcal{S}_i = \{a_1, \dots, a_{\bar{s}}\}$ of the known active configuration $i \in \mathcal{K}_a$, the outlet resistor $a_{\bar{s}+1}$ and the gas cooler $a_{\bar{s}+2}$. Note that a sub-arc a_j connects the sub-nodes j and $j + 1$ in contrast to the compressor model of the MINLP and MPEC. Figure 3.13 illustrates this build-up.

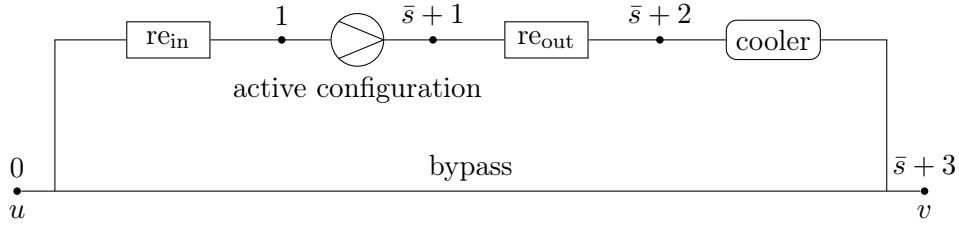


Figure 3.13. Subgraph of a compressor group

Associated with every inner sub-node is a variable vector, $x_j = (p_j, T_j)$, $j = 1, \dots, \bar{s} + 2$. The sub-nodes 0 and $\bar{s} + 3$ are synonyms for u and v , respectively.

The inlet and outlet resistors are modeled by (3.76), resulting in the constraints

$$\begin{aligned} 0 &= c_{\mathcal{E}, a_0}(x_u, x_1, x_a^{\text{base}}, x_{a_0}), & x_{a_0} &= (x_{a_0}^{\text{heat-cap}}, \mu_{\text{JT}, a, a_0}). \\ 0 &= c_{\mathcal{E}, a_{\bar{s}+1}}(x_{\bar{s}+1}, x_{\bar{s}+2}, x_a^{\text{base}}, x_{a_{\bar{s}+1}}), & x_{a_{\bar{s}+1}} &= (x_{a_{\bar{s}+1}}^{\text{heat-cap}}, \mu_{\text{JT}, a, a_{\bar{s}+1}}) \end{aligned}$$

in case of linear resistors. The nonsmooth maximum function in the model of the gas cooler (3.40) is smoothed by applying the smoothing function (3.50). This yields the constraint

$$0 = c_{\mathcal{E}, a_{s+2}}(p_{a,s+2}, p_v, T_{a,s+2}, T_{a:v}) = \left(T_{a:v} - T_{a:v}^+ + \frac{1}{2} \left(\sqrt{\Delta T_a^2 + \epsilon} - \Delta T_a \right) \right),$$

with $\Delta T_a = T_{a,s+2} - T_{a:v}^+$ and $\epsilon > 0$.

An active compressor group $a = (u, v)$ premises a flow in arc direction, i.e. $q_a \geq 0$. The model of stage a_j , $j \in \mathcal{S}_i$, consists of a constraint modeling the distribution of the arc flow q_a between the parallel units \mathcal{U}_j ,

$$0 = c_{a_j}^{\text{flow-dist}}(q_a, q_{\mathcal{U}_j}) = q_a - \sum_{k \in \mathcal{U}_j} q_k, \quad \text{for all } j \in \mathcal{S}_i,$$

the mixing of the outflow temperatures T_k^{out} , $k \in \mathcal{U}_j$, of the parallel units,

$$\begin{aligned} 0 &= c_{a_j}^{\text{mix-temp}}(q_{\mathcal{U}_j}, T_{a,j+1}, T_{\mathcal{U}_j}^{\text{out}}) \\ &= T_{a,j+1} \sum_{k \in \mathcal{U}_j} q_k - \sum_{k \in \mathcal{U}_j} q_k T_k^{\text{out}}, \end{aligned}$$

and the constraints representing the compressor units c_k , $k \in \mathcal{U}_j$. The constraints of compressor units are partly identical for both turbo compressors and piston compressors.

3. Validation of Nominations

The specific change in adiabatic enthalpy is modeled by the constraint

$$\begin{aligned} 0 &= c^{\text{adiabatic}}(H_{ad,k}, p_j, T_j, p_{j+1}, z_j, m_a, \kappa_k) \\ &= H_{ad,k} - z_j T_j \frac{R}{m_a} \frac{\kappa_k}{\kappa_k - 1} \left(\left(\frac{p_{j+1}}{p_j} \right)^{(\kappa_k - 1)/\kappa_k} - 1 \right) \end{aligned} \quad (3.79)$$

for a compressor $k \in \mathcal{U}_j$ of either type. The required power P_k is modeled by

$$c^{\text{power}}(P_k, q_k, H_{ad,k}, \eta_{ad,k}) = P_k - \frac{q_k H_{ad,k}}{\eta_{ad,k}}. \quad (3.80)$$

Equations (3.27) and (3.28) describe how the isentropic exponent κ_k is calculated, yielding the constraint

$$0 = c^{\text{isen-exp-lin}}(\kappa_k, \kappa_k^{\text{in}}, \kappa_k^{\text{out}}) = \kappa_k - \frac{1}{2}(\kappa_k^{\text{in}} + \kappa_k^{\text{out}}),$$

where κ_k^{in} and κ_k^{out} are defined by the constraint

$$0 = c^{\text{isen-exp-def}}(\kappa, p, T, z, c_p, X_a) = \kappa - \frac{Rc_p z}{Rc_p Z_p(z, p, T, p_c, T_c) - mZ_T(z, p, T, p_c, T_c)^2}.$$

For Z_p and Z_T , see (3.29) and (3.30). Extended by the constraints for the required heat capacity and using the additional variables

$$x_k^{\text{isen-exp}} = (\kappa_k, \kappa_k^{\text{in}}, \kappa_k^{\text{out}}, x_{k,\text{in}}^{\text{heat-cap}}, x_{k,\text{out}}^{\text{heat-cap}}), \quad (3.81)$$

the model of the isentropic exponent is

$$\begin{aligned} 0 &= c^{\text{isen-exp}}(p_j, T_j, z_j, p_{j+1}, T_k^{\text{out}}, z_k^{\text{out}}, x_a^{\text{base}}, x_k^{\text{isen-exp}}) \\ &= \begin{pmatrix} c^{\text{isen-exp-lin}}(\kappa_k, \kappa_k^{\text{in}}, \kappa_k^{\text{out}}) \\ c^{\text{isen-exp-def}}(\kappa_k^{\text{in}}, p_j, T_j, z_j, c_{p,k,\text{in}}, X_a) \\ c^{\text{isen-exp-def}}(\kappa_k^{\text{out}}, p_{j+1}, T_k^{\text{out}}, z_k^{\text{out}}, c_{p,k,\text{out}}, X_a) \\ c^{\text{heat-cap}}(p_j, T_j, X_a, x_{k,\text{in}}^{\text{heat-cap}}) \\ c^{\text{heat-cap}}(p_{j+1}, T_k^{\text{out}}, X_a, x_{k,\text{out}}^{\text{heat-cap}}) \\ c^z(z_k^{\text{out}}, p_{j+1}, T_k^{\text{out}}, p_{c,a}, T_{c,a}) \end{pmatrix}. \end{aligned}$$

A constraint modeling the compressibility factor z_j is outsourced since is involved in several model aspects of a compressor unit.

3.4. High Accuracy Optimization (ValNLP)

A alternative simplified model is based on a linear function of the temperature

$$\begin{aligned}
0 &= c^{\text{isen-exp}}(T_j, T_k^{\text{out}}, x_k^{\text{isen-exp}}) \\
&= \begin{pmatrix} \kappa_k - 1.29 + 5.8824 \times 10^{-4}(T_{m,k} - T_0) \\ T_{m,k} - \frac{1}{2}(T_j + T_k^{\text{out}}) \end{pmatrix}, \quad (3.82) \\
x_k^{\text{isen-exp}} &= (\kappa_k, T_{m,k}).
\end{aligned}$$

Last but not least, choosing $\kappa_k = 1.29$ as described in Section 3.2.8 yields the basic model

$$0 = c^{\text{isen-exp}}(\kappa_k) = \kappa_k - 1.29. \quad (3.83)$$

This constraint can either be added to the model directly or all occurrences of the isentropic exponent are replaced by the constant value instead.

The pressure change caused by a compressor unit results in a change of the temperature due to the Joule–Thomson effect. Equations (3.31) and (3.32) describe an empirical model. They result in the constraint

$$\begin{aligned}
0 &= c^{\text{temp-inc}}(p_j, T_j, z_j, p_{j+1}, T_k^{\text{out}}, z_k^{\text{init}}, T_k^{\text{init}}, \kappa_k, \eta_{\text{ad},k}, X_a) \\
&= \begin{pmatrix} T_k^{\text{out}} z_k^{\text{init}} - T_k^{\text{init}} z_j \\ T_k^{\text{init}} - T_j \left(\frac{p_{j+1}}{p_j} \right)^{(\kappa_k - 1)/(\kappa_k \eta_{\text{ad},k})} \\ c^z(z_k^{\text{init}}, p_{j+1}, T_k^{\text{init}}, p_{c,a}, T_{c,a}) \end{pmatrix}.
\end{aligned}$$

The models of both types of compressors involve the volumetric flow $Q = q/\rho$. To determine the density at the inlet of the compressor unit a constraint c^{eos} modeling the equation of state is further required. Similarly, the models of both types of compressors require the speed of the compressor n_k . Summarizing all constraints defined in this section

3. Validation of Nominations

so far results in the core model of a compressor unit,

$$\begin{aligned}
0 &= c_k^{\text{base}}(x_a^{\text{base}}, x_j, x_{j+1}, x_k^{\text{base}}) \\
&= \begin{pmatrix} c^{\text{adiabatic}}(H_{ad,k}, p_j, T_j, p_{j+1}, z_j, m_a, \kappa_k) \\ c^{\text{power}}(P_k, q_k, H_{ad,k}, \eta_{ad,k}) \\ c^{\text{isen-exp}}(p_j, T_j, z_j, p_{j+1}, T_k^{\text{out}}, z_k^{\text{out}}, x_a^{\text{base}}, x_k^{\text{isen-exp}}) \\ c^{\text{temp-inc}}(p_j, T_j, z_j, p_{j+1}, T_k^{\text{out}}, z_k^{\text{init}}, T_k^{\text{init}}, \kappa_k, \eta_{ad,k}, X_a) \\ c^z(z_j, p_j, T_j, p_{c,a}, T_{c,a}) \\ c^{\text{eos}}(p_j, T_j, \rho_j, m_a, z_j) \end{pmatrix}, \quad (3.84) \\
x_k^{\text{base}} &= (q_k, P_k, H_{ad,k}, \eta_{ad,k}, T_k^{\text{out}}, z_j, z_k^{\text{out}}, z_k^{\text{init}}, T_k^{\text{init}}, x_k^{\text{isen-exp}}, n_k).
\end{aligned}$$

This model of the common constraints is extended by type-specific constraints modeling the characteristic diagrams of the compressor units.

The characteristic diagram of a turbo compressor, see Figure 3.8a, is described by quadratic least-squares fits (3.33) and (3.34). The curved lower and upper border of the feasible operating range results from the technical limits of the compressor speed $n_k \in [n_k^-, n_k^+]$ and the constraint for the speed isolines (3.35)

$$\begin{aligned}
0 &= c^{\text{speed}}(H_{ad,k}, q_k, \rho_j, n_k) \\
&= H_{ad,k} - \chi\left(\frac{q_k}{\rho_j}, n_k; A_{H_{ad,k}}\right).
\end{aligned}$$

Here, the volumetric flow rate Q_k is replaced by q_k/ρ_j . To the left and right, the feasible operating range is bounded by the surpline and choke line

$$\begin{aligned}
0 &\leq c^{\text{surge}}(q_k, \rho_j, H_{ad,k}) = \psi\left(\frac{q_k}{\rho_j}, a_{s,k}\right) - H_{ad,k}, \\
0 &\leq c^{\text{choke}}(q_k, \rho_j, H_{ad,k}) = H_{ad,k} - \psi\left(\frac{q_k}{\rho_j}, a_{c,k}\right).
\end{aligned}$$

The adiabatic efficiency $\eta_{ad,k} \in [0, 1]$ of the turbo compressor is modeled by

$$\begin{aligned}
0 &= c^{\text{eff}}(\eta_{ad,k}, q_k, \rho_j, n_k) \\
&= \eta_{ad,k} - \chi\left(\frac{q_k}{\rho_j}, n_k; A_{\eta_{ad,k}}\right),
\end{aligned}$$

In summary, the complete model of a turbo compressor $k \in \mathcal{U}_j$ of stage j consists of the

3.4. High Accuracy Optimization (ValNLP)

common constraints (3.84) and the description of the feasible working range, yielding

$$\begin{aligned}
0 &= c_{\mathcal{E},k}(x_a^{\text{base}}, x_j, x_{j+1}, x_k) \\
&= \begin{pmatrix} c_k^{\text{base}}(x_a^{\text{base}}, x_j, x_{j+1}, x_k^{\text{base}}) \\ c^{\text{speed}}(H_{ad,k}, q_k, \rho_j, n_k) \\ c^{\text{eff}}(\eta_{ad,k}, q_k, \rho_j, n_k) \end{pmatrix}, \\
0 &\leq c_{\mathcal{I},k}(x_j, x_{j+1}, x_k) = \begin{pmatrix} c^{\text{surge}}(q_k, \rho_j, H_{ad,k}) \\ c^{\text{choke}}(q_k, \rho_j, H_{ad,k}) \end{pmatrix}, \\
x_k &= (x_k^{\text{base}}).
\end{aligned}$$

This model introduces the first inequalities so far to the ValNLP.

In contrast to the complex nonlinear model of turbo compressors, the model of a piston compressor $k \in \mathcal{U}_j$ is less sophisticated. Essentially, the maximum possible volumetric flow is restricted by the amount, the compressor can process per rotation,

$$0 = c^{\text{vol}}(q_k, \rho_j, n_k) = \frac{q_k}{\rho_j} - V_0 n_k,$$

and the maximum allowed torque is restricted on one of three possible ways:

$$\begin{aligned}
0 &= c^{\text{torque}}(\rho_j, M_k, H_{ad,k}) = M_k - \frac{V_0 H_{ad,k}}{2\pi \eta_{ad,k}} \rho_j, \\
0 &\leq c^{\text{limit}}(p_j, p_{j+1}, M_k) = \begin{cases} \varepsilon^+ - p_{j+1}/p_j, \\ p_j - p_{j+1} + \Delta p^+, \\ M_k^+ - M_k. \end{cases}
\end{aligned}$$

Details on the parameters are given in Section 3.2.8. These constraints are summarized in the model of a piston compressor $k \in \mathcal{U}_j$

$$\begin{aligned}
0 &= c_{\mathcal{E},k}(x_a^{\text{base}}, x_j, x_{j+1}, x_k) = \begin{pmatrix} c_k^{\text{base}}(x_a^{\text{base}}, x_j, x_{j+1}, x_k^{\text{base}}) \\ c^{\text{torque}}(\rho_j, M_k, H_{ad,k}) \\ c^{\text{vol}}(Q_k, n_k) \end{pmatrix}, \\
0 &\leq c_{\mathcal{I},k}(x_j, x_{j+1}, x_k) = c^{\text{limit}}(p_j, p_{j+1}, M_k),
\end{aligned}$$

with the variables

$$x_k = (x_k^{\text{base}}, \rho_j, z_j, M_k, n_k).$$

3. Validation of Nominations

Each compressor unit of either type has a drive d attached, which powers the compressor unit. The mapping from a compressor unit to its connected drive is denoted by $\sigma(k)$. The power P_k a compressor consumes is limited by the maximum power P_d^+ the connected drive d can create,

$$0 \leq c_{\mathcal{L},d}(P_k, P_d^+) = P_d^+ - P_k. \quad (3.85)$$

How this power is generated depends on the type of the drive. All drives are modeled as a subset of the constraints

$$\begin{aligned} 0 &= c^{\text{fuel}}(q_d^{\text{fuel}}, b_d, m_a, H_{c,a}) = q_d^{\text{fuel}} - \frac{b_d m_a}{H_{u,a}}, \\ 0 &= c^{\text{spec-ener}}(b_d, P_k) = b_d - \psi(P_k, a_{b_d}), \\ 0 &= c^{\text{quad-power}}(P_d^+, n_k) = P_d^+ - \chi(n_k; T_{\text{amb}}, A_P), \\ 0 &= c^{\text{lin-power}}(P_d^+, n_k) = P_d^+ - \psi(n_k; a_P). \end{aligned}$$

The subset of constraints applicable for gas turbines is

$$0 = c_{\mathcal{E},d}(x_k, x_d) = \begin{pmatrix} c^{\text{fuel}}(q_d^{\text{fuel}}, b_d, m_a, H_{c,a}) \\ c^{\text{spec-ener}}(b_d, P_k) \\ c^{\text{quad-power}}(P_d^+, n_k) \end{pmatrix}, \quad x_d = (q_d^{\text{fuel}}, b_d, P_d^+).$$

Gas driven motors are modeled by

$$0 = c_{\mathcal{E},d}(x_k, x_d) = \begin{pmatrix} c^{\text{fuel}}(q_d^{\text{fuel}}, b_d, m_a, H_{c,a}) \\ c^{\text{spec-ener}}(b_d, P_k) \\ c^{\text{lin-power}}(P_d^+, n_k) \end{pmatrix}, \quad x_d = (q_d^{\text{fuel}}, b_d, P_d^+),$$

and electric motors are either modeled by

$$0 = c_{\mathcal{E},d}(x_k, x_d) = \begin{pmatrix} c^{\text{spec-ener}}(b_d, P_k) \\ c^{\text{lin-power}}(P_d^+, n_k) \end{pmatrix}, \quad x_d = (b_d, P_d^+)$$

or

$$0 = c_{\mathcal{E},d}(x_k, x_d) = \begin{pmatrix} c^{\text{spec-ener}}(b_d, P_k) \\ c^{\text{quad-power}}(P_d^+, n_k) \end{pmatrix}, \quad x_d = (b_d, P_d^+).$$

Electric engines do not consume any fuel q_d^{fuel} however they cause electricity costs correlated to the generated power P_k .

All different compressor units, drives and connecting model aspects of a compression stage a_j , $j \in \mathcal{S}_i$ of the configuration i , are now defined. Putting all these parts together results in the stage model

$$\begin{aligned}
 0 = c_{\mathcal{E},a_j}(x_j, x_{j+1}, x_a^{\text{base}}, x_j) &= \begin{pmatrix} c_{a_j}^{\text{flow-dist}}(x_a^{\text{base}}, q_{\mathcal{U}_j}) \\ c_{a_j}^{\text{mix-temp}}(q_{\mathcal{U}_j}, T_{a,l+1}, T_j) \\ (c_{\mathcal{E},k}(x_a^{\text{base}}, x_j, x_{j+1}, x_k))_{k \in \mathcal{U}_j} \\ (c_{\mathcal{E},\sigma(k)}(x_k, x_{\sigma(k)}))_{k \in \mathcal{U}_j} \end{pmatrix}, \\
 0 \leq c_{\mathcal{I},a_j}(x_j, x_{j+1}, x_a^{\text{base}}, x_j) &= \begin{pmatrix} c_{\mathcal{I},k}(x_a^{\text{base}}, x_j, x_{j+1}, x_k) \\ c_{\mathcal{I},\sigma(k)}(x_k, x_{\sigma(k)}) \end{pmatrix}_{k \in \mathcal{U}_j}, \\
 x_j &= (q_{a_j}, (x_k, x_{\sigma(k)})_{k \in \mathcal{U}_j}).
 \end{aligned}$$

Finally, the complete model of a compressor group is represented in terms of its sub-arcs, the inlet resistor a_0 the compression stages a_j , $j \in \mathcal{S}_i = \{1, \dots, \bar{s}\}$, the outlet resistor $a_{\bar{s}+1}$ and the gas cooler $a_{\bar{s}+2}$. The model of a compressor group now reads

$$\begin{aligned}
 0 = c_{\mathcal{E},a}(x_u, x_v, x_a) &= \begin{pmatrix} c_{\mathcal{E},a_0}(x_u, x_1, x_a^{\text{base}}, x_{a_0}) \\ c_{\mathcal{E},a_j}(x_j, x_{j+1}, x_a^{\text{base}}, x_j)_{j=1}^{\bar{s}}, \\ c_{\mathcal{E},a_{\bar{s}+1}}(x_{\bar{s}+1}, x_{\bar{s}+2}, x_a^{\text{base}}, x_{a_{\bar{s}+1}}) \\ c_{\mathcal{E},a_{\bar{s}+2}}(x_{\bar{s}+2}, x_v, x_a^{\text{base}}) \end{pmatrix}, \\
 0 \leq c_{\mathcal{I},a}(x_a) &= \left(c_{\mathcal{I},a_j}(x_j, x_{j+1}, x_a^{\text{base}}, x_j) \right)_{j=1}^{\bar{s}}, \\
 x_a &= (x_a^{\text{base}}, (x_j)_{j=1}^{\bar{s}+2}, (x_{a_j})_{j=0}^{\bar{s}+1}).
 \end{aligned}$$

3.4.8. A Concrete Validation Model

For each network component introduced in Section 3.2 an NLP model has now been described. For a nonlinear problem of the form (3.58) an objective function is missing. For the sole purpose of validating a nomination no objective function is necessary, just a feasible point is required. To this end, the constant objective $f^{\text{const}}(\text{contVar}) = 0$ could be chosen. However, a zero objective leads to an ill-posed optimization problem and since an optimization problem is solved anyway, a sensible objective function does not harm.

3. Validation of Nominations

For a transport network operator the most intuitive objective function is probably a minimization of the operating cost. Besides mostly constant maintenance investments, the regular expenses are dominated by the fuel costs of compressor groups, strictly speaking the costs caused by gas-powered drives \mathbb{D}_{gas} and electricity-powered drives \mathbb{D}_{el} . When the cost per unit fuel is denoted by the coefficient ω_d an appropriate objective function is

$$f^{\text{cost}}(q_{\mathbb{D}_{\text{gas}}}^{\text{fuel}}, P_{\mathbb{D}_{\text{el}}}) = \sum_{d \in \mathbb{D}_{\text{gas}}} \omega_d q_d^{\text{fuel}} + \sum_{d \in \mathbb{D}_{\text{el}}} \omega_d P_d.$$

Under consideration of the increasing environmental awareness an ecological point of view may be preferable to the economical approach of cost minimization. To this end, minimizing the consumption of fossil natural gas may be an important aim, leading to

$$f^{\text{fuel}}(q_{\mathbb{D}_{\text{gas}}}^{\text{fuel}}) = \sum_{d \in \mathbb{D}_{\text{gas}}} q_d^{\text{fuel}}.$$

Alternatively, the focus may rest on minimum energy dissipation. For this, the power consumed by compressor groups is reduced instead of its cost,

$$f^{\text{power}}(P_{\mathbb{A}_{\text{cg}}}) = \sum_{a \in \mathbb{A}_{\text{cg}}} P_a.$$

Here, P_a denotes the combined power of all active compressor units of the compressor group a .

After choosing the desired optimization aim, the full validation NLP finally is

$$\min_x f(x) \tag{3.86a}$$

$$\text{s.t. } c_{\mathbb{V}}(x) = 0, \tag{3.86b}$$

$$c_{\mathcal{E}, \mathbb{A}}(x) = 0, \tag{3.86c}$$

$$c_{\mathcal{I}, \mathbb{A}_{\text{cg}}}(x) \geq 0, \tag{3.86d}$$

$$x \in [x^-, x^+], \tag{3.86e}$$

with the variables

$$x = (x_{\mathbb{V}}, x_{\mathbb{A}}).$$

Finally, the objective function and all constraints of (3.86) are smooth and standard NLP solvers are applicable.

3.4.9. Relaxations

Solving the ValNLP (3.86) has essentially two possible outcomes. The applied nonlinear solver either converges to a (local) minimum or it diverges. If the solver stops at a feasible point, the solution of the MPEC approach allows a feasible network operation under the physical and technical sophisticated model of the ValNLP. The MPEC solution is thus validated to be a sufficient approximation and is adjusted by the ValNLP with respect to the more detailed model. However, if model (3.86) does not yield a feasible point, no conclusion can be drawn. Since standard NLP solvers are local solvers, they may diverge even when a solution exists and usually they do not indicate any possible reasons in this case. Though global solvers exist and would resolve this dilemma, problem (3.86) is too hard for them to solve, see Section 4.1.

To gain additional information in case of an infeasible result, we introduce slack variables s^+ and s^- and relax the NLP (3.86) yielding

$$\min_{x, s^+, s^-} f^{\text{relax}}(x, s^+, s^-) \quad (3.87a)$$

$$\text{s.t. } c_{\mathcal{E}}(x) + s_{\mathcal{E}}^+ - s_{\mathcal{E}}^- = 0, \quad (3.87b)$$

$$c_{\mathcal{I}}(x) + s_{\mathcal{I}}^+ \geq 0, \quad (3.87c)$$

$$x \in [x^-, x^+], \quad (3.87d)$$

$$s^+, s^- \geq 0. \quad (3.87e)$$

The constraints $c_{\mathcal{E}, \mathbb{V}}$ and $c_{\mathcal{E}, \mathbb{A}}$ are summarized in $c_{\mathcal{E}}$ and $c_{\mathcal{I}}$ corresponds to $c_{\mathcal{I}, \mathbb{A}_{\text{cg}}}$. A constraint is called violated, if one of the associated slack variables is nonzero. The main focus lies on finding a feasible solution of (3.86). Thus, the objective function f^{relax} is a norm of the vector of slack variables, i.e. the objective function of (3.86) is omitted and (3.87) minimizes the violation of the original constraints. A standard choice for the objective function is the ℓ_1 -norm,

$$f^{\text{relax}}(x, s^+, s^-) = \|(s^+, s^-)\|_1 = \sum_{i \in \mathcal{E} \cup \mathcal{I}} s_i^+ + \sum_{i \in \mathcal{E}} s_i^-. \quad (3.88)$$

In practice, this results in a few (if any) positive slack variables and their indices give a hint of the network elements affected by the infeasibility. This information is of high interest for practitioners. A second natural choice is the ℓ_∞ -norm, which is gained by

3. Validation of Nominations

minimizing a common upper bound of all slack variables \bar{s} ,

$$f^{\text{relax}}(x, s^+, s^-, \bar{s}) = \bar{s}, \quad s^+, s^- \leq \bar{s}.$$

Numerical experiments show that the maximum slack value under the ℓ_∞ -norm is typically smaller than under the ℓ_1 -norm, but the ℓ_∞ -norm often results in a much larger number of non-vanishing slack variables when the value of the objective function is nonzero. No useful information for pin-pointing the infeasibility can be gained in this case.

The advantage of the relaxed nonlinear problem is that under the assumption of nonempty variable bounds problem (3.87) has always a feasible point. If \hat{x} is an infeasible point of the unrelaxed problem set $s_i^+ = -\min(c_i(\hat{x}), 0)$ and $s_i^- = \max(c_i(\hat{x}), 0)$ for all $i \in \mathcal{E}$ with $c_i(\hat{x}) \neq 0$. Additionally set $s_j^- = \max(c_j(\hat{x}), 0)$ for all $j \in \mathcal{I}$. The point $(\hat{x}, \hat{s}^+, \hat{s}^-)$ is then a feasible point of (3.87). It follows that the x -component of a feasible point of the relaxed problem is a feasible point of the original ValNLP, if and only if $f^{\text{relax}}(x, s^+, s^-) = 0$ holds, i.e. $s^+ = s^- = 0$. The chosen NLP solver should always be able to find a feasible point of the relaxed problem which may provide useful information about the constraints which are hard to satisfy, at least in a heuristic way. While the index of a nonzero slack variable may indicate a problematic network element, there is no direct information about the significance of the violation, since the slack variables are of different physical quantities. A slack value of 10 has a different impact if it is in bar or kW. In addition, the slack values have usually complex type depending on the exact formulation of the corresponding constraint. For evaluation and comparison of resulting slack values a simple common unit like bar or kg s^{-1} is preferable.

To derive an interpretable value from a slack variable value, two interpretation schemes are introduced. For both, a small set of physical quantities from the component model is selected, e.g. pressure and mass flow, and the slack value is interpreted in terms of one of these quantities. The first suggested way to translate slack values is to reorder the corresponding constraint until one of the reference quantities is singled out. For pressure as the reference quantity, the equation of state (3.64) is thus transformed into

$$0 = \frac{\rho z RT}{m} - p. \quad (3.89)$$

The reinterpreted slack value \bar{s} is then gained by setting the solution x^* into (3.89), yielding

$$\bar{s} = \frac{\rho^* z^* RT^*}{m^*} - p^*.$$

3.4. High Accuracy Optimization (ValNLP)

This approach has some drawbacks. If several nonzero slack values are associated with the same network element, each violated constraint will almost surely lead to a different interpreted value. These values have different physical units, if the constraints cannot be solved for the same reference quantity. Thus, the user has to judge several different values in different units for a single network element. Lastly, the transformation is only applicable if the constraint can be solved for one of the reference quantities.

As an alternative approach for arcs, an heuristic based on a small NLP for each network element $a = (u, v)$ with violated constraints is presented. The arc is modeled as described in the previous sections. The values at the incident nodes and the flow q_a are fixed according to the solution x^* of the relaxed ValNLP, except for the reference quantity. The difference between x_{ref} and its value in the solution x_{ref}^* is minimized. In summary, the following NLP is solved:

$$\min_x |x_{\text{ref}} - x_{\text{ref}}^*| \quad (3.90a)$$

$$\text{s.t. } c_{\mathcal{E},a}(x) = 0, \quad (3.90b)$$

$$c_{\mathcal{I},a}(x) \geq 0, \quad (3.90c)$$

$$x_i - x_i^* = 0, \text{ for all } x_i \in \{x_u, x_v, q_a\} \setminus \{x_{\text{ref}}\}, \quad (3.90d)$$

$$x \in [x^-, x^+]. \quad (3.90e)$$

The variable vector x summarizes x_u , x_v and x_a . The value of the objective function is returned as the interpretation of the violation at the element a after a successful solution of (3.90).

This approach has some desirable properties. The constraints of the validation NLP are reused without requiring any changes. The constraints do not need to satisfy any special properties except for the basics described in Section 2.1. In particular, implicit functions are possible. From the practitioner's point of view the main advantage of this approach is the single value it returns. However, there is also a drawback. This approach may fail, if the infeasibility cannot be expressed in a single quantity x_{ref} . As an example, if a turbo compressor has to be operated above its upper speed limit and to the right of the choke line in the relaxed solution, this infeasibility cannot be expressed in pressure or flow alone. In addition, the return value is not a direct interpretation of the nonzero slack values associated with arc a , but interpret the full local situation.

4. Numerical Experiments

In this chapter the models presented in Chapter 3 are further examined by numerical experiments. In Section 4.1 a short overview of the applicability of MINLP solvers for gas network problems is given. It is illustrated why another approach is required for large-scale problems like the validation of nominations (NoVa) on real-world networks.

In Section 4.2 the MPEC approach is applied on NoVa problems based on instances of the gas network library `GasLib` [56]. Several regularization strategies and parameter settings are compared with emphasis on the penalization strategy (2.9) and the relaxation approach (2.10) which are discussed in Section 2.2.4.

The accuracy of multiple model variants of the ValNLP is investigated in Section 4.3. To this end, the conditions of transported gas is computed for a large number of single network elements and several settings of pressure and flow based on the models described in Section 3.4. The results are compared to those gained by the commercial simulation software `SIMONE` 5.73 [120, 141].

All computations take place on a desktop PC with an Intel i7 920 CPU and 12 GB memory running openSUSE 12.3. Calculations based on the models described in Section 3 are conducted using `GAMS` 24.0.2 [55].

4.1. Solving Mixed-Integer Nonlinear Problems Directly

Since the problem of validation of nominations is in fact an MINLP, the usage of state-of-the-art MINLP solvers suggests itself. Some modifications of the model described in Section 3.2 are necessary, since MINLP solvers commonly require twice continuously differentiable constraints and objective functions. To this end, the techniques described in Section 3.3 and 3.4 can be re-used.

However, Pfetsch et al. [104] observed that MINLP solvers are not reliable on real-world network sizes. The authors tested an isothermal MINLP model with uniform

4. Numerical Experiments

gas composition including the quadratic pressure loss equation (3.43) and nonlinear representations of the characteristic diagrams of compressors, see Section 3.4.7, on a set of real-world network data. A feasible solution is found only for a small number of the tested instances within the time limit of 4 h and infeasibility is not proven for any infeasible case. Pfetsch et al. concluded that current general-purpose MINLP solvers cannot solve large-scale NoVa problems. Nevertheless, there exist further applications which may benefit from a global MINLP solver, e.g. solving the ValNLP (Section 3.4.8) to a global minimum, solving the interpretation NLPs (Section 3.4.9) to a global minimum and solving mixed-integer nonlinear models of small subnetworks like compressor groups.

Applying MINLP solvers on small-scale problems like single network elements or small subnetworks offers an alternative approach to the second stage of the MPEC heuristic. Instead of solving the NLP described in Section 3.3.8, each compressor group is solved for the pressure and flow demands at the incident nodes according to the solution of the first stage. The drawback of this approach is that the compressor groups are solved separately and overloaded compressor groups thus cannot be supported by other compressor groups. To test the applicability of MINLP solvers on these kinds of subnetwork problems, 16 feasibility problems concerning a compressor group incorporating 6 compressor units and 11 configurations are solved. Each problem defines a different combination of inflow pressure, outflow pressure and flow through the compressor group. All but one instances are solved successfully by BARON within the time limit of 10 min. The validation NLP is able to verify 14 of the gained solutions. In most successful cases BARON takes between one and three seconds, only two cases require 76 s and 158 s. SCIP decides 7 instances as feasible, all are verified by the validation NLP. The remaining instances however are decided as infeasible, which is not correct for at least those instances that are successfully verified based on the solution generated by BARON. SCIP also requires between 1 and 3 seconds per instance, except for one case that takes 23 seconds.

While SCIP performs quite poorly on this test set of small MINLP problems, only two instances do not result in a solution by BARON that can be verified by the validation NLP. The results show, that BARON is applicable for MINLP feasibility problems of small-scale networks and subnetworks. By applying a suitable objective function, BARON may also be applicable on cost minimization problems of compressor groups.

Solving the relaxed validation NLP to a global optimum increases the significance of any remaining non-zero relaxation variables and their interpretation for the practitioner, since the global solution indicates the location and quantity of the reason of violated constraints at least as accurate as a local solution does. The applicability of global MINLP solvers

for this task is tested on spot tests. To this end, ValNLP models of four instances of `gaslib-582` from GasLib [56] are selected. The models are generated during the numerical analysis of the MPEC, the required discrete decisions are thus generated by the MPEC, see Section 4.2 for details. Here, the ℓ_1 -objective function (3.88) was chosen. Two of the selected models are solved by `lpopt` 3.10[134] with vanishing objective value, one model is solved to optimality with a positive objective value and the fourth model is reported to be infeasible by `lpopt`. To fit the needs of global solvers the models are extended by lower and upper variable bounds if not yet existent. These adjusted models are solved by the global MINLP solvers BARON 11.9.1 [127] and SCIP 3.0 [1], and by the local NLP solver `lpopt` to check the impact of the additional variable bounds. The time limit is set to one hour for each computation.

The originally infeasible instance is confirmed to be infeasible by all solvers. Both global solvers detect the infeasibility in preprocessing, SCIP finishes after only 0.2s while BARON requires 35s. `lpopt` stops after 2.3s. In case of the instance with nonzero objective function, BARON comes to the same objective value than `lpopt`, but requires 22.3s compared to 3s. SCIP fails to find any feasible solution within the time limit. The first instance with originally vanishing objective value is solved by `lpopt` in 2.5s and by BARON in 11.6s. Both solvers confirm the vanishing objective value. SCIP fails again to find a feasible solution within the time limit. In contrast, the last instance shows a discrepancy in the results. `lpopt` converges with a vanishing objective value after 3.73s. BARON however spends 728s in preprocessing before concluding with the alleged global optimal solution with an objective value of 141.81. Clearly this cannot be the global optimum, since the local solver `lpopt` finds a solution with vanishing objective value (which is a global solution). Again, SCIP does not find any feasible solution within the time limit.

In summary, several observations are made. The additional variable bounds have no significant impact on the result of `lpopt` in any case. SCIP fails to find any feasible solution. The solver only concludes successfully in case of the infeasible instance. In contrast, all results computed by BARON are achieved during its preprocessing, the quality of BARONs results however are unsatisfactory. In three cases, BARON stops with the same objective value as `lpopt` but requires significantly more time. In the last described case, BARON calls a solution a global optimum which clearly is not. While the larger runtime may be regarded as a reasonable price for a global solution, the solutions of BARON seem not to be reliable enough to gain an advantage over a local solver. In contrast, in every tested case the solution of `lpopt` is the best in terms of required computation time and objective value.

4. Numerical Experiments

The reliability of MINLP solvers improves for small nonlinear problems. In the ForNe project MINLP solvers are successfully used to compute variable bounds of compressor units. For this purpose, a set of continuous nonlinear optimization problems is solved, minimizing and maximizing the desired variables with respect to the nonlinear model of the compressor unit. A similar field of application of global solvers are the interpretation problems 3.90 in Section 3.4.9. Knowing x_{ref} to correlate to the global minimum offers the practitioner a better basis for rating different solutions than the result of a local NLP solver.

In summary, general-purpose global MINLP solvers are applicable for small subnetworks and the analysis of single network elements as in case of the compressor group optimization. They are already applied in practice on nonlinear models of single arcs to generate global solutions. However, in case of large-scale gas transport networks however these approaches typically fail to generate reliable solutions. In case of large-scale continuous nonlinear models this improves slightly but the global solvers may stop in a false global optimum, thus offering no advantage over a significantly faster local NLP solver.

The following section examines if a multi-stage approach consisting of the MPEC approach presented in Section 3.3 and the validation NLP of Section 3.4 is better fitted for large-scale NoVa problems.

4.2. Solving NoVa with the MPEC Approach

In Section 3.3 a group of reformulation techniques were presented, that are suitable to derive an MPEC from the nonsmooth MINLP problem presented in Section 3.2. The aim of the combined approach of MPEC and ValNLP described in Chapter 3 is to find a solution of the NoVa problem by applying standard NLP solvers in short time. However, the MPEC resulting from the descriptions in Section 3.3 does not satisfy the necessary preconditions for most state-of-the-art NLP solvers, see Section 2.2. For this reason, regularization schemes introduced in Section 2.2 are applied to the MPEC (3.53).

The strategies introduced in Section 2.2 all are based on solving a sequence of NLPs in which a regularization parameter ξ is driven to zero and the sequence of solutions of the NLPs converges to the solution of the original MPEC. This approach has two drawbacks. First, for a successful run each NLP of the sequence needs to be solved to optimality. As soon as one of the NLP runs fails to converge, the whole process fails. Second, solving a sequence of NLP requires a lot of time which contradicts the aim of a fast validation.

Thus, the approaches presented in the following sections solve just a single optimization problem by handling the regularization parameter as part of the model.

Overall, the regularization parameter ξ is handled in three different ways. The first simply sets the regularization parameter ξ to a constant value. Another way to control the regularization parameter is to handle it as a variable that is minimized in the objective function. If the variable is minimized to zero, all complementarity constraints of the MPEC are satisfied. The third approach adds the constraint $e^\xi - 1 = 0$ to the problem, see Section 2.2.4. Again, the regularization parameter is handled as a variable. The variable ξ is zero for every feasible point, thus every feasible point is also feasible for the MPEC.

Not every combination of control mechanism and regularization approach is sensible. For example, an appropriately chosen constant value may result in good results for the penalization approach, while any nonzero value is not applicable in case of the relaxation approach. A constant nonzero value would not enforce the satisfaction of the complementarity constraints in any way.

The complementarity constraints of the MPEC (3.53) differ from the complementarity constraints handled in Section 2.2 since the factors are not always non-negative. As an example, both characteristic functions (3.45) and (3.46) of valves have no designated sign. Possible adjustments of the regularization approaches are described in the corresponding subsections.

Since there is no generally acknowledged superior regularization strategy and the suitability of regularization strategies is in fact problem-dependent, several adjusted strategies are tested. In addition, the success of the applied regularization schemes may depend on the choice of the NLP solver. Hence, the interior-point method `Ipopt` 3.10 [134], the SQP method `SNOPT` 7.2-12 [59] and the generalized reduced gradient method `CONOPT` in version 3 and 4 [31, 32, 33, 34] are applied.

The solvers and regularization schemes are compared based on the results of 500 randomly chosen instances of the network `gaslib-582` from `GasLib` [56]. The full list of tested instances is stated in Section A.3. For each instance a validation of nominations process is computed that consists of three stages. Stage 1 is the regularized version of the MPEC (3.53), in stage 2 the heuristic for finding active configurations (3.57) is applied on the instances passing the first stage and the instances passing the second stage are finally validated by a `ValNLP` run in the third stage. The objective function of the `ValNLP` is the ℓ_1 -norm of slack variables (3.88). A problem instance is considered to be validated successfully, if

4. Numerical Experiments

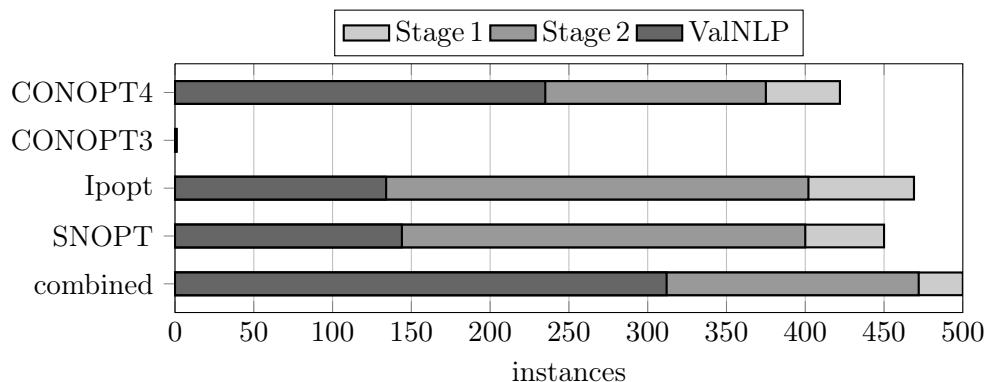


Figure 4.1. Successfully solved instances when solving the MPEC directly

the objective value of the ValNLP is at most 10^{-3} . This value results from experiences gained in the project ForNe [71] and offers a tradeoff between realizability of the solution and a successful solution process. The value is small enough, that occurring violations can typically be compensated in practice.

While the different solvers and regularization schemes are applied on the MPEC problem (3.53), both the heuristic (3.57) and the ValNLP are solved by `Ipopt`. None of the test instances contained a control valve without remote access, hence its model variant in the MPEC has not to be decided. For the validation NLP, an isothermal model variant with uniform gas composition and the quadratic pressure loss model (3.70) is chosen.

4.2.1. Direct Approach

Convergence theory of most standard NLP solvers is not applicable for the MPEC (3.53), since this problem does neither satisfy LICQ nor MFCQ. However, this does not imply that an NLP solver will fail to solve the MPEC (3.53) for all chosen instances. The solution process of an instance may result in a feasible point anyway, but with an assumably slow rate of convergence.

To see the effect of regularization approaches, the 500 chosen problem instances are first solved without a regularization scheme, i.e. this direct approach solves the unmodified complementarity constraints

$$\phi_i(x)\psi_i(x) = 0, \quad i \in \mathcal{C}. \quad (4.1)$$

The results of all solvers are illustrated in Figure 4.1. It shows the numbers of instances

solver	direct approach			modified direct approach		
	stage 1	stage 2	ValNLP	stage 1	stage 2	ValNLP
CONOPT4	3.7	1.9	1.4	9.2	1.7	2.2
CONOPT3	1.5	1.1	–	–	–	–
lpopt	49.5	1.3	1.8	68.2	1.6	1.9
SNOPT	5	1.6	1.4	19.5	1.7	2.2

Table 4.1. Average runtimes in seconds of the direct approach

solved successfully in the MPEC (stage 1), the heuristic for determining the active configurations (stage 2) and the ValNLP. While the solvers CONOPT4, SNOPT and lpopt successfully solve more than 400 instances of the MPEC, the quality of the gained MPEC results differ. lpopt finds 469 results in stage 1, of which 402 pass the second stage, but only 134 pass successfully the validation NLP. In contrast, applying CONOPT4 results in 422 successfully solved instances of stage 1, of which 375 pass the second stage and 235 are finally validated by the validation NLP. The older version of CONOPT seems not to cope well with the complementarity constraints. Only a single instance passes the first and second stage and was rejected by the ValNLP. SNOPT is comparable to lpopt. Combining the results of the different solvers shows that their sets of solved instances differ. In summary, all 500 instances pass the first stage, 472 the second stage for at least one solver and 312 instances are successfully validated by the ValNLP. These are 77 instances more than in case of the best single solver, CONOPT4.

Table 4.1 shows the average computation times of the successfully solved or validated instances. The second stage and the ValNLP take 1 s to 2 s. In contrast, the different solvers result in very different runtimes of the first stage. While CONOPT4 requires an average time of 3.7 s and SNOPT requires 5 s, lpopt has an average runtime of 49.5 s.

In summary, implementing the complementarity constraints directly without a regularization scheme works surprisingly well for most solvers. lpopt, SNOPT and CONOPT4 solve at least 84% of the test cases despite the drawbacks of complementarity constraints. The best solver of the tested ones for solving the MPEC (3.53) without adjustments is CONOPT4. It results in the largest rate of successfully validated instances and is comparably fast. CONOPT3 however seems to suffer under the loss of constraint qualifications. The changes between both versions of CONOPT significantly improve the results. lpopt and SNOPT result in a large number of cases that pass the second stage but are not validated. This indicates, that the heuristic in stage 2 is not able to suggest feasible configurations in these cases, i.e. the first stage solutions overestimate the possibilities

4. Numerical Experiments

of the compressor groups. Besides a more sophisticated model for compressor groups in the first stage this may be countered heuristically by minimizing the pressure increase at compressor groups or minimizing the distance of the working point to the center of the feasible working range as suggested for the MILP model in [71].

While `lpopt` solves the largest number of cases in the first stage, it often has to fall back to a restoration phase and an emergency mode in these cases. This is the main reason for the comparatively large computation time in the first stage and indicates, that the problems with complementarity constraints are hard to solve, despite the good rate of success.

Besides complementarity constraints the model of the first stage contains inequalities of type (3.54), which result also in a violation of LICQ and MFCQ in certain cases as described in Section 3.3.7. The direct approach is modified to tackle this problem by relaxing the inequality constraint and minimizing the value of the relaxation variable, yielding

$$\phi_i(x)\psi_i(x) + s_i \geq 0, \quad \phi_i(x) \geq 0, \quad s_i \geq 0, \quad i \in \mathcal{I}_{\text{Acv}} \cup \mathcal{I}_{\text{Acg}}, \quad (4.2a)$$

$$f^{\text{mod}}(x, s) = f(x) + \sum_{i \in \mathcal{I}_{\text{Acv}} \cup \mathcal{I}_{\text{Acg}}} s_i. \quad (4.2b)$$

This renews the idea of Scholtes' relaxation approach [117] and constraint qualifications are typically satisfied at every feasible point (x^*, s^*) with $s^* > 0$.

Besides violating LICQ in certain cases, the solutions computed by the direct approach without any modifications show a tendency to artificial flow in loops of arcs without pressure loss, e.g. bypassed control valve stations and compressor groups, shortcuts, and open valves. Here, additional flow of arbitrary size (within the variable bounds) may circle around the loops without entering or leaving the loop. This does not contradict the flow balance equations (3.10), but without countermeasures this may even influence the decision of complementarity constraints during computation. For example, artificial flow through a valve, which would have zero flow otherwise, prevents the closing of the valve. Thus, the sum of the flows through valves, compressor groups and control valve stations is minimized also. Applying the changes

$$\phi_i(x)\psi_i(x) + s_i \geq 0, \quad \phi_i(x) \geq 0, \quad s_i \geq 0, \quad i \in \mathcal{I}_{\text{Acv}} \cup \mathcal{I}_{\text{Acg}}, \quad (4.3a)$$

$$f^{\text{rel-flow}}(x, s) = f^{\text{mod}}(x, s) + \sum_{a \in \mathbb{A}_{\text{vl}} \cup \mathbb{A}_{\text{cg}} \cup \mathbb{A}_{\text{cv}}} q_a^2, \quad (4.3b)$$

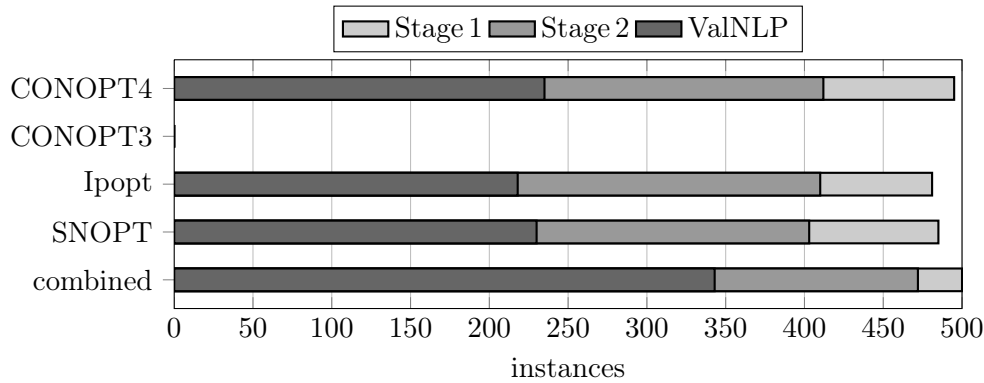


Figure 4.2. Successfully solved instances for the direct approach with modifications (4.3)

to the MPEC model (3.53) leads to improved results for `Ipopt` and `SNOPT`. Figure 4.2 and Table 4.1 illustrate the new test results. The number of instances passing the first stage increased for all solvers except `CONOPT3`, which now finds no solution at all. While the number of successfully validated instances does not change when `CONOPT4` is applied, it drastically increases for `Ipopt` and `SNOPT`, which now lead to 218 and 230 validated instances, respectively. A drawback is the increase of the runtimes, when (4.3) is applied. While the increased time of stage 2 and the ValNLP are small, the increase in stage 1 is between 5.5s and 18.7s.

In total, all instances passed the first stage and again 472 instances pass the second stage for at least one solver. Now 343 instances are successfully validated in total, this is an increase of 33 instances compared to the direct approach without (4.2a) and (4.3b).

Both applied modifications have different consequences for the MPEC approach. The relaxation (4.2a) reduces the number of constraints violating LICQ. This is the main reason for the increased numbers of successfully solved first-stage-instances for `SNOPT`, `Ipopt` and `CONOPT4`. The minimization of flow on active arcs is first and foremost a heuristic improving the coupling of the first and second stage. It results in better discrete decisions and initial values. The improved initial values also lead to a reduction of artificial flow in loops in the solutions of the second stage and thus to better initial values for the validation NLP. Minimization of the flows increase the problem complexity compared to the sole feasibility problem of the unmodified direct approach and leads to increased computation times.

Summarizing, the applied modifications support the solvers in the first stage and decrease the gap between the number of successfully solved second stage solutions and the successfully validated cases. Hence, they are also applied in the following, if possible.

4.2.2. Penalization Approach

The penalization approach (2.9) requires several adjustments before general NLP solvers can be applied. This approach must cope with complementarity constraints containing characteristic functions with arbitrary sign while it is designed for nonnegative factors ϕ and ψ . The characteristic functions cannot be shifted by a constant value since they have to evaluate to zero if their represented state is active and taking the absolute value is not a smooth function that is required for general NLP solvers. Therefore, the characteristic functions are squared if necessary, i.e. functions $\phi(x)$ and $\psi(x)$ are defined as

$$\phi(x) = \chi_1(x)^{\tau_1}, \quad \psi(x) = \chi_2(x)^{\tau_2},$$

with $\tau_i = 1$, $i \in \{1, 2\}$, if $\chi_i(x) \geq 0$ and $\tau_i = 2$ else. By doing so, the resulting complementarity constraint $\phi(x)\psi(x) = 0$ is consistent with Section 2.2.4 and can be handled by the penalization approach.

Since the modifications (4.3) have a significant positive influence on the results of `Ipopt` and `SNOPT` in case of the direct approach, they are also applied in combination with the penalization approach.

Three possible control mechanisms for the parameter ξ have been suggested so far: an appropriately chosen constant value, the minimization of a representing variable and the adding of the constraint (2.13). Practical experience shows, that minimizing ξ in the objective usually does not result in a vanishing ξ . Thus the penalization parameter is either chosen constant or handled by constraint (2.13).

A properly chosen small constant value leads to minimized violation of the complementarity constraints. Figure 4.3a shows the results gained for the penalization approach

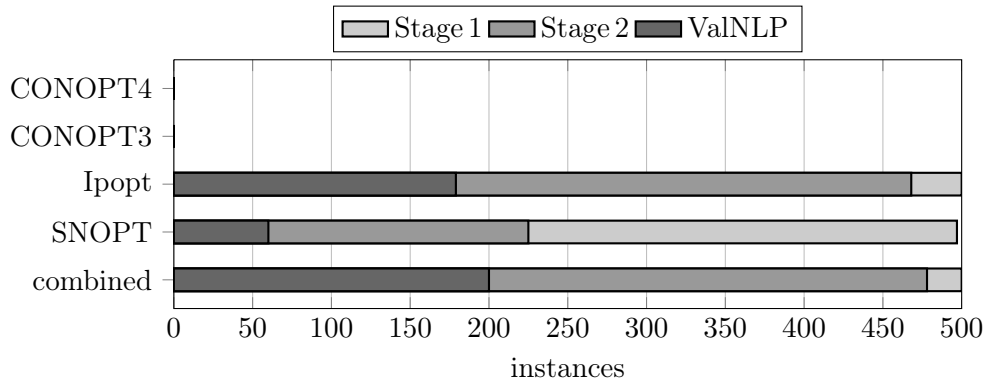
$$f^{\text{penalty}}(x) = f(x) + \frac{1}{\xi} \sum_{i \in \mathcal{C}} \phi_i(x)^{\tau_i} \psi_i(x)^{\tau_i}, \quad (4.4a)$$

$$\xi = 10^{-6}, \quad (4.4b)$$

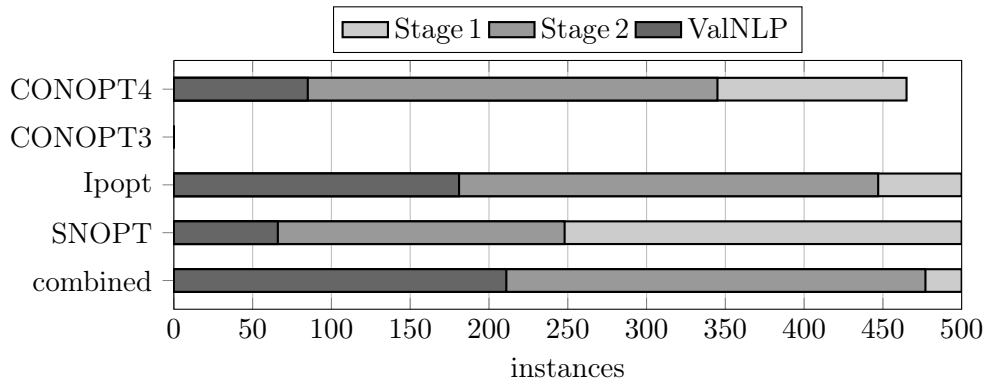
with constant penalization parameter. Figure 4.3b shows the results for

$$f^{\text{penalty}}(x) = f(x) + \frac{1}{\xi} \sum_{i \in \mathcal{C}} \phi_i(x)^{\tau_i} \psi_i(x)^{\tau_i}, \quad (4.5a)$$

$$\xi = 10^{-4}, \quad (4.5b)$$



(a) Constant parameter $\xi = 10^{-6}$



(b) Constant parameter $\xi = 10^{-4}$

Figure 4.3. Successful instances for the penalization approach with adjustments (4.3) and constant parameter ξ

While the choice of ξ has a rather marginal influence on the result of `Ipopt` and `SNOPT`, at least when it is small enough, it is critical for `CONOPT4`. If the penalization parameter is chosen as 10^{-4} , `CONOPT4` results in a feasible point for 465 instances of stage 1, of which 85 test cases are validated by the `ValNLP`. In contrast, no instance is solved successfully for $\xi = 10^{-6}$.

For both choices of the penalization parameter `Ipopt` proves to be the best solver in terms of validated instances. 181 cases are validated with $\xi = 10^{-4}$ and 179 are validated for the other choice. `CONOPT3` however does not find any solution for neither parameter setting.

Combining all solvers, all instances pass stage 1 for both choices of the penalization parameter. If the parameter ξ is set to 10^{-6} , 478 instances pass the second stage. 200 of

4. Numerical Experiments

solver	$\xi = 10^{-6}$			$\xi = 10^{-4}$		
	stage 1	stage 2	ValNLP	stage 1	stage 2	ValNLP
CONOPT4	–	–	–	32.3	3.2	1.6
CONOPT3	–	–	–	–	–	–
lpopt	12.3	3.2	3	6.1	1.7	1.7
SNOPT	168.8	5.9	2.3	113.2	19.8	1.7

Table 4.2. Average runtimes in seconds of the penalization approach

solver	stage 1	stage 2	ValNLP
CONOPT4	–	–	–
CONOPT3	–	–	–
lpopt	8.3	2.2	1.7
SNOPT	108.4	84.9	1.4

Table 4.3. Average runtimes of successful instances using the penalization approach (4.7) and the controlling constraint (4.6)

them are successfully validated in total. For $\xi = 10^{-4}$ one instance less passes the second stage, but 211 are successfully validated.

Table 4.2 shows the corresponding runtimes. `lpopt` profits considerably from the regularization, the average runtime of the first stage with $\xi = 10^{-4}$ is only one tenth of the average runtime required for the modified direct approach. In contrast, both `SNOPT` and `CONOPT4` take longer than when the direct approach is applied. The second stage and the validation NLP require about 2 s, except for `SNOPT` where the second stage takes significantly longer. A possible reason might be, that the complementarity constraints are not satisfied as good as with the other solvers.

Overall, the success rate of the first stage is considerably higher than in case of the direct approach for all instances. This is to be expected, since the penalization approach does not guarantee a satisfaction of all complementarity constraints and the resulting problems should be easier to solve. Interestingly, the penalization approach with a constant penalization parameter has no positive effect for any solver on the tested scenarios when compared to the direct approach with modifications. In fact, the number of successfully solved instances has decreased for every solver. The value 10^{-6} for the penalization parameter has a positive influence on `lpopt` only, all other solvers gain better results for the larger value. It is possible that the smaller value leads to numerical difficulties in the solution process.

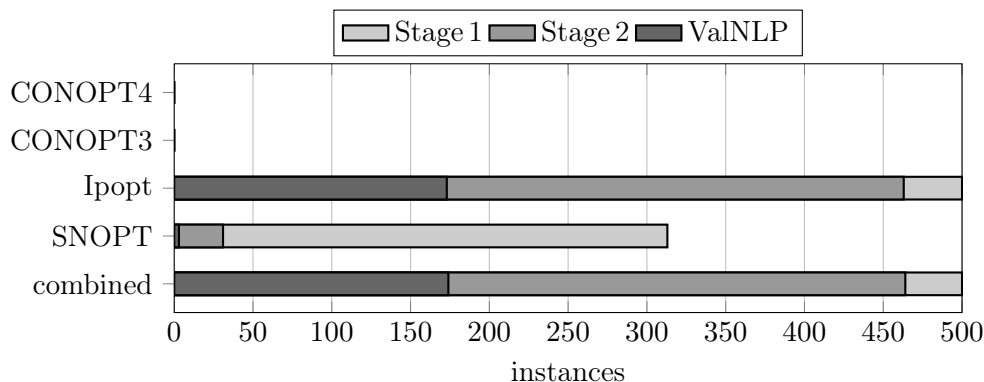


Figure 4.4. Number of successful instances using the penalization approach (4.7) and the controlling constraint (4.6)

Controlling the penalization parameter by the constraint

$$0 = e^{\xi} - 1, \quad (4.6)$$

and an initial value of 1 for ξ yields the penalization approach

$$f^{\text{penalty}}(x) = f(x) + \frac{1}{\xi} \sum_{i \in \mathcal{C}} \phi_i(x)^{\tau_i} \psi_i(x)^{\tau_i}, \quad (4.7a)$$

$$0 = e^{\xi} - 1. \quad (4.7b)$$

This setting does not harmonize well with CONOPT3, CONOPT4 and SNOPT, see Figure 4.4. Both versions of CONOPT do not find any solution in stage one, while SNOPT solves 313 instances, but only 31 pass the second stage of which 3 are successfully validated. The results of Ipopt however are comparable to a constant choice of ξ . All instances pass the first stage, 463 the second stage and 173 are successfully validated. Ipopt finds feasible solutions faster in all instances with the additional constraint than with a constant parameter, see Table 4.3. The average times are 8.3 s, 2.2 s and 1.7 s for stage 1, stage 2 and the validation NLP, respectively. In combination, 174 instances are successfully validated, meaning SNOPT only contributes a single instance not solved by Ipopt.

The controlling constraint (4.7b) results in a penalization parameter of 0. This may result in numerical difficulties in the evaluation of the objective function and to a ill-conditioned problem. The same holds for very small constant choices of the regularization parameter. Because of this, CONOPT4 fails for $\xi = 10^{-6}$ and problem formulation (4.7). As a

4. Numerical Experiments

countermeasure (4.7b) may be replaced by

$$0 = e^{\xi - \epsilon} - 1,$$

with $\epsilon > 0$, resulting in $\xi \rightarrow \epsilon$ during computation.

On the chosen test set, the penalization approach is an improvement over the unmodified direct approach only for `lpopt`, independent of the handling of the regularization parameter. Based on the validation NLP results, the modified direct approach is superior even for `lpopt`, despite a larger number of solved first stage instances. The large number of instances failing the second stage in case of `SNOPT` for all tested variants of the penalization approach indicates that the complementarity terms in the objective functions are not minimized to zero for many test cases resulting in infeasible decisions. In case of `lpopt` most instances fail the validation NLP. The reasons are twofold. First, the abilities of compressor groups are again overestimated in the first stage. Second, some cases of nonzero complementarity terms in the first stage are compensated by positive slacks in the second stage heuristic.

4.2.3. Relaxation Approach

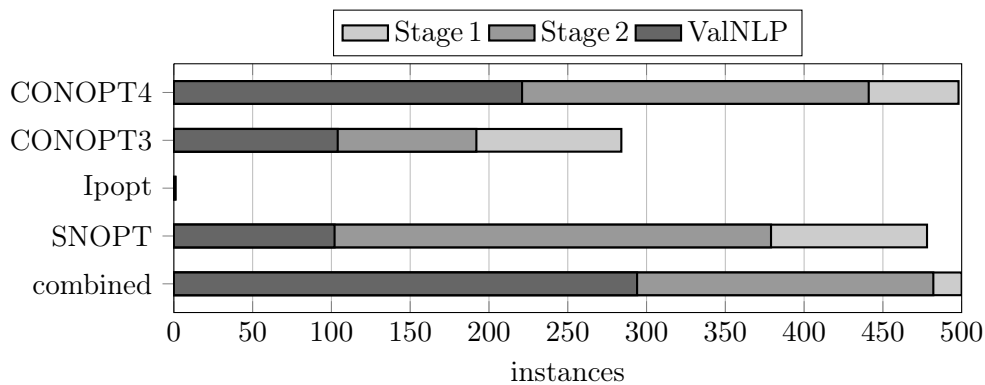
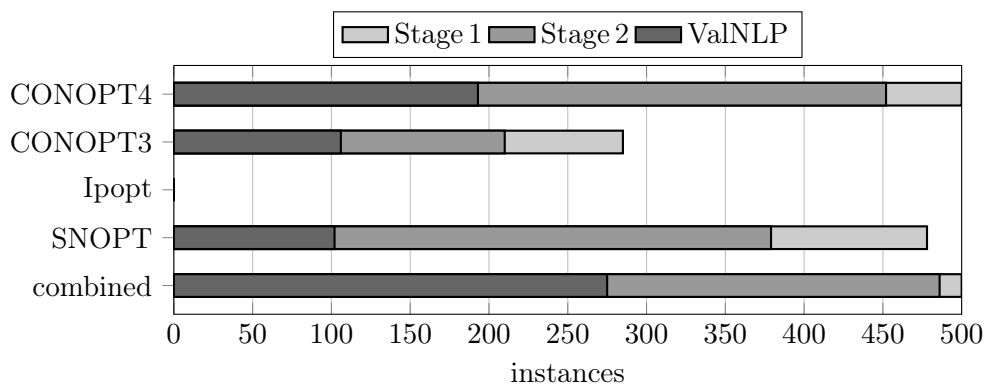
The second relaxation scheme presented in Section 2.2 is the relaxation scheme suggested by Scholtes [117]. Every complementarity constraint is replaced by an inequality constraint

$$\phi(x)\psi(x) \leq \xi, \tag{4.8}$$

with $\phi(x), \psi(x) \geq 0$ and $\xi \geq 0$. Note that setting the relaxation parameter ξ to zero coincides with the direct approach, since $\phi, \psi \geq 0$.

The handling of the relaxation parameter differs from the previous section. When choosing a constant nonzero value the product $\phi(x)\psi(x)$ is not forced to zero by any means and the original complementarity constraint is typically not satisfied. Two control mechanisms of the relaxation parameter ξ are therefore tested. First, the relaxation parameter is minimized in the objective. If it is minimized to zero, the original complementarity constraint is satisfied. Second, the constraint (2.13) is applied instead with a sufficiently large initial value for ξ .

Similar to the penalization approach, the relaxation approach cannot be applied directly, if ϕ or ψ does not have a nonnegative lower bound. Without zero as a lower bound, the product $\phi\psi$ can become negative and the inequality (4.8) of the relaxation approach does

(a) Initial value $\xi_0 = 1$ (b) Initial value $\xi_0 = 100$ **Figure 4.5.** Successfully solved instances of the relaxation approach minimizing ξ (4.9)

not converge to the complementarity constraint for $\xi \rightarrow 0$. Squaring all relevant factors as suggested for the penalization approach resolves this issue.

Figure 4.5 shows the number of feasible instances for the relaxation scheme

$$f^{\text{relax}}(x) = f(x) + \xi, \quad (4.9a)$$

$$\xi \geq \phi_i(x)^{\tau_i} \psi_i(x)^{\tau_i}, \quad i \in \mathcal{C}, \quad (4.9b)$$

and two different choices for the initial value of the relaxation parameter, $\xi_0 \in \{1, 100\}$. In addition, the modification (4.2) is applied. The impact of the initial value is negligible, the number of feasible instances in each stage is nearly the same, except for CONOPT3, where 18 instances more are solved for the larger initial value in stage 2, and CONOPT4, where 28 instances more are successfully validated by the validation NLP. This is the first approach presented, where CONOPT3 solves a noteworthy number of instances. In

4. Numerical Experiments

solver	$\xi_0 = 1$			$\xi_0 = 100$		
	stage 1	stage 2	ValNLP	stage 1	stage 2	ValNLP
CONOPT4	31.7	1.1	1.5	28.4	1.2	1.5
CONOPT3	15.3	1.2	1.5	28.6	2.7	2.7
lpopt	146.1	1	–	–	–	–
SNOPT	28.6	1.2	1.6	36.4	1.6	2.4

Table 4.4. Average runtimes in seconds for the relaxation approach minimizing ξ (4.9)

contrast, **lpopt** seems not to cope well with the relaxation approach. The best result is a single instance that passed the second stage for the smaller initial value. The best solver in this setting is **CONOPT4**. For the small choice of the initial value 498 instances pass the first stage, of which 441 succeed in the second stage. 221 instances are finally validated.

The main reason of the differences is the handling of infeasible initial points. The initial primal infeasibility is about 10^9 to 10^{10} due to the squared complementarity constraints. All solvers perform significant work to get to a feasible point. **CONOPT** and **SNOPT** cope better with the large primal infeasibility than **lpopt**, which often fails in its restoration phase [134].

Combining the results of all solvers, all instances pass the first stage for both choices of the initial value. The second stage is passed by 482 and 486 instances for the small and large initial value, respectively. Of all instances, 294 ($\xi_0 = 1$) and 275 ($\xi_0 = 100$) instances are validated in at least one setting.

Table 4.4 lists the average runtimes. When ignoring the single instance solved by **lpopt**, the runtimes of the solvers are more equal than in previous approaches and the largest average runtime is 36 s in the first stage, while the other stages take between 1 s and 2.7 s. Finding feasible solutions in about half a minute is a significant improvement over the manual determination by sequential simulation, however most settings of the direct approach are significantly faster, see Section 4.2.1.

When the relaxation parameter is controlled by the additional constraint (2.13), i.e. the relaxation model

$$\xi \geq \phi_i(x)^{\tau_i} \psi_i(x)^{\tau_i}, \quad i \in \mathcal{C}, \quad (4.10a)$$

$$0 = e^\xi - 1, \quad (4.10b)$$

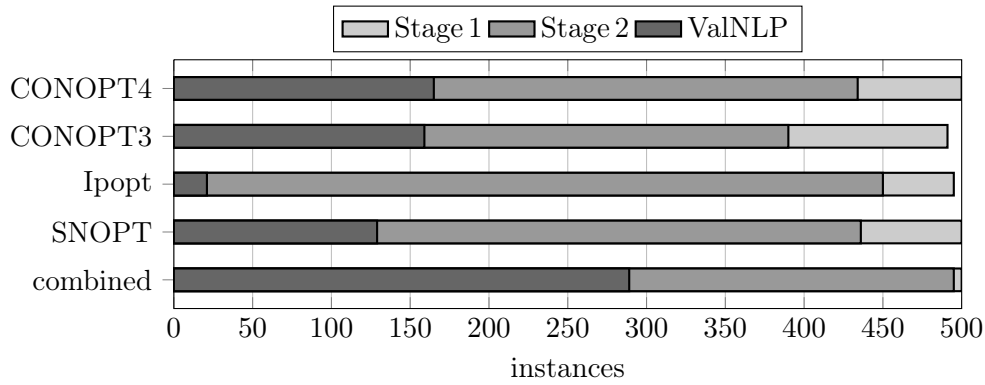
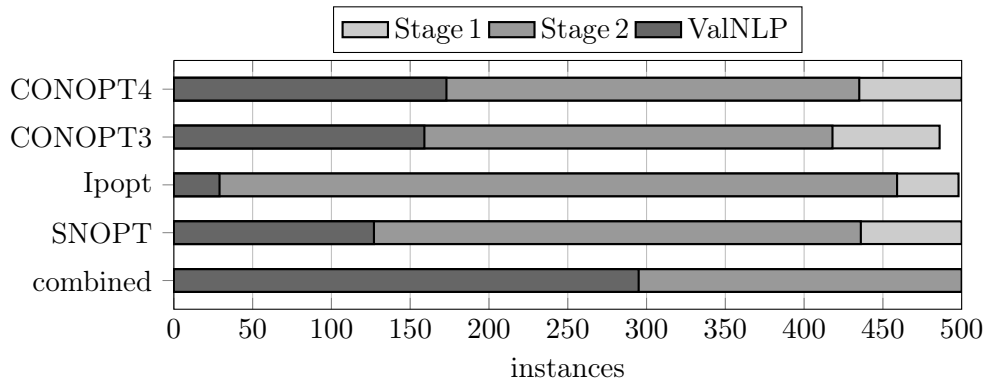
(a) Initial value $\xi_0 = 1.0$ (b) Initial value $\xi_0 = 100.0$

Figure 4.6. Successfully solved instances of the symmetric relaxation approach (4.11) minimizing ξ

replaces the complementarity constraints, only CONOPT4 and SNOPT find solutions in the first stage. CONOPT4 solves 18 instances in stage 1, 9 in stage 2 and 6 are successfully validated. The average runtime of the first stage is 122.6s. SNOPT performs better, solving 393, 289 and 115 instances. Here, the average runtime of the first stage is 105.7s. The sets of successfully validated instances are disjunctive, so 121 instances are validated in total. The controlling constraint performs worse than minimizing the relaxation parameter in the objective function. Significantly less instances if any are solved and the average runtime is more than three times larger.

The drawback of squaring the factors of the complementarity function is a worsening of the condition of the optimization problem. This may be the reason why Ipopt has problems finding a feasible point. In the following, two alternative approaches are presented that do not increase the problem complexity significantly.

4. Numerical Experiments

solver	$\xi_0 = 1.0$			$\xi_0 = 100.0$		
	stage 1	stage 2	ValNLP	stage 1	stage 2	ValNLP
CONOPT4	8.2	1.1	1.4	6.9	2.5	1.8
CONOPT3	7.5	1.3	1.5	5.5	1.5	1.6
lpopt	6.6	1.6	1.4	11.9	3.3	3
SNOPT	15.3	2.1	1.4	25.6	2	2.7

Table 4.5. Average runtimes in seconds for the symmetric relaxation approach

The first alternative is called the symmetric relaxation approach. Complementarity constraints without lower bound zero are now symmetrically relaxed in both directions,

$$f^{\text{relax}}(x) = f(x) + \xi, \quad (4.11a)$$

$$-\xi \leq \phi_i(x)\psi_i(x) \leq \xi, \quad i \in \mathcal{C}. \quad (4.11b)$$

Figure 4.6 illustrates the computation results for two initial values of ξ . The number of feasible instances in the first stage improves for all solvers, at least 486 instances are solved. The same holds for the second stage except for CONOPT4, which solves 7 and 17 less instances for $\xi_0 = 1.0$ and $\xi_0 = 100.0$, respectively. The number of successfully validated instances increases for all solvers except for CONOPT4 where the number decreased slightly. In total, all instances are solved by at least one solver in the first stage, 495 and 500 instances pass the second stage. With 289 and 295 cases, the combined number of validated instances is comparable to the relaxation approach with squared factors.

While the number of feasible instances in stage 1 increases for all solvers, the required average runtime decreases significantly as stated in Table 4.5. Five of eight settings have an average runtime of less than nine seconds in the first stage while most settings of the relaxation approach with squared factors require about 30 seconds in average.

In summary, the symmetric relaxation improves the performance in the first stage significantly. More instances are solved by every solver in considerably less time. However, while the number of validated instances increases, it is still smaller than the direct approach, except for CONOPT3.

If the relaxation parameter is not minimized in the objective but handled by

$$-\xi \leq \phi_i(x)\psi_i(x) \leq \xi, \quad i \in \mathcal{C}, \quad (4.12a)$$

$$0 = e^\xi - 1, \quad (4.12b)$$

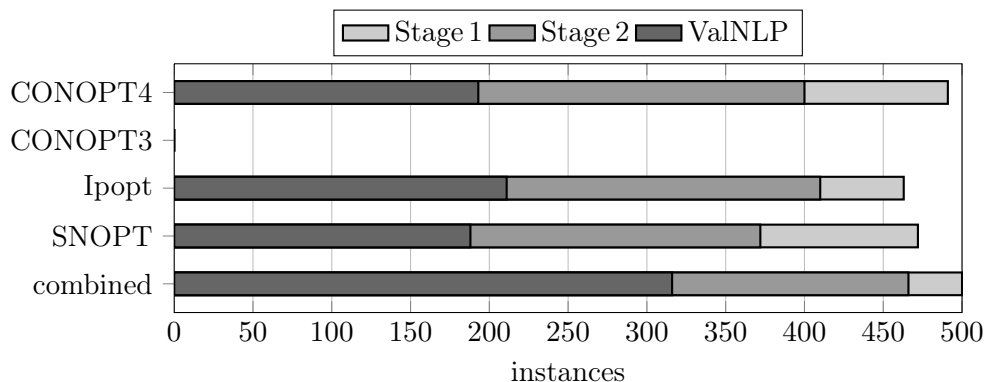


Figure 4.7. Successfully solved instances of the symmetric relaxation approach (4.11) with additional constraint (4.12b)

the number of instances passing the first stage drops a bit for each solver except CONOPT3, which solves no instance anymore. However, the number of instances finally validated increases for the three other solvers, as can be seen in Figure 4.7. As a drawback, only CONOPT4 keeps a small average runtime of the first stage with 5.7s. The average runtime of Ipopt increases to 317.7s and the one of SNOPT increases to 43.4s. The second stage and the ValNLP takes between one and two seconds in average in any case.

The second alternative seizes the idea of taking the absolute value. To avoid nonsmooth functions, the absolute value is not applied directly, but a variable splitting is applied on every factor of the complementarity constraint without lower bound zero. If both factors ϕ and ψ have to be treated, the resulting set of constraints replacing the complementarity constraint reads

$$0 = \phi_i(x) + s_{\phi_i}^+ - s_{\phi_i}^-, \quad s_{\phi_i}^+, s_{\phi_i}^- \geq 0, \quad (4.13a)$$

$$0 = \psi_i(x) + s_{\psi_i}^+ - s_{\psi_i}^-, \quad s_{\psi_i}^+, s_{\psi_i}^- \geq 0, \quad (4.13b)$$

$$\xi \geq (s_{\phi_i}^+ + s_{\phi_i}^-)(s_{\psi_i}^+ + s_{\psi_i}^-). \quad (4.13c)$$

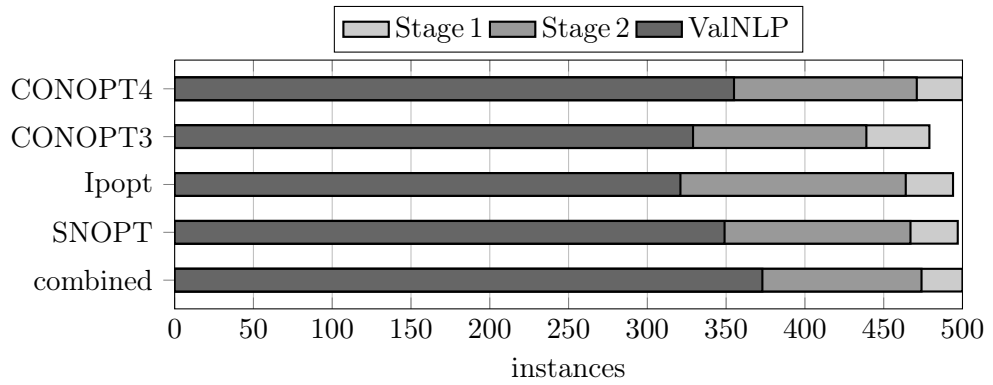
To prevent unnecessarily large splitting variables without adding additional complementarity constraints, the splitting variables are added to the objective function.

The results stated in Figure 4.8 show, that the variable splitting (4.13) with the objective function

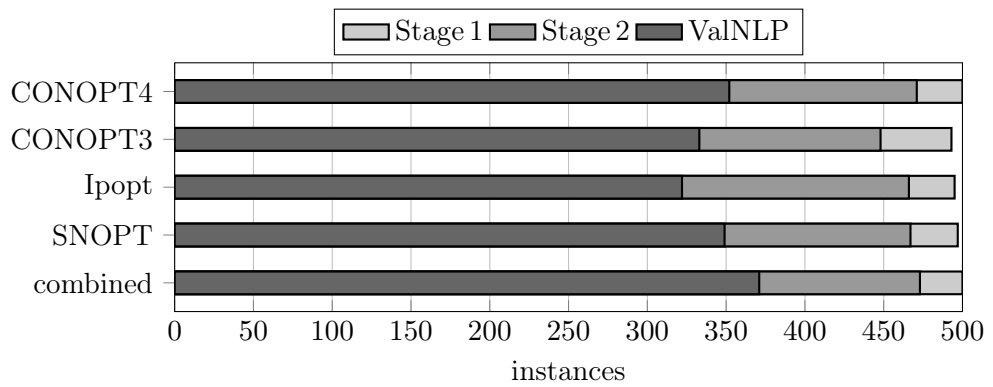
$$f^{\text{split}}(x, s) = f^{\text{relax}}(x, s) + \sum_{i \in \mathcal{C}} (s_{\phi_i}^+ + s_{\phi_i}^-) \quad (4.14)$$

and the inequality modification (4.2) is a huge improvement over the squaring of the

4. Numerical Experiments



(a) Initial value $\xi_0 = 1.0$



(b) Initial value $\xi_0 = 100.0$

Figure 4.8. Successfully solved instances of the relaxation approach with variable splitting and minimized ξ

solver	$\xi_0 = 1.0$			$\xi_0 = 100.0$		
	stage 1	stage 2	ValNLP	stage 1	stage 2	ValNLP
CONOPT4	4.9	0.9	1.3	9.3	1.5	2.5
CONOPT3	4.9	0.8	1.3	9.5	1.7	2.4
lpopt	9.2	0.9	1.3	5.2	1.4	1.3
SNOPT	7.2	0.8	1.3	7.2	0.9	1.3

Table 4.6. Average runtimes in seconds for the relaxation approach with variable splitting and minimized ξ

factors and the symmetric relaxation. At least 493 instances pass the first stage for all NLP solvers independent of the initial value, except for CONOPT3 that solves 479 instances successfully in the first stage for $\xi_0 = 1.0$. Compared to the regularization schemes presented so far, the number of validated instances is by far the best: between 321 instances in case of lpopt with $\xi_0 = 1.0$ and 355 instances in case of CONOPT4 with $\xi_0 = 1.0$ are successfully validated by the ValNLP. The choice of the initial value of the relaxation parameter hardly makes a difference. In total, all instances pass the first stage of at least one solver. Only for 26 ($\xi_0 = 1.0$) and 27 ($\xi_0 = 100.0$) instances no active configurations can be found in the second stage and 373 and 371 instances are successfully validated for $\xi_0 = 1.0$ and $\xi_0 = 100.0$, respectively.

Besides generating validated solutions for a large number of instances, the relaxation approach with variable splitting is even faster in many cases than the symmetric relaxation approach previously presented, see Table 4.6. Noteworthy is the very small average runtime of about 0.8s of the second stage for $\xi_0 = 1.0$ and every solver and the average runtime of about 1.3s of the validation NLP. A reason might be, that the solution of the previous stage is a very good initial value.

If the relaxation parameter is not a part of the objective function but is controlled by the constraint (2.13), the results are not as good in terms of validated instances, see Figure 4.9. The average runtimes are about 4 seconds for CONOPT3 and CONOPT4 and about 31 seconds for lpopt and SNOPT.

4.2.4. Further Approaches

Besides the penalization approach and the relaxation approach, the Fischer–Burmeister function (2.11) and the smoothed minimum function (2.12) are suggested as regularization

4. Numerical Experiments

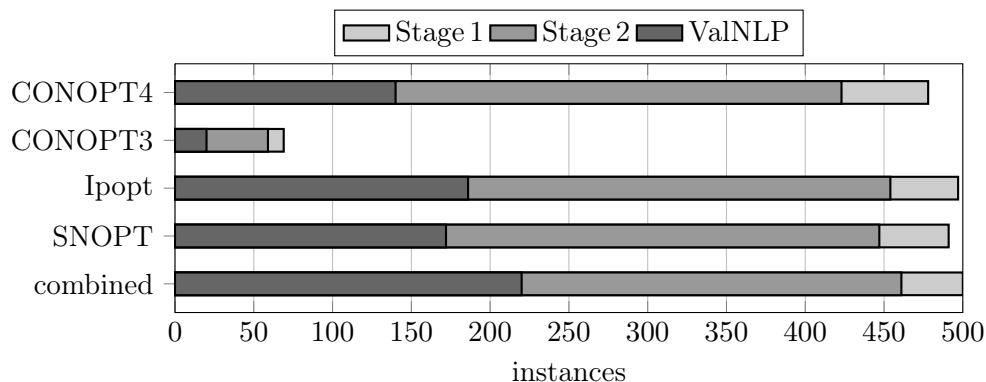


Figure 4.9. Successfully solved instances of the relaxation approach with variable splitting and constraint (2.13)

schemes in Section 2.2.4. Both NCP functions are applied on complementarity constraints with squared factors if necessary.

The regularization parameter of the Fischer–Burmeister function is minimized in the objective. This approach results in 24 successfully solved instances in the first stage when CONOPT4 is chosen as the solver and 31 successfully solved instances for SNOPT. Only 5 and 7 instances pass the validation stage, respectively. Neither CONOPT3 nor Ipopt finds any solution in the first stage at all.

The smoothed minimum function is tested with a constant choice of the regularization parameter, $\xi = 10^{-6}$. Only SNOPT was able to find any solutions. Of the 19 instances passing the first stage, 18 pass the second and 5 are finally validated.

Neither tested NCP function can compete with the other regularization schemes or the direct approach. Due to the bad results of all solvers and the similarity of the functions, other mechanisms to control the regularization parameter inside the model are not to be expected to lead to significantly better results.

4.2.5. Conclusion

In total, the MPEC formulation of the first stage and the configuration heuristic of the second stage is solved for all instances by at least one solver. The validation NLP accepts discrete decisions determined by the second stages in 386 cases. It is unknown, for how many instances discrete decisions exist, that result in a feasible state with respect to the model of the validation NLP. However, the large variety of different solution strategies

applied in this chapter lets assume, that the actual number is not much larger than 386, if at all.

Of all approaches, those involving the objective function, e.g. the penalization schemes or the relaxation schemes with minimized regularization parameter, show the best first stage results. This is to be expected, since these approaches relax the feasible range of the original MPEC and do not guarantee the satisfaction of the original complementarity constraints. However, the small gap between the number of successful solutions of the first stage and the second stage indicates, that the first stage solutions can be interpreted as sensible discrete decisions in most cases. Only the penalization approaches solved by SNOPT results in large gaps.

In most cases the majority of the unsuccessful instances pass the second stage but are rejected by the validation NLP. Possible reasons of failure are an overestimation of the capabilities of the compressor groups by the first stage and a bad choice of the active configuration in the second stage.

Figure 4.10 groups the results of the regularization schemes listed in Table 4.7 by solvers. Each solver has some approaches that harmonizes well and some do not. CONOPT3 gains results for only half of the tested approaches whereas the newer version CONOPT4 shows a better behavior with problems in case of the penalization approach and the use of the constraint (2.13). The interior point method `lpopt` does not cope well with the relaxation approach. Of all solvers SNOPT offers the most balanced results with a large number of first stage solution for all approaches.

Despite the violation of LICQ and MFCQ, the direct approach works well with all solvers except CONOPT3. In combination with the modifications (4.3) more instances are successfully validated than by many of the other tested approaches. The best solution approach is the relaxation approach with variable splitting (4.13). In combination with CONOPT4, 355 of the 386 solved instances are validated (92%).

Results of the MPEC approach applied on different data sets are given in [71] for a smaller number of solution approaches, excluding the relaxation approach with variable splitting. In comparison, the success rate of the combinations of solver and solution approach differ between the data sets, e.g. `lpopt` and the penalization approach (4.4) was the best setting for one data set. In consequence, the best choice of solver and solution approach depends on the data set and there is no unique recommendation. Nevertheless, the very good results of the relaxation approach with variable splitting in combination with all tested

4. Numerical Experiments

solvers indicates a suitability of this approach in many situations, not only for the data set tested in this work.

(D) direct approach (4.1)	(Re) relaxation, $e^\xi - 1 = 0$ (4.10)
(mD) modified direct approach (4.3)	(sR1) symmetric, $\xi_0 = 1$ (4.11)
(P6) penalization, $\xi_0 = 10^{-6}$ (4.4)	(sR2) symmetric, $\xi_0 = 100$ (4.11)
(P4) penalization, $\xi_0 = 10^{-4}$ (4.5)	(sRe) symmetric, $e^\xi - 1 = 0$ (4.12)
(Pe) penalization, $e^\xi - 1 = 0$ (4.7)	(S1) splitting, $\xi_0 = 1$ (4.13), (4.14)
(R1) relaxation, $\xi_0 = 1$ (4.9)	(S2) splitting, $\xi_0 = 100$ (4.13), (4.14)
(R2) relaxation, $\xi_0 = 100$ (4.9)	(Se) splitting, $e^\xi - 1 = 0$ (4.13)

Table 4.7. Compared regularization approaches

4.2. Solving NoVa with the MPEC Approach

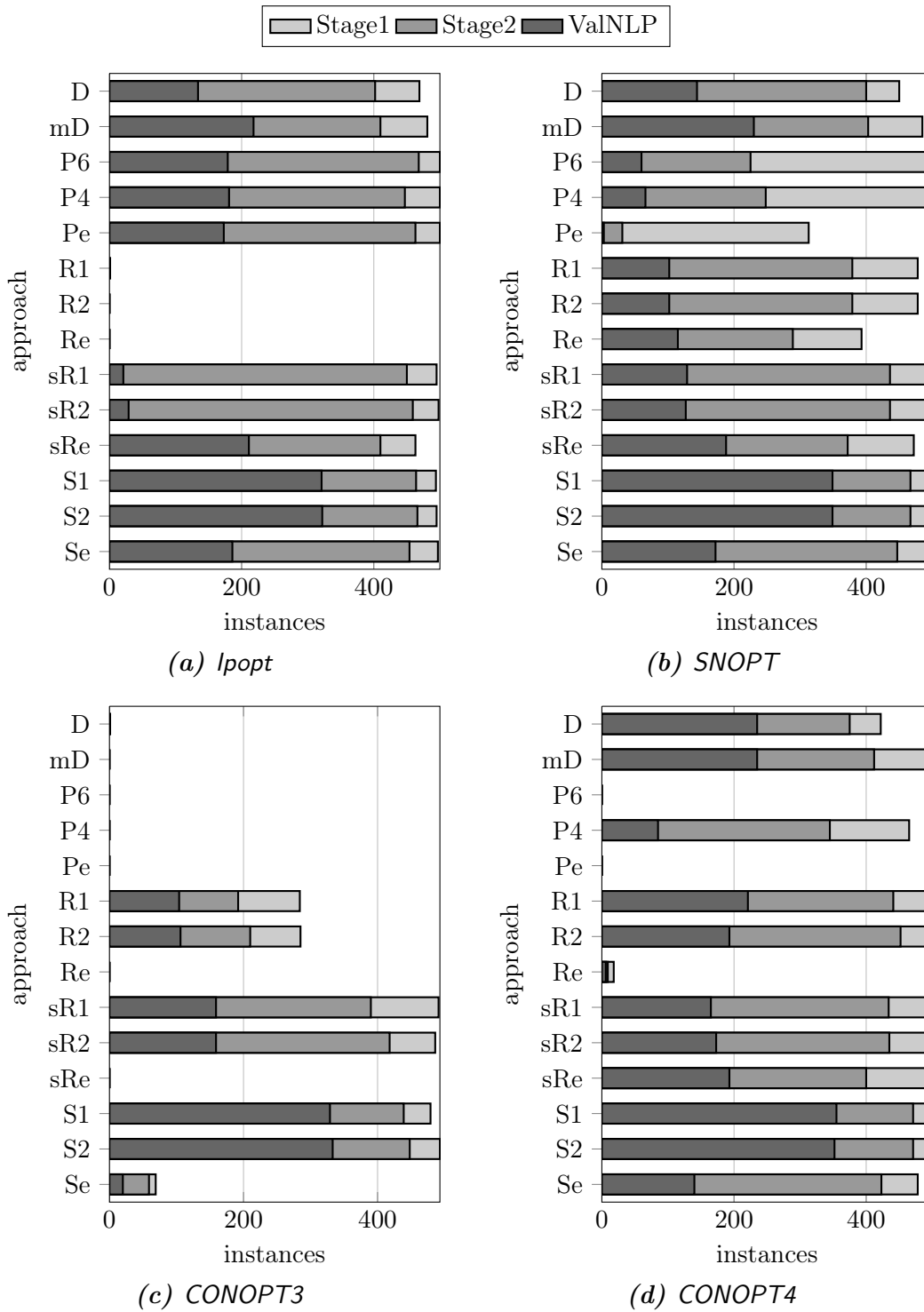


Figure 4.10. Solvers and their numbers of feasible instances for all solution approaches listed in Table 4.7

4.3. Accuracy of the Validation NLP

The model of the validation NLP (ValNLP) described in Section 3.4 is created with the purpose to gain a highly detailed mathematical description of a gas network, which is applicable for optimization. In this section it is evaluated how well the aim of high accuracy is met.

Since gaining a sufficient amount of test data at real-world gas networks for stationary gas flow is impractical, the validation is based on a comparison to the commercial gas network simulation software **SIMONE** [120, 140], version 5.73. To this end, each gas component is analyzed separately for different technical and physical settings. Each test case models an entry u , an exit v and an arc $a = (u, v)$. For a proper comparison, the settings have to be identical in both the ValNLP and **SIMONE**. Thus, the settings are restricted to the mutual possible ones. The highest common level of detail was chosen, including temperature and gas parameter tracking. In addition, the test cases describe a unique flow situation for deterministic reference values, i.e. the technical parameters (e.g. length, diameter, drag factor, characteristic diagram, ...) and the gas parameters ($p_c, T_c, \rho_0, z_0, \tilde{A}, \tilde{B}, \tilde{C}, m, H_c, \dots$) are chosen identical and the transport situation incorporating $Q_0, p_u, T_u, T_{\text{soil}}, \dots$ is fixed such that no degree of freedom remains.

The main focus lies on the comparison of realistic parameters of network devices. Since real-world network data is available in the project ForNe, a comparison based on the elements of this network suggests itself. However, the API of **SIMONE** does not offer control over every required parameter like the slope of the pipe, so each network element would have to be generated manually. Since this is not practical for the intended large amount of test cases, data for the externally controllable parameters are extracted from a real-world network supplied by the industrial partner OGE. For each technical parameter the 10 %, 35 %, 65 % and 90 % quantiles are chosen. For the remaining quantities, like inflow pressure, inflow temperature and flow, a small set of cases are created manually. The Cartesian product of the manually created parameter set and the quantiles define the set of test cases.

The lower and upper 10 % are discarded to eliminate the risk of outliers, which would result in unrealistic test cases for most parameter combinations and would distort the analysis. However, unrealistic combinations are not prevented completely, e.g. very long pipes with a small diameter and high value of roughness. These combinations may still have a distorting impact on the results, thus stating maximum deviations is pointless and the following results concentrate on average deviations.

Three different measures of deviation are regarded for an examined quantity x , e.g. outflow pressure or outflow temperature. Probably the most intuitive are the absolute deviation

$$e_{\text{abs}}(x) = |x^{\text{NLP}} - x^{\text{Sim}}|,$$

and the relative deviation

$$e_{\text{rel}}(x) = \frac{|x^{\text{NLP}} - x^{\text{Sim}}|}{|x^{\text{Sim}}|},$$

between the result of the ValNLP x^{NLP} and the result of SIMONE x^{Sim} . A third measure is applied for values which change along an arc, e.g. gas temperature. Here, the relative deviation is computed with respect to the change along the arc, i.e.

$$e_{\Delta}(x) = e_{\text{rel}}(\Delta x), \quad \Delta x = x_u - x_v.$$

Since the inflow values are fixed a priori, this is identical to

$$e_{\Delta}(x) = \frac{|x_v^{\text{NLP}} - x_v^{\text{Sim}}|}{|x_u^{\text{Sim}} - x_v^{\text{Sim}}|}.$$

This value is only computed when the change is at least 1% of the inflow value.

There exists a known model difference in case of zero flow for all elements. In SIMONE the outflow temperature is set to the soil temperature, while in case of the NLP the outflow temperature is set to the inflow temperature. For this reason, the case of zero flow is not considered for any element.

SIMONE and the ValNLP also differ in the handling of several variable bounds. While all variable bounds are part of the model of the ValNLP, SIMONE does not regard all bounds during computation, e.g. the bounds of gas velocity. Thus, several instances are computed successfully in SIMONE but not in the ValNLP. For this reason, only those cases are regarded for the analysis that converge in both the ValNLP and SIMONE.

4.3.1. Pipes

For pipes the values computed by SIMONE are compared to the values gained by the quadratic approximation (3.70), (3.71) and the discretized differential equations (3.69a), (3.69b).

The compressibility factor is computed using the AGA formula (3.59) and Papay's formula (3.60). The data sets for the technical parameters and transportation situations are stated

4. Numerical Experiments

quantity	samples	unit
L_a	0.01, 0.1, 0.9, 46	km
D_a	150, 310, 405, 1185	mm
k_a	0.006, 0.02, 0.1, 0.5	mm
h_v	-500, 0, 500	m
p_u	3.9, 15.3, 53.8, 74.4	bar
T_u	288.15, 298.15, 308.15, 318.15	K
$Q_{0,u}$	50, 250, 500, 750	1000 Nm ³ /h

Table 4.8. Parameters for test cases of pipes

setting	valid pairs	x	$e_{\text{abs}}(x)$	$e_{\text{rel}}(x)$	$e_{\text{rel}}(\Delta x)$
approximation, AGA	2419	p_v	0.11	0.008 61	0.058
		T_v	1.10	0.003 84	0.161
approximation, Papay	2651	p_v	0.10	0.009 42	0.059
		T_v	1.00	0.003 49	0.150
ODE, AGA	2658	p_v	0.05	0.003 07	0.032
		T_v	0.23	0.000 75	0.046
ODE, Papay	2659	p_v	0.05	0.003 33	0.033
		T_v	0.15	0.000 51	0.029

Table 4.9. Mean deviations of pressure (bar) and temperature (K) of pipes

in Table 4.8. The height of the entry u is fixed to 0 m. In summary, four model choices are examined for 12 288 parameter choices, resulting in 49 152 different test cases. Test cases with an unrealistic large slope are skipped.

Table 4.9 shows the resulting average deviations. The deviations between **SIMONE** and the discretized ODE model are smaller than between **SIMONE** and the quadratic approximation. This is to be expected, since **SIMONE** solves the differential equations (3.18) by numerical integration [140].

A mean deviation of about 1 K is visible in the outflow temperatures of the approximation model and **SIMONE**. Thus, the deviations in case of the approximation is about ten times larger than in case of the discretized ODEs. A possible reason is visible in Figure 3.12b. The approximation lacks the convex part for small temperatures. In many cases the approximation seems to overestimate the outflow temperature at least for most realistic flow values. However, the mean absolute deviation of about 1 K lies within the range of

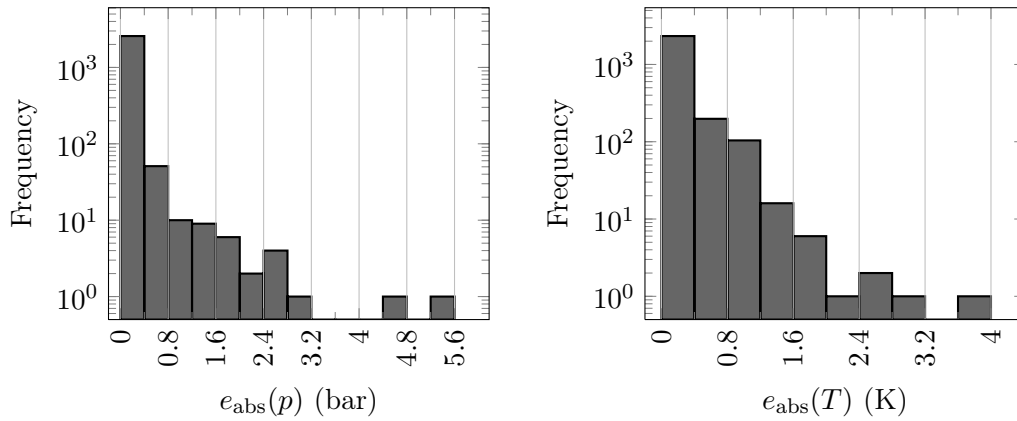


Figure 4.11. Logarithmically scaled frequencies of absolute deviations of pressure and temperature for discretized ODEs and Papay’s formula

technical parameters	scenario
$L = 46$ km	$p_{\text{in}} = 74.44$ bar
$D = 1185$ mm	$T_{\text{in}} = 318.15$ K
$k = 0.006$ mm	
$s = 0.01$	

Table 4.10. Exemplary setting of a pipe with large deviation in temperature compared to SIMONE

data accuracy, since more accurate temperature forecasts are typically not available in mid-term planning.

The logarithmically scaled histograms in Figure 4.11 show the distribution of the absolute errors. The majority of test cases concentrates on the far left, i.e. they result in very small absolute deviations. A handful of cases lie further to the right. Spot tests show that these cases mainly coincide with atypical parameter combinations resulting in a very large pressure loss along the pipe. The standard deviation for pressure is about 0.24 and in case of temperature it is about 0.29.

Table 4.10 shows exemplary data of a pipe for which a large deviation in the outlet temperature occurs. The outflow pressure in dependence of the normal volumetric flow are given in Figure 4.12. The outflow temperature is visualized in Figure 4.13. The graphs of the discretized ODE model and SIMONE run next to each other for pressure and temperature. The quadratic approximation model offer comparable pressure values for a moderate pressure loss but it underestimates the pressure loss for larger flow values

4. Numerical Experiments

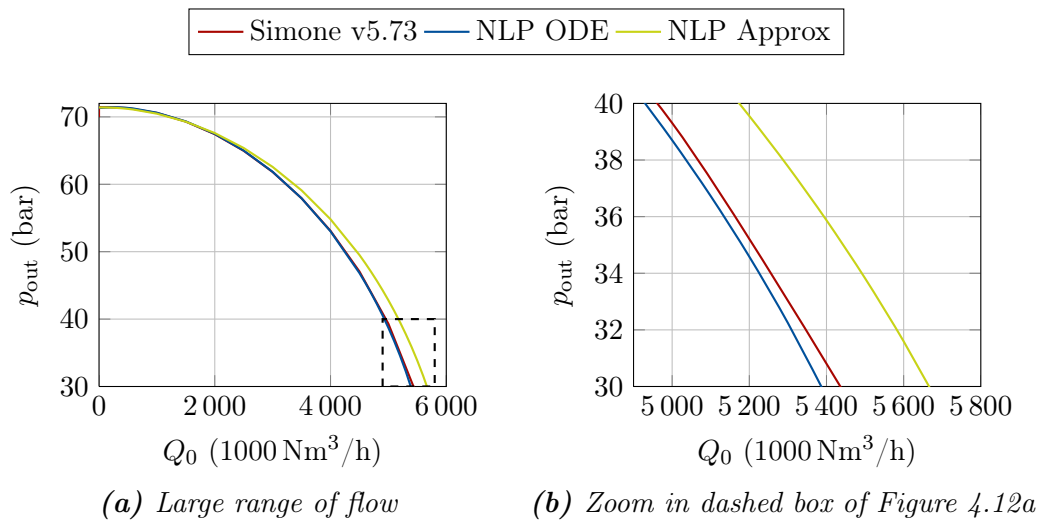


Figure 4.12. Outflow pressure vs. normal volumetric flow for the pipe of Table 4.10

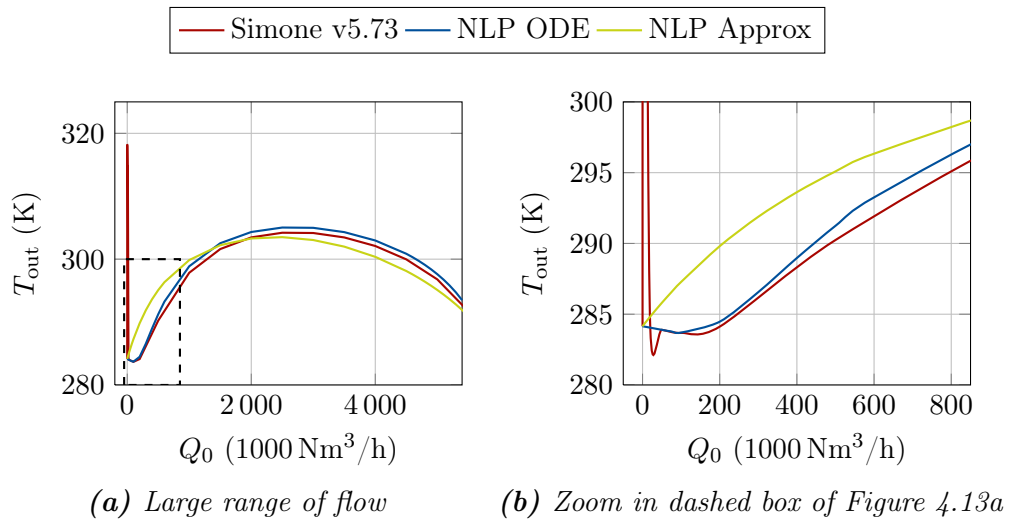


Figure 4.13. Outflow temperature vs. normal volumetric flow for the pipe of Table 4.10

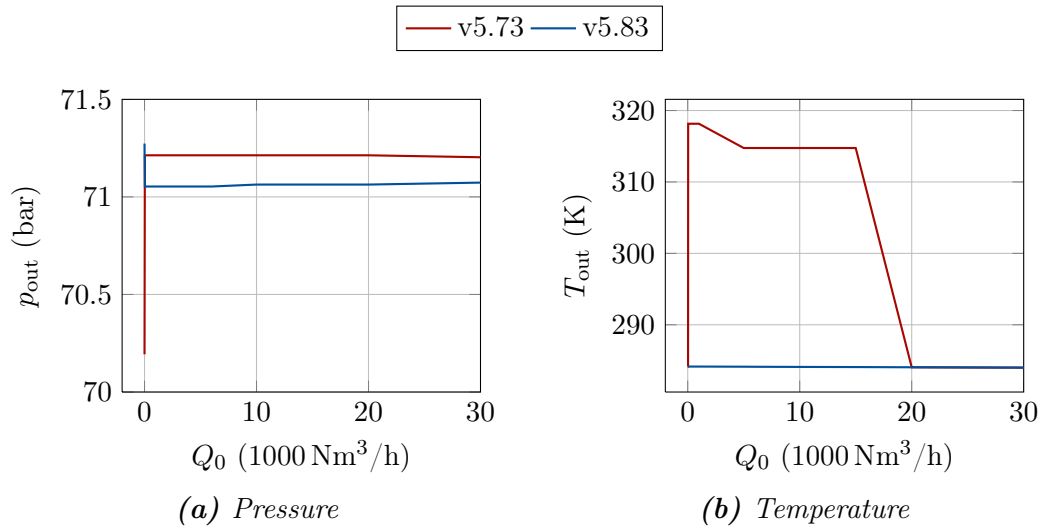


Figure 4.14. Comparison of outflow pressure and temperature values for two versions of SIMONE and small normal volumetric flows (for pipe data see Table 4.10)

in this example. In Figure 4.13a the lack of the convex curvature information in case of the approximation model is again visible. While the graph of the approximation model follows the trends of the other two models and is qualitatively comparable, this difference results in an absolute temperature deviation up to 5 K, see Figure 4.13b.

Another noteworthy phenomenon in Figure 4.13 is the spike for small flows in the graph of SIMONE. This temperature spike has no physical reason. Spot checks with version 5.83 of SIMONE do not show the same behavior, see Figure 4.14b. Thus the nonsmooth spike seems to be a bug in SIMONE version 5.73, which is fixed in version 5.83. Nevertheless, both versions have a nonsmooth transition in pressure between zero flow and positive flow, but with different amplitude. This is shown in Figure 4.14a. The pressure and temperature values also differ between both versions, despite identical settings. The maximum pressure difference for this example is 1.1 bar and the maximum temperature difference is 0.5 K.

4.3.2. Resistors

The parameters used for both resistor models (3.73), (3.74) are stated in Table 4.11. They result in 90 test cases for the linear model and 360 cases for the nonlinear model. The inflow pressure, the inflow temperature and the supplied flow are fixed and the outflow pressure (bar) and temperature (K) are computed and compared. The results of the comparisons for the linear model are stated in Table 4.12. The distribution of

4. Numerical Experiments

quantity	samples	unit
ξ_a	2, 4, 6, 8, 10	bar
D_a	300, 525, 775, 1000	mm
ζ_a	5, 20, 50, 70, 90	1
p_u	20, 40, 60	bar
T_u	283.15, 300.15, 318.15	K
$Q_{0,u}$	500, 1000	1000 Nm ³ /h

Table 4.11. Parameters of test cases of resistors

setting	valid pairs	x	$e_{\text{abs}}(x)$	$e_{\text{rel}}(x)$	$e_{\text{rel}}(\Delta x)$
AGA	90	p_v	5.05×10^{-5}	2.05×10^{-6}	1.16×10^{-5}
Papay	90	p_v	5.03×10^{-5}	2.05×10^{-6}	1.15×10^{-5}
AGA	90	T_v	8.85×10^{-1}	3.01×10^{-3}	3.37×10^{-1}
Papay	90	T_v	9.83×10^{-2}	3.34×10^{-4}	3.57×10^{-2}

Table 4.12. Mean deviations of pressure (bar) and temperature (K) in case of the linear pressure loss model of a resistor

the absolute temperature deviation is given in Figure 4.15a for the AGA formula (3.59) and Figure 4.15a states the same for Papay’s formula (3.60). If the AGA formula is chosen for the compressibility factor, the mean deviation of temperature is about ten times larger than in case of Papay’s formula, and the absolute deviation is not better than 0.2. The standard deviation of the absolute values is 0.44 in case of AGA and 0.08 in case of Papay.

Since the pressure loss equation in case of the linear model is linear, the mean deviation in the outflow pressure of about 5×10^{-5} bar for both choices of the compressibility factor offers an indication for the accuracy of SIMONE. Since the results of the NLP are computed and stored at least with double precision, the SIMONE API seems to return pressure values in single precision. Either SIMONE computes in single precision, or the API does not return the full accuracy.

The results for the nonlinear pressure loss model are stated in Table 4.13 and the absolute deviations are visualized in Figure 4.16 and Figure 4.17. Note that the axis of the frequency is logarithmically scaled. The absolute pressure deviation is small but measurable for both choices of the compressibility factor. The reason may be a larger internal precision of SIMONE or discrepancies between the implemented model and its documentation in SIMONE.

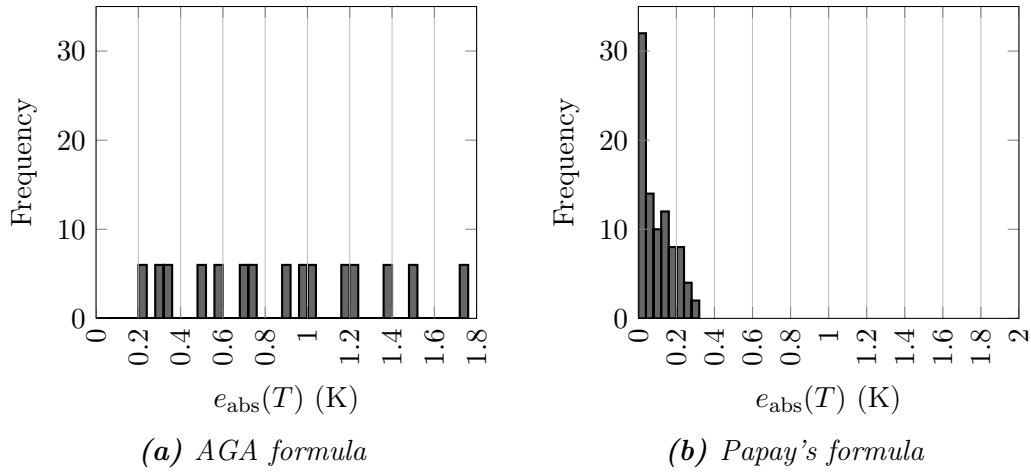


Figure 4.15. Frequencies of absolute deviations of outflow temperature in case of the linear pressure loss model of a resistor

setting	valid pairs	x	$e_{\text{abs}}(x)$	$e_{\text{rel}}(x)$	$e_{\text{rel}}(\Delta x)$
AGA	317	p_v	6.01×10^{-3}	6.31×10^{-4}	1.31×10^{-3}
Papay	318	p_v	8.27×10^{-3}	8.34×10^{-4}	1.82×10^{-3}
AGA	317	T_v	6.83×10^{-1}	2.35×10^{-3}	3.34×10^{-1}
Papay	318	T_v	2.23×10^{-1}	8.04×10^{-4}	7.39×10^{-2}

Table 4.13. Mean deviations of pressure (bar) and temperature (K) in case of the nonlinear pressure loss model of a resistor

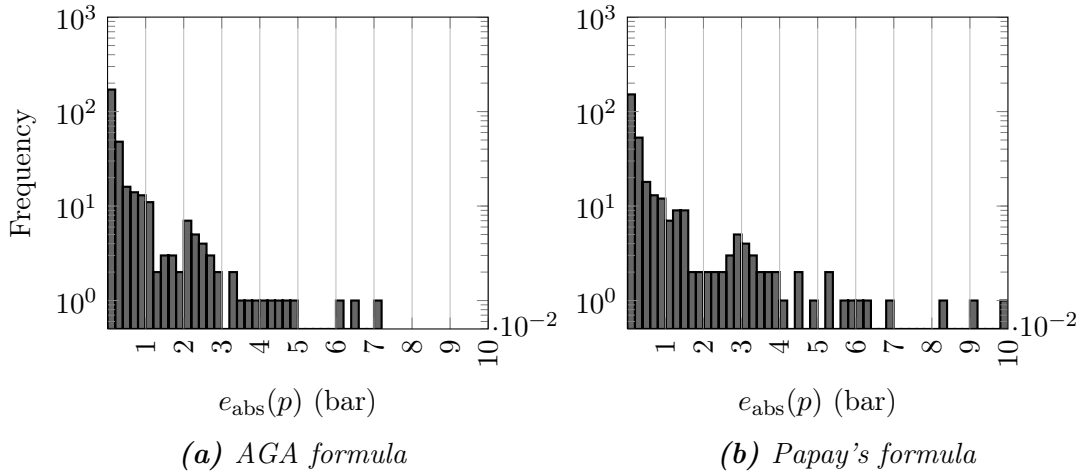


Figure 4.16. Logarithmically scaled frequencies of absolute deviations of outflow pressure in case of the nonlinear pressure loss model of a resistor

4. Numerical Experiments

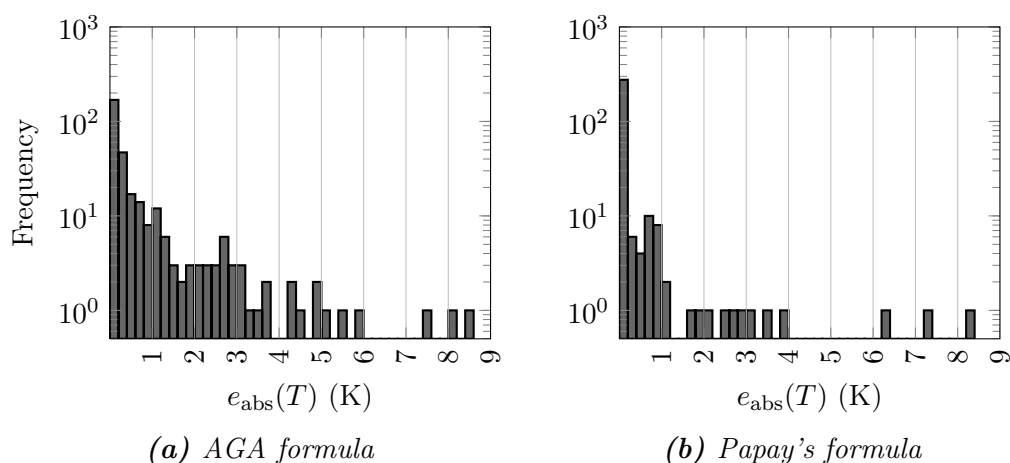


Figure 4.17. Logarithmically scaled frequencies of absolute deviations of outflow temperature in case of the nonlinear pressure loss model of a resistor

When applying the AGA formula, 317 tested cases are feasible in both programs and 318 cases are valid in case of Papay's formula. The failed test cases lead to an outlet pressure below 1.0325 bar. While the major part of the valid test cases result in an absolute temperature deviation up to 0.2 K for both models of the compressibility factor, some few outliers cause a deviation up to 8.5 K. These outliers coincide with resistor settings that cause a very large pressure loss. The largest outlier for the temperature and the AGA formula corresponds to a resistor with $\zeta = 50$ and $D = 300$ mm. The normal volumetric flow of $10^6 \text{ Nm}^3/\text{h}$ is supplied with a pressure of 50 bar, resulting in a pressure loss of 45.95 bar in **SIMONE**. Since no pressure loss at resistors with nonlinear model above 3.2 bar occurred in the successfully validated cases of a validation process containing 4227 nominations on a real-world network and 22 275 pressure loss values in total, it can be safely assumed that such large pressure losses and their causing parameter settings are unrealistic. Furthermore, the temperature change in both resistor models is identically based on the Joule–Thomson effect (3.63) and the fixed pressure loss settings in case of the linear model do not result in such large outliers. Ignoring all test cases with a pressure loss above 4 bar in **SIMONE** the mean absolute deviation reduces to 5.96×10^{-3} K with a standard deviation of 9.9×10^{-3} . The average relative deviation is 1.76585×10^{-5} .

For both linear and nonlinear pressure loss model there is a visible difference in the mean temperatures between the choices for the compressibility factor. The results computed with the AGA formula result in three to ten times larger deviations.

quantity	samples	unit
Δp	0, 5, 10	bar
p_u	20, 40, 60	bar
T_u	283.15, 300.15, 318.15	K
$Q_{0,u}$	500, 1000	1000 Nm ³ /h

Table 4.14. Parameters of test cases of control valves

setting	valid pairs	x	$e_{\text{abs}}(x)$	$e_{\text{rel}}(x)$	$e_{\text{rel}}(\Delta x)$
AGA	54	p_v	4.47×10^{-5}	1.44×10^{-6}	6.77×10^{-6}
Papay	54	p_v	4.47×10^{-5}	1.44×10^{-6}	6.77×10^{-6}
AGA	54	T_v	7.39×10^{-1}	2.51×10^{-3}	3.38×10^{-1}
Papay	54	T_v	9.38×10^{-2}	3.19×10^{-4}	4.09×10^{-2}

Table 4.15. Mean deviations of pressure (bar) and temperature (K) of control valves

4.3.3. Control Valves with Remote Access

To get a deterministic situation for a control valve with remote access, the inflow pressure, inflow temperature, the pressure reduction and thus the outflow pressure are a priori fixed. The data samples are given in Table 4.14. They result in 108 different test cases. Due to these fixations, the NLP model is equivalent to that of the resistor model with linear pressure loss. The pressures are coupled linearly and the temperature change is modeled by Joule–Thomson (3.63). The resulting deviations are stated in Table 4.15 and the frequencies of the absolute deviations of temperature are illustrated in Figure 4.18. As to be expected, the results are very similar to the results of resistors with linear pressure loss model. Again, there exists a mean absolute deviation in pressure of about 5×10^{-5} bar.

4.3.4. Compressors

In case of compressors, the inflow pressure, the pressure increase, the flow through the unit and the inflow temperature are fixed to receive a deterministic scenario. Based on the fixed values, the specific change in adiabatic enthalpy (kJ kg^{-1}), power (MW) and outflow temperature (K) are compared for 18 model settings, including different choices for the compressibility factor, isentropic exponent and temperature rise equations. In summary, 1458 test cases are examined for both piston compressors and turbo compressors. Tables 4.16 and 4.17 list the settings used for piston compressors and turbo compressors. They

4. Numerical Experiments

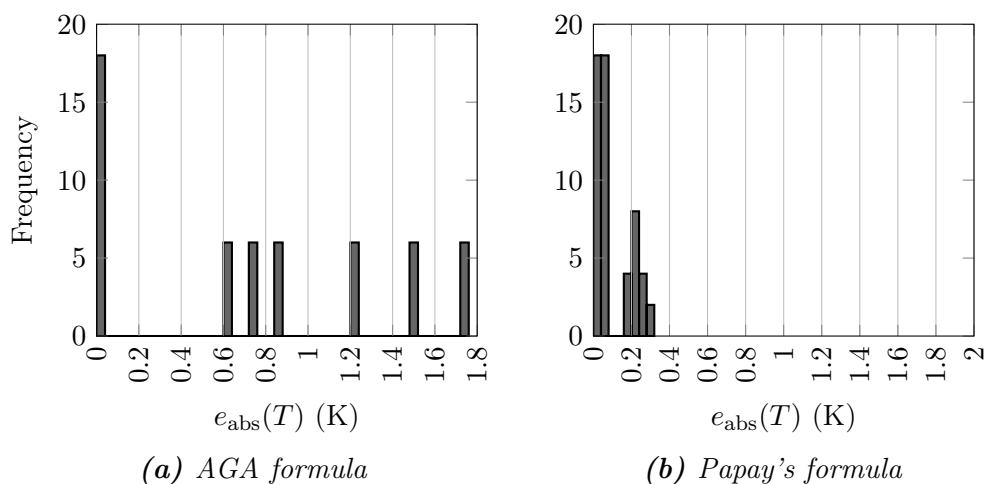


Figure 4.18. Frequencies of absolute deviations of outflow temperature of control valves

quantity	samples	unit
Δp	10, 15, 20	bar
p_u	45, 50, 55	bar
T_u	283.15, 300.15, 318.15	K
$Q_{0,u}$	300, 400, 500	1000 Nm ³ /h

Table 4.16. Parameters of test cases of piston compressors

differ only in the flow values, which are slightly larger for turbo compressors. The results are given in Table 4.18 and Table 4.19. All relative pressure deviations are at most 0.2% and the relative deviations with respect to the temperature change are about 2%. The reason for the remaining differences may lie in the calculated isentropic exponent and adiabatic efficiency. Since both sizes cannot be accessed directly in SIMONE and thus cannot be compared directly to the values computed by the NLP, further examination is difficult.

quantity	samples	unit
Δp	10, 15, 20	bar
p_u	45, 50, 55	bar
T_u	283.15, 300.15, 318.15	K
$Q_{0,u}$	400, 500, 600	1000 Nm ³ /h

Table 4.17. Parameters of test cases of turbo compressors

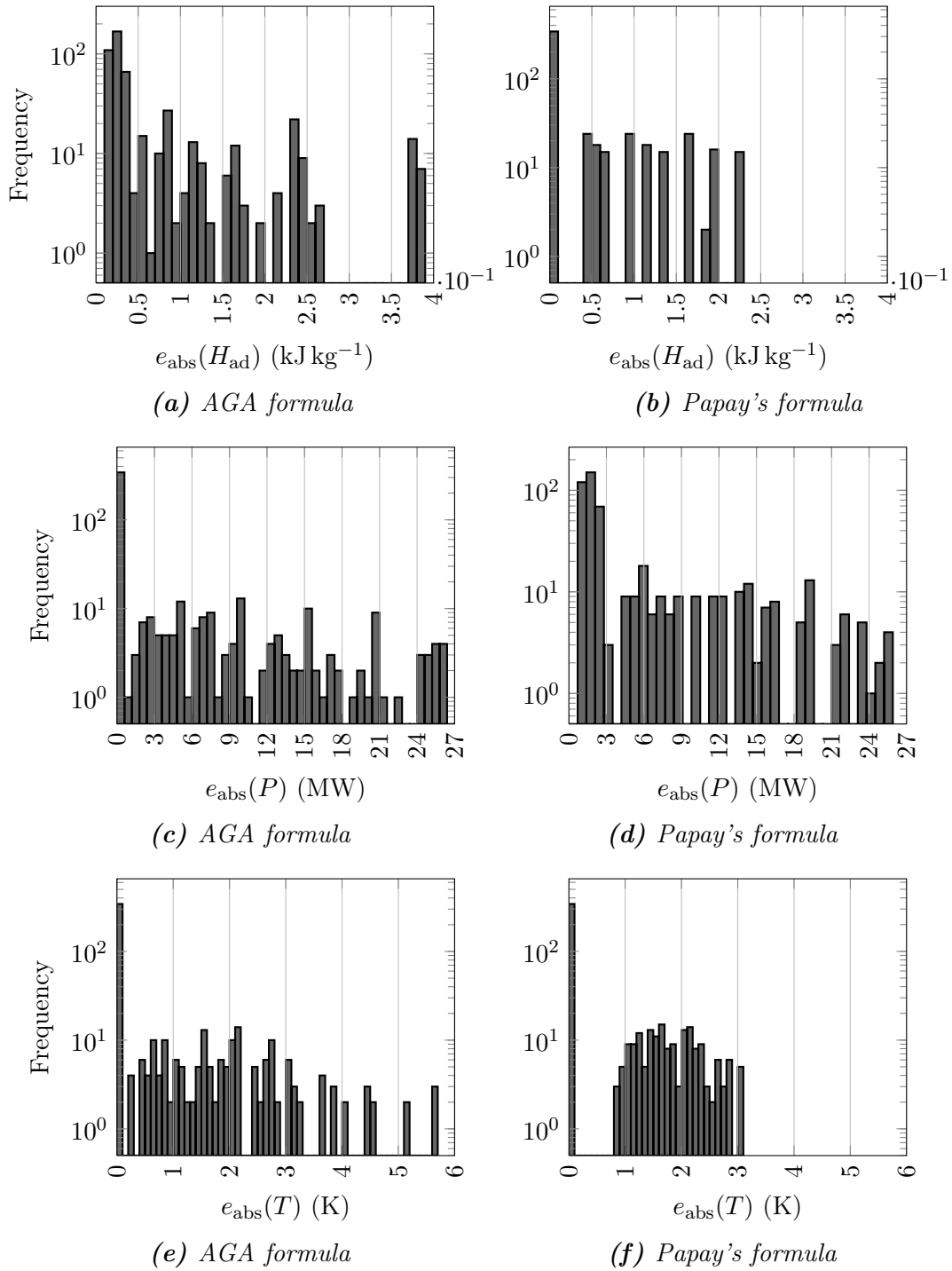


Figure 4.19. Frequencies of absolute deviations of specific change in adiabatic enthalpy, power and outflow temperature for piston compressors

4. Numerical Experiments

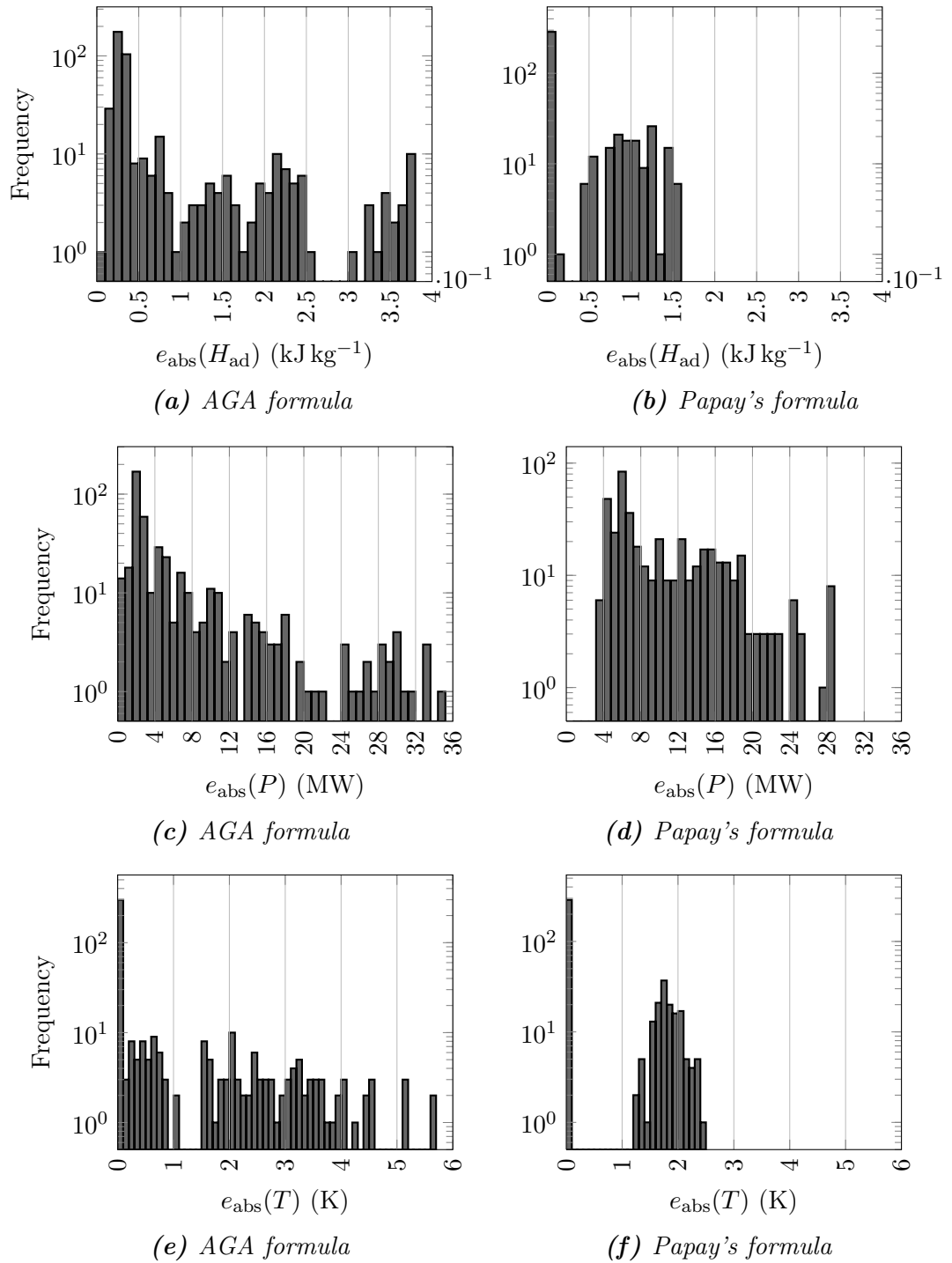


Figure 4.20. Frequencies of absolute deviations of specific change in adiabatic enthalpy, power and outflow temperature for turbo compressors

setting	valid pairs	x	$e_{\text{abs}}(x)$	$e_{\text{rel}}(x)$	$e_{\text{rel}}(\Delta x)$
AGA	513	H_{ad}	7.21×10^{-2}	2.08×10^{-3}	–
AGA	513	P	4.36×10^{-3}	1.40×10^{-3}	–
AGA	513	T_v	6.60×10^{-1}	2.07×10^{-3}	2.63×10^{-2}
Papay	513	H_{ad}	4.37×10^{-2}	1.20×10^{-3}	–
Papay	513	P	5.32×10^{-3}	1.70×10^{-3}	–
Papay	513	T_v	6.06×10^{-1}	1.86×10^{-3}	2.43×10^{-2}

Table 4.18. Mean deviations of piston compressors

setting	valid pairs	x	$e_{\text{abs}}(x)$	$e_{\text{rel}}(x)$	$e_{\text{rel}}(\Delta x)$
AGA	513	H_{ad}	7.29×10^{-2}	1.85×10^{-3}	–
AGA	513	P	5.83×10^{-3}	8.93×10^{-4}	–
AGA	513	T_v	6.81×10^{-1}	2.08×10^{-3}	1.99×10^{-2}
Papay	513	H_{ad}	3.88×10^{-2}	9.61×10^{-4}	–
Papay	513	P	1.05×10^{-2}	1.58×10^{-3}	–
Papay	513	T_v	6.20×10^{-1}	1.85×10^{-3}	1.88×10^{-2}

Table 4.19. Mean deviations of turbo compressors

Figure 4.19 shows histograms of the absolute deviations in specific change in adiabatic enthalpy, power and outflow temperature for piston compressors, Figure 4.20 shows the same for turbo compressors. Note that the frequencies are logarithmically scaled. In the figures 4.19b, 4.19f, 4.20b and 4.20f there is a visible partition. A large part of instances results in a very small absolute deviation, while a second group of instances results in a noteworthy deviation in outflow temperature and specific change in adiabatic enthalpy. The groups coincide with the model choice for the isentropic exponent κ . While the constant model (3.83) and the linear model (3.82) result in mean absolute temperature deviations of 10^{-3} K to 7×10^{-3} K, the nonlinear model (3.81) corresponds to the other group of instances and results in mean temperature deviations of 1.8 K to 2 K. This strongly indicates a difference in the implementation of the model (3.81) between the ValNLP and SIMONE.

4.3.5. Conclusion

The comparisons point out several differences between the ValNLP and SIMONE. Besides known issues like the different handling of variable bounds and a different model for temperature in case of zero flow, the results indicate additional discrepancies. The deviations of the outflow temperatures of resistors and control valves are larger when the

4. Numerical Experiments

AGA formula is chosen for the compressibility factor than when Papay's formula is chosen. Since this difference is not observed in case of pipes, there seems to be a discrepancy in the Joule–Thomson model or the associated compressibility factor. Another observed discrepancy lies with the nonlinear model of the isentropic exponent. The mean deviation is significantly larger than in case of the other model choices. Furthermore, the differences in the outflow temperature of linear resistors despite the linear model indicate a low accuracy of the values returned by the API of SIMONE and a low internal accuracy cannot be ruled out.

Despite the observed differences in modeling, data handling and accuracy, the resulting mean relative deviations are in the range of 10^{-6} to 10^{-3} for all settings. Differences are always to be expected even when the models are based on the same equations due to differences in the solution method and implementation. As seen, this holds true even for the comparison of different versions of the same software. The conducted experiments show that the presented models are on par with the level of detail provided by the commercial simulation software SIMONE. Since the source codes of simulation packages are usually not available, there is no practical way of eliminating the remaining differences, but the reach level of accuracy is sufficient for the validation of nominations and similar midterm planing tasks.

5. Technical Capacities of Gas Networks

Recent developments of European and German regulations of the gas market established new tasks for transport system operators which results in new mathematical problems of significant practical importance. A central topic is the obligation of transport system operators to determine for every entry or exit the maximum bookable amount of supplyable and dischargable gas, such that the integrity of the network and the network operation is ensured [16]. The maximum bookable amount q_u^{TC} at a boundary node $u \in \mathbb{V}^\circ$ is called the technical capacity of u . The operator is furthermore obligated to publish the available capacities, i.e. the difference between the technical capacities and the already sold capacity rights. The definition of a technical capacity induces that all partial nominations of the published capacities must result in a feasible state of the network.

In the following sections, a mathematical formulation of the determination of technical capacities is developed and its properties are examined.

5.1. Problem Description

Given a gas network $\mathbb{G} = (\mathbb{V}, \mathbb{A})$, the vector of capacities $q^{\text{TC}} \in \mathbb{R}_{\geq 0}^{|\mathbb{V}^\circ|}$ is a technical capacity, if and only if all possible (in particular balanced) nominations $0 \leq q^{\text{ext}} = (q_u^{\text{ext}})_{u \in \mathbb{V}^\circ} \leq q^{\text{TC}}$ result in a feasible network state. To render this definition more precisely, several sets of flows are introduced. To ease notation and illustrations the definition of discharged flow at exits is aligned to general linguistic usage in gas business. Since capacities of entries and exits are usually stated in positive numbers, the sign of discharged flow at exits is switched compared to the models in Chapter 3, i.e. $q_u \geq 0$, for all $u \in \mathbb{V}_-$. This induces switched signs the mass balance equations (3.10), (3.42), and (3.65).

The set of bounded flows at the boundary nodes is defined by

$$\mathcal{Q} = \{q: q_u \in [q_u^-, q_u^+] \forall u \in \mathbb{V}_+, q_v \in [-q_v^+, -q_v^-] \forall v \in \mathbb{V}_-\}.$$

5. Technical Capacities of Gas Networks

This is a $|\mathbb{V}^\circ|$ -dimensional cuboid. The set of balanced and bounded boundary flows, i.e. nominations, is the intersection of the cuboid \mathcal{Q} and the $(|\mathbb{V}^\circ| - 1)$ -dimensional hyperplane of the balance equation

$$\sum_{u \in \mathbb{V}_+} q_u^{\text{ext}} - \sum_{u \in \mathbb{V}_-} q_u^{\text{ext}} = 0.$$

It is denoted by

$$\mathcal{B} = \left\{ q^{\text{ext}} \in \mathcal{Q} : \sum_{u \in \mathbb{V}_+} q_u^{\text{ext}} = \sum_{u \in \mathbb{V}_-} q_u^{\text{ext}} \right\}.$$

A nomination has to be balanced, however not all balanced nominations result in a feasible network state. In the following, feasibility is defined in terms of a discrete-continuous model of the gas network,

$$\begin{aligned} c_{\mathcal{E}}(x, z; q^{\text{ext}}) &= 0, \\ c_{\mathcal{I}}(x, z; q^{\text{ext}}) &\geq 0, \end{aligned}$$

with $x \in \mathbb{R}^{n_x}$ and $z \in \{0, 1\}^{n_z}$. The set of feasible nominations is hence defined as

$$\mathcal{F}_q = \{ q^{\text{ext}} \in \mathcal{B} : \exists (x, z) \in \mathbb{R}^{n_x} \times \{0, 1\}^{n_z} : c_{\mathcal{E}}(x, z; q^{\text{ext}}) = 0, c_{\mathcal{I}}(x, z; q^{\text{ext}}) \geq 0 \}.$$

Since mass balance is one of the most fundamental aspects of gas physics, equation (3.10) is assumed to part of every mathematical model describing gas networks, it follows that $\mathcal{F}_q \subseteq \mathcal{B}$.

The technical capacity q^{TC} defines itself a cuboid of flow ranges

$$\mathbb{T}(q^{\text{TC}}) = \{ q^{\text{ext}} \in \mathcal{Q} : q^{\text{ext}} \leq q^{\text{TC}} \},$$

such that all nominations within have to be feasible. Hence, the problem of finding a technical capacity is to find a maximized vector q^{TC} such that $\mathcal{B} \cap \mathbb{T}(q^{\text{TC}}) \subseteq \mathcal{F}_q$, i.e.

$$\forall q^{\text{ext}} \in \mathcal{B} \cap \mathbb{T}(q^{\text{TC}}) : q^{\text{ext}} \in \mathcal{F}_q. \quad (5.1)$$

Figure 5.1 depicts the described sets for a network containing three boundary vertices and illustrates their relations.

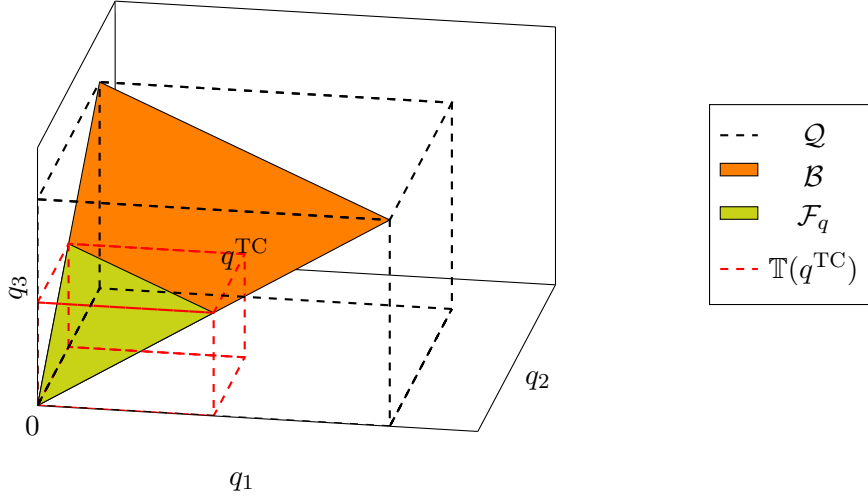


Figure 5.1. Flow sets concerning technical capacities

Given a stationary gas network model

$$\begin{aligned} c_{\mathcal{E}}(x, z; q^{\text{ext}}) &= 0, \\ c_{\mathcal{I}}(x, z; q^{\text{ext}}) &\geq 0, \end{aligned}$$

with the corresponding feasible set $\mathcal{F}(q^{\text{ext}})$, the problem of determining technical capacities can similarly be formulated as

$$\max f(q^{\text{TC}}) : \forall q^{\text{ext}} \in \mathbb{T}(q^{\text{TC}}) \exists (x, z) \in \mathbb{R}^{n_x} \times \mathbb{R}^{n_z} : (x, z) \in \mathcal{F}(q^{\text{ext}}). \quad (5.2)$$

Define the maximum exchanged amount of gas of a set of nodes $P \subseteq \mathbb{V}^\circ$ by

$$q_P^+ = \max \left\{ \sum_{u \in P} |q_u| : c_{\mathcal{E}}(x, z) = 0, c_{\mathcal{I}}(x, z) \geq 0 \right\}.$$

The constraints $c_{\mathcal{E}}$ and $c_{\mathcal{I}}$ do not depend on a nomination q^{ext} , instead, the boundary flows $q_{\mathbb{V}^\circ}$ are bounded. The following lemma defines some upper bounds of the technical capacity of node u .

Lemma 4. Let $\mathcal{P}(\mathbb{V})$ denote the power set of \mathbb{V} .

1. $q_u^{\text{TC}} \leq q_u^+$, for all $u \in \mathbb{V}^\circ$.
2. $q_u^{\text{TC}} \leq q_{\mathbb{V}_-}^+ = q_{\mathbb{V}_+}^+$, for all $u \in \mathbb{V}^\circ$.

5. Technical Capacities of Gas Networks

3. Let $\gamma_{\mathbb{V}_-} = \min\{q_P^+ : P \in \mathcal{P}(\mathbb{V}_-), u \in P\}$ denote the smallest maximum discharged gas of all subsets of exits containing u and let $P_u^-(\mathbb{V}_-)$ denote the corresponding set. It holds that $q_u^{\text{TC}} \leq \gamma_{\mathbb{V}_-}$ for all $u \in \mathbb{V}_-$.
4. Let $\gamma_{\mathbb{V}_+} = \min\{q_P^+ : P \in \mathcal{P}(\mathbb{V}_+), u \in P\}$ denote the smallest maximum supplied gas of all subsets of exits containing u and let $P_u^-(\mathbb{V}_+)$ denote the corresponding set. It holds that $q_u^{\text{TC}} \leq \gamma_{\mathbb{V}_+}$ for all $u \in \mathbb{V}_+$.

Proof. 1. Follows directly from the fact, that all subnominations of the technical capacity have to be feasible.

2. Assume $q_{\mathbb{V}_-}^+ > q_{\mathbb{V}_+}^+$, then there exists a feasible nomination discharging $q_{\mathbb{V}_-}^+$ and hence supplying more gas than $q_{\mathbb{V}_+}^+$, since the nomination is balanced. This contradicts the definition of $q_{\mathbb{V}_+}^+$. Accordingly, $q_{\mathbb{V}_-}^+ < q_{\mathbb{V}_+}^+$ leads to a similar contradiction.
3. Assume $q_u^{\text{TC}} > \gamma_{\mathbb{V}_-}$. It follows that

$$q_u^{\text{TC}} > \max \left\{ \sum_{u \in P_u^-(\mathbb{V}_-)} |q_u| : c_{\mathcal{E}}(x, z) = 0, c_{\mathcal{I}}(x, z) \geq 0 \right\} \\ \geq \max \{ |q_u| : c_{\mathcal{E}}(x, z) = 0, c_{\mathcal{I}}(x, z) \geq 0 \}.$$

This contradicts the feasibility of the technical capacity of node u .

4. Similar to 3. □

5.2. Relation to Robust Optimization

Optimization with respect to all possible realizations of a parameter is subject of robust optimization. This area of research has its source in operation research of the 1970s. Originally, it focused on planning tasks under uncertainty, where the optimal result x needs to be valid under all possible occurrences of the unknown parameter p with its uncertainty set \mathcal{U} . Robust optimization stands in contrast to stochastic optimization, where the validity is guaranteed with a given probability. While the traditional subjects of robust optimization are linear programming (LP), second-order cone programming (SOC) and semi-definite programming (SDP)[8], in recent years several advances in nonlinear robust optimization have been made [23, 29, 142].

The general robust optimization problem can be stated as the optimization over a set of optimization problems

$$\left\{ \min_x \{f(x; p); c_{\mathcal{E}}(x; p) = 0, c_{\mathcal{I}}(x; p) \leq 0\} \right\}_{p \in \mathcal{U}}. \quad (5.3)$$

A vector x is called a robust feasible solution of (5.3), if it satisfies

$$c_{\mathcal{E}}(x; p) = 0, \quad c_{\mathcal{I}}(x; p) \leq 0,$$

for all realizations of $p \in \mathcal{U}$ and the robust objective value $\hat{f}(x)$ is defined as the largest value of the objective over all possible data values:

$$\hat{f}(x) = \sup_{p \in \mathcal{U}} f(x; p).$$

The optimization of the robust objective value under all robust feasible solutions leads to the robust counterpart of the robust optimization problem (5.3). It is defined as the optimization problem

$$\min_x \left\{ \hat{f}(x); c_{\mathcal{E}}(x; p) = 0, c_{\mathcal{I}}(x; p) \leq 0, \forall p \in \mathcal{U} \right\}. \quad (5.4)$$

and substantiate the solution of (5.3): the solution of (5.4) is called robust optimal solution of (5.3) and its optimal value is called the robust optimal value of (5.3).

The general principle of robust optimization is based on three assumptions [8]:

- A1 The optimization variables x are independent of the actual realization of p .
- A2 The optimum is only valid for parameters in \mathcal{U} but not necessarily for other realizations.
- A3 For all $p \in \mathcal{U}$ the constraints are hard, i.e. no violations are tolerated.

Some work is done to relax these assumptions under certain conditions, see [8].

Considering the technical capacity problem, it would stand to reason that the nomination q^{ext} is regarded as the uncertain parameter and $\mathbb{T}(q^{\text{TC}})$ is its uncertainty set.

Lemma 5. *Given a general gas network $\mathbb{G} = (\mathbb{V}, \mathbb{A})$, $|\mathbb{V}^{\circ}| \geq 1$, the determination of a maximum q^{TC} cannot be formulated as a robust optimization problem.*

5. Technical Capacities of Gas Networks

Proof. As already mentioned, mass flow balance is part of the physical model, i.e. the optimization problem contains the linear constraints (3.10) and the fixations of the supplied and discharged gas due to the nomination,

$$q_u = q_u^{\text{ext}}, u \in \mathbb{V}_+, \quad -q_u = q_u^{\text{ext}}, u \in \mathbb{V}_-.$$

This results in a linear equation system

$$A \begin{pmatrix} q_{\mathbb{A}} \\ q_{\mathbb{V}^\circ} \end{pmatrix} = \begin{pmatrix} 0 \\ q^{\text{ext}} \end{pmatrix},$$

with $A_{ij} \in \{-1, 0, 1\}$. For each nomination q^{ext} several feasible flow distributions $q_{\mathbb{A}}$ between the arcs may exist, but each vector $q = (q_{\mathbb{A}}, q_{\mathbb{V}^\circ})$ corresponds to exactly one nomination. Thus it is not possible to find a solution x containing q that is valid for several nominations, let alone all nominations within $\mathbb{T}(q^{\text{TC}})$. \square

There exist some significant differences between the technical capacity problem and a general robust optimization problem.

- D1 In case of the technical capacity problem, all nominations $q^{\text{ext}} \in \mathbb{T}(q^{\text{TC}})$ must lead to a feasible solution and the solutions usually depend on the nomination, contradicting Assumption A1.
- D2 The uncertainty set \mathcal{U} is not a fix set of possible realizations but depends on the optimization variables q^{TC} .

In case of $q^{\text{TC}} > 0$ Difference D2 can be eliminated by the parameter transformation

$$\begin{aligned} q^{\text{ext}} &\in \mathbb{T}(q^{\text{TC}}) \\ \iff q_u^{\text{ext}} &\in [0, q_u^{\text{TC}}], \text{ for all } u \in \mathbb{V}^\circ \\ \iff \frac{q_u^{\text{ext}}}{q_u^{\text{TC}}} &\in [0, 1], \text{ for all } u \in \mathbb{V}^\circ. \end{aligned}$$

Difference D1 induces, that applying robust optimization on the problem of determining technical capacities is too conservative. Looking for a solution that is feasible for all nominations within $\mathbb{T}(q^{\text{TC}})$ is obviously more restricting than just confirming, that all nominations within $\mathbb{T}(q^{\text{TC}})$ result in a feasible network state. Difference D1 is subject of adjustable robust optimization [8, 7], also known as quantified optimization [35, 36].

5.3. Properties of Technical Capacities and the Set of Feasible Nominations

Adjustable robust optimization consists of a collection of optimization problems, called instances,

$$\mathcal{P} = \left\{ \min_x \{f(x; p), c(x; p) \leq 0\} : p \in \mathcal{U} \right\}.$$

The objective $f(x; p)$ and the constraints $c(x; p)$ depend on the uncertain data p inside the uncertainty set \mathcal{U} . The corresponding adjustable robust counterpart is

$$\min_{t, X} \{t; \forall p \in \mathcal{U} : f(X(p); p) \leq t, c(X(p); p) \leq 0\}.$$

Here, the dependence on p , or adjustability, can be modeled by defining a variable x_i by a decision rule

$$x_i = X(p).$$

The technical capacity problem (5.2) can now be seen as the adjustable robust optimization problem

$$\mathcal{P} = \left\{ \max \{f(q^{\text{TC}}) : (x, z) \in \mathcal{F}(q^{\text{ext}})\}; q^{\text{ext}} \in \mathbb{T}(q^{\text{TC}}) \right\}.$$

5.3. Properties of Technical Capacities and the Set of Feasible Nominations

The size of the technical capacities of a gas transport network depend substantially on the properties of the set of feasible nominations \mathcal{F}_q . Thus, knowledge of the properties of \mathcal{F}_q and their influence on the technical capacity is crucial for the design of solution methods. The main properties can already be observed at very small exemplary networks and simplified physical models. However, a systematic analysis of all networks up to a given size becomes rapidly impracticable due to the large numbers of possible topologies and element types. Figure 5.2 lists some possible topologies, all of these can be combined with several types of arcs. The graph notation is explained in Section A.1. Several of these topologies will be used in the following sections to illustrate specific properties of technical capacities and the set of feasible nominations. Some properties do not require a full nonlinear mixed-integer model of the network to occur. Three levels of detail will thus be used for the underlying model. First, a basic flow model incorporating flow bounds, supplied and discharged flow values and the mass balance equations (3.10). The second model adds pressure bounds and a pressure loss model for pipes, see Section 3.4.3. Third, the most detailed model used for the illustrating examples incorporates also active network elements like compressor groups.

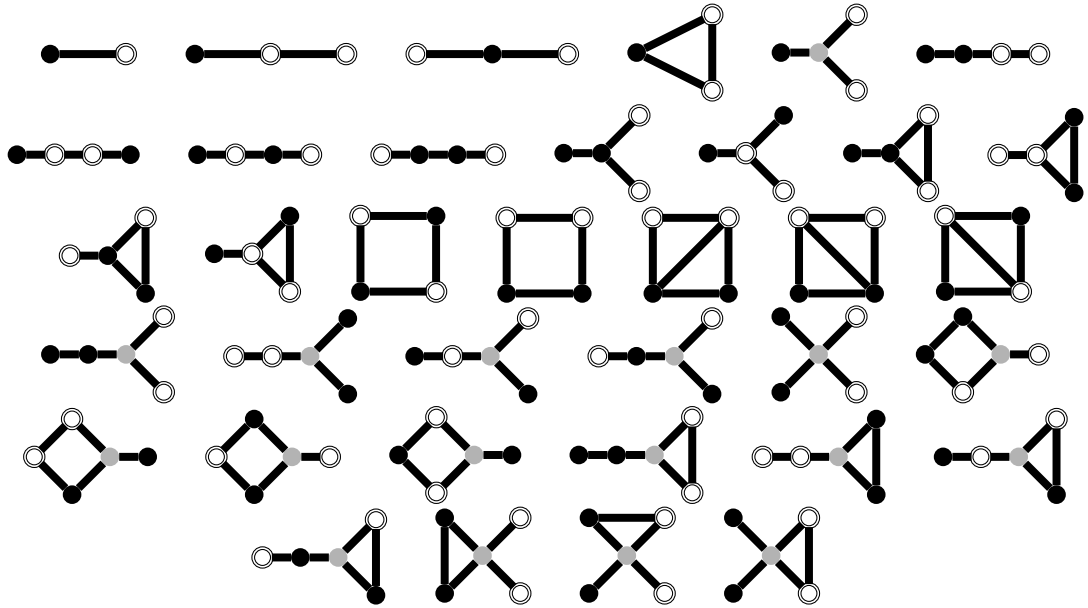


Figure 5.2. All network topologies with at most two entries, two exits, one required inner node and five arcs

5.3.1. Existence and Uniqueness of Technical Capacities

The regulations concerning technical capacities presume the existence of technical capacities in any case. Looking at the problem definition (5.1) the zero vector is the smallest possible candidate according to amount. It is equivalent to shutting down the transport network which seems to be a drastic but possible state of any network. However, it is theoretically possible to design networks with a strictly positive supply at an entry based on the models described in Section 3. A strictly positive flow for the single pipe a in Figure 5.3 may be caused in several ways. Different pressure requirements of supplier and discharger may result in $p_u^+ < p_v^-$, i.e. a pressure loss is required along the pipe. This induces a positive flow through the pipe, if the pipe is not sloped. Having a strong downward slope at the pipe and the lower pressure bound at the entry is hardly smaller than the upper pressure bound at the exit may also result in a strictly positive flow to satisfy the pressure bounds. In these cases the zero vector is not part of \mathcal{F}_q , thus there exists no technical capacity such that $\mathbb{T}(q^{\text{TC}}) \subset \mathcal{F}_q$ since it is impossible to nominate nothing.

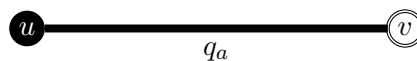


Figure 5.3. Single pipe a connecting entry u and exit v

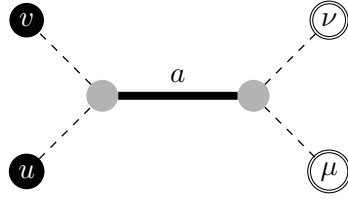


Figure 5.4. Network with infinite possible technical capacities

While it is interesting from a theoretical point of view that technical capacities may not be defined for a network and a given physical model, both described situations are usually prohibited by either the network operator or safety regulations. In the following examples, the zero vector is hence considered a feasible nomination. As already mentioned, the technical capacity is defined as the maximum capacity that the network operator can offer any transport customers with respect to the integrity of the network. However, this definition is ill-defined. As the following example illustrates, the technical capacities of the boundary nodes are correlated and there typically exists no unique maximum.

Figure 5.4 shows a network with two entries on the left side and two exits on the right, connected by a pipe a and four shortcuts. The pipe acts as a bottleneck in this example by restricting the maximum flow through the network. A basic flow model is sufficient for illustrating the ambiguity and correlation of technical capacities. Assume flow bounds $q_a^- = 0 \text{ kg s}^{-1}$ and $q_a^+ = 50 \text{ kg s}^{-1}$ at the pipe and no other bounds, thus 50 kg s^{-1} is the largest amount of gas that can be discharged, thus $q_\mu^{\text{TC}}, q_\nu^{\text{TC}} \leq 50 \text{ kg s}^{-1}$. The same holds for the technical capacities at the entries. In addition, the upper flow bound q_a^+ restricts the sum of supply capacities or the sum of discharge capacities to 50 kg s^{-1} . If the supplied gas is limited, i.e. $q_u^{\text{TC}} + q_v^{\text{TC}} = 50 \text{ kg s}^{-1}$, the technical capacities of the exits can both be set to 50 kg s^{-1} . All nominations within these technical capacities are feasible, since a nomination is balanced by definition. Every nomination within the technical capacities supplies at most 50 kg s^{-1} gas and thus discharges at most the same amount, never violating the only restriction of the network at the connecting pipe. The technical capacities of the exits are never exhausted at the same time. This example shows that the vector of technical capacities q^{TC} of a network with $|\mathbb{V}^\circ| > 2$ is not necessarily balanced itself and due to the symmetry of the network similar observations hold for $q_\mu^{\text{TC}} + q_\nu^{\text{TC}} = 50 \text{ kg s}^{-1}$. Either way, this results in a infinite number of possible choices for the technical capacities, some examples are listed in Table 5.1.

The example in Figure 5.4 also shows that there may exist a set $P \in \mathcal{P}(\mathbb{V}_-)$ or $P \in \mathcal{P}(\mathbb{V}_+)$ with $u \in P$ and $\sum_{v \in P} q_v^{\text{TC}} > q_P^+$. However, the following relation between the technical capacities and the supplied or discharged flow holds.

5. Technical Capacities of Gas Networks

q_u^{TC}	q_v^{TC}	q_μ^{TC}	q_ν^{TC}
50	0	50	50
50	50	0	50
50	50	25	25
50	50	10	40

Table 5.1. Some valid choices for technical capacities in kg s^{-1} of the network in Figure 5.4

Lemma 6. *In every gas network \mathbb{G} it holds that either $\sum_{u \in \mathbb{V}_+} q_u^{\text{TC}} \leq q_{\mathbb{V}_+}^+$, $\sum_{u \in \mathbb{V}_-} q_u^{\text{TC}} \leq q_{\mathbb{V}_-}^+$, or both.*

Proof. Assume that $\sum_{u \in \mathbb{V}_+} q_u^{\text{TC}} > q_{\mathbb{V}_+}^+$ and $\sum_{u \in \mathbb{V}_-} q_u^{\text{TC}} > q_{\mathbb{V}_-}^+$. Due to Lemma 4 $q_{\mathbb{V}_+}^+ = q_{\mathbb{V}_-}^+$. Then there exists a nomination q^{ext} within the bounds of the technical capacities with $q^{\text{ext}} \leq q^{\text{TC}}$ and $\sum_{u \in \mathbb{V}_+} q_u^{\text{ext}} > \sum_{u \in \mathbb{V}_+} q_{\mathbb{V}_+}^+$. This nomination is infeasible since more gas supply is demanded than possible. This conflicts with the requirement of technical capacities, that all partial nominations have to be feasible. \square

Lemma 6 is also valid for each connected component of a network graph, since each component is itself a gas network.

In a nutshell, the technical capacities of the boundary nodes compete with each other. Increasing the capacity of one node decreases the capacities of others. The legal regulations do not define an objective function incorporating the vector q^{TC} . A possible interpretation of the legal regulations is the maximization of a (weighted) sum of the capacities. However, this interpretation is very restrictive since there are nodes where customers are not interested in buying more capacities. The least restrictive interpretation sees the capacity problem as a Pareto optimization problem.

In any case, the weighting of the boundary nodes lies in the hands of the network operator. In the upper example, the operator has the choice to lay the focus of the technical capacities either on the entries or on the exits by setting their technical capacities to 50 kg s^{-1} and he decides the distribution between the nodes of the other type.

5.3.2. Geometry of the Set of Feasible Nominations

Knowing the possible geometric features of the set of feasible nominations \mathcal{F}_q is important for the development of solution algorithms for the determination of technical capacities,

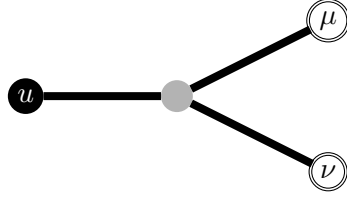


Figure 5.5. Y-shaped network with entry u and exits μ and ν

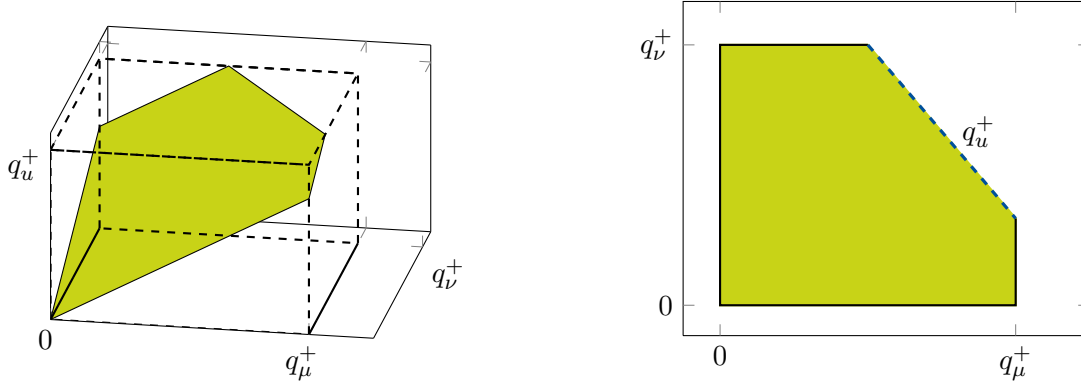


Figure 5.6. Set of feasible flows of the Y-shaped network in Figure 5.5 and its projection into the q_μ - q_ν -plane in case of a linear flow model

since \mathcal{F}_q is a central part of their definition. The following examples will examine connectivity and convexity of \mathcal{F}_q and smoothness of its border.

Applying a flow model with the bounds $q_u \in [q_u^-, q_u^+]$, $q_\mu \in [q_\mu^-, q_\mu^+]$, and $q_\nu \in [q_\nu^-, q_\nu^+]$ on the network shown in Figure 5.5 results in a linearly bounded set of feasible flows, see Figure 5.6. The technical capacity of every node is unique in this case. It is the smallest maximum amount of suppliable or dischargable gas of the network.

Figure 5.7 illustrates the change when a nonlinear pressure loss model is regarded at the pipes. Here, the isothermal quadratic approximation (3.70) is chosen. Upper mass flow limits are set to $q_u = 1000 \text{ kg s}^{-1}$, $q_\mu = 800 \text{ kg s}^{-1}$ and $q_\nu = 600 \text{ kg s}^{-1}$. The inflow pressure p_u is set to 70 bar. The set of feasible nominations is piecewise nonlinear bounded, both upper right boundaries are slightly curved. These boundaries are caused by reaching the lower pressure limit of 1.01325 bar at one of the exits.

In contrast to the linear model, the technical capacities are not unique when the nonlinear pressure loss model is added. Three technical capacities are intuitive and relate to three vertices of the feasible set. The vertex marked by A in Figure 5.7 corresponds to the nomination $q_A^{\text{ext}} = (q_u^{\text{ext}}, q_\mu^{\text{ext}}, q_\nu^{\text{ext}}) = (800, 199, 600)$ that maximizes the exit flow

5. Technical Capacities of Gas Networks

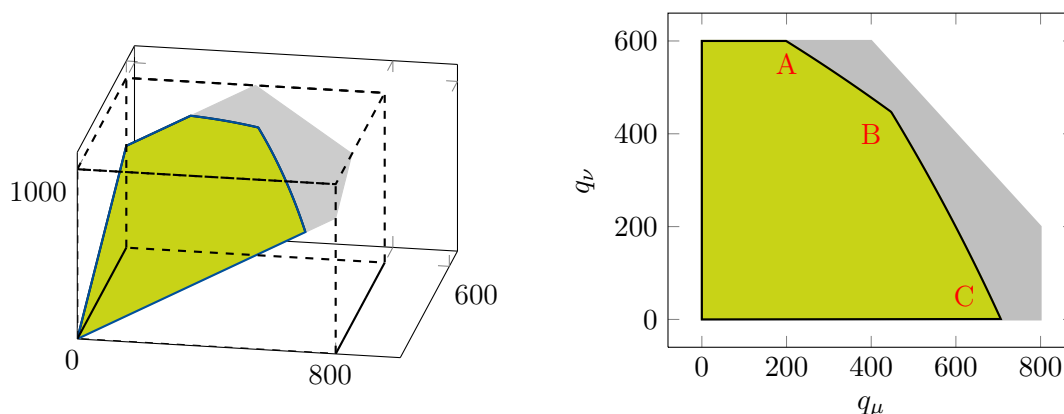


Figure 5.7. Set of feasible flows of the Y-shaped network in Figure 5.5 and its projection into the q_μ - q_ν -plane regarding nonlinear pressure loss at pipes (each $L = 50$ km, $D = 1.1$ m, $k = 0.01$ mm) and an inflow pressure of $p_u = 70$ bar

q_ν . This nomination can be extended to the (unbalanced) technical capacity $q^{\text{TC}} = (q_u^{\text{TC}}, q_\mu^{\text{TC}}, q_\nu^{\text{TC}}) = (800, 600, 600)$ by following the line $q_\mu + q_\nu = 800$ through \mathcal{F}_q until it hits another boundary of \mathcal{F}_q , i.e.

$$\begin{aligned} \max \quad & q_\mu \\ \text{s.t.} \quad & q_\mu + q_\nu - q_u = 0, \\ & q_u = 800, \\ & (q_u, q_\mu, q_\nu) \in \mathcal{F}_q. \end{aligned}$$

This is possible since \mathcal{F}_q is convex and $0 \in \mathcal{F}_q$ in this example, so every partial nomination of every feasible flow combination is feasible too. The nomination $q^{\text{ext}} = (707, 707, 0)$ in vertex C maximizes q_μ and leads by similar means to the technical capacity $q^{\text{TC}} = (707, 707, 600)$. Finally, $q^{\text{ext}} = (896, 448, 448)$ in vertex B is itself a technical capacity maximizing q_u , since no other flow can be increased further. In addition to these technical capacities, there exists an infinite number in between.

So far, the set of feasible nominations has been connected and convex. However, this is not necessarily the case. Consider the network in Figure 5.8 which is similar to the network Figure 5.5 except for the compressor group. All pipes stay unchanged. The compressor group has a minimum flow q_{CS}^{min} required for the active operation mode. The schematic illustration in Figure 5.9 shows the change caused by adding the compressor group. The compressor group has no effect on the capability of exit ν , but due to the pressure increase in case of $q_\mu \geq q_{CS}^{\text{min}}$, the possible pressure loss along the pipe leading to

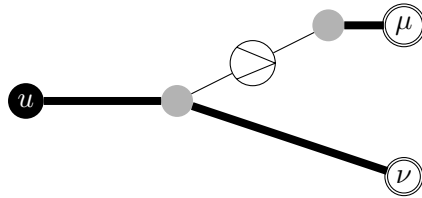


Figure 5.8. Y-shaped network with a compressor group

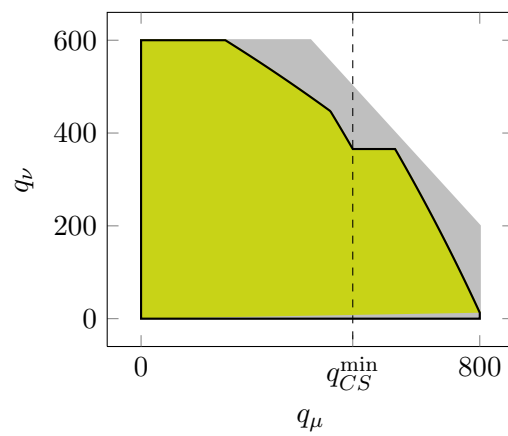
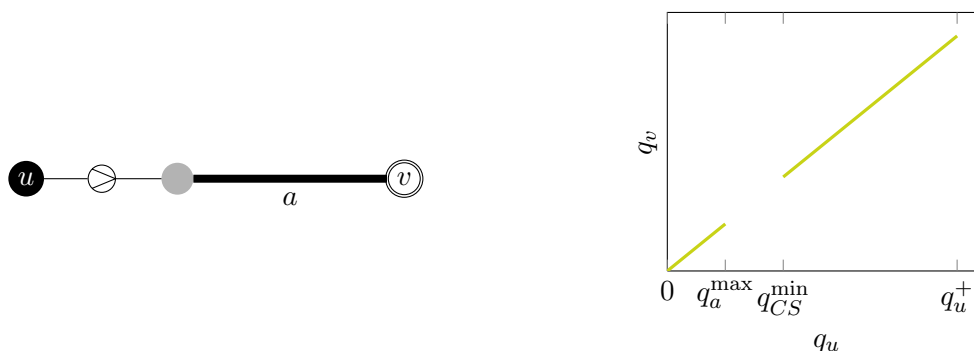


Figure 5.9. Nonconvex set of feasible nominations of the Y-shaped network with a compressor group in Figure 5.8 (schematic representation)



(a) Network consisting of a compressor group and a pipe with high pressure loss

(b) Two disjunctive areas of feasible nominations

Figure 5.10. Series of a compressor group and a pipe resulting in two disjunctive sets of feasible nominations

μ grows and larger amounts of gas can be discharged from exit μ . The discrete activation of the compressor group results in a kink in the boundary at $q_\mu = q_{CS}^{\min}$ and \mathcal{F}_q becomes nonconvex.

The discrete states of active elements also may result in a set of feasible nominations not being connected. Proper choices of the parameters of the network in Figure 5.10a results in \mathcal{F}_q with disjunctive sets. If the maximum possible flow through the pipe due to pressure loss q_a^{\max} is smaller than the minimum flow required by the compressor group be active, the feasible set looks like Figure 5.10b. The lower left part of the feasible set corresponds to the situation when the compressor is in bypass while the upper right part is valid for an active compressor. For the computation of the technical capacities only the lower left part can be considered, otherwise not all partial nominations would be possible – those lying in the gap. The technical capacity is hence $q_u^{\text{TC}} = q_v^{\text{TC}} = q_a^{\max}$. This is also one of the most basic examples showing that monotonicity is not valid for nominations, i.e. given a feasible nomination $q^{\text{ext}*}$ not all nominations q^{ext} with $q_i^{\text{ext}} \leq q_i^{\text{ext}*}$ have to be feasible too.

In summary, the set of feasible nominations of a complex gas transport network cannot be assumed to be convex and it may consist of disjunctive subsets. The existence of gaps as in Figure 5.10b lets assume that holes inside \mathcal{F}_q are possible for more complex

networks when the sets of feasible nominations of different choices of discrete network aspects partially overlap.

5.4. Approaches

In summary, determining technical capacities based on a detailed physical and technical model is a nonconvex, mixed-integer nonlinear robust Pareto optimization problem. So it combines several different areas of mathematical optimization which are hard to handle by themselves. There exists currently no general solution approach to tackle this problem class.

The current approach in practice is usually based on the validation by simulation of several nominations which are assumed to be worst-case. A technical capacity is conducted from these computations. This manual approach heavily depends on a deep knowledge of the network and a proper choice of the test cases. It also assumes convexity and monotonicity of the set of feasible nominations since all nominations between the test cases are assumed to be feasible.

A possible solution approach uses the fact that technical capacities are related to maximum bookings, see Section 5.1. Solution approaches for validating bookings have been developed in the ForNe project and could be used as an oracle [71]. However, validating a single booking is very time-consuming and testing several bookings may contain redundant tests of very similar nominations [71].

Other approaches determine a description of the set of feasible nominations and conducts the technical capacity based on this information. The feasible set shown in Figure 5.7 was determined by tracking the borders of the feasible set using a homotopy method. This procedure is impractical for larger networks since it contains rasterizing flow variables and setting other variables and inequalities to their bounds. The number of combinations of variable bounds and inequality ranges that have to be considered grow exponentially with the model complexity and network size.

Another possibility is to dissect the set of possible nominations \mathcal{Q} within the bounds of the flow variables and apply a validation of nomination on each grid point. If an infeasible nomination $q^{\text{ext}*}$ is found, all nominations with $q_i^{\text{ext}} \geq q_i^{\text{ext}*}, i \in \mathbb{V}^\circ$ are irrelevant for the technical capacity and can be skipped, see Figure 5.11. This bears some similarities to filters in nonlinear programming [52], however in a higher dimension. Such a grid approach is based on the assumption that a feasible nomination possesses a neighborhood

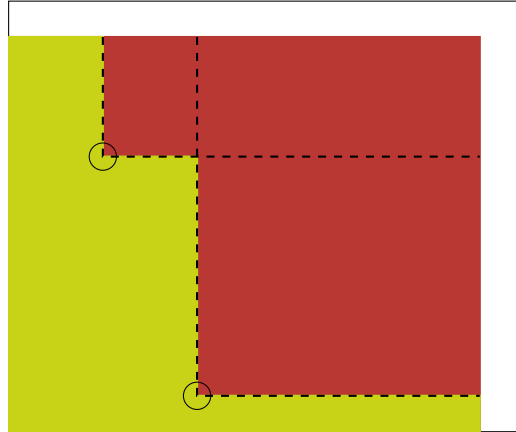


Figure 5.11. Two instances validated as infeasible (circled) cut off a large part of nominations (red)

of technically feasible nominations as large as the grid size, so all nonconvexities are covered. Furthermore, the dissected flows need lower and upper bounds. If not already given, these can be gained in a preprocessing step by computing the maximum and minimum possible flow using the same optimization model as for the technical capacity.

This approach has some advantages over the homotopy method. The dimension of the grid only depends on the number of entries and exits, not on the network layout or the chosen optimization model. The validation of a grid point can be handled by a NoVa solver, see Section 3. Since the proposed MPEC approach cannot prove infeasibility, i.e. a failed validation does not necessarily imply an infeasible nomination, it will yield an inner approximation of the set of feasible nominations, if failed validations are treated as infeasible anyway. In contrast, choosing a MIP approach or global MINLP approach for the determination of the discrete decisions leads to a detailed description of the set of feasible nominations depending on the grid size. These approaches can prove infeasibility, however longer computation times than the MPEC approach are to be expected.

Hayn et al. [71] are working on a related approach based on the same assumptions. Here, the space of nominations is also rasterized. A grid block is treated as a feasible area, if a valid nomination is found within the block. For this, a modified validation of nominations run based on a MIP model is performed, where the nomination is replaced by flow bounds according to the grid block.

All approaches based on a subdivision of variable spaces suffer from curse of dimensionality. The complexity increases exponentially with the dimension of the subdivided space. Thus, only a small number of boundary vertices can be handled. For large scale networks the

solution time of the subproblems has to be very small. Besides accelerating the solution process, implementing expert knowledge to aggregate or skip nodes decrease the number of computed capacities and thus the problem complexity.

6. Conclusion

The role of optimization in the gas industry has drastically increased in recent years. New requirements due to market regulations and the foreseeable shortage of this natural resource is driving the need for improved network efficiency. This thesis covers two of the current main problems in gas transportation, validation of nominations and the determination of technical capacities.

Based on a stationary mixed-integer nonlinear model of a gas network and a two-stage solution framework developed in the project ForNe, a solution approach for the problem of validation of nominations is presented.

The first stage determines the discrete settings of the active network elements and the general situation in the gas network while the second stage validates the solution against a high-detailed NLP model, resulting in a very accurate description of the network state. In this work an MPEC approach is suggested for the first stage. Differential equations and nonsmooth model aspects of the underlying MINLP model are replaced by smooth approximations and discrete model aspects modelling decisions of active network elements like valves, control valves and compressors are transformed into smooth constraints using complementarity constraints. Detailed decisions within a compressor group are heuristically determined separately. To be able to apply general-purpose NLP solvers on the resulting MPEC problem several well-known regularization schemes are suggested. They are adjusted to fit the special needs of the network model.

To prove the practical relevance of the results gained from the MPEC approach they are validated in a second step. To this end, a class of NLP models is suggested with alternatives for many model aspects. The model variants offer the possibility to adjust the model for the best trade-off between required model accuracy and run-time.

The complexity of the underlying MINLP model is thus divided into two separate problems, offering an advantage over the direct application of current MINLP solvers. Numerical experiments in the literature and in this work show, that state-of-the-art MINLP solvers

6. Conclusion

are not yet capable of reliably solving large-scale network problems with a detailed mixed-integer nonlinear model of gas physics and technical devices in acceptable time.

Extensive numerical experiments on realistic network instances of the library **GasLib** [56] prove the practicability for many regularization techniques and solvers. Validated solutions are generated for a large number of test instances. It is safe to assume that the major part of the unsolved instances are infeasible. Modifications of a relaxation scheme originally proposed by Scholtes stand out with the largest rate of success and an average solution time of about ten seconds. The automated determination of feasible network settings within seconds is a significant improvement over the established process based on simulation runs. The numerical analysis underlines the practicability of the suggested MPEC approach as a primal heuristic for MIP and MINLP approaches as well as a stand-alone approach.

Despite the successful application on realistic large-scale problems there is still room for improvement. Some well-established regularization schemes like the Fischer-Burmeister function do not perform as well as expected. While some possible reasons are discussed, the actual cause is not known by certainty. Further research at this point is required.

The MPEC model covers the most important network elements and restrictions, however, further interesting aspects of gas networks exist. So far, the reformulation based on complementarity constraints focuses on discrete states of the same network element. In practice, the states of network elements are sometimes correlated, e.g. in complex structures of compressor groups and valves. Here, only a subset of the discrete decisions is permitted. Further research is required to include this type of constraints into the MPEC model without the application of integer variables.

Numerical analysis of MINLPs in Section 4.1 indicates a possible alternative for the current heuristic in the second MPEC stage. Further research has to show, if the operation modes of compressor groups within the gas transport network can be determined in separated optimization runs and which model formulations are best fitted for compressor group optimization.

The NLP model that is used to validate the results of the MPEC approach features a high level of detail. The numerical results on the **GasLib** instances show, that a solution for a problem of validation of nominations on a large-scale network is computed in only a few seconds despite the high level of detail of the model. A comparison with the commercial simulation software **SIMONE** is conducted on a large number of single network elements.

It shows that the accuracy of the validation NLP model is on par with current simulation software.

The solution process of both the MPEC and the validation NLP can be increased further by eliminating the overhead of the modeling system. This would have a significant impact on the determination of technical capacities based on a discretized set of nominations, since the overhead would fall away for every verified nomination.

With increased model complexity the demands on the initial value and the applied NLP solver increase as well, since raising model accuracy typically makes a problem harder to solve. A sequence of NLPs with increasing complexity, where a solution is used as the initial point in the next step, may improve the rate of success. An automatic choice of the model variant for single network elements based on indicators like pressure bounds, would make the model locally adaptable, which would improve the trade-off between practical solvability and model accuracy. However, the proposed model variants are not strictly ordered, hence such a sequence of models or an automatic choice does not suggest itself. The variety of model choices with multiple interdependences show some generic properties, that are not gas-specific but relevant for most transport and distribution network problems. The generalization of these structures is topic of current research and may lead to a guiding toolbox for future network modelers.

Having a reliable and fast solution approach for the problem of validation of nomination may be a keystone in solving the technical capacity problem. It is shown, that the legal definition of the technical capacity is an ill-posed mathematical problem. Reasonable interpretations of the legal requirements result in an adjustable robust optimization problem. Central properties of this problem class are discussed and illustrated by means of basic network examples. So far, no solution approach exists that covers all aspects of technical capacities. Further research in this area is strongly required, since an accurate determination of the capacities is crucial for all gas transport system operators.

A. Appendix

A.1. Symbols of Network Elements







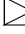
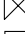

network element	symbol
entry	
exit	
inner node	
pipe	
shortcut	
compressor (group)	
control valve (group)	
valve	
resistor	

Table A.1. Network elements used in the network graphs throughout this work

A.2. Physical Quantities

The equations describing the physics of a gas network are based on many quantities of natural gas, but a small group are inherent to almost all model components. This group consists of the pressure p , given in Pa or bar, temperature T in K, density ρ in kg m^{-3} , and mass flow q in kg s^{-1} .

Besides the mass flow, two other quantities describe the amount of gas flowing through an element. Some technical devices are described by models in volumetric flow Q ($\text{m}^3 \text{s}^{-1}$), while calculations of the gas industry are often based on the normal volumetric flow Q_0 under normal conditions, $p_0 = 1.013\,25$ bar, $T_0 = 273.15$ K. These flow quantities are translated by

$$q = \rho Q = \rho_0 Q_0.$$

A. Appendix

symbol	explanation	unit
A	cross sectional area	m^2
D	diameter	m
h	height above sea level	m
k	integral roughness	m
L	length	m
λ	friction factor	1
M	shaft torque of a piston compressor	Nm
n	speed of a compressor	s^{-1}
V_0	operating volume of a piston compressor	m^3
ξ_a	linear pressure loss of a resistor	Pa
ζ_a	resistance coefficient of a resistor	1

Table A.2. Technical parameters of network elements

symbol	explanation	value and unit
g	gravitational acceleration	$9.806\,65\,\text{m s}^{-2}$
p_0	normal pressure	$101\,325\,\text{Pa}$
R	universal gas constant	$8.314\,462\,1\,\text{J mol}^{-1}\,\text{K}^{-1}$
T_0	normal temperature	$273.15\,\text{K}$

Table A.3. Constants required for the optimization models

The norm density ρ_0 (kg m^{-3}) is a gas parameter, which is constant for a given gas composition. Other composition-specific parameters are molar mass m (kg mol^{-1}), pseudocritical pressure p_c (bar), pseudocritical temperature T_c (K), molar calorific value H_c J mol^{-1} , and parameters of the molar heat capacity \tilde{A} ($\text{J mol}^{-1}\,\text{K}^{-1}$), \tilde{B} ($\text{J mol}^{-1}\,\text{K}^{-2}$), and \tilde{C} ($\text{J mol}^{-1}\,\text{K}^{-3}$). Table A.4 lists physical quantities inherent to the models of several arc types described in this work and Table A.3 lists required constants. Technical parameters of the network elements are listed in Table A.2.

symbol	explanation	unit
$\tilde{A}, \tilde{B}, \tilde{C}$	coefficients of isobaric molar heat capacity	$\text{J mol}^{-1} \text{K}^{-\alpha}$, $\alpha = 1, 2, 3$
b_d	specific energy consumption rate	W
c_p	specific isobaric heat capacity	$\text{J kg}^{-1} \text{K}^{-1}$
\tilde{c}_p	molar heat capacity	$\text{J mol}^{-1} \text{K}^{-1}$
c_{HT}	heat transfer coefficient	$\text{W m}^{-2} \text{K}^{-1}$
η_{ad}	adiabatic efficiency	1
η	dynamic viscosity	$\text{kg m}^{-1} \text{s}^{-1}$
H_{ad}	specific change in adiabatic enthalpy	J kg^{-1}
H_c	calorific value	J mol^{-1}
H_u	lower calorific value	J kg^{-1}
κ	isentropic exponent	1
m	molar mass	kg mol^{-1}
μ_{JT}	Joule–Thomson coefficient	K Pa^{-1}
p	pressure	Pa
p_c	pseudocritical pressure	Pa
P	energy flow rate (heating power)	W
q	mass flow rate	kg s^{-1}
Q	volumetric flow rate	$\text{m}^3 \text{s}^{-1}$
Q_0	normal volumetric flow rate	$\text{m}^3 \text{h}^{-1}$
ρ	density	kg m^{-3}
ρ_0	normal density	kg m^{-3}
R_s	specific gas constant	$\text{J kg}^{-1} \text{K}^{-1}$
Re	Reynolds number	1
T	temperature	K
T_c	pseudocritical temperature	K
T_{amb}	ambient temperature	K
T_{soil}	soil temperature	K
v	velocity	m s^{-1}
z	compressibility factor	1
z_0	compressibility factor under normal conditions	1

Table A.4. Physical quantities used in the model descriptions

A.3. List of Used GasLib-582 Instances

The following 500 randomly selected instances of GasLib v1 [56] are processed for the computations described in Section 4.2:

cold_1028	cold_1037	cold_1126	cold_1235	cold_1268
cold_1033	cold_1108	cold_1137	cold_1255	cold_1283

A. Appendix

cold_1336	cold_2606	cold_3562	cold_771	cool_1588
cold_1338	cold_2635	cold_365	cold_782	cool_1600
cold_1373	cold_2646	cold_3655	cold_796	cool_1643
cold_1403	cold_265	cold_3669	cold_8	cool_1696
cold_1482	cold_2653	cold_3788	cold_801	cool_1708
cold_1539	cold_2693	cold_3806	cold_89	cool_1719
cold_1548	cold_2715	cold_382	cold_929	cool_1723
cold_1626	cold_2727	cold_3929	cold_942	cool_1744
cold_1629	cold_2746	cold_3999	cold_959	cool_1752
cold_1728	cold_2757	cold_4006	cold_978	cool_1777
cold_1742	cold_2815	cold_4016	cold_983	cool_1782
cold_1768	cold_2840	cold_4039	cool_1052	cool_1790
cold_1810	cold_2901	cold_4041	cool_1059	cool_1816
cold_1817	cold_2908	cold_4051	cool_1063	cool_1822
cold_1842	cold_2936	cold_4088	cool_1079	cool_1837
cold_1860	cold_2944	cold_4106	cool_1133	cool_1875
cold_1939	cold_2968	cold_4128	cool_1135	cool_1893
cold_1944	cold_3002	cold_4143	cool_115	cool_1934
cold_1948	cold_3035	cold_4148	cool_1168	cool_1945
cold_1988	cold_309	cold_4182	cool_1175	cool_1949
cold_202	cold_310	cold_4199	cool_1188	cool_195
cold_2056	cold_3103	cold_4201	cool_1227	cool_196
cold_2061	cold_3120	cold_4214	cool_1256	cool_1985
cold_2067	cold_3159	cold_447	cool_1275	cool_200
cold_2119	cold_3163	cold_491	cool_1297	cool_2014
cold_2143	cold_3165	cold_509	cool_1308	cool_2022
cold_2232	cold_3195	cold_528	cool_131	cool_2095
cold_2256	cold_3218	cold_571	cool_1316	cool_2126
cold_2261	cold_3240	cold_574	cool_1319	cool_2153
cold_2266	cold_3271	cold_587	cool_1325	cool_2187
cold_232	cold_3304	cold_598	cool_1369	cool_2207
cold_2376	cold_3321	cold_623	cool_1380	cool_2251
cold_2428	cold_334	cold_638	cool_1384	cool_2388
cold_2439	cold_3353	cold_717	cool_1411	cool_2434
cold_2501	cold_3426	cold_723	cool_1438	cool_2447
cold_2535	cold_3436	cold_729	cool_1488	cool_2461
cold_2561	cold_3472	cold_73	cool_1543	cool_250

A.3. List of Used GasLib-582 Instances

cool_2506	cool_3422	cool_472	freezing_207	freezing_3556
cool_2620	cool_3495	cool_55	freezing_2115	freezing_3566
cool_2624	cool_3500	cool_555	freezing_2163	freezing_3581
cool_2627	cool_351	cool_584	freezing_2183	freezing_3617
cool_2649	cool_3511	cool_601	freezing_2242	freezing_3683
cool_271	cool_3543	cool_639	freezing_2331	freezing_3703
cool_2713	cool_3644	cool_657	freezing_2380	freezing_3704
cool_272	cool_366	cool_757	freezing_2385	freezing_3744
cool_2721	cool_3668	cool_803	freezing_2415	freezing_376
cool_275	cool_3684	cool_818	freezing_2574	freezing_3857
cool_2751	cool_3689	cool_832	freezing_2593	freezing_3859
cool_2775	cool_3692	cool_836	freezing_26	freezing_3885
cool_2863	cool_3708	cool_939	freezing_2603	freezing_3927
cool_287	cool_3738	cool_966	freezing_2619	freezing_3951
cool_2878	cool_3741	cool_998	freezing_2741	freezing_3973
cool_2926	cool_3790	freezing_10	freezing_2864	freezing_407
cool_2937	cool_3805	freezing_1035	freezing_2868	freezing_4073
cool_2946	cool_3817	freezing_1065	freezing_2881	freezing_4074
cool_2959	cool_3831	freezing_1096	freezing_2892	freezing_4084
cool_2972	cool_3839	freezing_1098	freezing_2893	freezing_4085
cool_2974	cool_3841	freezing_1151	freezing_2952	freezing_4094
cool_2996	cool_3867	freezing_1222	freezing_2957	freezing_4112
cool_3069	cool_3874	freezing_1257	freezing_2975	freezing_4138
cool_3082	cool_3887	freezing_1360	freezing_3042	freezing_4142
cool_3137	cool_391	freezing_1376	freezing_3050	freezing_4180
cool_314	cool_3938	freezing_1432	freezing_3061	freezing_4227
cool_315	cool_4014	freezing_1468	freezing_3142	freezing_437
cool_3222	cool_4078	freezing_1497	freezing_3202	freezing_542
cool_3258	cool_4090	freezing_1532	freezing_3210	freezing_586
cool_326	cool_4100	freezing_1658	freezing_3316	freezing_592
cool_3273	cool_4119	freezing_1669	freezing_3324	freezing_614
cool_3299	cool_4122	freezing_1745	freezing_3339	freezing_648
cool_3320	cool_4141	freezing_176	freezing_3362	freezing_666
cool_333	cool_4147	freezing_1851	freezing_3398	freezing_67
cool_3346	cool_4194	freezing_2058	freezing_3430	freezing_682
cool_337	cool_4206	freezing_2063	freezing_3434	freezing_698
cool_3402	cool_453	freezing_2069	freezing_346	freezing_71

A. Appendix

freezing_804	mild_1935	mild_3390	mild_533	warm_2239
freezing_85	mild_1958	mild_3420	mild_568	warm_2247
freezing_955	mild_2044	mild_3485	mild_629	warm_2342
freezing_96	mild_2101	mild_3493	mild_686	warm_2754
mild_1074	mild_2231	mild_350	mild_714	warm_2786
mild_1085	mild_2346	mild_3513	mild_769	warm_2839
mild_1105	mild_2460	mild_3545	mild_863	warm_3036
mild_114	mild_2497	mild_3546	mild_87	warm_3056
mild_1171	mild_2602	mild_3705	mild_870	warm_3247
mild_1209	mild_262	mild_3784	mild_914	warm_3337
mild_1234	mild_2631	mild_3794	mild_961	warm_3462
mild_1277	mild_264	mild_3845	mild_99	warm_3533
mild_1294	mild_2647	mild_3897	warm_1000	warm_3553
mild_1391	mild_2666	mild_3926	warm_112	warm_3630
mild_1412	mild_2703	mild_3953	warm_1260	warm_3767
mild_1435	mild_2725	mild_3957	warm_154	warm_3946
mild_1469	mild_2771	mild_3998	warm_1721	warm_4113
mild_1506	mild_2922	mild_4023	warm_180	warm_4135
mild_1642	mild_3089	mild_4066	warm_1844	warm_4145
mild_1679	mild_3172	mild_4068	warm_1938	warm_4155
mild_1869	mild_3176	mild_4179	warm_1959	warm_4174
mild_1873	mild_3221	mild_4205	warm_1999	warm_496
mild_1892	mild_3365	mild_503	warm_2025	warm_986
mild_1920	mild_3375	mild_529	warm_2097	warm_993

Bibliography

- [1] T. ACHTERBERG, *Constraint Integer Programming*, PhD thesis, Technische Universität Berlin, 2007.
- [2] AMERICAN GAS ASSOCIATION. PIPELINE RESEARCH COMMITTEE AND R. H. ZIMMERMAN, *A.G.A. manual for the determination of supercompressibility factors for natural gas: PAR research project NX-19 Extension of range of supercompressibility tables*, American Gas Association, New York, 1963.
- [3] J. D. ANDERSON, JR., J. DEGROOTE, G. DEGREGZ, E. DICK, R. GRUNDMANN, AND J. VIERENDEELS, *Computational Fluid Dynamics An Introduction*, Springer Berlin, Heidelberg, 3rd ed., 2009.
- [4] M. ANITESCU, *On using the elastic mode in nonlinear programming approaches to mathematical programs with complementarity constraints*, *SIAM Journal on Optimization*, 15 (2005), pp. 1203–1236.
- [5] P. BALES, *Hierarchische Modellierung der Eulerschen Flussgleichungen in der Gasdynamik*, Master's thesis, Technische Universität Darmstadt, 2005.
- [6] B. T. BAUMRUCKER, J. G. RENFRO, AND L. T. BIEGLER, *MPEC problem formulations and solution strategies with chemical engineering applications*, *Computers & Chemical Engineering*, (2008), pp. 2903–2913.
- [7] A. BEN-TAL, S. BOYD, AND A. NEMIROVSKI, *Extending scope of robust optimization: Comprehensive robust counterparts of uncertain problems*, *Mathematical Programming*, 107 (2006), pp. 63–89.
- [8] A. BEN-TAL, L. EL GHAOUI, AND A. NEMIROVSKI, *Robust Optimization*, Princeton Series in Applied Mathematics, Princeton University Press, October 2009.
- [9] H. G. BOCK, E. KOSTINA, H. X. PHU, AND R. RANNACHER, eds., *Modeling, Simulation and Optimization of Complex Processes*, Springer, Berlin, 2005.

Bibliography

- [10] C. BORRAZ-SÁNCHEZ AND R. Z. RÍOS-MERCADO, *A procedure for finding initial feasible solutions on cyclic natural gas networks*, in Proceedings of the 2004 NSF Design, Service and Manufacturing Grantees and Research Conference, Dallas, USA, January 2004.
- [11] ———, *A hybrid meta-heuristic approach for natural gas pipeline network optimization*, in Hybrid Metaheuristics, M. Blesa, C. Blum, A. Roli, and M. Sampels, eds., vol. 3636 of Lecture Notes in Computer Science, Springer, 2005, pp. 54–65.
- [12] E. A. BOYD, L. R. SCOTT, AND S. WU, *Evaluating the quality of pipeline optimization algorithms*, in PSIG 29th Annual Meeting, Tucson, Arizona, Pipeline Simulation Interest Group, 1997.
- [13] D. BRKIĆ, *Determining friction factors in turbulent pipe flow*, AICHE J., (2012), pp. 34–39.
- [14] J. BROUWER, I. GASSER, AND M. HERTY, *Gas pipeline models revisited: Model hierarchies, nonisothermal models, and simulations of networks*, Multiscale Model. Simul., 9 (2011), pp. 601–623.
- [15] BUNDESAMT FÜR WIRTSCHAFT UND AUSFUHRKONTROLLE, *Entwicklung der Erdgaseinfuhr in die Bundesrepublik Deutschland, Bilanzen 1998 – 2013 (development of natural gas import to the federal republic of germany, 1998 – 2013)*, tech. rep., Bundesamt für Wirtschaft und Ausfuhrkontrolle, 2014. http://www.bafa.de/bafa/de/energie/erdgas/ausgewaehlte_statistiken/egashist.pdf.
- [16] BUNDESREGIERUNG DEUTSCHLAND, *Verordnung über den Zugang von Gasversorgungnetzen (Gasnetzzugangsverordnung – GasNZV)*, 2010.
- [17] J. BURGSCHWEIGER, B. GNÄDIG, AND M. C. STEINBACH, *Optimization models for operative planning in drinking water networks*, Optim. Eng., 10 (2009), pp. 43–73.
- [18] J. BURGSCHWEIGER, B. GNÄDIG, AND M. C. STEINBACH, *Nonlinear programming techniques for operative planning in large drinking water networks*, The Open Appl. Math. J., 3 (2009), pp. 14–28.
- [19] R. G. CARTER, *Compressor station optimization: Computational accuracy and speed*, in 28th Annual Meeting, no. PSIG 9605, Pipeline Simulation Interest Group, 1996.

- [20] R. G. CARTER, D. W. SCHROEDER, AND T. D. HARBICK, *Some causes and effects of discontinuities in modeling and optimizing gas transmission networks*, in 25th Annual Meeting, no. PSIG 9308, Pipeline Simulation Interest Group, 1993.
- [21] CENTRAL INTELLIGENCE AGENCY, *World Factbook*. <https://www.cia.gov/library/publications/the-world-factbook/>. Accessed: 2014-04-06.
- [22] B. CHEN, X. CHEN, AND C. KANZOW, *A penalized fischer-burmeister NCP-function*, Math. Program., 88 (2000), pp. 211–216.
- [23] C. CHEN, Y. LI, G. HUANG, AND Y. ZHU, *An inexact robust nonlinear optimization method for energy systems planning under uncertainty*, Renewable Energy, 47 (2012), pp. 55 – 66.
- [24] J.-S. CHEN AND S. PAN, *A family of NCP functions and a descent method for the nonlinear complementarity problem*, Comput. Optim. Appl., 40 (2008), pp. 389–404.
- [25] I. J. CHODANOWITSCH AND G. E. ODISCHARIJA, *Analiž žavisimosti dlja koefizienta hidravličeskogo soprotivlenija (analysis of the relations of friction coefficients)*, gazovaya promyšlennost, 11 (1964), pp. 38–42.
- [26] C. F. COLEBROOK, *Turbulent flow in pipes with particular reference to the transition region between smooth and rough pipe laws*, Journal of the Institution of Civil Engineers, 11 (1939), pp. 133–156.
- [27] D. DE WOLF AND Y. SMEERS, *The gas transmission problem solved by an extension of the simplex algorithm*, Management Sci., 46 (2000), pp. 1454–1465.
- [28] A.-V. DEMIGUEL, M. P. FRIEDLANDER, F. J. NOGALES, AND S. SCHOLTES, *A two-sided relaxation scheme for mathematical programs with equilibrium constraints*, SIAM J. Optim., 16 (2005), pp. 587–609.
- [29] M. DIEHL, H. G. BOCK, AND E. KOSTINA, *An approximation technique for robust nonlinear optimization*, Math. Program., 107 (2006), pp. 213–230.
- [30] P. DOMSCHKE, B. GEISSLER, O. KOLB, J. LANG, A. MARTIN, AND A. MORSI, *Combination of nonlinear and linear optimization of transient gas networks*, INFORMS Journal of Computing, 23 (2011), pp. 605–617.
- [31] A. S. DRUD, *CONOPT - a large-scale GRG code*, ORSA J. Comput., 6 (1992), pp. 207–216.
- [32] ———, *CONOPT - a large-scale GRG code*, INFORMS J. Comput., 6 (1994), pp. 207–216.

Bibliography

- [33] ———, *CONOPT: A system for large scale nonlinear optimization, tutorial for CONOPT subroutine library*, tech. rep., ARKI Consulting and Development A/S, Bagsvaerd, Denmark, 1995.
- [34] ———, *CONOPT: A system for large scale nonlinear optimization, reference manual for CONOPT subroutine library*, tech. rep., ARKI Consulting and Development A/S, Bagsvaerd, Denmark, 1996.
- [35] T. EDERER, U. LORENZ, A. MARTIN, T. OPFER, AND J. WOLF, *Polyhedral properties and algorithmic aspects of quantified linear programs*, preprint 2650, Technische Universität Darmstadt, 2012.
- [36] T. EDERER, U. LORENZ, A. MARTIN, AND J. WOLF, *Quantified linear programs: A computational study*, in *Proceeding ESA 2011*, Springer, 2011, pp. 203–214.
- [37] K. EHRHARDT AND M. C. STEINBACH, *KKT systems in operative planning for gas distribution networks*, *Proc. Appl. Math. Mech.*, 4 (2004), pp. 606–607.
- [38] ———, *Nonlinear optimization in gas networks*, in Bock et al. [9], pp. 139–148.
- [39] M. FEISTAUER, *Mathematical Methods in Fluid Dynamics*, vol. 67 of Pitman Monographs and Surveys in Pure and Applied Mathematics Series, Longman Scientific & Technical, Harlow, 1993.
- [40] M. C. FERRIS AND J.-S. PANG, *Engineering and economic applications of complementarity problems*, *SIAM Review*, 39 (1997), pp. 669–713.
- [41] M. C. FERRIS AND F. TIN-LOI, *On the solution of a minimum weight elastoplastic problem involving displacement and complementarity constraints*, *Computer Methods in Applied Mechanics and Engineering*, 174 (1999), pp. 108–120.
- [42] M. C. FERRIS AND F. TIN-LOI, *Nonlinear programming approach for a class of inverse problems in elastoplasticity*, *Structural Engineering and Mechanics*, 6 (1998), pp. 857–870.
- [43] A. FINCHAM AND M. GOLDWATER, *Simulation models for gas transmission networks*, *Transactions of the Institute of Measurement and Control*, 1 (1979), pp. 3–13.
- [44] E. J. FINNEMORE AND J. E. FRANZINI, *Fluid Mechanics with Engineering Applications*, McGraw-Hill, 10th ed., 2002.
- [45] A. FISCHER, *A special Newton-type optimization method*, *Optimization*, 24 (1992), pp. 269–284.

- [46] R. FLATT, *Unsteady compressible flow in long pipelines following a rupture*, International Journal for Numerical Methods in Fluids, 6 (1986), pp. 83–100.
- [47] M. L. FLEGEL, *Constraint Qualifications and Stationarity Concepts for Mathematical Programs with Equilibrium Constraints*, PhD thesis, University of Würzburg, 2005.
- [48] M. L. FLEGEL AND C. KANZOW, *Abadie-type constraint qualification for mathematical programs with equilibrium constraints*, Journal of Optimization Theory and Applications, 124 (2005), pp. 595–614.
- [49] M. L. FLEGEL AND C. KANZOW, *On m -stationary points for mathematical programs with equilibrium constraints*, Journal of Mathematical Analysis and Applications, 310 (2005), pp. 286–302.
- [50] M. L. FLEGEL AND C. KANZOW, *On the guignard constraint qualification for mathematical programs with equilibrium constraints*, Optimization, 54 (2005), pp. 517–534.
- [51] ———, *A direct proof for m -stationarity under mpec-gcq for mathematical programs with equilibrium constraints*, in Optimization with Multivalued Mappings, S. Dempe and V. Kalashnikov, eds., vol. 2 of Springer Optimization and Its Applications, Springer US, 2006, pp. 111–122.
- [52] R. FLETCHER AND S. LEYFFER, *Nonlinear programming without a penalty function*, Math. Program., 91 (2000), pp. 239–269.
- [53] L. R. FORD AND D. R. FULKERSON, *Flows in Networks*, Princeton University Press, 1962.
- [54] A. FÜGENSCHUH, B. GEISSLER, R. GOLLMER, C. HAYN, R. HENRION, B. HILLER, J. HUMPOLA, T. KOCH, T. LEHMANN, A. MARTIN, R. MIRKOV, A. MORSI, W. RÖMISCH, J. RÖVEKAMP, L. SCHEWE, M. SCHMIDT, R. SCHULTZ, R. SCHWARZ, J. SCHWEIGER, C. STANGL, M. C. STEINBACH, AND B. M. WILLERT, *Mathematical optimization for challenging network planning problems in unbundled liberalized gas markets*, Energy Systems, (2013), pp. 1–25.
- [55] *General algebraic modeling system (GAMS)*. <http://www.gams.com/>.
- [56] *GasLib – a library of gas network instances*. gaslib.zib.de.
- [57] C. GEIGER AND C. KANZOW, *Theorie und Numerik restringierter Optimierungsprobleme*, Springer, 2002.

Bibliography

- [58] B. GEISLER, *Towards Globally Optimal Solutions for MINLPs by Discretization Techniques with Applications in Gas Network Optimization*, PhD thesis, Friedrich-Alexander-Universität Erlangen-Nürnberg, 2011.
- [59] P. E. GILL, W. MURRAY, AND M. S. SAUNDERS, *SNOPT: An SQP algorithm for large-scale constrained optimization*, SIAM J. Optim., 12 (2002), pp. 979–1006.
- [60] P. HACKLÄNDER, *Integrierte Betriebsplanung von Gasversorgungssystemen*, PhD thesis, Universität Wuppertal, 2002.
- [61] R. HENRION, *On constraint qualifications*, J. Optim. Theory Appl., 72 (1992), pp. 187–197.
- [62] P. HOFER, *Beurteilung von Fehlern in Rohrnetzrechnungen (error evaluation in calculation of pipelines)*, GWF Gas / Erdgas, 11 (1973), pp. 113–119.
- [63] X. M. HU AND D. RALPH, *Convergence of a penalty method for mathematical programming with complementarity constraints*, J. Optim. Theory Appl., 123 (2004), pp. 365–390.
- [64] T. JENÍČEK, *Steady-state optimization of gas transport*, in SIMONE [121], pp. 26–38.
- [65] T. JENÍČEK, J. KRÁLIK, J. ŠTĚRBA, Z. VOŠTRÝ, AND J. ZÁWORKA, *Study to analyze the possibilities and features of an optimization system (optimum control system) to support the dispatching activities of Ruhrgas*. Vertrauliche Dokumentation, LIWACOM Informationstechnik GmbH Essen, 1993.
- [66] H. JIANG AND D. RALPH, *Smooth sqp methods for mathematical programs with nonlinear complementarity constraints*, SIAM Journal on Optimization, 10 (1997), pp. 779–808.
- [67] H. T. JONGEN, J.-J. RÜCKMANN, AND V. SHIKHMAN, *Mpcc: critical point theory*, SIAM Journal on Optimization, 20 (2009), pp. 473–484.
- [68] C. KANZOW, N. YAMASHITA, AND M. FUKUSHIMA, *New NCP-functions and their properties*, J. Optim. Theory Appl., 94 (1997), pp. 115–135.
- [69] D. L. V. KATZ, *A thermodynamic analysis of frictional heat in pipeline flow*, Oil and Gas Journal, 70 (1972).
- [70] S. KAZEMPOUR, A. CONEJO, AND C. RUIZ, *Strategic generation investment considering futures and spot markets*, Power Systems, IEEE Transactions on, 27 (2012), pp. 1467–1476.

- [71] T. KOCH, D. BARGMANN, M. EBBERS, A. FÜGENSCHUH, B. GEISLER, N. GEISLER, R. GOLLMER, U. GOTZES, C. HAYN, H. HEITSCH, R. HENRION, B. HILLER, J. HUMPOLA, I. JOORMANN, V. KÜHL, T. LEHMANN, H. LEÖVEY, A. MARTIN, R. MIRKOV, A. MÖLLER, A. MORSI, D. OUCHERIF, A. PELZER, M. E. PFETSCH, W. RÖMISCH, J. RÖVEKAMP, L. SCHEWE, M. SCHMIDT, R. SCHULTZ, R. SCHWARZ, J. SCHWEIGER, K. SPRECKELSEN, C. STANGL, M. C. STEINBACH, A. STEINKAMP, S. VIGERSKE, I. WEGNER-SPECHT, AND B. M. WILLERT, *Evaluating Gas Network Capacities*, MOS-SIAM Series on Optimization, 2014. In preparation.
- [72] J. KRÁLIK, *Compressor stations in SIMONE*, in SIMONE [121], pp. 93–117.
- [73] J. KRÁLIK, P. STIEGLER, Z. VOSTRÝ, AND J. ZÁWORKA, *Dynamic Modeling of Large-Scale Networks with Application to Gas Distribution*, vol. 6 of Studies in Automation and Control, Elsevier Sci. Publ., New York, 1988.
- [74] O. KUNZ, R. KLIMECK, W. WAGNER, AND M. JAESCHKE, *The GERG-2004 Wide-Range Equation of State for Natural Gases and Other Mixtures*, no. 557 in Fortschritt-Berichte VDI, Reihe 6, VDI Verlag, Düsseldorf, 2007. GERG Technical Monograph 15.
- [75] S. LEYFFER, *Complementarity constraints as nonlinear equations: Theory and numerical experience*, in Optimization with Multivalued Mappings, S. Dempe and V. Kalashnikov, eds., Springer, 2006, pp. 169–208.
- [76] S. LEYFFER, G. LÓPEZ-CALVA, AND J. NOCEDAL, *Interior methods for mathematical programs with complementarity constraints*, SIAM J. Optim., 17 (2004), pp. 52–77.
- [77] S. LEYFFER AND T. S. MUNSON, *A globally convergent filter method for MPECs*, preprint ANL/MCS-P1457-0907, Argonne National Laboratory, Mathematics and Computer Science Division, 2007.
- [78] LIWACOM INFORMATIONS GMBH AND SIMONE RESEARCH GROUP S.R.O., *Gleichungen und Methoden*, 2004.
- [79] Z.-Q. LUO, J.-S. PANG, AND D. RALPH, *Mathematical programs with equilibrium constraints*, Cambridge University Press, 1996.
- [80] M. V. LURIE, *Modeling of Oil Product and Gas Pipeline Transportation*, Wiley-VCH, 2008.

Bibliography

- [81] A. MARTIN, B. GEISSLER, C. HAYN, B. HILLER, J. HUMPOLA, T. KOCH, T. LEHMANN, A. MORSI, M. PFETSCH, L. SCHEWE, M. SCHMIDT, R. SCHULTZ, R. SCHWARZ, J. SCHWEIGER, M. C. STEINBACH, AND B. M. WILLERT, *Optimierung Technischer Kapazitäten in Gasnetzen*, in *Optimierung in der Energiewirtschaft*, vol. 2157 of VDI-Berichte, 2011, pp. 105–114.
- [82] A. MARTIN, D. MAHLKE, AND S. MORITZ, *A simulated annealing algorithm for transient optimization in gas networks*, *Math. Methods Oper. Res.*, 66 (2007), pp. 99–115.
- [83] A. MARTIN AND M. MÖLLER, *Cutting planes for the optimization of gas networks*, in Bock et al. [9], pp. 307–329.
- [84] A. MARTIN, M. MÖLLER, AND S. MORITZ, *Mixed integer models for the stationary case of gas network optimization*, *Math. Program.*, 105 (2006), pp. 563–582.
- [85] E. MENON, *Gas Pipeline Hydraulics*, Taylor & Francis Group, 2005.
- [86] J. MISCHNER, *Notices about hydraulic calculations of gas pipelines*, *GWf Gas / Erdgas*, 4 (2012), pp. 158–273.
- [87] M. MÖLLER, *Mixed Integer Models for the Optimisation of Gas Networks in the Stationary Case*, PhD thesis, Technische Universität Darmstadt, 2004.
- [88] L. F. MOODY, *Friction factors for pipe flow*, *Transactions of the A.S.M.E.*, 66 (1944), pp. 671–684.
- [89] A. A. MORE, *Analytical solutions for the Colebrook and White equation and for pressure drop in ideal gas flow in pipes*, *Chemical Engineering Science*, 61 (2006), pp. 5515 – 5519.
- [90] S. MORITZ, *A Mixed Integer Approach for the Transient Case of Gas Network Optimization*, PhD thesis, Technische Universität Darmstadt, 2007.
- [91] NASA, *Axial compressor*. <http://www.grc.nasa.gov/WWW/K-12/airplane/caxial.html>. Accessed: 2013-07-23.
- [92] J. NIKURADSE, *Strömungsgesetze in rauhen Röhren*, Forschungsheft auf dem Gebiete des Ingenieurwesens, VDI-Verlag, 1933.
- [93] ———, *Laws of Flow in Rough Pipes*, vol. 1292 of Technical Memorandum, National Advisory Committee for Aeronautics, Washington, 1950.

- [94] J. NOCEDAL AND S. J. WRIGHT, *Numerical Optimization*, Springer, Berlin, 2nd ed., 2006.
- [95] F. M. ODOM AND G. L. MUSTER, *Tutorial on modeling of gas turbine driven centrifugal compressors*, Tech. Rep. 09A4, Pipeline Simulation Interest Group, 2009.
- [96] A. OSIADACZ, *Nonlinear programming applied to the optimum control of a gas compressor station*, Int. J. Numer. Methods Eng., 15 (1980), pp. 1287–1301.
- [97] A. J. OSIADACZ, *Simulation and analysis of gas networks*, E. & F.N. Spon, London, 1987.
- [98] J. OUTRATA, M. KOCVARA, AND J. ZOWE, *Nonsmooth Approach to Optimization Problems with Equilibrium Constraints*, Kluwer Academic Publishers, Dordrecht, The Netherlands, 1998.
- [99] J. V. OUTRATA, *On optimization problems with variational inequality constraints*, SIAM Journal on Optimization, 4 (1994), pp. 340–357.
- [100] J. V. OUTRATA, *Optimality conditions for a class of mathematical programs with equilibrium constraints*, Mathematics of Operations Research, 24 (1999), pp. 627–644.
- [101] J.-S. PANG, G. LO, AND J. C. TRINKLE, *A complementarity approach to a quasistatic rigid body motion problem*, tech. rep., Texas A & M University, 1994.
- [102] J.-S. PANG AND J. C. TRINKLE, *Complementarity formulations and existence of solutions of dynamic multi-rigid-body contact problems with coulomb friction*, Mathematical Programming, 73 (1994).
- [103] I. PAPAY, *A termelestechnologiai parameterek változása a gázleplek művelese során*, OGIL Musz. Tud. Kozl., (1968), pp. 267–273.
- [104] M. E. PFETSCH, A. FÜGENSCHUH, B. GEISSLER, N. GEISSLER, R. GOLLMER, B. HILLER, J. HUMPOLA, T. KOCH, T. LEHMANN, A. MARTIN, A. MORSI, J. RÖVEKAMP, L. SCHEWE, M. SCHMIDT, R. SCHULTZ, R. SCHWARZ, J. SCHWEIGER, C. STANGL, M. C. STEINBACH, S. VIGERSKE, AND B. M. WILLERT, *Validation of nominations in gas network optimization: Models, methods, and solutions*, Optimization Methods and Software, (2014).
- [105] K. F. PRATT AND J. G. WILSON, *Optimization of the operation of gas transmission systems*, Transactions of the Institute of Measurement and Control, 6 (1984), pp. 261–269.

Bibliography

- [106] O. REDLICH AND J. N. S. KWONG, *On the Thermodynamics of Solutions. V. An Equation of State. Fugacities of Gaseous Solutions*, Chemical Reviews, 44 (1949), pp. 233–244.
- [107] R. Z. RÍOS-MERCADO, S. KIM, AND A. E. BOYD, *Efficient operation of natural gas transmission systems: A network-based heuristic for cyclic structures*, Computers & Operations Research, 33 (2006), pp. 2323–2351.
- [108] R. Z. RÍOS-MERCADO, S. WU, L. R. SCOTT, AND A. E. BOYD, *A reduction technique for natural gas transmission network optimization problems*, Ann. Oper. Res., 117 (2002), pp. 217–234.
- [109] H. ROUSE, *Evaluation of boundary roughness*, in Proc. 2nd Hydraulics Conf, 1943.
- [110] J. M. SALEH, ed., *Fluid Flow Handbook*, McGraw-Hill Handbooks, McGraw-Hill, 2002.
- [111] H. SCHEEL AND S. SCHOLTES, *Mathematical programs with complementarity constraints: Stationarity, optimality and sensitivity*, Math. Oper. Res., 25 (2000), pp. 1–22.
- [112] D. SCHEIBE AND A. WEIMANN, *Dynamische Gasnetzsimulation mit GANESI*, GWF Gas / Erdgas, 9 (1999), pp. 610–616.
- [113] M. SCHMIDT, *A Generic Interior-Point Framework for Nonsmooth and Complementarity Constrained Nonlinear Optimization*, PhD thesis, Gottfried Wilhelm Leibniz Universität Hannover, 2013.
- [114] M. SCHMIDT, M. C. STEINBACH, AND B. M. WILLERT, *A primal heuristic for nonsmooth mixed integer nonlinear optimization*, in Facets of Combinatorial Optimization, M. Jünger and G. Reinelt, eds., Springer Berlin Heidelberg, 2013, pp. 295–320.
- [115] ———, *High detail stationary optimization models for gas networks*, Optimization and Engineering, (2014), pp. 1–34.
- [116] M. SCHMIDT, M. C. STEINBACH, AND B. M. WILLERT, *High detail stationary optimization models for gas networks — Part 2: Validation and results.*, Optimization and Engineering, (2014). In preparation.
- [117] S. SCHOLTES, *Convergence properties of a regularization scheme for mathematical programs with complementarity constraints*, SIAM J. Optim., 11 (2001), pp. 918–936.

- [118] E. SEKIRNJAK, *Mixed integer optimization for gas transmission and distribution systems*. Presentation manuscript, INFORMS-Meeting, Seattle, Oct. 1998.
- [119] ———, *Transiente Technische Optimierung (TTO-Prototyp)*. Vertrauliche Dokumentation, PSI AG, Berlin, 1999.
- [120] *SIMONE software*. <http://www.liwacom.de>.
- [121] *Proceedings of 2nd International Workshop SIMONE on Innovative Approaches to Modeling and Optimal Control of Large Scale Pipeline Networks*, Prague, 1993.
- [122] K. E. STARLING AND J. L. SAVIDGE, *Compressibility factors of natural gas and other related hydrocarbon gases*, Transmission Measurement Committee report, American Gas Association, New York, 1992.
- [123] M. C. STEINBACH, *On PDE solution in transient optimization of gas networks*, J. Comput. Appl. Math., 203 (2007), pp. 345–361.
- [124] M. STÖHR, *Nonsmooth Trust Region Methods and Their Applications to Mathematical Programs with Equilibrium Constraints*, PhD thesis, Universität Fridericiana zu Karlsruhe, 1999.
- [125] C.-L. SU, *Equilibrium problems with equilibrium constraints: stationarities, algorithms, and applications*, PhD thesis, Stanford University, 2005.
- [126] D. SUN AND L. QI, *On NCP-functions*, Comput. Optim. Appl., 13 (1999), pp. 201–220. Computational Optimization - a Tribute to Olvi Mangasarian, Part II.
- [127] M. TAWARMALANI AND N. V. SAHINIDIS, *A polyhedral branch-and-cut approach to global optimization*, Mathematical Programming, 103 (2005), pp. 225–249.
- [128] J. B. TAYLOR, A. L. CARRANO, AND S. G. KANDLIKAR, *Characterization of the effect of surface roughness and texture on fluid flow—past, present, and future*, International Journal of Thermal Sciences, 45 (2006), pp. 962 – 968.
- [129] T. TAYLOR, N. WOOD, AND J. POWERS, *A computer simulation of gas flow in long pipelines*, Old SPE Journal, 2 (1962), pp. 297–302.
- [130] F. TIN-LOI, *On the numerical solution of a class of unilateral contact structural optimization problems*, Structural optimization, 17 (1999), pp. 155–161.
- [131] Y. VILLALOBOS-MORALES, D. COBOS-ZALETÁ, H. J. FLORES-VILLARREAL, C. BORRAZ-SÁNCHEZ, AND R. Z. RÍOS-MERCADO, *On NLP and MINLP formulations and preprocessing for fuel cost minimization of natural gas transmission*

Bibliography

- networks*, in Proceedings of the 2003 NSF Design, Service and Manufacturing Grantees and Research Conference, Birmingham, USA, January 2003.
- [132] Z. VOSTRÝ, *Transient optimization of gas transport and distribution*, in SIMONE [121], pp. 53–62.
- [133] Z. VOSTRÝ AND J. ZÁWORKA, *Heat dynamics in gas transport*, in Proceedings of the SIMONE Congress '95, Espoo, 5 1995, LIWACOM, pp. 64–75.
- [134] A. WÄCHTER AND L. T. BIEGLER, *On the implementation of an interior-point filter line-search algorithm for large-scale nonlinear programming*, Math. Program., 106 (2006), pp. 25–57.
- [135] A. WEIMANN, *Modellierung und Simulation der Dynamik von Gasnetzen im Hinblick auf Gasnetzführung und Gasnetzüberwachung*, PhD thesis, Technische Universität München, 1978.
- [136] S. WRIGHT, M. SOMANI, AND C. DITZEL, *Compressor station optimization*, in 30th Annual Meeting, Pipeline Simulation Interest Group, 1998. Paper 9805.
- [137] S. WU, *Steady-State Simulation and Fuel Cost Minimization of Gas Pipeline Networks*, PhD thesis, University of Houston, 1998.
- [138] S. WU, R. Z. RÍOS-MERCADO, A. E. BOYD, AND L. R. SCOTT, *Model relaxations for the fuel cost minimization of steady-state gas pipeline networks*, Mathematical and Computer Modelling, 31 (2000), pp. 197 – 220.
- [139] J. J. YE, *Necessary and sufficient optimality conditions for mathematical programs with equilibrium constraints*, J. Math. Anal. Appl., 307 (2005), pp. 305–369.
- [140] J. ZÁWORKA, *Project SIMONE—Achievements and running development*, in SIMONE [121], pp. 1–24.
- [141] J. ZÁWORKA, *Project SIMONE - achievements and running development*, tech. rep., Institute of Information Theory and Automation, Czech Republic, 2004.
- [142] Y. ZHANG, *A general robust-optimization formulation for nonlinear programming*, J. Optim. Theory Appl., (2005).

Curriculum Vitae

Persönliche Informationen

Geburtsdatum	10.02.1984
Geburtsort	München, Deutschland
Geburtsname	Sack

Bildungsgang

09/2009 — 07/2014	Promotion an der Leibniz Universität Hannover
10/2004 — 08/2009	Studium der Mathematik mit Nebenfach Informatik an der Leibniz Universität Hannover, Diplom mit Auszeichnung Diplomarbeit: „Strukturierte Trajektorienoptimierung mechanischer Systeme“
1994 — 2003	Curie-Gymnasium Neubrandenburg, Abitur

Berufserfahrung

09/2009—02/2014	Wissenschaftlicher Mitarbeiter am Institut für angewandte Mathematik, AG Algorithmische Optimierung (Prof. Dr. Steinbach), Leibniz Universität Hannover
07/2008—02/2009	Praktikum und Werkstudententätigkeit bei HDI-Gerling
04/2007—08/2007	Praktikum bei STIHL Incorporated, Virginia Beach, USA
2006 — 2009	Wissenschaftliche Hilfskraft am Institut für angewandte Mathematik der Leibniz Universität Hannover
2005 — 2007	Wissenschaftliche Hilfskraft am Institut für Versicherungsbetriebslehre der Leibniz Universität Hannover
2003 — 2004	Grundwehrdienst

Veröffentlichungen

M. SCHMIDT, M. C. STEINBACH, AND B. M. WILLERT, *High detail stationary optimization models for gas networks*, Optimization and Engineering, (2014), pp. 1–34.

M. E. PFETSCH, A. FÜGENSCHUH, B. GEISSLER, N. GEISSLER, R. GOLLMER, B. HILLER, J. HUMPOLA, T. KOCH, T. LEHMANN, A. MARTIN, A. MORSI, J. RÖVEKAMP, L. SCHEWE, M. SCHMIDT, R. SCHULTZ, R. SCHWARZ, J. SCHWEIGER, C. STANGL, M. C. STEINBACH, S. VIGERSKE, AND B. M. WILLERT, *Validation of nominations in gas network optimization: Models, methods, and solutions*, Optimization Methods and Software, (2014).

A. FÜGENSCHUH, B. GEISSLER, R. GOLLMER, C. HAYN, R. HENRION, B. HILLER, J. HUMPOLA, T. KOCH, T. LEHMANN, A. MARTIN, R. MIRKOV, A. MORSI, W. RÖMISCH, J. RÖVEKAMP, L. SCHEWE, M. SCHMIDT, R. SCHULTZ, R. SCHWARZ, J. SCHWEIGER, C. STANGL, M. C. STEINBACH, AND B. M. WILLERT, *Mathematical optimization for challenging network planning problems in unbundled liberalized gas markets*, Energy Systems, (2013), pp. 1–25.

M. SCHMIDT, M. C. STEINBACH, AND B. M. WILLERT, *A primal heuristic for nonsmooth mixed integer nonlinear optimization*, in Facets of Combinatorial Optimization, M. Jünger and G. Reinelt, eds., Springer Berlin Heidelberg, 2013, pp. 295–320.

A. MARTIN, B. GEISSLER, C. HAYN, B. HILLER, J. HUMPOLA, T. KOCH, T. LEHMANN, A. MORSI, M. PFETSCH, L. SCHEWE, M. SCHMIDT, R. SCHULTZ, R. SCHWARZ, J. SCHWEIGER, M. C. STEINBACH, AND B. M. WILLERT, *Optimierung Technischer Kapazitäten in Gasnetzen*, in Optimierung in der Energiewirtschaft, vol. 2157 of VDI-Berichte, 2011, pp. 105–114.